Dissertation

submitted to the

Combined Faculty of Natural Sciences and Mathematics

of the Ruperto Carola University Heidelberg, Germany

for the degree of

Doctor of Natural Sciences

Presented by

M.Sc. Stefan Ralf Kurzhals

Born in: Heidelberg, Germany

Oral examination: 05th October 2021

Functional characterization of

human resident intestinal lamina propria dendritic cells

under inflammatory conditions in health and disease

Referees: **Prof. Dr. Tobias Dick**

Prof. Dr. Stefan Meuer

Index of contents

Abbreviations

°C	degrees celcius
µg	microgram
µm	micrometer
15-HETE	15-Hydroxyeicosatetraenoic acid
AA	Arachidonic acid
Ab	Antibody
ALOX15B	Arachidonate 15-Lipoxygenase type B
APCs	antigen presenting cells
aRNA	antisense RNA
BDCA	Blood Dendritic Cell Antigen
CCL	CC chemokine ligand
CCR	CC chemokine receptor
CD	Crohn's disease
CD#	cluster of differentiation (number)
cDC1	conventional dendritic cell 1
cDC2	conventional dendritic cell 2
cDNA	complementary desoxyribonucleic acid
CED	chronisch entzündliche Darmerkrankungen
CM	complete mucosa
Co-IP	Co-immunoprecipitation
CTSK	Cathepsin K
DCs	dendritic cells
DE	differentially expressed
DN	double negative
DP	double positive
dsDNA	double-stranded DNA
DSS	dextran sodium sulfate
DTT	Dithiothreitol
EGFR	epidermal growth factor receptor
EIM	extraintestinal manifestation
ELISA	enzyme linked immunosorbant assay
FACS	Fluorescence-activated cell sorting
FBS	fetal bovine serum
FcR	Fragment crystallizable receptor
FcRn	neonatal fragment crytallizable receptor
FDR	false discovery rate
FFPE	formalin fixed paraffin embedded
Fig.	Figure
g	relative centrifugal force
GALT	gut-associated lymphoid tissues
GWAS	genome-wide association studies
HEK	human embryonic kidney
HRP	horseradish peroxidase
IBD	Inflammatory Bowel Diseases
iCD	inflamed Crohn's disease

IDO	indoleamine 2,3-dioxygenase
IELs	intraepithelial lymphocytes
IF	immunofluorescence
IFN	interferon
IgG	Immunoglobulin G
IL	Interleukin
ILFs	isolated lymphoid follicles
IPA	Ingenuity Pathway Analysis
iUC	inflamed ulcerative colitis
LEL	loss of epithelial layer
lfc	linear fold change
lncRNA	long non-coding RNA
M cell	microfold cell
mAb	monocolonal antibody
MACS	magnetic-activated cell sorting
MAdCAM-1	mucosal addressin cell adhesion molecule-1
MALT	mucosa-associated lymphoid tissues
MAMPs	microbe-associated molecular patterns
mDCs	myeloid dendritic cells
ml	millilitre
mLPDCs	lamina propria myeloid dendritic cells
MMP	matrix metalloproteinase
MNP	mononuclear phagocyte
mRNA	messenger ribonucleic acid
Mϕ	Macrophage
NC	normal colon
NFDM	non-fat dry milk
niCD	non-inflamed Crohn's disaese
niUC	non-inflamed ulcerative colitis
NLR	NOD-like receptor
nm	nanometer
PBDCs	peripheral blood dendritic cells
PBMOs	peripheral blood mononuclear cells
PBS	phosphate buffered saline
pDCs	plasmacytoid dendritic cells
PEI	Polyethylenimine
PGE2	prostaglandin E2
pIgR	polymeric immunoglobulin receptor
PLA	proximity ligation assay
PRR	pattern recognition receptor
PVDF	Polyvinylidene fluoride
r	recombinant
rpm	rounds per minute
RT	room temperature
SDE	statistical significant differentially expressed
sfTSLP	short form thymic stromal lymphopoietin
SIgA	secretory immunoglobulin A

SNP	single-nucleotide polymorphism
ssDNA	single-stranded DNA
STAT	signal-transducing activator of transcription
STING	stimulator of interferon genes
TBS	Tris buffered saline
TGF-β	transforming growth factor β
Th cell	T helper cell
TIMP2	tissue inhibitor of matrix metalloproteinases 2
TLRs	Toll like receptors
TNBS	trinitrobenzene sulfonic acid
TNF-α	tumor necrosis factor α
TPM	transcripts per million
U	units
UC	ulcerative colitis
VE-cadherin	vascular endothelial cadherin

Summary

Inflammatory Bowel Diseases (IBD) are a group of intestinal disorders which are increasing in prevalence in industrialized countries. Dynamics of intestinal inflammatory disorders are manifold and investigation of coherences might help developing new therapeutic strategies harnessing the acquired knowledge. Keeping a homeostatic balance in the intestinal environment is vital for normal gut functions, regulating inflammatory and anti-inflammatory processes. Dendritic cells are known as key players in the regulation of intestinal homeostasis as they scavenge their surroundings for antigens followed by the induction of an adaptive immune response. The aim of this study was to investigate the functional properties of resident lamina propria myeloid dendritic cells (mLPDCs) in the shift from a homeostatic to an inflammatory milieu. Utilization of an organ culture model (LEL) made it possible to collect migratory lamina propria mDCs from an acute inflammatory environment. Gene expression analysis of LEL mDCs compared to peripheral blood DCs (PBDCs) revealed a variety of functions attributed to their environment and activation status. The LEL mDCs showed a gene expression profile which hinted at contribution to tissue remodeling and wound healing processes. Moreover, the majority of emigrated LEL mDCs could be attributed to the cDC2 fraction of DCs which exhibit mostly anti-inflammatory functionalities. Upregulation of the IL-12 family member mRNAs encoding for the protein subunits IL-23p19 and EBI3 was striking, hinting at the formation of the newly discovered heterodimeric cytokine IL-39. Both subunit proteins could be detected in LEL mDCs but not in PBDCs. Experiments using recombinant proteins confirmed IL-39 heterodimer formation in vitro as well as in cell culture experiments. However, technical difficulties prevented confirmation of heterodimer presence in primary human lamina propria mDCs. Scientific publications and initial experiments might hint at a possible contribution to wound healing processes related to IL-39 or its subunits.

A follow up experiment explored the gene expression profiles of mLPDCs from enzymatically digested IBD patients biopsies under inflammatory and non-inflammatory conditions as well as in healthy individuals. The extracted cells displayed a mixture of cDC1 and cDC2 cells with conserved functional properties across all samples including MHCII dependent antigen presentation and T cell regulatory processes amongst others. The gene expression analysis uncovered new aspects of mLPDCs including involvement in epithelial cell proliferation, humoral immunity and neuronal system development and signaling. Epithelial cell proliferation might contribute to wound healing properties of mLPDCs. Furthermore, the data hints at a mutual influence between mLPDCs and neuronal cells. Another striking observation was the detection of immunoglobulin related mRNAs hinting at yet unexplored functional properties of mLPDCs involving the expression of antibodies. Moreover, differential gene expression in mLPDCs varied for different IBD patient groups compared to healthy individuals.

Zusammenfassung

Die Prävalenz chronisch entzündlicher Darmerkrankungen (CED) steigt stetig in industrialisierten Ländern. Ursachen der CEDs sind dabei vielfältig und ein genaueres Verständnis dieser kann dazu genutzt werden, neue Therapien zu entwickeln. Die Regulation von pro- und anti-inflammatorischen Reaktionen im Darm ist wichtig um ein homöostatisches Gleichgewicht aufrecht zu erhalten. Dendritische Zellen sind dafür bekannt hauptsächlich an der Aufrechterhaltung der Homöostase beteiligt zu sein indem sie Antigene ihrer Umgebung prozessieren und dazu eine passende adaptive Immunantwort einleiten. Ziel dieser Studie war es funktionelle Eigenschaften gewebeständiger myeloider dendritischen Zellen unter akuten inflammatorischen Bedingungen zu untersuchen. Durch die Anwendung eines Organkulturmodells (LEL) war es möglich, migratorische mDCs aus einer akut inflammatorischen Umgebung zu isolieren und analysieren. Der Vergleich der Genexpressionsdaten von LEL mDCs mit aus Blut extrahierten DCs (PBDCs) offenbarte neue Funktionen der gewebeständigen Zellen, welche auf ihre Umgebung oder den Aktivierungszustand zurückzuführen sind. So zeigten die LEL mDCs Funktionen zum Gewebeumbau oder einer möglichen Beteiligung an Wundheilungsprozessen anhand des genetischen Profils. Die emigrierten LEL mDCs konnten hauptsächlich dem cDC2 Phänotyp zugewiesen werden, welcher in der Regel anti-inflammatorische Prozesse fördert. Besondere Aufmerksamkeit gebührte der Expression der Interleukin 12 Familie mRNAs für die Proteinuntereinheiten EBI3 und IL-23p19, was auf eine mögliche Expression des erst kürzlich beschriebenen Interleukin 39 hindeutete. Beide Proteinuntereinheiten konnten in LEL mDCs nachgewiesen werden, aber nicht in PBDCs. Die Heterodimerisierung beider Untereinheiten konnte in Experimenten mit rekombinanten Proteinen gezeigt werden, sowohl außerhalb von Zellen als auch in überexprimierenden Zellkulturen. Aufgrund technischer Unzulänglichkeiten konnten diese Beobachtungen nicht für Zellen aus Patientenmaterial gezeigt werden. Bisherige Veröffentlichungen zu IL-39, als auch experimentelle Hinweise, deuten auf eine mögliche Beteiligung dieses Proteins an Wundheilungsprozessen hin.

In einem Folgeexperiment wurden Lamina propria mDCs aus enzymatisch verdautem Biopsiegewebe von CED Patienten mit und ohne Entzündung als auch gesunden Probanden untersucht. Extrahierte mDCs beinhalteten sowohl cDC1 als auch cDC2 Zellen und wiesen unter anderem eine Beteiligung bei MHCII assozierter Antigenpräsentation als auch der Regulation von T Zellen auf. Die Genexpressionanalysen deckten drei größere Bereiche auf an denen mLPDCs beteiligt sind: Epithelzellproliferation, humorale Immunität, und Entwicklung und Signaltransduktion von und mit neuronalen Zellen. Die Epithelzellproliferation deutet auf eine Beteiligung an Wundheilungsprozessen hin. Die Daten lieferten außerdem Hinweise auf eine gegenseitige Regulation neuronaler Zellen mit mLPDCs im Darmgewebe. Des Weiteren zeigten mLPDCs von CED Patienten eine stark differentielle Expression von Immunglobulin assoziierten Genen, welche auf eine

Beteiligung an humoralen Mechanismen hindeuten. Zudem wurden deutliche Unterschiede in der Expression statistisch signifikant differentiell regulierter Gene bei verschiedenen Gruppen von CED Patienten im Vergleich zu gesunden Individuen beobachtet.

1.0 Introduction

1.1 Mucosal surfaces in the human body

A large portion of scientific discoveries in the immunological field throughout the past decades were made examining the adaptive immune system in secondary lymphoid organs (lymph nodes and spleen), because these are the main effector sites when antigen is introduced via the skin or injected into the blood stream. The ease of use with these infection routes made it very popular to examine the adaptive immune system in response to antigen injections or skin applications in the beginnings of immunological science. But far more common routes of antigen entry into the human body are via the mucosal surfaces. Mucosal surfaces are the inner parts of the body which have direct contact to many different kinds of antigens introduced from the commensal microflora or from external sources, mainly via food intake, but also through e.g. breathing (dust, pollen) or intercourse. Therefore the mucosal surfaces are the main entry points for invading pathogens or innocuous antigens into the human body. The three main mucosal surfaces are the (1) respiratory tract with the sinuses (paranasal), trachea and lungs, (2) urogenital tract which comprises the bladder, urethra, uterus and vagina and (3) the gastrointestinal tract spanning the oral cavity, esophagus, stomach, gall bladder, billiary tract and the intestine (Fig.I1) (Duan and Mukherjee 2016). The main causes of death from transmissible diseases are linked to respiratory tract infections and diarrheal disorders, which emphasizes on the importance of understanding immunity at mucosal surfaces (Lozano et al. 2012).

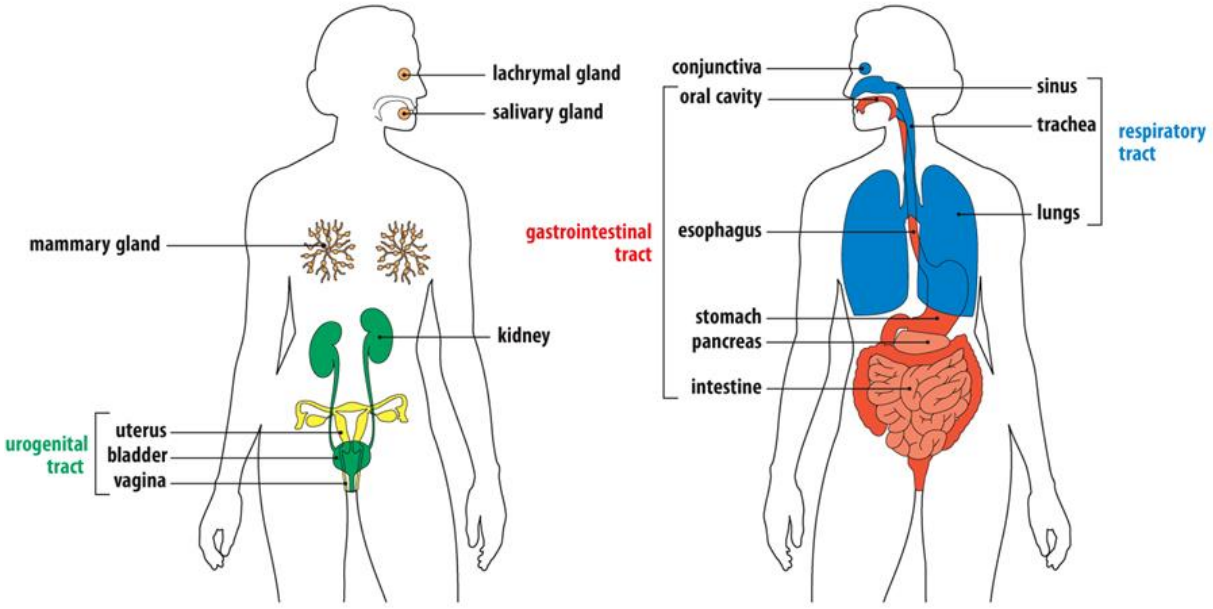

Fig.I1: The mucosal surfaces in the human body.

source: (Duan and Mukherjee 2016)

1.2 Anatomy of the intestinal tract

The intestine is by far the largest compartment of the immune system, with the small intestine having a length of ~6-7m and the large intestine which has a length of ~1,5m (Hounnou et al. 2002). The small intestine is located caudal of the stomach and is divided into 3 parts namely the duodenum, jejunum and ileum, followed by the large intestine which can be subdivided into the caecum with the appendix, colon (ascending/transverse/descending/sigmoid) and rectum (Fig. I2). Each of those parts has a unique morphology and fulfills different tasks like e.g. absorption of nutrients in the small intestine and reabsorption of water in the large intestine.

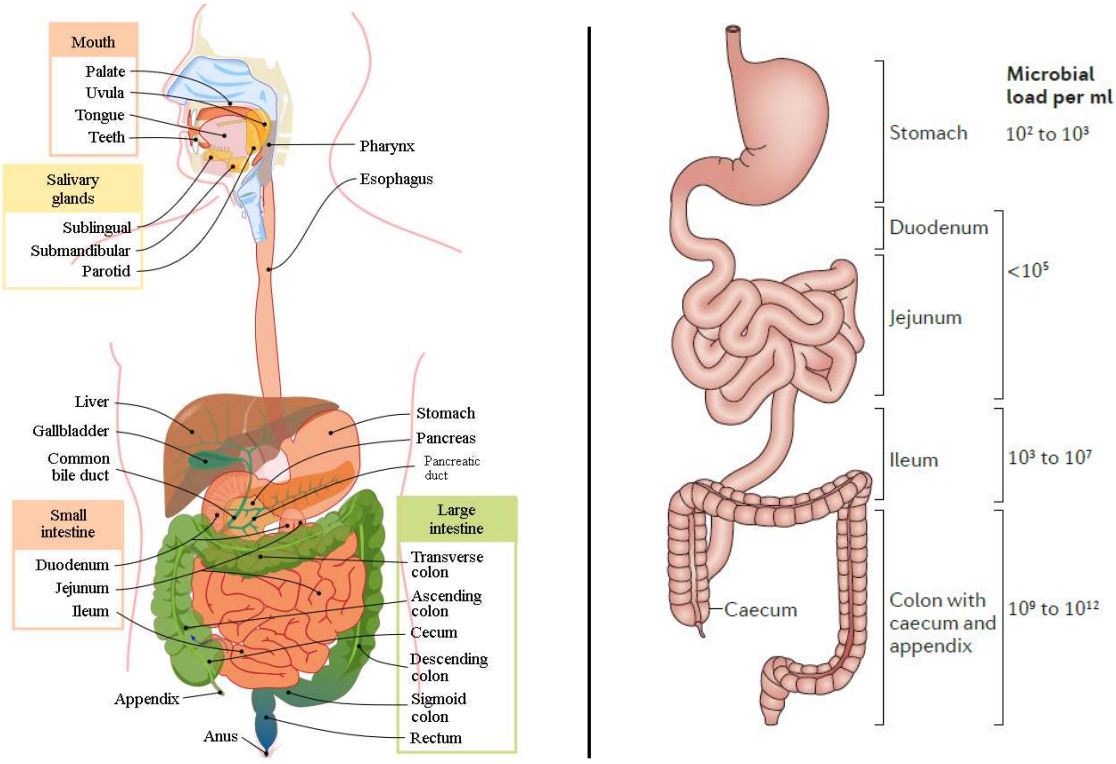

Fig.I2: Arrangement of the gastro intestinal system in human beings (left) and the amount of microbial load throughout the intestinal system (right).

sources: [http://www.turkupetcentre.net/petanalysis/pic/digestive_system.svg] and (Mowat and Agace 2014)

The surface area of the intestine is highly increased due to the formation of villi, which are protrusions of small intestinal tissue into the lumen, accompanied by microvilli structures of epithelial cell membranes, resulting in a surface area of approximately 32m² (Helander and Fändriks 2014). This huge amount of surface is aiding the efficiency of nutritional absorption but leaves also a large area for possible unwanted microbial or viral invasions and therefore needs to be protected by a substantial amount of immune cells.

The intestinal tissue is covered by a mucus layer which is filled with antibodies and antimicrobial peptides, traps luminal contents and is additionally shielding the tissue from invasion by microbial or other foreign antigens (Johansson and Hansson 2016). The small intestine has a single layer of mucus which is loose enough to allow food to get in contact with the tissue for digestive purposes. In the large intestine there is an additional tight layer of mucus right above the epithelial cells that does not allow penetration of microorganisms but only smaller molecules. Other than the villus structures, which are only present in the small intestine, the crypts of Lieberkühn can be found throughout the whole intestine (Fig.I3). At the base of those crypts reside multipotent stem cells which are producing seven different types of cells: enterocytes, goblet cells, enteroendocrine cells, paneth cells, microfold (M) cells, cup cells and tuft cells which have different functional properties like production of mucus, defensins or uptake of commensal and nutritional antigens or pathogens in a controlled way (Clevers 2013). Enterocytes, which are the most numerous cell type, are simple columnar epithelial cells that are covered with mucus (containing digestive enzymes) and absorb nutrients from the food. Additionally, they express pattern recognition receptors (PRRs) like Toll-like receptors (TLRs) to sense microbe-associated molecular patterns (MAMPs) and produce different cytokines, chemokines and other mediators to recruit innate immune cells like dendritic cells (DCs), macrophages or neutrophils depending on homeostatic or inflammatory conditions. They are generated by the multipotent stem cells in a continuous fashion, pushing older cells to the outside with a tremendous turnover rate of 4-5 days for every epithelial cell. Beneath the single layer of epithelial cells is the thin basal membrane which separates the lamina propria, a loosely packed connective tissue crowded with immune cells, from the epithelium. Underneath the lamina propria is a muscle layer called muscularis mucosae whose function is to keep the mucosa in a constant motion to expel mucus from the crypts. Additionally this movement increases the contact of enterocytes with the luminal content, contributing to the overall absorption efficiency. The epithelium, lamina propria and muscularis mucosae combined are termed mucosa (Fig.I3). These compartments harbour a variety of innate and adaptive immune cells and the majority of intestinal immunological processes are happening there.

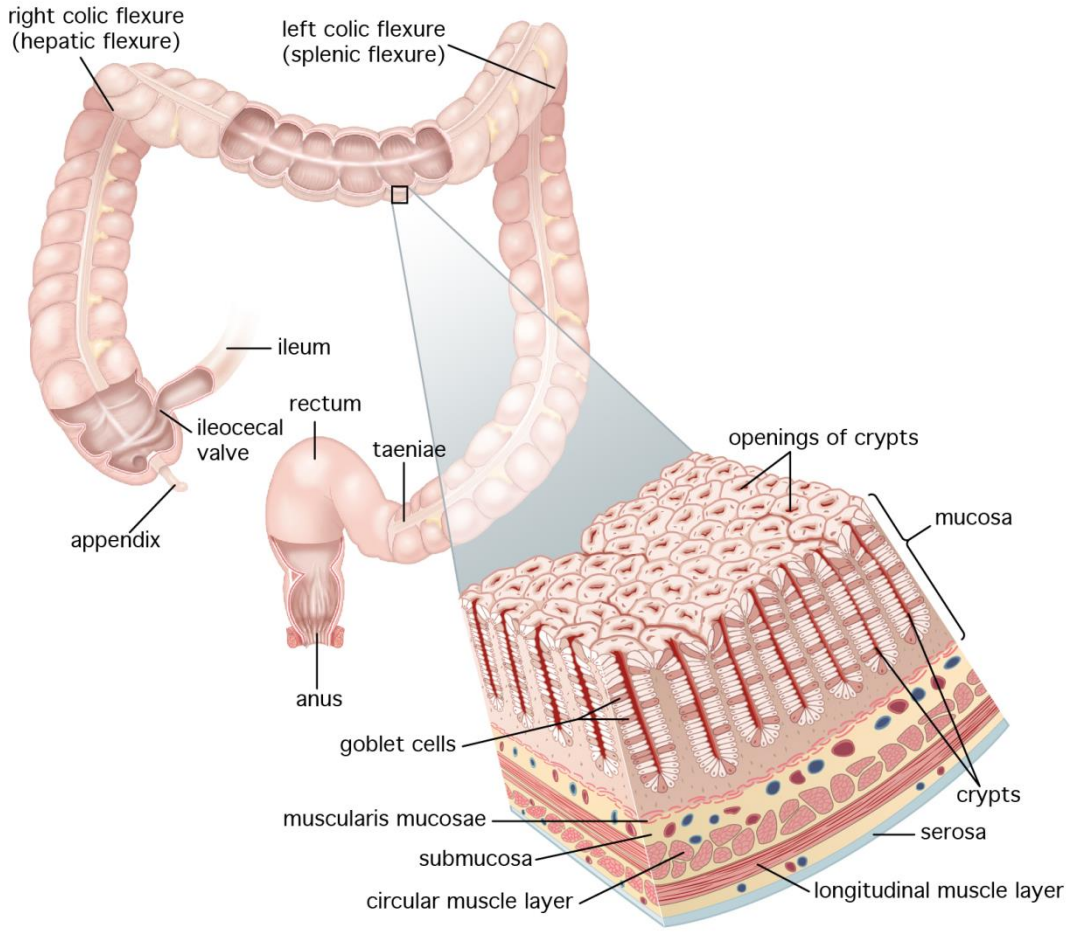

Fig.I3: Structure of the large intestine and mucosal layers.

source: https://cdn.britannica.com/19/74319-050-A0139604/intestine-rectum-Structures-human-crypts-mucosa-anus.jpg

1.3 The intestinal immune system

Nearly 75% of all lymphocytes in the human body are associated with the mucosal immune system. The entirety of immune cells from mucosal tissues is referred to as mucosa-associated lymphoid tissues (MALT). In regard to the gastro intestinal tract these cells are combined under the term: gut-associated lymphoid tissues (GALT) (Brandtzaeg et al. 2008). In the large intestine, lymphocytes are either scattered throughout the layer of epithelial cells (intraepithelial lymphocytes (IELs)) as well as the lamina propria or they inhabit organized lymphoid structures, the isolated lymphoid follicles (ILFs). Above organized lymphoid structures that are located in close contact to the epithelial layer, like ILFs, are specialized epithelial cells, the so called microfold (M) cells. M cells have no thick glycocalix, in contrast to the rest of the enterocytes, and serve as an entry point for antigens (Mabbott et al. 2013). Everything that enters via M cells comes directly in contact with immune cells

in the organized lymphoid structures underneath. Dendritic cells take up the antigen, process it and present it to B cells which, if being activated and differentiated into plasma cells, produce antigen specific IgA molecules after class switching. IgA is the predominant antibody at mucosal surfaces which helps to keep commensal microorganisms and possible invaders in check (Fagarasan et al. 2010). The DCs can also travel to the mesenteric lymph node, activating naïve T cells and B cells which recognize the presented antigen. These activated B and T cells are also imprinted by the DC, leading to an expression of specific markers on the B & T cells to favourably home back into the large intestine after extravasation into the bloodstream(Iwata et al. 2004; Mora and von Andrian 2008). Activated B and T cells become effector cells until they reach the intestine again, where they then inhabit the lamina propria or organized lymphoid structures.

Intraepithelial lymphocytes (IEL) are mainly comprised of antigen experienced TCRαβ^{+} CD8+ T cells (~80%), γδT cells (10%), CD4 T cells as well as some T cell receptor negative subsets (Olivares-Villagómez and Van Kaer 2018). In the intestinal epithelial cell layer there are approximately 10 IELs for every 100 enterocytes present. Most of these cells are part of the first line of defense, inhibiting intruders crossing the epithelial barrier. Additionally, the γδT cells are able to sense epithelial stress signals and promote cell healing and tissue repair (Dalton et al. 2006). Because of the plethora of effector cells being present in the intestinal tissues, healthy tissue shares characteristics with inflammatory responses due to the constant responses to innocuous antigens (Niess et al. 2008). Key components to achieve this type of homeostatic balance are regulatory T cells and anti-inflammatory cytokines like IL-10 (Maynard and Weaver 2009). Macrophages, which are patrolling the lamina propria, phagocytose invaders and release cytokines to favour T cell differentiation into the Treg phenotype under homeostatic conditions (Barnes and Powrie 2009). There is a strong bias towards tolerance in the intestine but there are always cells present which produce pro-inflammatory mediators like TNFα, IL-6 and IL-23; molecules which drive differentiation of T cells into the Th17 phenotype. In a healthy individual, effector Th17 T cells can be found in the colon and ileum probably due to the high bacterial load in these areas (Khader, Gaffen, and Kolls 2009). The Th17 cells produce IL-22, which in turn leads to a production of antimicrobial peptides by paneth cells, sitting at the base of the crypts. The constant reaction towards commensals leads also to presence of Th1 and Th2 cells. In case of an overwhelming intrusion into the subepithelial space, those pro-inflammatory reactions are boosted. In case of an initiating inflammation activated immune cells can act pro-inflammatory and also recruit other immune cells like neutrophils and eosinophils (Duan and Mukherjee 2016).

1.4 Intestinal immune homeostasis

The intestinal immune system does not only have to deal with harmless food antigens or possible harmful pathogens like bacteria and viruses but also with antigens from the commensal microflora. The commensal microflora varies in amount throughout the gut with 10^2 bacteria per ml in the small intestine and up to 10^{14} bacteria per ml in the colon with 1000 different species and a genome that is roughly 100 times larger than that of the inhabited body itself (Fig.I2) (Mowat and Agace 2014). The key to a healthy gut environment is to be in a homeostatic equilibrium were harmless antigens strengthen the intestinal barrier integrity and serious immune reactions against harmful invaders are only applied when really necessary. If this delicate balance is disturbed it can lead to serious inflammation or in the worst case to chronic diseases like inflammatory bowel diseases (IBD) and cancer.

The first line of defense is immune exclusion which describes the ability to prevent antigens from getting in contact with epithelial cells through a coating of secretory IgA (SIgA) (Corthësy 2009). Following production by intestinal plasma cells, SIgA is transcytosed from the lamina propria into the lumen via the polymeric immunoglobulin receptor (pIgR) through epithelial cells. If a virus or a bacterium has entered an epithelial cell it is even possible to expel it back into the lumen with the SIgA transport system (Johansen and Kaetzel 2011). The influx of antigens into the human body is as tightly regulated as possible. Usually there are four routes of controlled luminal antigen uptake into the body: first (1) via M cells residing on top of a lymphoid follicle (Peyer's Patches or ILFs) passing the antigen onto underlying antigen presenting cells (APCs), second (2) by being bound to IgG and transcytosed via the neonatal Fc receptor (FcRn), third (3) via apoptotic epithelial cells which contain the antigen and fourth (4) via lamina propria DCs which actively sample luminal antigens by extension of dendrites through the epithelial layer and subsequent transport into organized GALT structures for priming of adaptive immune cells. The priming results in the generation of gut-specific T effector cells as well as the maturation of B cells into plasmablasts which subsequently migrate to mucosal sites. There, plasmablasts develop into plasma cells producing large amounts of SIgA. Under homeostatic conditions epithelial and mesenchymal cells are producing molecules such as transforming growth factor β (TGF-β), IL-10, prostaglandin E_2 (PGE_2) or short form thymic stromal lymphopoietin (sf TSLP) in a constitutive fashion which leaves DCs in a quiescent state (Kurashima et al. 2017; Rimoldi et al. 2005). When DCs are now, after antigen uptake, traveling to the mesenteric lymph nodes (MLNs) they induce Treg cells which help to maintain the homeostatic balance via production of IL-10 and TGF-β at mucosal effector sites. When pathogenic bacteria (or commensal bacteria following injury of the mucus/epithelial barrier) pass the epithelium in an uncontrolled manner and get in direct contact with the DCs, than the latter acquire an active state, characterized

by the upregulation of pro-inflammatory cytokines and many co-stimulatory molecules on their surface, which enables them to induce Th1 and Th17 cells shifting into a pro-inflammatory adaptive immune response (Stagg 2018).

DCs are the most important orchestrators in gut homeostasis as they are responsible for the interpretation of incoming threats and innocuous antigens, mounting the right response at the right time and activating adaptive immune responses if necessary.

1.5 Inflammatory bowel diseases

Inflammatory bowel disease (IBDs) is the hypernym for a group of inflammatory conditions which affect the gastrointestinal tract. The most prominent ones are ulcerative colitis (UC), which affects mainly the colon and the rectum, and Crohn's disease (CD) which can affect every part from mouth to anus. (Bernstein et al. 2016). Besides the chronic relapsing inflamed regions at gastrointestinal sites these diseases share some symptoms like e.g. diarrhea, abdominal pain, rectal bleeding, muscle spasms & cramps (G.-F. Wang et al. 2012). Some patients also suffer from additional diseases, so called extraintestinal manifestations (EIMs) which, depending on the disease, are directly or indirectly linked to the underlying IBD. Associated EIMs, amongst others, are Type 1 arthritis and erythema nodosum, which are directly linked to IBD and are ameliorated as soon as IBD treatment is started; ankylosing spondylitis and uveitis which are independent of the IBD activity status; pyoderma gangrenosum (Plumptre, Knabel, and Tomecki 2018) and primary sclerosing cholangitis (Ricciuto, Kamath, and Griffiths 2018) which may or may not be linked to IBD but most likely are considered as an EIM (Vavricka et al. 2014).

The occurrence of IBD was only sporadical in ancient times and is growing from year to year in industrialized nations (Kirsner 1988). As of today IBD is not curable yet but although the mortality rate is relatively low, the quality of life from patients is severely affected (Kaplan 2015).

The global IBD burden in 2017 was an estimated of 5 million people. In Germany for instance one per 300 persons is suffering from Crohn's disease (Ng et al. 2017). In Europe, Norway has the highest prevalence of ulcerative colitis with one patient per 200 inhabitants (Ng et al. 2017). Having a closer look at the aetiology of IBD it seems like the disease is driven by the environment that surrounds us (Hou, El-Serag, and Thirumurthi 2009). One clue is that people who are living in an urban area are more likely to develop IBD compared to people from rural parts or people who were born and raised in a rural area and moved into an urban area at a later point in their life (Benchimol et al. 2017).

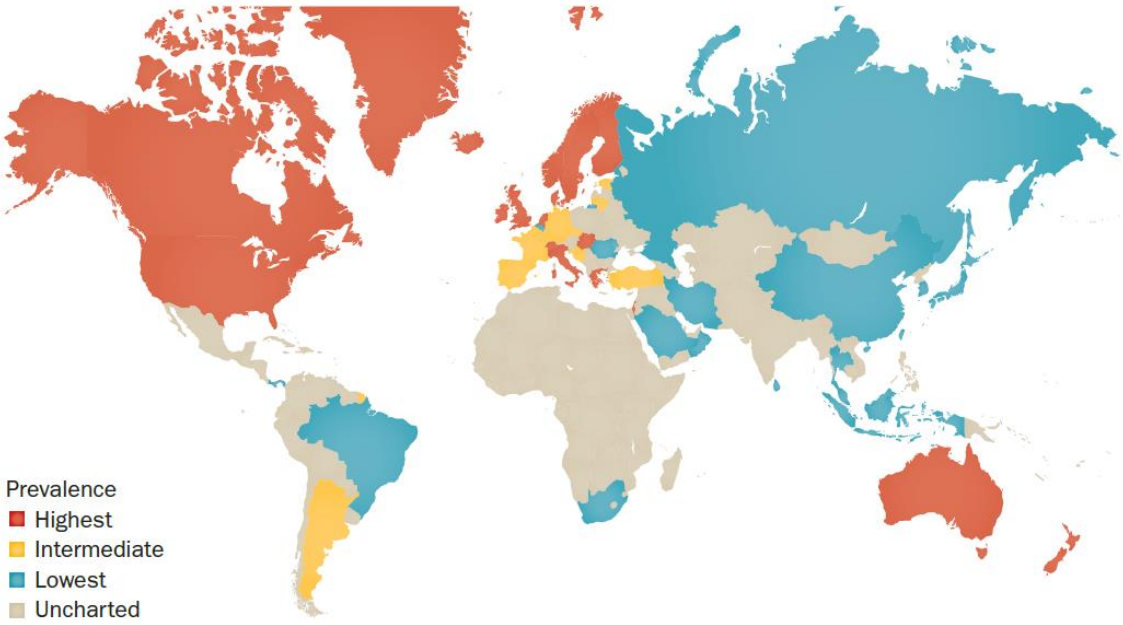

Fig.I4: Colour coded world map showing the prevalence of IBD cases (2015).

source: (Kaplan 2015)

IBDs are multifactorial diseases which means that there is not only one single cause but a combination of circumstances which leads to the manifestation of the disease. Additionally the elicitors vary between individuals and are not always the same. Given the complexity of this topic, it will not be discussed in minute detail in this short overview.

What is to be believed as the main driver of IBDs is a disturbed reaction of the immune system towards the intestinal (commensal) microbiota, leading to dysbiosis (a change in the microbial ecology in the intestine) and, in the end, inflammation. (Loh and Blaut 2012). The intestinal microbiota is therefore important in the maintenance of a healthy state but - if this can not be kept up - also the driver of the disease (Kåhrström, Pariente, and Weiss 2016; Lynch and Pedersen 2016). The composition of the microbiota is one key aspect of IBD and equally influenced by host and environmental factors. The biodiversity of the commensal microbiota in IBD is drastically reduced, between 30%-50%, compared to non-affected individuals. The ratio of the bacterial phyla of Firmicutes to Bacteroidetes can be used as an indicator for biodiversity and to identify IBD dysbiotic conditions (a lower ratio is associated with IBD) (Kabeerdoss et al. 2015). One aspect of a possible susceptibility towards IBD is that a good third of the microbial taxa residing in the gut are heritable (Turpin et al. 2016). Further events in early childhood which shape the composition of the intestinal microbiota are e.g. breastfeeding, which lowers the risk of IBD development (Klement et al. 2004),

and the use of antibiotics within the first year of life which leads to an increase in cases compared to controls (Shaw, Blanchard, and Bernstein 2010). But besides the fact that those factors can be the first turning point towards a dysbiotic microbiota, the intestinal microflora is malleable at every point in life. A more frequent use of antibiotics increases the risk of IBD by a factor of 1.5 in adults (Shaw, Blanchard, and Bernstein 2010) and worsens the clinical condition in people already suffering from Crohn's disease (Gevers et al. 2014). Another important determinant of microbial composition is diet. In a murine model, the impact of alterations in diet and genetic mutations were examined with regard to modulation of the composition of the commensal microflora: dietary changes explained 57% of the total variation in gut microbiota whereas genetics could only be made responsible for 12% (Zhang et al. 2010). And it was also shown in humans that changes in the dietary composition, for example switching from a carnivorous diet to a more plant-based diet, lead to rapid changes regarding the gut microbiome (David et al. 2014). Diversity is key to a healthy intestinal environment because every niche that is not occupied by a commensal microorganism gives room for colonization with pathogens or pathobionts (Gevers et al. 2014). The individual microflora compositions are one hint as to why the risk of heritability in IBD is relatively low, as people might have a similar genetic predisposition but the differences in their microflora can lower or heighten the risk of an IBD onset (Khor, Gardet, and Xavier 2011). However, the genome of one person is responsible for the organic structural framework with all its traits and how the immune system is behaving in this environment. Approximately 12% of all IBD cases are attributable to heritability, with ulcerative colitis being less likely inherited to the offspring compared to Crohn's disease (Moller et al. 2015; Jostins et al. 2012). In genome-wide association studies (GWAS) over 230 single-nucleotide polymorphisms (SNPs) have been identified to be associated with IBD (de Lange et al. 2017; J. Z. Liu et al. 2015). Having a SNP means that a single nucleotide in the DNA sequence of a gene is altered and therefore able to affect the protein sequence if the gene is expressed. The complex nature of IBD can not be explained solely by the genetic profile yet but scientists try constantly to find new approaches for a deeper understanding of the disease like e.g. the participation of rare copy number variations (CNV) of genes (Frenkel et al. 2019). CNVs are either insertions or deletions of DNA Sequences in the genome, resulting in duplication or deletion of genes leading to a predisposition towards certain diseases (Shaikh 2017).

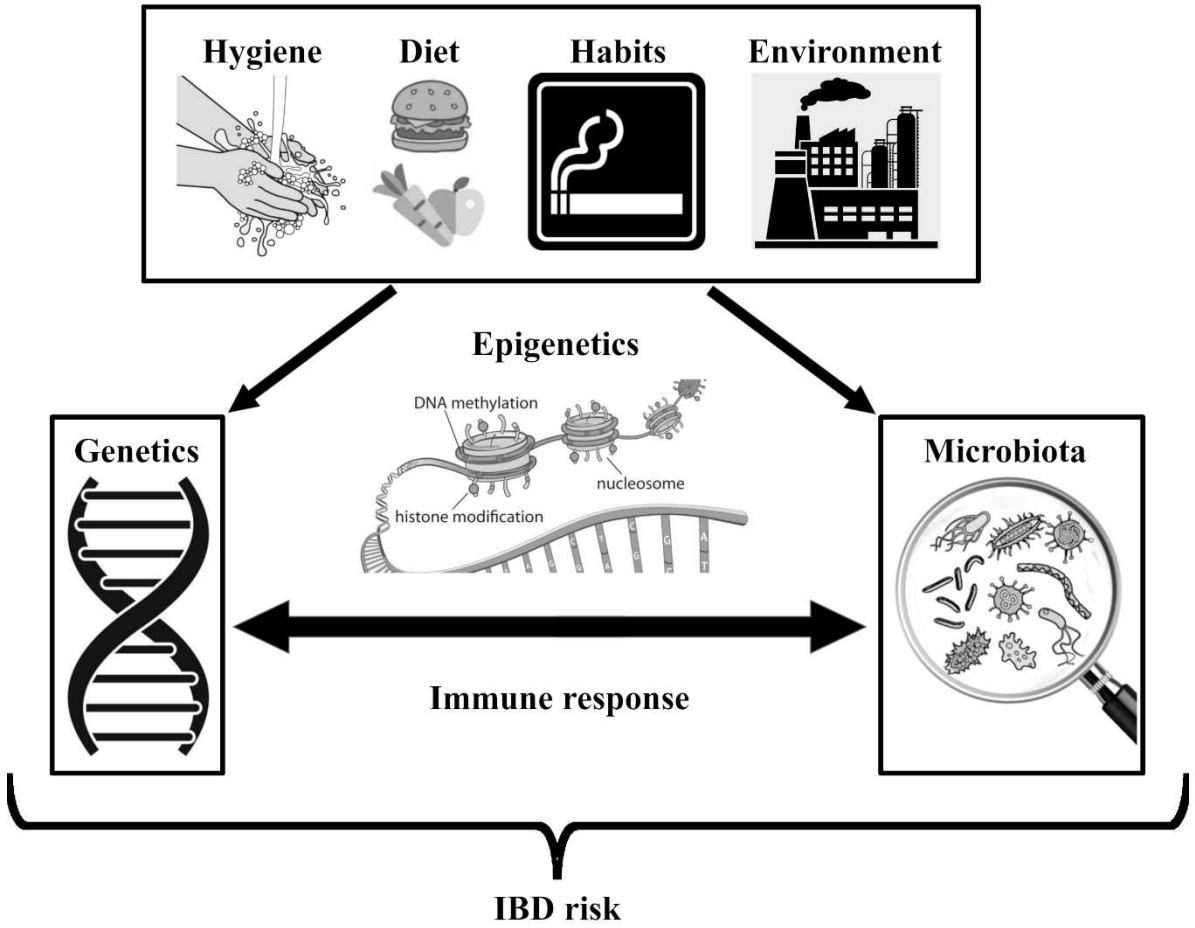

Fig.I5: Schematic of factors influencing the risk of IBD emergence.

For every discovered SNP, odds ratios can be calculated as a measure of how the risk of disease is increased in an individual carrying a certain type of SNP (J. Z. Liu et al. 2015). The two strongest genetic risk loci identified so far are *NOD2* with an odds ratio of 3.1 in Crohn's disase, and *IL23R* with an odds ratio of 2.0 in IBD (Jostins et al. 2012). The *NOD2* gene encodes a cytosolic pattern recognition receptor which is responsible for the recognition of muramyl dipeptide, a building block of the bacterial cell wall. This gene is expressed in intestinal epithelial cells and lamina propria leukocytes (most strongly in macrophages and monocytes) (Gutierrez et al. 2002; Zanello et al. 2013, 2). *IL23R* on the other hand encodes for one subunit of the IL-23 receptor which binds to the cytokine IL-23 and mediates activation of T-cells, NK cells and macrophages/myeloid cells. Genetic variants of IL-23 receptor differ in their phosphorylation activity of the downstream molecules signal-transducing activator of transcription 3 (STAT3) and STAT4 in response to IL-23 mediated IL-23 receptor signaling. Variants with higher STAT3 and STAT4 phosphorylation activity raise the susceptibility to IBD (Sivanesan et al. 2016).

Besides IBD, *IL23R* is also associated with psoriasis, a chronic inflammatory disease of the skin which is mediated by an aberrant crosstalk between antigen presenting cells & immunocytes towards epidermal keratinocytes (Ayala-Fontánez, Soler, and McCormick 2016). Features from both, innate

and adaptive immunity have been linked to the inflammatory responses taking place in IBD patients. Given the important role of innate and adaptive immune responses in the pathogenesis of IBD, modulation of the controlled intervention of immune system actions represents the main approach of how IBDs are treated to date. There are drugs available like e.g. Adalimumab and Infliximab, which target and reduce available TNF-α (Hu et al. 2013). Furthermore, Ustekinumab blocks the action of IL-12/IL-23 by targeting the common p40 subunit of these cytokines (Deepak and Loftus 2016). And there is also the drug Vedolizumab, which blocks the interaction of α4β7 integrin to mucosal addressin cell adhesion molecule-1 (MAdCAM-1), inhibiting white blood cell traversal into the inflamed gut (Rosario et al. 2017). So far, drugs for IBD treatment interfere with cytokines, receptors, cell adhesion molecules and signaling pathways trying to ameliorate disease severity via a controlled intervention of immune system actions. The environment in the gut is changing and behaves differently under normal versus inflammatory conditions and the early and late stages of IBD. For example, a typical Th1 response can be mounted during an acute infection, however this ability is lost at later disease stages (Kugathasan et al. 2007). Therefore different therapeutic approaches might be helpful at different stages of disease progression.

1.6 Importance of DCs in IBD

Some key aspects of dendritic cell functions in the intestinal environment have been described in sections 1.3 and 1.4. The brief version is, in regard to innate immune mechanisms, DCs are mononuclear phagocytes of the innate immune system which have a variety of pattern recognition receptors (PRRs) like Toll-like receptors (TLRs) or NOD-like receptors (NLRs). With these receptors DCs can identify common structures from microorganisms and phagocytose target cells or viruses for subsequent antigen presentation to cells from the adaptive immune system. Depending on several factors, the DC decides whether to induce an immunogenic or tolerogenic adaptive immune response. The DC itself releases cytokines and chemokines to modulate other cells, like T cells, neutrophils or epithelial cells, and amplify the desired outcome (tolerogenic or immunogenic).

In regard to the adaptive immune system, DCs prime antigen specific T and B cells in secondary lymphoid organs and imprint them simultaneously, giving those lymphocytes the ability to home back into the intestinal tissue after maturation. Plasma cells home into lymphoid follicles where they produce sIgA and, under homeostatic conditions, T cells are favourably differentiated into Treg cells, regulating the activity of effector cells. In case of a pathogenic invasion, DCs drive differentiation of T cells into the Th1 or Th17 phenotype (depending on the intruder), to achieve an immunogenic response.

Dendritic cells are the main orchestrators of immune homeostasis in the intestine and there is some evidence that DCs may play a key role when it comes to IBD.

In a study done in a murine model by Yamazaki et al., bone marrow derived DCs were generated, lacking the expression of CD40, CD80 and CD86 molecules using DNA antisense technology. Without these surface molecules the dendritic cells resemble immature tolerogenic DCs, leading to the differentiation of naïve CD4+ T cells into the CD25+, FoxP3+, regulatory T cell phenotype (Yamazaki and Steinman 2009). Transfer of these co-stimulation impaired DCs into dextran sodium sulfate (DSS) treated mice resulted in a protection from experimental colitis symptoms. Control mice who had not received additional DCs developed disease symptoms. Besides an increase in the frequency of CD4+ Treg cells they also found a higher number of IL-10 expressing regulatory B-cells in mice which received the altered DCs (Engman et al. 2018).

In another study, it was shown that IL-10 signaling decreased IL-1β release from human monocyte-derived DCs, which itself influences the IFN-γ release from CD4+ T cells in a direct manner. This means that when there is no IL-10 present, the DC releases more IL-1β which leads to a higher release of IFN-γ by CD4+ T cells. IFN-γ, which is also released in response to constituents of intestinal microbiota by CD4+ T cells, induces IL-12 release from DCs, which itself increases the IFN-γ release of CD4+ T cells, resulting in an unfavorable feedback loop (Veenbergen et al. 2019). IL-12 is a driver of IBD by participation in the disruption of epithelial barrier integrity (Eftychi et al. 2019). IFN-γ has an influence on vascular barrier integrity by disruption of the adherens protein VE-cadherin (vascular endothelial cadherin) (Langer et al. 2019). A disturbed IL-10 presence or responsiveness can therefore result in an inflammatory response accompanied by an increased danger of bacterial invasion. In this specific study it could be shown that a subset of pediatric IBD patients had an increase in IL-1β in inflamed tissue as well as an overall less pronounced responsiveness to IL-10 in PBMCs (Veenbergen et al. 2019).

Another study, comprised of 37 pediatric IBD cases versus 14 healthy controls, found differences in the expression of the inhibitory receptor CD200R1 on DCs between those two groups. The amount of CD200R1 and CD200 on peripheral blood DCs was assessed as well as the amount of circulating Treg and IL-17 producing CD4+ Th17 cells. In a murine model DCs have shown to express indoleamine 2,3-dioxygenase (IDO) after CD200R1 binding via CD200, which favours differentiation of naïve CD4+ T cells into the Treg phenotype and suppresses effector T cells (Fallarino et al. 2004; Mellor, Lemos, and Huang 2017). The results showed that the amount of CD200R1 on DCs was significantly decreased in IBD patients. The amount of Th17 cells was significantly increased, concurrently the amount of regulatory T cells was significantly decreased in patients with IBD (Elshal et al. 2015). This data again suggests a direct correlation of DC contribution to the IBD severity status.

These were just three short examples of how DCs can potentially influence IBD disease progression. Dendritic cells might also have some abilities to directly influence their environment apart from orchestrating the adaptive immune system.

1.7 Outlook

With all those facts in mind we chose dendritic cells as targets for our investigation of IBD inflammatory process regulation. These cells are the bridge between the innate and the adaptive immune system and influence both groups on multiple levels. Besides that, there are several subsets of DCs inhabiting different regions of the intestine and there is not much information about possible functions of DCs in the lamina propria, other than activating innate and inducing adaptive immune cells. Being closely related to macrophages on many levels suggests that DCs could have several abilities to influence cells like e.g. mesenchymal cells in the intestinal environment. Having a closer look at functional properties on a genetic level during different disease progression states might give a hint at how the environment and adaptive immunity is shaped by those cells. Additionally, we might uncover new mechanistic targets which widen our understanding of the diseases and lead to new starting points for possible future treatments of inflammatory disorders.

2.0 Material and Methods

2.1 Chemicals, solutions & kits

Name	Product Number	Company/ Retailer	Stock concentration	Abbreviation/ synonymous
[Leu^{15}]-Gastrin I human	G9145	Sigma-Aldrich	-	Gastrin
2-Mercaptoethanol	M6250	Sigma-Aldrich	78,13g/mol	2-ME
A 83-01	2939	Tocris	421,52g/mol	-
Acrylamid/Bis-Solution, 37.5:1	1068801	SERVA	30% w/v	Acrylamid
Advanced DMEM/F12	12634028	Gibco	-	-
Albumin Fraction V	8076.2	Roth	66.000 g/mol	Albumin
Amersham ECL Prime Western Blotting Detection Reagent	RPN2232	GE Healthcare	-	ECL
Ammonium Persulfate 10% in ddH2O	1610700	Bio-Rad	10%	APS
Amphotericin B	15290018	Gibco	250µg/ml	-
Anti-rabbit IgG, HRP-linked Antibody	7074	Cell Signaling	-	HRP anti rabbit
B27 Supplement	17504044	Gibco	50x	-
BD Matrigel Basement Membrane Matrix	356234	BD Biosciences	-	Matrigel
Bovine Serum Albumin	A4919	Sigma-Aldrich	66.000 g/mol	BSA
Bromphenolblau Natriumsalz wasserlöslich Indikator ACS	1117460005	Merck	-	-
Calyculin A, protein phosphatase inhibitor	9902S	Cell Signaling	-	-
Ciprofloxacin Kabi	PZN: 3277618	Fresenius Kabi	2mg/ml	Ciprofloxacin
Cotrim-ratiopharm	PZN: 3928197	480mg/5ml	Ratiopharm	Cotrim
DCS Antikörperverdünnungspuffer	AL120R100	DCS	-	DCS antibody diluent
Direct-zol RNA Microprep	R2061	Zymo research	-	-
DL-Dithiothreitol	D5545	Sigma-Aldrich	154,25 g/mol	DTT
dNTP-Mix, 10mM each	R0191	Thermo Fisher	-	-
d-Sorbitol	S3889	Sigma-Aldrich	182,17g/mol	-
Dulbecco's Phosphate Buffered Saline	D8537	Sigma-Aldrich	-	PBS
Duolink In Situ Mounting Medium with DAPI	DUO82040	Sigma-Aldrich	-	-
Duolink In Situ Orange Starter Kit Mouse/Rabbit	DUO92102-1KT	Sigma-Aldrich	-	-
Dynabeads Co-Immunoprecipitation Kit	14321D	Thermo Scientific	-	-
Ethanol	32205	Sigma-Aldrich	46,07g/mol	-
Fetal Bovine Serum, Virus and mycoplasma tested	P30-3302	PAN Biotech	-	FBS
FicoLite-H	GTF1511	Linaris blue	-	-
FLAG Immunoprecipitation Kit	FLAGIPT1	Sigma-Aldrich	-	-

FreeStyle 293 Expression Medium	12338018	Gibco	-	-
FreeStyle 293-F-Zellen	R79007	Thermo Fisher	-	HEK293F
Gelatin from cold water fish skin	G7765	Sigma-Aldrich	40-50% in H2O	-
Gentamicin	15750037	Gibco	50mg/ml	-
GlutaMAX	35050038	Gibco	100x	-
Glycerol anhydrous p.A	A3552	AppliChem	92,10g/mol	-
Glycine p A	A1377	AppliChem	75,07g/mol	-
Hanks' Balanced Salt Solution	14170088	Gibco	-	HBSS
hEGF	E9644	Merck	-	-
Heparin Natrium Leo	PZN: 15261203	LEO Pharma GmbH	25.000 I.E./5ml	Heparin
HEPES	15630080	Gibco	1M	-
Hydrochloric acid	H1758	Sigma-Aldrich	36.5-38.0%	HCl
Invitrogen UltraPure 0.5M EDTA, pH 8.0	11568896	Thermo Scientific	0,5M	EDTA pH8
Potassium Chloride	104936	Merck	74,55g/mol	KCl
Monopotassium phosphate	3246-01	J.T. Baker	136,09g/mol	KH_2PO_4
L-Glutamine	25030024	Gibco	200mM	-
Methanol	32213	Sigma-Aldrich	32,04g/mol	-
Milchpulver, Blotting-Grade	T145.3	Roth	-	Milk powder
Myeloid Dendritic Cell Isolation Kit, human	130-094-487	Miltenyi Biotec	-	-
N2 Supplement	17502048	Gibco	100x	-
Disodium phosphate	S374	Fisher Scientific	141,957g/mol	Na_2HPO_4
N-acetylcystein	A9165	Sigma-Aldrich	163,19g/mol	-
Sodium bicarbonate	3510-05	J.T. Baker	84,01g/mol	$NaHCO_3$
Sodium chloride	9265	Roth	58,44g/mol	NaCl
nCounter Human Immunology V2	-	Nanostring	-	-
Nicotinamid	N0636	Sigma-Aldrich	122,12g/mol	-
Noggin	120-10C	Peprotech	-	-
Oligo dT	-	biomers	5'-AAGCAGTGGTATCAACGCAGAGTACT30VN-3'	-
Opal Kit	NEL811001KT	Akoya Biosciences	-	-
Panel Plus	-	IDTDNA	-	-
Paraformaldehyde Solution 4%, methanol free		A. Brenzinger	4%	PFA solution
Penicillin-Streptomycin	15140122	Gibco	10.000 U/ml Penicillin 10.000 µg/ml Streptomycin	PenStrep
Peroxidase AffiniPure Goat Anti-Mouse IgG (H+L)	115-035-146	Jackson Immuno Research	-	HRP anti mouse
pH-Pufferlösungen CaliMat Set pH 4,00 / 7,00 / 9,00 (20°C)	CSPSET479	Knick	-	-
hEBI3 pEF6-Flag	72491	addgene	-	Plasmid EBI3-FLAG
hIL23p19 pEF6-V5	72492	addgene	-	Plasmid IL23p19-V5

Polyethylenimine, branched	408727	Sigma-Aldrich	-	PEI
Precision Plus Protein Dual Color Standards	1610374	Bio-Rad	-	Protein standard
Prostaglandin E_2	P5640	Sigma-Aldrich	-	PGE2
Recombinant ribonuclease inhibitor	2313A	Takara	-	RNase inhibitor
RPMI 1640 Medium	21876034	Gibco	-	RPMI
R-Spondin	120-38	Peprotech	-	-
SB202190	S7067	Sigma-Aldrich	331,35g/mol	-
SDS Solution, 20 %	20767	SERVA	20%	SDS
SIGMAFAST OPD	P9187	Sigma-Aldrich	-	OPD
Sodium Hydroxide	S8045	Sigma Aldrich	-	NaOH
Sodium pyrophosphate tetrabasic decahydrate	S6422	Sigma-Aldrich	446,06g/mol	$Na_4P_2O_7 \cdot 10H_2O$
Sucrose	84097	Sigma-Aldrich	342,30g/mol	-
Sulfuric acid	30743	Sigma-Aldrich	98,08g/mol	H_2SO_4
TEMED	1610800	Bio-Rad	-	-
Titriplex III (EDTA·2Na·2H_2O)	108418	Merck	372,24 g/mol	EDTA
TRI Reagent	R2050-1-200	Zymo research	-	-
TRIS	4855.2	Roth	121,14g/mol	-
Triton X-100	T9284	Sigma-Aldrich	-	-
Trypan Blue solution	T8154	Sigma-Aldrich	0,40%	-
Tween 20	9127	Roth	-	-
UltraPure 0,5M EDTA, pH8	15575020	Invitrogen	0,5M	-
UltraPure DNase/RNase-freies destilliertes Wasser	10977035	Invitrogen	18,02g/mol	-
Western Lightning Plus-ECL	NEL103001EA	Perkin Elmer	-	ECL plus
Wnt3A Medium	Cell culture supernatant	-	-	-
Xylol	X/0250/15	Fisher Chemical	-	-
Y-27632 dihydrochloride	Y0503	Sigma-Aldrich	320,26g/mol	Rock inhibitor
Zombie NIR Fixable Viability Kit	423105	BioLegend	-	-

2.2 Labware

Name	Product number	Company/Retailer	Abbreviation/synonymous
50ml BD Plastipak Spritze	300866	BD	-
Amersham Hyperfilm ECL	28906836	GE Healthcare	ECL
Ampliseal Abdeckfolie	676040	Greiner bio-one	Ampliseal
C Tubes	130-096-334	Miltenyi Biotech	-
Corning 850cm² Polystyrene Roller Bottle with Easy Grip Vent Cap	431198	Corning	Roller bottle
Corning Costar Stripette serological pipettes	CLS4489	Sigma-Aldrich	5/10/25/50 ml pipette
Dual Gel Caster	SE245	Hoefer	Casting frame
Eppendorf Safe-Lock Tubes, 1,5 mL	30120086	Eppendorf	1,5ml safe-lock tube

Falcon 5 mL Round Bottom PP Test Tube	352053	Corning	5ml FACS tube
FluoroTrans W PVDF Transfer Membrane	BSP0161	Pall	PVDF membrane
GE Healthcare Whatman Grade 3MM Chr Cellulose Chromatography Paper: Sheets	3030-335	GE Healthcare	Whatman paper
Glasplatten, ausgeschnitten, 10 x 10,5 cm	SE262GN-5.01	Serva	Glass plates
Kamm, Standard, 10 Taschen, 1,5 mm dick	SE211A-10-1.5.01	Serva	Comb
LD Columns	130-042-901	Miltenyi Biotech	-
Lumi-Film Chemiluminescent detection film	11666916001	Roche	-
MACS SmartStrainers	130-098-463	Miltenyi Biotech	100µm cell strainer
Microscope Slides 24x50mm	-	Knittel Gläser	Coverslip
Mikroröhre 1,5ml mit Verschluß	72692	Sarstedt	1,5ml tube
Mini PAP Pen	8877	Thermo Scientific	PAP pen
Minisart High Flow Spritzenvorsatzfilter	16532 – K	Sartorius	0,22µm filter
Nalgene Rapid-Flow Sterile Einweg-Filtrationsgeräte mit SFCA-Membran	155-0020	Thermo Scientific	0,2µm, 115ml filter unit
Nalgene Rapid-Flow Sterile Einweg-Filtrationsgeräte mit SFCA-Membran	156-4020	Thermo Scientific	0,2µm, 500ml filter unit
Nalgene Rapid-Flow Sterile Filtratflaschen	455-0250	Thermo Scientific	250ml plastic bottle
Nunc MaxiSorp flat-bottom	44-2404-21	Thermo Scientific	96-well ELISA plate
Röhrchen, 15ml, PP, 17/120mm	188271	Greiner bio-one	15ml tube
Röhrchen, 50ml, PP, 30/115mm	227261	Greiner bio-one	50ml tube
Röhrchenstreifen, 0.2 ml	AB0266	Thermo Fisher	Strip tube
SAPPHIRE MICROPLATTE, 96 WELL	652270	Greiner bio-one	Sorting plate
Shandon Cytoclip	59910052	Thermo Scientific	-
Shandon filter cards	5991022	Thermo Scientific	Filter card
Shandon Single Cytofunnel	5991040	Thermo Scientific	cytofunnel
Spacer flach 10,6 cm x 1,5 mm	SHS10-150.01	Serva	spacer
Staining cuvettes by Hellendahl and Coplin	11-0021	Langenbrinck	Hellendahl cuvette
Superfrost Plus Adhesion Microscope Slides	10149870	Thermo Scientific	Superfrost slide
Vivaspin 20, 10.000 MWCO PES	VS2001	Sartorius	-
Zählkammer Neubauer	717805	Brand	Cell counting chamber
ZELLKULTUR SCHALE, PS, 145/20 MM	639160	Greiner bio-one	Petri dish

2.3 Devices

Name	Product number	Company/Retailer	Abbreviation/synonymous
2100 Bioanalyzer Instrument	-	Agilent	-
AGFA CP100 Entwicklungsmaschine	CP100	Agfa	Film processor
BD FACSAria III	-	BD Biosciences	Cell sorting machine
CFI Plan Apochromat Lambda 10X	-	Nikon	-
CFI Plan Apochromat Lambda 20X	-	Nikon	-
CFI Plan Apochromat Lambda 40X	-	Nikon	-
CFI SR HP Apochromat TIRF 100XC Oil	-	Nikon	-
Cytospin 4 Zytozentrifuge	A78300003	Thermo Scientific	Cytospin centrifuge
Eppendorf Mastercycler gradient	Z316083	Eppendorf	PCR cycler
Gefrierschrank GNP 3056 Premium NoFrost	4016803184423	Liebherr	-20°C
Heidolph Duomax 2030 Rocking Shaker	BL11380	Heidolph	Rocking platform
Heidolph REAX 2 mixer	541-21001-00	Heidolph	Rotator
Heracell 240i CO2 Incubators	51026556	Thermo Scientific	Incubator
Heraeus Fresco 21	75002425	Thermo Scientific	centrifuge
IKA VXR Vibrax	2819000	IKA	Orbital shaker
Integra acu	612-0926	Integra biosciences	pipetboy
Labor-pH-Meter 766	-	Knick	-
Midi MR 1 digital (Magnetrührer)	25002968	IKA	-
Model 680 Microplate Reader	-	Bio-Rad	Microplate reader
Multifuge 3 S-R	75004371	Thermo Scientific	centrifuge
nCounter SPRINT Profiler	-	Nanostring	-
New Brunswick Scientific U57085 Ultra Low Temp - 85° Freezer	U57085	Eppendorf	-80°C
Nikon Eclipse Ti Microscope	-	Nikon	-
polystar 401 M	-	Polystar	Welding unit
Power Pac 300	1645050	Bio-Rad	Power supply
Quadro MACS	-	Miltenyi Biotech	MACS magnet
Rotator, 5-50 UpM	2-1185	NeoLab	Rotator disc
Sartorius Feinwaage	BP211D	Sartorius	scale
Sartorius Waage	L2200P-D2	Sartorius	scale
Schüttelwasserbad GFL	1083	GFL	Shaking water bath
SE 260 miniVE Integrierte Vertikale Elektrophorese und Blotting Einheit	SE260-10A-.75	Hoefer	running chamber
Sicherheitswerkbank HERASAFE HS18	51011623	Heraeus	Biological safety cabinet
Thermomixer, Eppendorf Model 5436	-	Eppendorf	Heating shaker

Trans-Blot SD Semi-Dry Transfer Cell	1703940	Bio-Rad	-
Universal-Kühlgerät mit statischer Kühlung FKU 1803	9005382220757	Liebherr	4°C refrigerator
Vortex Schüttler VF2	-	IKA	vortexer

2.4 Buffers

Intestine wash buffer			
Ingredient	**Amount**	**Stock concentration**	**End concentration**
RPMI	500ml	100%	97,37%
PenStrep	5ml	10.000 U/ml Penicillin 10.000 µg/ml Streptomycin	97,4U/ml Penicillin 97,4µg/ml Streptomycin
Amphotericin B	5ml	250µg/ml	2,43µg/ml
Ciprofloxacin	2,5ml	2mg/ml	9,74µg/ml
Gentamicin	500µl	50mg/ml	48,69µg/ml
Cotrim	500µl	96mg/ml	93,48µg/ml
Total	513,5ml		

HBSS/PSACGB			
Ingredient	**Amount**	**Stock concentration**	**End concentration**
HBSS	500ml	100%	97,37%
PenStrep	5ml	10.000 U/ml Penicillin 10.000 µg/ml Streptomycin	97,4U/ml Penicillin 97,4µg/ml Streptomycin
Amphotericin B	5ml	250µg/ml	2,43µg/ml
Ciprofloxacin	2,5ml	2mg/ml	9,74µg/ml
Gentamicin	500µl	50mg/ml	48,69µg/ml
Cotrim	500µl	96mg/ml	93,48µg/ml
Total	513,5ml		

H/D			
Ingredient	**Amount**	**Stock concentration**	**End concentration**
HBSS/PSACGB	100ml	100%	100%
DTT	15,4mg	154,25 g/mol	0,1mM

-The solution was filtered through a 0,2µm, 115ml filter unit

H/E			
Ingredient	**Amount**	**Stock concentration**	**End concentration**
HBSS/PSACGB	360ml	100%	100%
Titriplex III	93,8mg	372,24 g/mol	0,252mM

-The pH was adjusted to pH:7,35 with $NaHCO_3$ and sterile filtered with a 0,2µm, 500ml filter unit.

Walk-Out medium			
Ingredient	**Amount**	**Stock concentration**	**End concentration**
RPMI	500ml	100%	87,95%
PenStrep	5ml	10.000 U/ml Penicillin 10.000 µg/ml Streptomycin	87,95U/ml Penicillin 87,95µg/ml Streptomycin
Amphotericin B	5ml	250µg/ml	2,2µg/ml
Ciprofloxacin	2,5ml	2mg/ml	8,795µg/ml
Gentamicin	500µl	50mg/ml	43,98µg/ml
Cotrim	500µl	96mg/ml	84,43µg/ml
FBS	50ml	100%	8,8%
L-Glutamine	5ml	200mM	1,76mM
Total	568,5ml		

Digestion buffer			
Ingredient	**Amount**	**Stock concentration**	**End concentration**
RPMI	500ml	100%	94,6%
PenStrep	5ml	10.000 U/ml Penicillin 10.000 µg/ml Streptomycin	94,6U/ml Penicillin 94,6µg/ml Streptomycin
Amphotericin B	5ml	250µg/ml	2,37µg/ml
Ciprofloxacin	2,5ml	2mg/ml	9,461µg/ml
Gentamicin	500µl	50mg/ml	47,3µg/ml
Cotrim	500µl	96mg/ml	90,82µg/ml
FBS	10ml	100%	1,89%
L-Glutamine	5ml	200mM	1,89mM
Total	528,5ml		

FACS staining buffer			
Ingredient	**Amount**	**Stock concentration**	**End concentration**
PBS	500ml	100%	95,7%
FBS	5ml	100%	0,95%
L-Glutamine	5ml	200mM	1,91mM
HEPES	12,5ml	1M	23,92mM
Total	522,5ml		

WC lysis buffer			
Ingredient	**Amount**	**Stock concentration**	**End concentration**
Tris pH8	120µl	1M	40mM
Na-pyrophosphate	1ml	180mM	60mM
EDTA pH8	60µl	0,5M	10mM
ddH2O	1,82	100%	60,67%
Total	3ml		

-WC lysis Buffer C = 500µl WC lysis buffer + 5µl Caliculin A (10µM in DMSO)

5X sample buffer			
Ingredient	**Amount**	**Stock concentration**	**End concentration**
TRIS pH6,8	1ml	1M	0,1M
Glycerol	5ml	92,10g/mol	68,4mmol
SDS	2,5ml	20%	5%
Bromphenolblau	0,25ml	10%	0,25%
ddH2O	1,25ml	100%	12,5%
Total	10ml		

-Before usage: mix 200µl 5X sample buffer with 50µl 2-ME

Protein standard buffer			
Ingredient	**Amount**	**Stock concentration**	**End concentration**
WC lysis buffer	400µl	100%	40%
10% SDS	400µl	10%	4%
5x sample buffer	160µl	100%	16%
2-ME	40µl	100%	4%
Total	1000µl		

Running buffer			
Ingredient	**Amount**	**Stock concentration**	**End concentration**
TRIS	30,26g	121,14g/mol	0,25M
Glycin	144g (231,84ml)	75,07g/mol	1,92M
SDS	50ml	20%	1%
ddH2O	Ad 1L		
Total	1L		

Western transfer buffer			
Ingredient	**Amount**	**Stock concentration**	**End concentration**
TRIS	5,81g	121,14g/mol	47,96mM
Glycin	2,93g	75,07g/mol	39,03mM
SDS	1,875ml	20%	0,0375%
Methanol	200ml	100%	20%
ddH2O	Ad 1L		
Total	1L		

10X TBS (Tris Buffered Saline)			
Ingredient	**Amount**	**Stock concentration**	**End concentration**
TRIS pH 7,5	100ml	1M	0,1M
NaCl	87,8g	58,44g/mol	1,502M
ddH2O	Ad 1L		
Total	1L		

-TBS-T= 500ml 1xTBS + 500µl Tween20

-Antibody buffer: 25ml TBS-T + 1,25g BSA V

-2nd stage Buffer Block: 40ml TBS + 2g Milchpulver

ELISA wash buffer			
Ingredient	**Amount**	**Stock concentration**	**End concentration**
PBS	500ml	100%	99,95%
Tween 20	250µl	100%	0,05%
Total	500,25ml		

-ELISA block buffer: ELISA wash buffer + 3% BSA

-ELISA Ab buffer: ELISA wash buffer + 0,1%BSA

Blood wash buffer			
Ingredient	**Amount**	**Stock concentration**	**End concentration**
RPMI	500ml	100%	96,15%
PenStrep	5ml	10.000 U/ml Penicillin 10.000 µg/ml Streptomycin	96,15U/ml Penicillin 96,15µg/ml Streptomycin
L-Glutamin	5ml	200mM	1,92mM
FBS	10ml	100%	1,92%
Total	520ml		

Transport buffer			
Ingredient	**Amount**	**Stock concentration**	**End concentration**
PBS	95,9ml	100%	95,9%
PenStrep	1ml	10.000 U/ml Penicillin 10.000 µg/ml Streptomycin	100U/ml Penicillin 100µg/ml Streptomycin
Amphotericin B	1ml	250µg/ml	2,5µg/ml
Ciprofloxacin	1ml	2mg/ml	20µg/ml
Gentamicin	100µl	50mg/ml	50µg/ml
FBS	1ml	100%	1%
Total	100ml		

Chelation Buffer			
Ingredient	**Amount**	**Stock concentration**	**End concentration**
Na_2HPO_4	0,8 g	141,96g/mol	5,6 mM
KH_2PO_4	1,1 g	136,09g/mol	8,0 mM
NaCl	5,6 g	58,44g/mol	95,8 mM
KCl	0,12 g	74,55g/mol	1,6 mM
Sucrose	14,9 g	342,30g/mol	43,5 mM
d-Sorbitol	10 g	182,17g/mol	54,9 mM
DTT	0,077 g	154,25g/mol	0,5 mM
ddH_2O	Ad 1l		
Total	1l		

-Adjust to pH 7,4 before filling up to 1l

-Before usage take out 30ml of chelation buffer and add 120µl of 0,5M EDTA solution (2mM EDTA end concentration)

Crypt wash buffer			
Ingredient	**Amount**	**Stock concentration**	**End concentration**
Advanced DMEM/F12	93ml	100%	93%
GlutaMAX	1ml	200mM	2mM
HEPES	1ml	1M	10mM
FBS	5ml	100%	5%
Total	100ml		

RNAseq lysis buffer			
Ingredient	Amount	Stock concentration	End concentration
Triton X100	0,4µl	100%	0,2%
Oligo dt	50µl	10µM	2,5µM
dNTPs	50µl	10µM each	2,5µM each
RNase inhibitor	5µl	100%	2,5%
H_2O	94,6µl	100%	47,3%
Total	200µl		

Crypt growth medium			
Chemical	**Amount**	**Stock concentration**	**End concentration**
A-83-01	1µl	500µM	500nM
Noggin	1µl	100µg/ml	100ng/ml
SB202190	1µl	10mM	10µM
PGE2	1µl of 1:100	1mM	10nM
R-Spondin	10µl	100µg/ml	1µg/ml
Gastrin	10µl of 1:100	100µM	10nM
EGF	10µl of 1:100	500µg/ml	50ng/ml
Nicotinamid	10µl	1M	10mM
HEPES	10µl	1M	10mM
N2	10µl	100x	1x
B27	20µl	50x	1x
N-acetylcystein	2µl	500mM	1mM
GlutaMAX	10µl	200mM	2mM
Penicillin/Streptomycin	10µl	10.000 U/ml Penicillin 10.000 µg/ml Streptomycin	100U/ml Penicillin 100µg/ml Streptomycin
Amphotericin B	10µl	250µg/ml	2,5µg/ml
Ciprofloxacin	10µl	2mg/ml	20µg/ml
Gentamicin	1µl	50mg/ml	0,5mg/ml
Wnt3A Medium	500µl	100%	50%
Advanced DMEM/F12	363µl	100%	36,3%
Rock inhibitor Y-27632	10µl	1mM	10µM
Total	1ml		

2.5 Antibodies

2.5a Antibodies used in assays regarding IL-23p19 and EBI3

Name	Target	Clonality	Host	Synonymous	Product number	Company
Anti-IL-23 antibody	IL23p19	polyclonal	rabbit	IL23R	ab45420	Abcam
Human IL-23 p19 Antibody	IL23p19	monoclonal	rabbit	IL23R2	MAB12901	R&D Systems
Human IL-23 p19 Antibody	IL23p19	monoclonal	mouse	IL23M	MAB17161	R&D Systems
Human/Canine IL-23 p19 Antibody	IL23p19	polyclonal	sheep	IL23S	AF6250	R&D Systems
Recombinant Anti-EBI3 antibody	EBI3	monoclonal	rabbit	EBI3R	ab124694	Abcam
Human EBI3 Antibody	EBI3	monoclonal	mouse	EBI3M	MAB6456	R&D Systems
ANTI-FLAG M2 antibody	Flag Tag	monoclonal	mouse	FLAG	F3165	Sigma-Aldrich
V5-Tag antibody	V5 Tag	monoclonal	mouse	V5	MCA1360	Bio-Rad
EBI3 (G4)	EBI3	monoclonal	mouse	G4	sc-166158	Santa Cruz Biotechnology
EBI3 (H6)	EBI3	monoclonal	mouse	H6	sc-365342	Santa Cruz Biotechnology
IL-23 (C3)	IL-23	monoclonal	mouse	C3	sc-271279	Santa Cruz Biotechnology
IL-23 (D12)	IL-23	monoclonal	mouse	D12	sc-271349	Santa Cruz Biotechnology

Table M1: List of antibodies used in ELISA and immunofluorescence microscopy experiments.

2.5b Antibodies used in flowcytometry

#	Fluorophor	Specificity	µl/1x	Product number	Company
1	FITC	CD64	5	305006	BioLegend
2	PE	CD326	5	130-091-253	Miltenyi Biotec
3	PE-Cy5	CD56	5	A07789	Beckman Coulter
4	PE-Cy7	CD11c	2,5	561356	BD Biosciences
5	Alexa Fluor 700	CD45	0,5	304024	BioLegend
6	APC-H7	CD3	4	641415	BD Biosciences
7	APC-H7	CD19	2,5	560727	BD Biosciences
8	APC-H7	CD20	2,5	641414	BD Biosciences
9	APC-eFluor 750	CD66b	2	B08756	Beckman Coulter
10	V450	CD14	2,5	560349	BD Biosciences
11	V500	HLA-DR	2,5	561224	BD Biosciences
12	BV605	CD117	1,25	562687	BD Biosciences
13	BV711	CD33	1,25	563171	BD Biosciences
14	BV650	CD1c	2	742749	BD Biosciences
15	BV786	CD141	2	741006	BD Biosciences

Table M2: List of antibodies used for the cell sorting procedure.

2.6 Loss of epithelial layer (LEL) model (walk-out)

Intestinal tissue was acquired from a surgical resection. The mucosal layer was dissected from the intestinal tissue using forceps and a scissor. The mucosa was then transferred into a 250ml plastic bottle containing 150ml of cold intestine wash buffer and transported into the laboratory. All following steps were performed within a biological safety cabinet. A petri dish filled with 80ml of cold intestine wash buffer was placed on an orbital shaker (150rpm) inside a refrigerator and used to wash the mucosa for 90 minutes at 4°C. During that time the intestine wash buffer was replaced every 30 minutes. After that, the mucosa was washed twice for 10 minutes in 80ml of cold HBSS/PSACGB at 4°C. The medium was then replaced with 80ml of room temperature (RT) warm H/D, to remove the mucous layer, and the dish was placed on an orbital shaker (150rpm) at RT for 15 minutes. To remove any traces of H/D the tissue was washed two times in 80ml RT warm HBSS/PSACGB for 5 minutes on an orbital shaker (150rpm). A 250ml plastic bottle was filled with 100ml of RT warm H/E, the mucosa was put inside and the bottle was placed in a shaking water bath at 37°C for 30 minutes to remove the epithelial cells from the mucosa. During the 30 minute incubation the bottle was shaken vigorously by hand twice. Afterwards the mucosa was transferred into a new 250ml plastic bottle containing 100ml of RT warm HBSS/PSACGB and incubated for 10 minutes at 37°C in a shaking water bath. The previous two steps were repeated twice followed by 3 consecutive washing steps, each for 10 minutes in 100ml HBSS/PSACGB in a shaking water bath at 37°C. The mucosa was then washed twice for 5 minutes in 80ml walk-out medium at RT and transferred into a large petri dish. The orientation of the tissue was adjusted so that the side facing towards the intestinal lumen in vivo was facing down in the petri dish. The tissue was then incubated for 12 hours in an incubator at 37°C and a CO2 level of 7%. After the incubation, the tissue was discarded and the medium harbouring the cells was filtered through a 100µm cell strainer and collected in a 50ml tube and placed on ice. The petri dish was then filled with ice cold walk-out medium and incubated on ice for 20 minutes. Using a pipetboy and a 10ml pipette, the cold medium was taken up and remaining adherent cells were washed off from the bottom of the petri dish utilizing the slight force of medium release from the pipette. This walk out medium was filtered through a 100µm cell strainer and added to the previously stored medium on ice. The bottom of the petri dish was washed with ice cold PBS to remove any residual adherent cells. The PBS solution containing the adherent cells was filtered (100µm cell strainer) and added to the already collected medium and centrifuged for 10 minutes with 300g at 4°C. The cells were washed in 50ml of FACS staining buffer and stained for FACS procedure (according to protocol 2.10).

2.7 Preparation of whole cell lysate samples for SDS PAGE

Approximately 200.000 sorted cells were washed in 1,2ml PBS in a 1,5ml safe-lock tube. The cells were centrifuged for 5 minutes with 900g at 4°C. The supernatant was aspirated completely and 28µl of WC lysis buffer C were added to the cell pellet. An additional 28µl of 95°C hot 10%SDS were added to the mixture and then vortexed. The tube was incubated for 10 minutes at 95°C on a heating shaker (900rpm). Within those 10 minutes of incubation the cells were vortexed twice. After the incubation the tube was centrifuged for 10 seconds with 900g to remove residual evaporated liquid from the lid. 14µl of 5x sample buffer + 2ME were added to the mix followed by another 10 minutes incubation at 95°C on a heating shaker. After the incubation, the evaporated liquid was again centrifuged for 10 seconds at 900g, the tube was snap frozen in liquid nitrogen and stored at -80°C until further use. Before running on a SDS gel, the samples were heated again for 10 minutes at 95°C on a heating shaker.

The protein standard for weight approximation was prepared by mixing 10µl of protein standard with 50µl of protein standard buffer and applied in 1 well of the SDS PAGE gel to run alongside with the other samples.

2.8 SDS PAGE

Glass plates were cleaned with 70% ethanol to remove any traces of proteins und dirt. The glass plates were put together with a pair of spacers in between them leaving a gap of 1,5mm. The set up was fixated in a casting frame with a rubber bottom to prevent the gel from leakage. Components of the resolving gel were pipetted together, mixed, and immediately pipetted in between the glass plates until 7,5cm from the bottom up.

Resolving gel					
Chemical	**Amount**	**Stock concentration**	**End concentration**	**Manufacturer**	**Order number**
H2O	13,58ml	100%	33,95%		
Acrylamid/Bis-Solution, 37.5:1	16ml	30% w/v	12%	SERVA	1068801
TRIS 1,5M pH8,8	10ml	1,5M	375mM		
20% SDS	200µl	20%	0,1%	SERVA	20767
10% APS	200µl	10%	0,05%	Bio-Rad	1610700
TEMED	20µl	100%	0,05%	Bio-Rad	1610800
Total	40ml				

Table M3: SDS PAGE resolving gel components.

The liquid gel was overlayed with ethanol to get a straight gel border during polymerization. After polymerization the ethanol was removed and the remaining space above the gel washed twice with water. Components of the stacking gel were pipetted together, mixed and pipetted on top of the resolving gel.

Stacking gel					
Chemical	**Amount**	**Stock concentration**	**End concentration**	**Manufacturer**	**Order number**
H2O	9,64ml	100%	30,095%		
Acrylamid/Bis-Solution, 37.5:1	2,12ml	30% w/v	1,99%	SERVA	1068801
TRIS 0,5M pH6,8	4ml	0,5M	62,44mM		
20% SDS	80µl	20%	0,05%	SERVA	20767
10% APS	160µl	10%	0,05%	Bio-Rad	1610700
TEMED	16µl	100%	0,05%	Bio-Rad	1610800
Total	32,032ml				

Table M4: SDS PAGE stacking gel components.

A comb was immediately placed inside the stacking gel to receive wells for the samples after the polymerization. The gel was placed into a running chamber and covered with running buffer. The comb was removed, samples and protein standard were pipetted into the wells and a constant electric current of 28mA was applied until the samples reached the resolving gel. As soon as the samples had transitioned into the resolving gel the current was raised to 80mA for 60 minutes. The gel was removed from the glass plates and incubated in western transfer buffer for 15 minutes. In parallel, a PVDF membrane was activated in pure methanol for 1 minute and then washed in water for 5 minutes. In a semi-dry blot machine 3 layers of, in running buffer soaked, whatman paper were placed in the middle, followed by the PVDF membrane, the gel, and another 3 layers of soaked whatman paper on top. At a constant current of 80mA for 60 minutes, the proteins transferred from the gel into the PVDF membrane. Afterwards the PVDF membrane was incubated for 1 hour in 5% milk powder in 1xTBS, followed by two washing steps for 10 minutes in TBS on a rocking platform. The primary antibody was diluted in antibody buffer, applied to the PVDF membrane, which were then together sealed in plastic foil and incubated on a rotator at 4°C over night. The next day the membrane was washed twice in TBS-T and once in TBS each for 10 minutes, followed by the incubation of HRP coupled secondary antibody in 5% milk powder in TBS for 60 minutes on a rocking platform. Lastly, two washing steps for 10 minutes in TBS-T and one washing step for 10 minutes in TBS were done. Both ECL components had been mixed in a ratio of 1:1, heated to room temperature in a water bath and applied onto the PVDF membrane for 60 seconds. In a darkroom, a

chemiluminescent detection film was placed for a varying amount of minutes onto the PVDF membrane and developed afterwards with a film processor. The blots had been scanned and were subsequently analyzed with Image Studio Lite (version 5.2.5, Licor).

2.9 ELISA

Throughout different experiments the amount of coated antibody and the blocking agent may differ. Changes from the standard protocol are mentioned whenever they had been applied.

The wells of a high binding 96-well ELISA plate were coated with 2,5µg/ml capture antibody for polyclonal antibodies and 5µg/ml for monoclonal antibodies in 100µl PBS respectively and incubated at 4°C over night. The wells were then washed three times with 200µl ELISA wash buffer and afterwards blocked with ELISA block buffer for 2 hours at RT. After another 3 washing steps with 200µl ELISA wash buffer, 100µl of cell culture supernatant or negative/positive control were pipetted into the wells and incubated for 1 hour at RT. The wells were washed 3 times with 200µl ELISA wash buffer and then incubated with 100µl detection antibody (5µg/ml) for 1 hour at RT. After another 3 washes with 200µl ELISA wash buffer for each well, 100µl of a horseradish peroxidase (HRPO) coupled antibody, directed against the species of the detection antibody, were incubated at 1:5.000 in ELISA Ab buffer for 1 hour at RT. A final wash step with 3 times 200µl ELISA wash buffer was done. To generate a measurable signal, 100µl of OPD solution were pipetted into the wells and incubated for 30 minutes at RT in the dark. The chemical reaction of the HRPO was stopped with 50µl of H_2SO_4 (1,8M) in each well. The wells were directly measured with a microplate reader at 450nm and the results calculated in a statistics program (GraphPad Prism, Version 6). Antibodies tested with this technique are listed in table M1.

2.10 FACS staining and sorting

Cells were washed in a FACS tube with 4ml of FACS staining buffer and centrifuged with 300g for 10 minutes at 4°C. The supernatant was removed and 1x of the antibody staining cocktail (table M2), filled up to 100µl with FACS staining buffer, was added per $1x10^6$ cells. The mixture was incubated for 30 minutes at 4°C in the dark. The tube was filled up to 4ml with FACS staining buffer and centrifuged for 10 minutes with 300g at 4°C. The supernatant was aspirated and the remaining cells were taken up in 300µl FACS staining buffer per $1x10^6$ cells. The cells were then sorted using a cell sorting machine and FACSDiva software (Version 8).

2.11 Cytospin and proximity ligation assay

Walk-out cells were acquired according to protocol 2.6. Cells were washed with ice cold PBS, centrifuged with 300g for 10 minutes and the supernatant was discarded. The cells were then adjusted to a density of 30.000 cells/250µl in ice cold PBS. A filter card was placed on a superfrost slide with a cytofunnel above and then locked in position with a clamp. The setup was placed into the cytospin centrifuge and 250µl of cell solution were pipetted into the opening on top. After a centrifugation of 5 minutes at 250rpm the superfrost slides were removed and air dried over night at RT. All following steps were performed at RT and the majority of the chemicals needed were provided within the "Duolink™ In Situ Orange Starter Kit". The next morning, a circle with a PAP pen was drawn around the cells for liquid retention. The slides were fixated with 1,7% PFA solution for 10 minutes and washed twice with 1X TBS. Increase in cell membrane permeability and blockade of unspecific antibody binding sites was achieved by incubating the cells with DCS antibody diluent for 10 minutes. The blocking solution was discarded and the primary antibody was diluted in DCS antibody diluent and incubated for 1 hour. The slides were washed three times for 5 minutes with 70ml TBS in a Hellendahl cuvette. The two PLA probes were diluted 1:5 in DCS buffer and incubated on the cells for 60 minutes at 37°C. The slides were washed twice with 1x wash buffer A for 5 minutes. The ligation stock solution was diluted 1:5 in H_2O and the ligase diluted 1:40 in that solution. The ligase was then incubated for 30 minutes at 37°C. After incubation the slides were washed twice in wash buffer A for 2 minutes. The amplification stock was diluted 1:5 in H_2O and the polymerase diluted 1:80 in that solution. The mix was applied to the samples and incubated for 100 minutes at 37°C. The slides were washed twice in 1x wash buffer B for 10 minutes followed by a short wash in 0,01x wash buffer B for 1 minute at RT. 30µl of DAPI mounting solution had been applied on the cells and then covered by a coverslip.

2.12 RNA purification of isolated cells

Cells were sorted into a solution of PBS and FCS (30%) in a 5ml round-bottom polystyrene tube, filled up with PBS to 4,5ml and centrifuged at 300g for 10 minutes at 4°C. The supernatant was discarded and the cells were washed with 4,5ml PBS and centrifuged again. The supernatant was aspirated completely and the cells were lysed in TRI reagent. If less than 10^6 cells were sorted, 100µl of TRI reagent had been used, and for 10^6 cells and above 300µl had been used for cell lysis. An equal amount of pure ethanol was added to the lysed cells and mixed vigorously. The "Direct-zol® RNA microprep kit" was used for the following purification process and provided all mentioned chemicals. The solution was then transferred into a Zymo-Spin IC column, placed into a collection tube and

centrifuged for 30 seconds at 14.000g. All following centrifugation steps were made at 14.000g for 30 seconds. The Zymo-Spin IC column was placed into a new collection tube and 400µl of RNA wash buffer were added. The tube was centrifuged and the flow through discarded. A mixture of 5µl DNase I (6U/µl) and 35µl digestion buffer were pipetted directly onto the column matrix. The solution was incubated for 15 minutes at room temperature. Two washing steps with 400µl Direct-zol RNA PreWash followed by centrifugation were made. 700µl of RNA wash buffer were added to the column followed by a centrifugation for 2 minutes at 14.000g to dry the membrane containing the RNA. Depending on the starting amount of cells, between 6µl and 15µl of DNase/RNase-Free water had been applied directly onto the column matrix followed by a 1 minute incubation and centrifugation at 16.000g for 1 minute into an RNase/DNase free tube. The RNA was snap frozen in liquid nitrogen and stored at -80°C.

2.13 Co-Immunoprecipitation (Co-IP)

The Co-IP was performed with the "FLAG Immunoprecipitation kit" (FLAGIPT1), which provided all of the following chemicals and buffers. All centrifugation steps were done at 4°C. The wash buffers were precooled. The Anti-FLAG M2 affinity gel was vortexed to make a uniform suspension of the resin. Per sample 100µl of the suspension were transferred into a new 5ml test tube. The resin was centrifuged at 6.000g for 30 seconds and the tube wasn't moved for 2 minutes to ensure that the resin was completely settled. The supernatant was removed completely without taking up any resin. The resin was then washed twice with 1ml wash buffer. 4ml of cell culture supernatant was pipetted onto the beads and incubated over night at 4°C on a rotator disc. For the negative control, only lysis buffer without protein was added. The positive control consisted of 4ml wash buffer mixed with 1µg FLAG-BAP fusion protein. The resin was then centrifuged at 6.000g for 30 seconds and the supernatant removed. The beads were washed three times with 500µl 1x wash buffer. 20µl of 2x sample buffer were added to the beads and then boiled for 3 minutes at 100°C. The samples were centrifuged at 6.000g for 30 seconds and the sample buffer containing now the eluted protein was analyzed via SDS-PAGE (according to protocol 2.8).

2.14 Transfection of HEK293 cells

2.14a Production of branched Polyethylenimine for the transfection of cells

In a 500ml glas beaker, 450ml of ddH2O were mixed with 500mg of branched Polyethylenimine (PEI). Under stirring and with the addition of HCl the pH was kept under pH>2 until the PEI was dissolved

completely. With the drop-wise addition of NaOH the pH was then adjusted to pH 7. The volume was filled up until 500ml had been reached and was filtered through a 0,22µm membrane. The solution was stored at -20°C.

2.14b HEK 293F Medium

HEK293 F cells were grown in 40ml HEK "Freestyle Expression Medium" with 100µl PenStrep and 10µl Amphotericin B. For transfection, the amount of PenStrep and Amphotericin B were halved to achieve an increase in transfection efficiency.

2.14c Transfection of HEK293F cells

15ml of PBS were mixed with 75µg of each plasmid containing the information for IL-23p19V5 or EBI3FLAG. The mixture was vortexed for 3 seconds and then incubated at RT for 20 minutes. The 15ml were then added to a roller bottle with 165ml of HEK293F medium containing $1x10^6$ HEK 293F cells/ml and incubated at 37°C with 7%CO2 for 48 hours. After the incubation period the cells were centrifuged in 50ml tubes with 300g for 10 minutes at 4°C. The cell pellet was flash frozen in liquid nitrogen until further use. The supernatant was transferred into a new 1,5ml collection tube and centrifuged at 12.000g for 10 minutes at 4°C to get rid of any remaining debris. The supernatant was again transferred into a new collection tube, flash frozen in liquid nitrogen and stored at -80°C.

2.15 DC purification from whole blood

4x50ml of whole blood were taken from a voluntary blood donor with a 50ml syringe harbouring a drop of heparin. The blood was mixed with an equal amount of RT warm blood wash buffer. 20ml of RT warm FicoLite-H were pipetted into a 50ml tube. 28ml of the blood wash buffer mixture were carefully overlayed on top of the FicoLite-H. The tubes were then centrifuged at 600g for 20 minutes at RT. The upper phase was aspirated and the second phase, containing the peripheral blood mononuclear cells, was carefully transferred into a new 50ml tube until 15ml had been reached, transferring as less FicoLite-H as possible, using a 5ml pipette. Everything above 15ml was put in additional 50ml tubes. The tubes were then filled up to 50ml with blood wash buffer and centrifuged at 600g for 12 minutes. The supernatant was aspirated and the tubes put on ice. The next steps were performed with utilization of the "myeloid dendritic cell isolation kit". The tube was filled up with ice cold MACS buffer. A fraction of the cell solution was stained with trypan blue and counted using a cell counting chamber. The cells were centrifuged with 300g at 4°C for 10 minutes. The supernatant was aspirated completely and the cells were resuspended in 300µl MACS buffer per $1x10^8$ cells. 100µl of FcR blocking reagent and 100µl of "non-myeloid dendritic cell antibody-biotin cocktail" had been

added per 1x10^8 cells, mixed and incubated for 10 minutes in a 4°C refrigerator. The cells were washed with 10ml of MACS buffer per 1x10^8 cells and centrifuged for 10 minutes with 300g at 4°C. The supernatant was aspirated and the cells were washed again. After centrifugation and aspiration of the supernatant the cells were resuspended in 400µl MACS buffer per 1x10^8 cells. 100µl of anti-biotin microbeads had been added to the cells and the mixture was then incubated for 15 minutes at 4°C in the refrigerator. After the incubation the cells were washed in 10ml MACS buffer per 1x10^8 cells, centrifuged, and resuspended in 500µl per 1x10^8 cells. The cells were filtered through a pre wetted 100µm filter and filled into a pre rinsed LD column inside a MACS magnet. After the LD column reservoir was emptied the LD column was washed twice with 1,5ml ice cold MACS buffer. The flow through contained the cells and was subjected to FACS staining and sorting (according to protocol 2.10).

2.16 nCounter® analysis

Dendritic cells from the walk-out model (protocol 2.6) and blood isolation (protocol 2.15) were sorted according to protocol 2.10 and the RNA was isolated as described in protocol 2.12. The purified RNA was then handed over to the nCounter core facility, university campus INF366 Heidelberg, for further processing. The gene expression for the defined human immunology V2 panel and codeset plus (adding 30 personalized genes) was determined.

A thermal cycler was set to 65°C with a lid temperature of 70°C. A hybridization master mix was pipetted containing 3µl “reporter CodeSet”, 2µl “reporter plus” and 5µl hybridization buffer per reaction. 10µl of the hybridization master mix were pipetted to a strip tube and 5µl of RNA sample, diluted to 10µg/µl, added. A master capture mix was created by mixing 14µl of “capture plus” with 28µl “core capture probe set”. 3µl of the master capture mix were added to each sample. Tubes were closed, mixed, spun down, placed inside the pre-heated thermocycler and incubated for 16-48 hours. After the hybridization, samples were stored short term at 4°C and immediately transferred to analysis with the nCounter® Sprint system. 30-35µl of each sample preparation were loaded onto a nCounter® cartridge (in case of a hybridization volume under 30µl, missing liquid was compensated with RNAse free water). Samples were analyzed with the nanostring nCounter® Sprint system and the resulting data was analyzed using Nanostring nSolver (4.0.70) software with the advanced analysis package (version 2.0.115).

2.17 DC isolation from biopsy samples (digestion)

Biopsy samples were taken from either inflamed or non-inflamed sites from the colon of patients and directly put into 8ml intestine wash buffer inside a 15ml S-tube. The samples were incubated at 4°C on an orbital shaker for 60 minutes. During the 60 minutes of incubation the intestine wash buffer was renewed twice. Biopsies were then transferred into 4°C cold 8ml HBSS/PSACGB in a new S-tube and incubated for 10 minutes on an orbital shaker. The biopsies were then placed into a new S-tube filled with 8ml of H/D and incubated on an orbital shaker at RT for 15 minutes. The samples were then washed in 8ml HBSS/PSACGB for 10 minutes and afterwards put into a new S-tube filled with 8ml of H/E. An incubation step followed in a shaking water bath at 37°C for 30 minutes, whilst every 10 minutes the S-tube had been shaken vigorously by hand. Another 10 minutes incubation in HBSS/PSACGB followed by 30 minutes in H/E was repeated twice. Biopsies were washed in a new S-tube with 8ml digestion buffer. The samples were then transferred into a C-tube filled with 10ml digestion buffer containing ~120 units/ml collagenase and ~120 Kunitz units/ml DNase. The tissue was digested for 90-120 minutes in a shaking water bath at 37°C. Every 30 minutes the C-tube was shaken vigorously by hand. After the digestion period the C-tube was centrifuged for 10 minutes with 300g at 4°C. The supernatant was removed and the cell pellet was resuspended in 2x1ml of FACS staining buffer. The resuspended cells were transferred into a 50ml tube through a pre-wetted 100µm cell strainer and filled up to 45ml with FACS staining buffer. The 50ml tube was centrifuged with 300g for 10 minutes at 4°C. The supernatant was removed and the cell pellet resuspended with 1ml of FACS staining buffer, transferred into a pre-cooled FACS-tube and filled with additional 3,5ml FACS staining buffer. The tube was again centrifuged at 300g for 10 minutes at 4°C. The cells were then stained and sorted according to protocol 2.10.

2.18 DC isolation from biopsy samples (walk-out)

Biopsy samples were taken from non-inflamed sites from the colon of healthy individuals and directly put into 8ml intestine wash buffer inside a 15ml S-tube. The samples were incubated at 4°C on an orbital shaker for 60 minutes. During the 60 minutes of incubation the intestine wash buffer was renewed twice. Biopsies were then transferred into 4°C cold 8ml HBSS/PSACGB in a new S-tube and incubated for 10 minutes on an orbital shaker. The tissues were then transferred into a new S-tube filled with 8ml of H/D and incubated on an orbital shaker at RT for 15 minutes. Biopsies were then washed in 8ml HBSS/PSACGB for 10 minutes and afterwards put into a new S-tube filled with 8ml of H/E. They were then incubated in a shaking water bath at 37°C for 30 minutes whilst every 10 minutes the S-tube had been shaken vigorously by hand. The biopsies were washed three times for

10 minutes in HBSS/PSACGB in a S-tube and then transferred into a FACS tube filled with 1,3ml of RT warm walk-out medium. The samples were incubated for 12 hours at 37°C and 7%CO2 in an incubator. The tissue was removed, the tube filled to the top with FACS staining buffer and then incubated for 20 minutes on ice. Cells were pelleted at 300g and 4°C for 10 minutes. The supernatant was removed and the pellet was again washed with 4ml of FACS staining buffer followed by centrifugation. The supernatant was aspirated and the cells were now stained according to protocol 2.10 (FACS staining and sorting).

2.19 RNA sequencing

Cells were acquired according to protocols 2.17 or 2.18 and then stained like described in protocol 2.10. Up to 100 DCs were sorted into 16µl of RNAseq lysis buffer in a well of a 96-well sorting plate. The plate was sealed with an adhesive foil (ampliseal), centrifuged at 700g for 30 seconds and then stored at -80°C until further processing. The samples were then handed over to the Deep Sequencing Core Facility on the university campus INF267 in Heidelberg. The RNA was transcribed into cDNA and amplified. The amplified material was then sequenced using an Illumina NextSeq 550 (sequencing method: 75 base pairs, single end). Bionformatic analysis was done by Dominik Schaack from the Department of Anesthesiology, based in the INF110 in Heidelberg. FastQC (Babraham Bioinformatics) was used to assess overall quality of the data and identify ribosomal RNA. Following datamanagement included rRNA contamination removal (SortMeRNA; bonsai bioinformatics), trimming (Trimmomatic; usadellab) and mapping/alignment (STAR; illumina). Alignment of the data was done with help of the reference genome “GRCh38.primary_assembly.genome.fa”. Conversion of sequence alignment maps into binary alignment maps was done using samtools. Read counting was done using htseq-count. Downstream processing utilized the statistics program R including the packages DESeq2, FactoMieR, factoextra and NMF to obtain data on differential gene expression and clustering followed by visualization of the received data.
Gene Ontology analysis based on differential gene expression was done using the bioinformatics tool GOrilla (Eden et al. 2009).

2.20 Opal™/FFPE staining for confocal microscopy

2.20a Immunofluorescence staining

All following steps had been performed at room temperature if not stated otherwise. Tissue sections which had been placed and dried on a “SuperFrost Plus” slide, had been treated with the following

substances for deparaffination and rehydration. Xylol - two times for 5 minutes; 100% Ethanol - two times for 3 minutes; 95% Ethanol - ones for 3 minutes; 70% Ethanol - once for 3 minutes, and two times in H_2O for 3 minutes each. This was followed by a demasking process in a pressure cooker. The slides were placed into a metal chamber filled with 400ml of citrate buffer (adjusted to pH6 with 2N HCl), put into a pressure cooker and added water until half of the outside of the metal chamber was covered with water. The lid was closed and the pot was heated up until the maximum pressure was reached; the heat source was turned off and the slides were incubated 5 more minutes inside the closed pressure cooker. After that the pot was cooled with water, the lid opened and the slides washed with H_2O once and then stored in H_2O until further processing. The tissue on the slides was encircled with a PAP pen for liquid retention. Slides were washed twice in TBS. An incubation in DCS antibody dilution buffer for 10 minutes followed. 50µl of the diluted primary antibodies in DCS antibody dilution buffer were incubated on the tissues for 60 minutes. The slides were washed 3 times in TBS for 5 minutes. 50µl of secondary antibodies diluted in DCS antibody dilution buffer were incubated for 30 minutes. The slides were washed 3 times for 5 minutes with TBS. After two final washing steps in H_2O for 5 minutes each, 1 drop of "Rotimount Fluorocare +DAPI" was pipetted onto the tissue and sealed bubble free with a coverslip. The slides were stored at 4°C until further investigation with a confocal microscope.

2.20b Opal™ staining

Tissue sections, which had been placed and dried on a "SuperFrost Plus" slide, had been treated with the following substances for deparaffination and rehydration. Xylol - two times for 5 minutes; 100% Ethanol - two times for 2 minutes; 95% Ethanol - ones for 2 minutes; 70% Ethanol - once for 2 minutes; H_2O - two times in 2 minutes, followed by 2 final washing steps for 2 minutes in TBST. The tissues were then fixated for 20 minutes in 4% PBS-buffered formalin and washed twice in H_2O for 2 minutes each. The slides were then placed in a plastic Hellendahl staining cuvette filled with 130ml of AR6 buffer. The cuvette was heated in a microwave oven until boiling (~45 seconds at the highest setting) and then kept at 20% of the maximum microwave output for 15 minutes. After the slides had cooled to room temperature (~30 minutes) the tissue pieces were encircled with a PAP pen for liquid retention. The slides were washed 3 times with TBST. The following incubation steps were performed in a slide humidity chamber. The tissues were blocked for 10 minutes, incubating with DCS antibody diluent. The primary antibody was incubated in DCS antibody diluent for 1 hour at RT. The slides were washed two times with TBST. Incubation of the secondary antibody polymer HRP mouse & rabbid was performed for 10 minutes at RT. The slides were washed with TBST twice for 2 minutes

each. A 1:50 working solution with Opal 520 was incubated at RT for 10 minutes. The slides were washed with TBST for 2 minutes two times. Heat retrieval of antibodies was performed in the microwave as before: The cuvette was heated until boiling (~45 seconds at the highest setting) and then kept at 20% of the maximum microwave output for 15 minutes. Slides were washed twice in H_2O followed by two washes with TBST for 2 minutes each. The process of adding a new primary antibody, secondary antibody and Opal signal generation (there are different fluorophores available) was repeated for every desired additional antibody target. In the end a DAPI counterstain was performed with a solution containing 1 Drop of DAPI in 500µl TBST. Slides were incubated with the DAPI solution for 5 minutes at RT followed by three washes in TBST and two washes in H2O. The tissue was mounted with "Diamond AntiFade Mounting Medium" and sealed with a coverslip. The slides were stored at 4°C until further investigation.

2.21 Wound healing assay

Lamina propria was dissected from colonic resected material and put into transport buffer followed by transportation into the safety cabinet. A petri dish was filled with transport buffer, the tissue placed inside and all visible fat and vein residues were removed with a scissor and forceps. The cleaned mucosa was put into a 50ml tube filled with 40ml transport buffer and shaken vigorously by hand. This process was repeated until the buffer remained visibly clear after shaking. The tissue was then placed in a 50ml tube filled with 40ml of chelation buffer and placed onto a spinning wheel at 4°C for 30 minutes, and shaken every 10 minutes by hand. Six 50ml tubes with 3ml cold PBS each were prepared and the tissue was placed into the first one, shaken vigorously then transferred into the next tube until each six tubes were processed this way. The 3ml of PBS from each tube were inspected with a bright-field microscope and the sample with the most intact crypts were processed further. The crypt solution was then transferred into a pre-blocked 50ml tube filled with 5ml of 5% FBS in PBS, filled up with crypt wash buffer and centrifuged with 100g for 3 minutes at 4°C. The supernatant was discarded and the crypt pellet was resuspended in 1ml ice cold crypt wash buffer. Crypt density was then adjusted to approximately 50 crypts per 50µl crypt wash buffer. 300µl of the crypt solution were then transferred into a 1,5ml safe-lock tube and centrifuged with 1000g for 3 minutes at 4°C. The supernatant was aspirated and 50µl pre-cooled Matrigel were pipetted with a pre-cooled tip onto the crypt pellet. The Matrigel crypt solution was then pipetted onto the bottom of a 37°C pre-heated 24-well plate and incubated for 15 minutes at 37°C in an incubator with 7%CO2. The well was then filled with 37°C warm 500µl crypt growth medium and incubated until further processing. The crypt growth medium was changed every 2 days.

Organoids were removed from the Matrigel, dissolving it with ice cold transport buffer, pipetting the solution in a 1,5ml safe-lock tube and centrifuging at 4°C with 500g for 3 minutes. The supernatant was removed, organoids washed in cold transport buffer and again centrifuged. The cell pellet was resuspended in 1ml of Trypsin-EDTA (0,05%) and incubated at 37°C for 5minutes to break cell-cell adhesions. Organoids were disrupted by progressively pipetting up and down. The cell dilution was filled ad 14ml with 4°C cold Advanced DMEM F12 containing 10% FBS and centrifuged with 300g at 4°C for 10 minutes. The washing step was repeated twice with 4°C cold Advanced DMEM F12 without FBS. Cells were resuspended in 100µl crypt growth medium and pipetted evenly into the wells of a collagen treated 2 well 35mm µ-Dish. Medium was changed every 2 days until 95% confluency was reached. The 2D layer procedure was done with the help of Megan Stanifer from the lab of Steeve Boulant on the university campus in Heidelberg INF 344. Each well was washed with 70µl Advanced DMEM F12 twice. The insert was removed and the dish filled with 1ml of Advanced DMEM F12 containing either nothing (control), 1µg IL-23p19, 1µg EBI3 or 1µg IL-23p19+1µg EBI3. Over 24-36 hours, a picture (stitched large image) of the gap between both cell layers was taken every 3 hours with the bright-field setting of the confocal microscope. The areas between the cell layers were calculated using GIMP (version 2.10.8) and growth rates were calculated based on that data.

2.22 Patients samples acquisition and ethics statement

All patients that participated in this study were educated about this study by their authorized doctor and gave written consent. The studies were approved by the ethics committee of the University of Heidelberg. All tests were performed in accordance with the principles of the Declaration of Helsinki.

3.0 Results

3.1 Generation of acute inflammatory intestinal dendritic cells - loss of epithelial layer (LEL) model

Understanding what happens at the initiation of an inflammatory response in the gut is the key to a more complete picture of gastrointestinal health itself. Examining acute inflammatory reactions leads to a deeper understanding of the processes which maintain intestinal homeostasis and may be used to ascertain which mechanisms are disturbed or malfunctioning in patients unable to resolve an inflammatory state. To mimic an acute inflammation a previously established organ culture model was utilized in this study. A piece of human mucosa from a colonic resection was chemically ablated of its epithelial cells, hence it is referred to as loss of epithelial layer (LEL) model (Fig.R1). Due to the missing signals from the epithelium and the disruption of that important barrier the tissue becomes inflamed. After an incubation period of 12 hours, where the tissue culture mRNA levels for inflammatory mediators like e.g. *IL1B*, *IL23A*, *IL6*, *IL8*, *TNFA* and *CXCL2* were strongly increased (Schröder-Braunstein et al. 2014), a significant amount of cells had emigrated out of the tissue into the culture dish (~0,25x10^{6}cells/cm²) (Szikszai et al. 2015). From this mixture of motile cells, myeloid dendritic cells (mDCs) were isolated via fluorescence activated cell sorting (FACS) and used for various downstream experiments. Due to the mechanism of DC recovery in this experiment they are also referred to as “walk-out” or LEL mDCs.

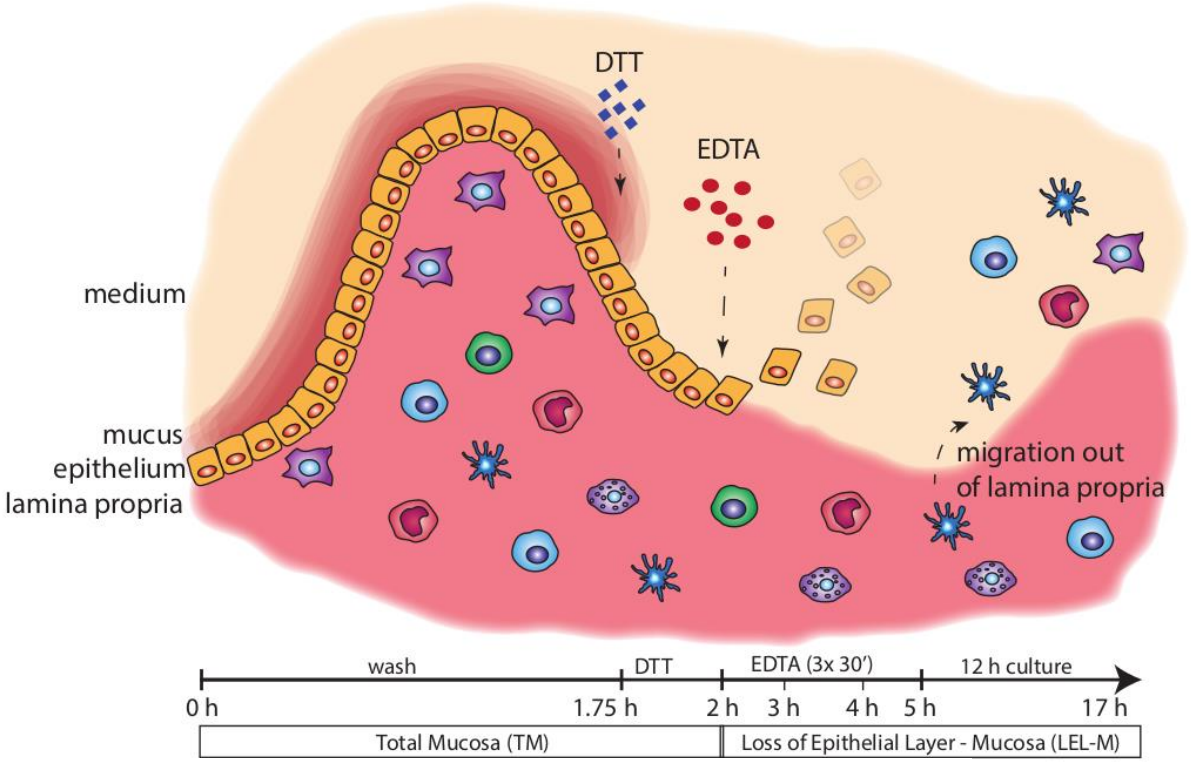

Fig.R1: Figure legend on next page

Fig.R1: Loss of epithelial layer (LEL) model. This schematic shows the critical steps of the LEL model. A piece of colonic mucosal tissue is treated with DTT and EDTA to remove the mucus and epithelial cell layer. This is followed by a 12 hour incubation in cell culture medium, during which immune cells migrate out of the tissue. Figure used with permission by Dr. Judith Gras.

3.2 Sorting procedure for the isolation of dendritic cells

In order to separate dendritic cells from the entirety of emigrated cells of the organ culture model the following sorting procedure was applied. First of all, cell aggregates (cell doublets) were excluded using the forward scatters H and A (Fig.R2 A) (Cossarizza et al. 2019). From all the stained singlet cells debris was excluded via forward and side scatter settings (Fig.R2 B). All non-$CD45^+$ cells were omitted, leaving only leukocytes for further gating steps (Fig.R2 C). A dump gate was used to exclude all $CD3^+$, $CD19^+$, $CD20^+$ and $CD66b^+$ cells which include T cells, B cells and granulocytes respectively (Fig.R2 D). $CD56^+$ NK cells (Fig.R2 E), $CD117^+$ mast cells (Fig.R2 F) and $CD326^+$ epithelial cells (Fig.R3 G) were neglected as well. For the identification of antigen presenting cells, only cells with a high expression of HLA-DR^{++} were incorporated (Fig.R3 G) (Villadangos, Schnorrer, and Wilson 2005; Reis e Sousa 2006; Landsverk et al. 2012). In order to exclude macrophages from the $CD33^+$ myeloid cells, only $CD14^-$ cells were considered (Fig.R3 H) (von Gunten and Bochner 2008). All of those remaining cells were $CD64^{-/low}$ and $CD11c^+$, which is a characteristic for myeloid dendritic cells (Fig.R3 I) (Segura 2016). These cells were also positive for CD1c and CD141 which is again a hallmark for dendritic cells (Fig.R3 J) (Haniffa et al. 2012; Chu et al. 2012).

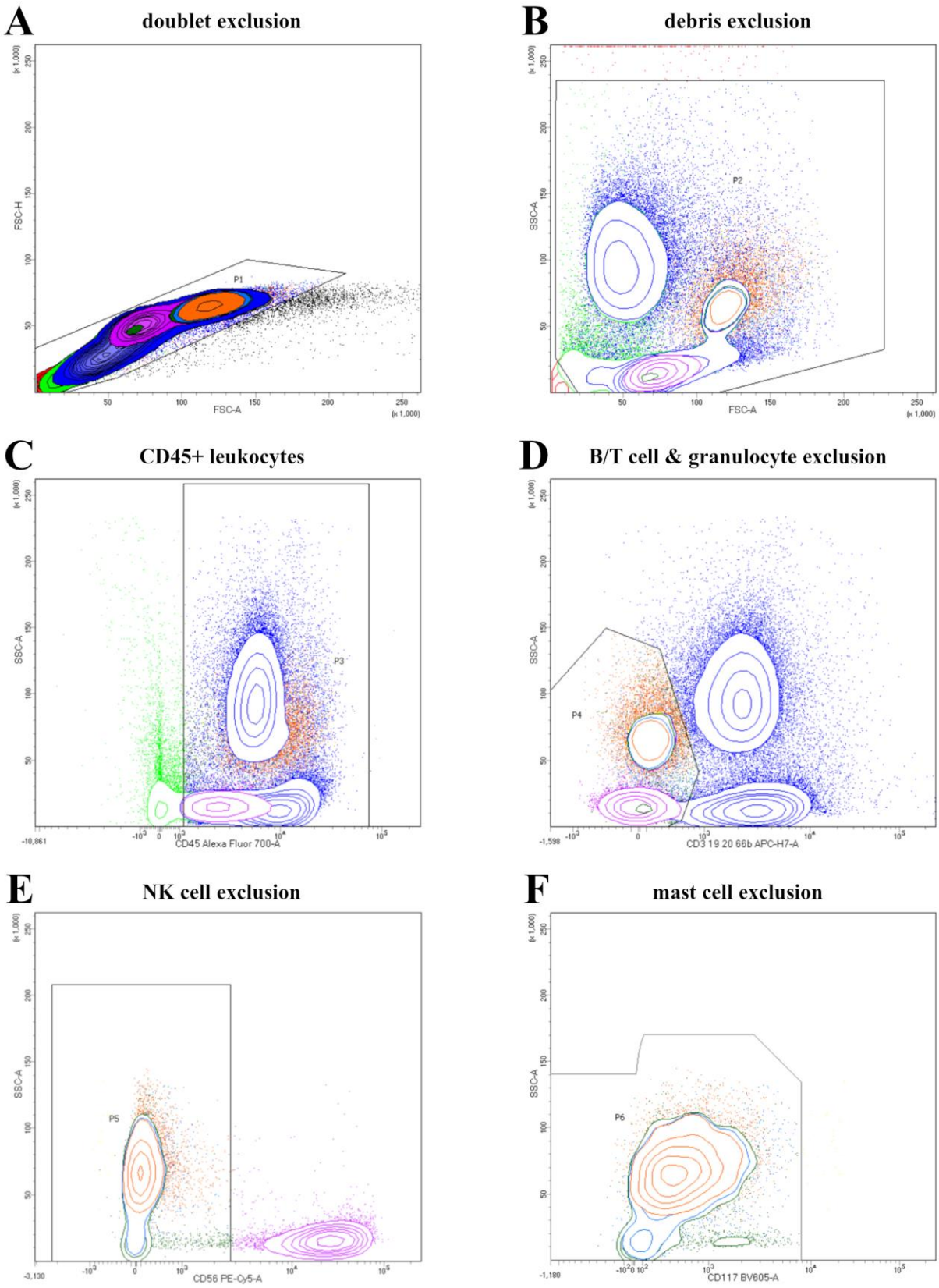

Fig.R2: FACS gating strategy for LEL mDCs. Please see next page for figure legend.

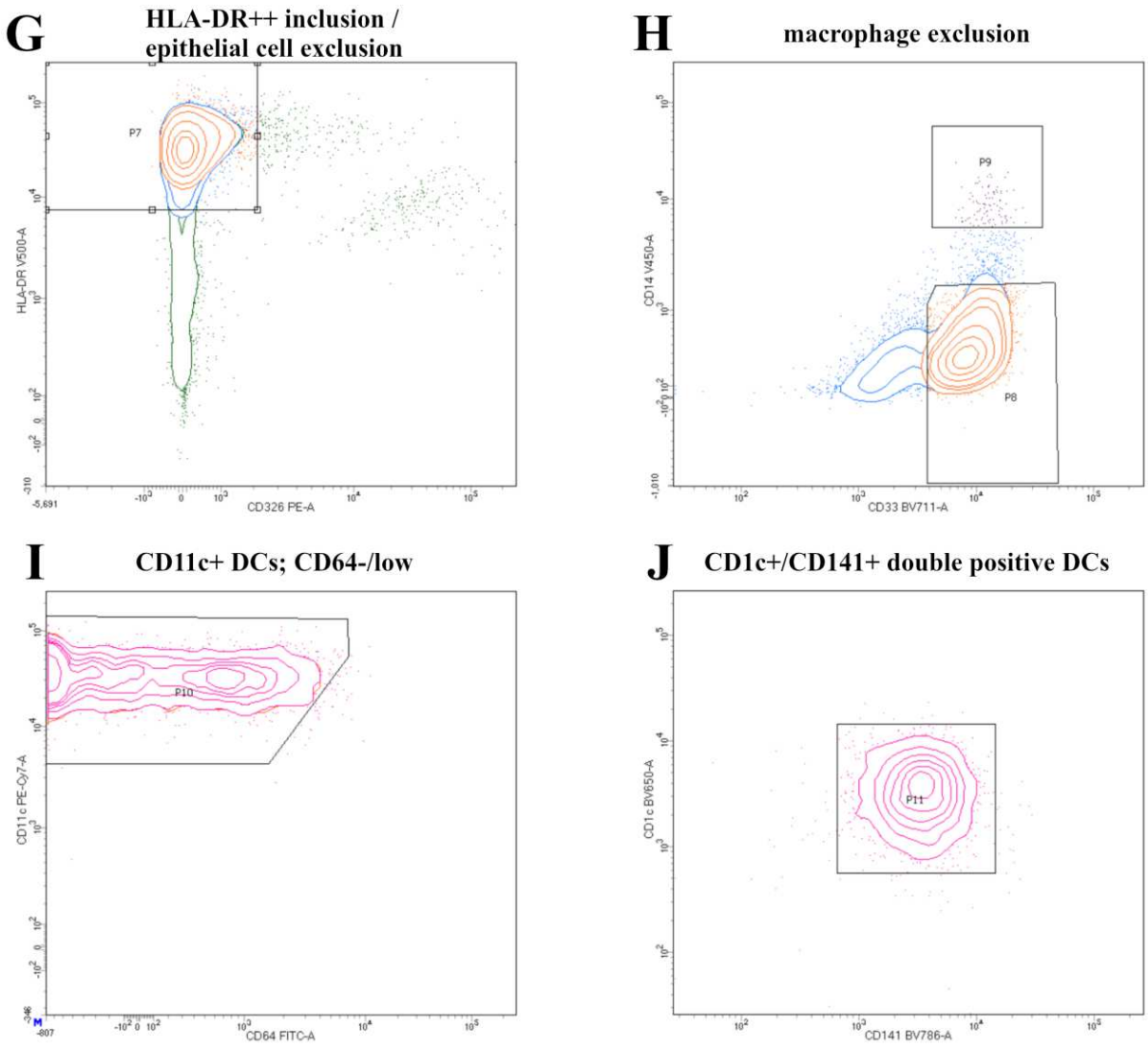

Fig.R3: FACS gating strategy for LEL mDCs. Cell aggregates were excluded via FSC-H and FSC-A (A). Too large, small and granular particles were excluded via FSC-A and SSC-A (B). All leukocytes were included via $CD45^+$ (C). Only $lineage^-$ negative cell populations were considered ($CD3^-$, $CD19^-$, $CD20^-$) and also granulocytes excluded ($CD66b^+$) (D). NK-cells were removed ($CD56^+$) (E) and mast cells as well ($CD117^+$) (F). Epithelial cells were excluded ($CD326^+$) and only $HLA\text{-}DR^{++}$ high cells included (G). Macrophages were neglected via $CD14^+$ (H) and $CD64^+$ (I) and only $CD33^+$ myeloid cells included (H). These cells had a high surface expression of $CD11c^+$ (I) and expressed both markers $CD1c^+$ and $CD141^+$ (J).

For further clarification of the gating strategy regarding the sorting procedure, figure R4 provides more insight. Since the gating strategy in figures R2 & R3 A-J was demonstrated on a sample of emigrated leukocytes from a LEL experiment, there are nearly no CD117 positive cells found in the sample. Figure R4 A shows data from the flow cytometric analysis of cells obtained following digestion of intestinal lamina propria, and a population of CD117 positive cells, presumably mast cells, is clearly visible (marked by the black arrow) compared to the LEL model (Fig.R2 F). The next 2

panels (Fig.R4 B & C) again reflect flowcytometric data of cells emigrated out of the tissue using the LEL model. Figure R4 B shows expression levels of CD11c and CD64 on CD33 positive, CD14 positive cells. The CD14 positive cells can be clearly distinguished from CD14 negative cells by the high level of CD64 (Fig.R4 B) on $CD14^+$ cells (Fig.R3 I). Additionally, the level of CD11c is slightly higher on CD14 negative cells compared to CD14 positive cells. Based on this expression profile CD14 positive cells can be considered as macrophages (Caër and Wick 2020). Figure R4 C shows the expression of CD1c and CD141 on HLA-DR low/intermediate cells which are consequently also low and intermediate in their CD33 expression, and those cells can be clearly distinguished from the $CD1c^+$, $CD141^+$ positive dendritic cells in figure R3 J.

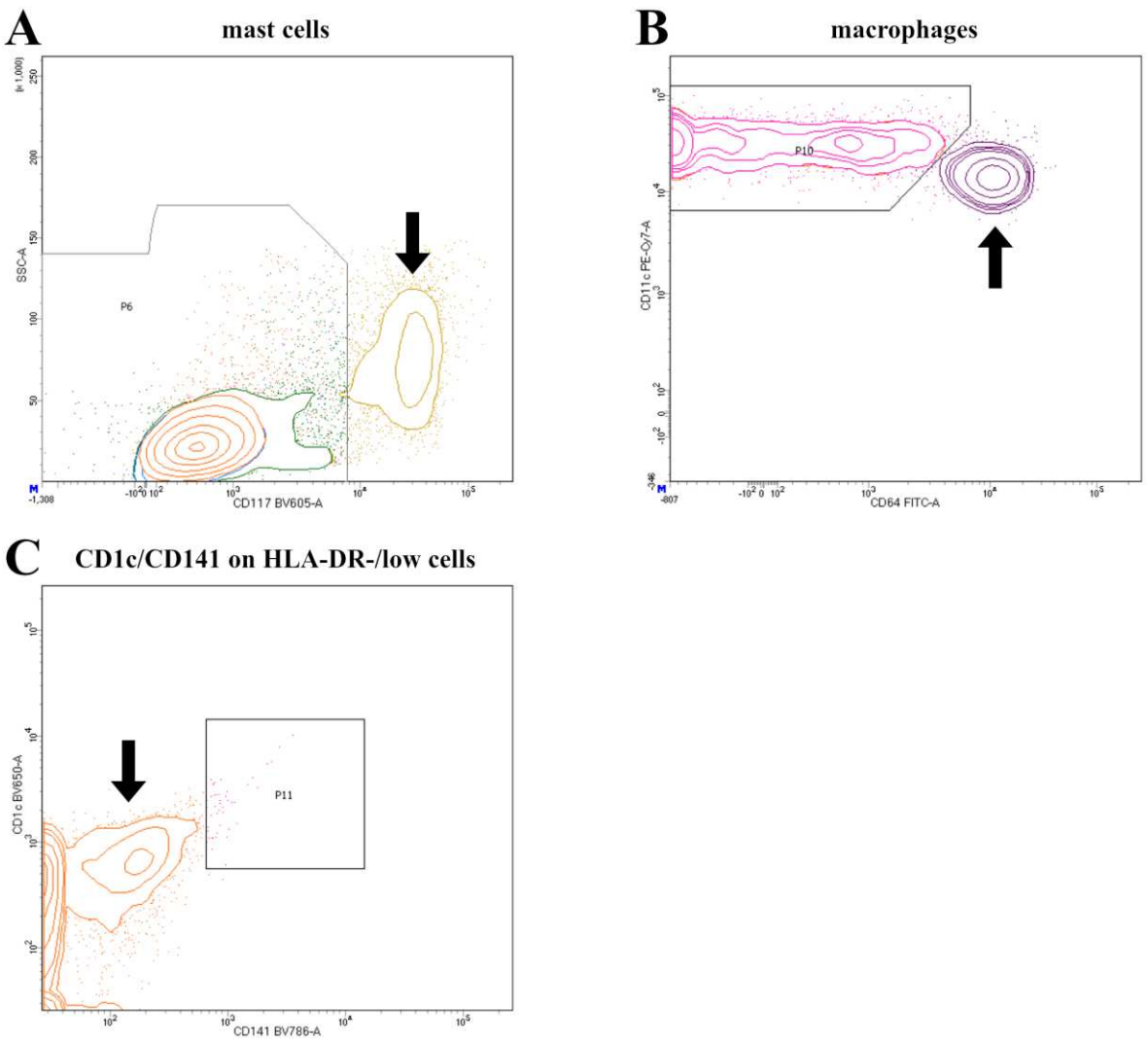

Fig.R4: Ancillary FACS gating strategy blots. These blots provide additional information on the gating strategy from figures R2 and R3. A population of CD117 positive mast cells is shown, acquired after enzymatic digestion of lamina propria tissue (A, arrow). Among LEL leukocytes, CD64 positive macrophages (B, arrow) can be distinguished from CD64 negative dendritic cells. Compared to the low expression of CD141 and CD1c on cells

that are HLA-DR$^{+/low}$ and CD33 intermediate/low (C, arrow), LEL mDCs can be considered as CD141^{+}/CD1c^{+} positive cells.

3.2.1 Cellular composition of emigrated lamina propria leukocytes in the LEL model

The flowcytometric analysis of emigrated lamina propria leukocytes obtained via the LEL model was performed with mucosal tissue of 20 different patients (13 male, 7 female; mean age: 67). For each cellular subpopulation the arithmetic mean was calculated on the basis of cells per 100.000 CD45^{+} leukocytes (Fig.R5). The majority of cells which migrated out of the tissue were B and T cells (52.542 cells; 52,54%) followed by granulocytes (27.475 cells; 27,48%). Dendritic cells account for approximately 5.415 cells (5,42%) per 100.000 CD45 positive cells. NK cells and macrophages were the least motile cell types analyzed with 4.767 and 499 cells per 100.000 CD45^{+} cells, respectively (NK cells: 4,77%; macrophages: 0,5%) (Fig.R5).

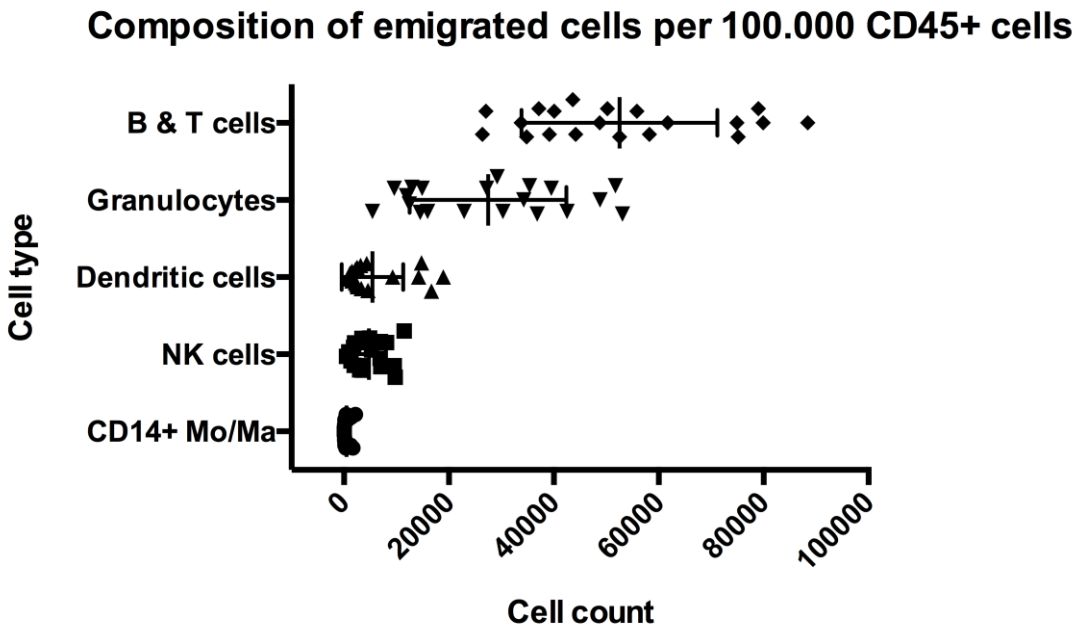

Fig.R5: Cellular composition of emigrated LEL leukocytes. This graph shows the numbers for different cell types emigrated out of the lamina propria as observed in 20 experiments, with mucosal tissue from 20 individual donors. The data for each cell type and subject refers to a common denominator of events per 100.000 CD45 positive cells.

The remaining cells were not categorized into a specific subgroup due to limitations in surface marker targets. Lineage negative, CD56 negative cells, which were also low in HLA-DR, accounted for approximately 4642 cells (4,64%). A small amount of those 4642 cells were CD326 positive epithelial cells. HLA-DR^{++} positive cells that were neither DCs nor macrophages were counted at 2528 cells

(2,53%). The majority of those lineage$^-$ negative non-DC, non-macrophage HLA-DR^{++} positive cells were CD33 low or negative. A precise subgroup gating strategy led to a loss of approximately 2,13% of cells on average due to the avoidance of overlapping gates and undeterminable events. The percentages of all emigrated LEL subgroups are depicted in figure R6.

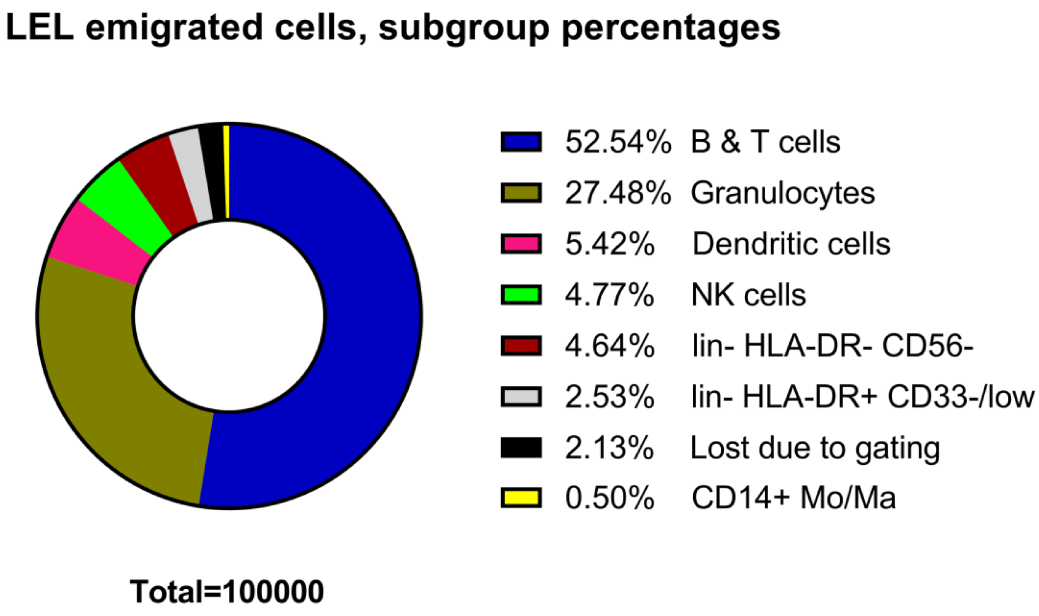

Fig.R6: Average percentages of emigrated LEL cell subgroups. This graph shows the average percentage of cells for different subgroups emigrating out of the lamina propria during the LEL model. The measurement was done with flowcytometric data from 20 individual patients.

3.3 Nanostring nCounter® mRNA analysis of colonic LEL mDCs

Emigrated leukocytes were acquired using the LEL model with colonic mucosa from four different patients (3 male, 1 female, mean age 59 years).Myeloid dendritic cells were sorted and mRNA was extracted. Analogously, peripheral blood dendritic cells were sorted from buffy coats of four healthy volunteer blood donors, followed by RNA extraction. All eight mRNA samples were analyzed via Nanostring nCounter® technology using the human immunology V2 panel+ with 30 additional selected genes, gathering mRNA expression data from 609 genes in total.

3.3.1 Validation of the sorted cell type using mRNA expression data

The mRNA data was used to verify the categorization of the sorted cells, comparing LEL mDCs and PBDCs to typical DC markers. Peripheral blood monocytes (PBMOs) were also analyzed and

incorporated into the analysis for further clarification of monocyte/macrophage associated marker expression levels. The gene expression profile shows that the cells, which emigrated out of the lamina propria, have a common gene expression profile for dendritic cells, with a high mRNA transcript amount of *HLA-DRA*, *CD86*, *CD80* and *FLT3* (HLA-DR/MHC-II (Kleijmeer et al. 2001), CD80/86 (Caux et al. 1994), FLT3 (Karsunky et al. 2003) (Fig.R7). mRNAs as common markers for monocytes/macrophages like *CD14* and *CD163* (CD14 (Grage-Griebenow, Flad, and Ernst 2001), CD163 (Kristiansen et al. 2001)) could only be found in peripheral blood monocytes to a higher extent. Peripheral blood dendritic cells had also low mRNA levels for monocyte markers like *CD14* and high levels for DC markers like *FLT3* and *HLA-DRA*. The macrophage specific marker *CD64* (*FCGR1A*) was also not present in LEL mDCs as seen in the appendix table AX3. LEL mDCs showed exclusively additional gene activity for *CCR7,* which is a marker for DC activation in peripheral tissues (Riol-Blanco et al. 2005). The LEL mDCs acquired with the sorting procedure in Fig.R7 show a clear gene expression profile for dendritic cells.

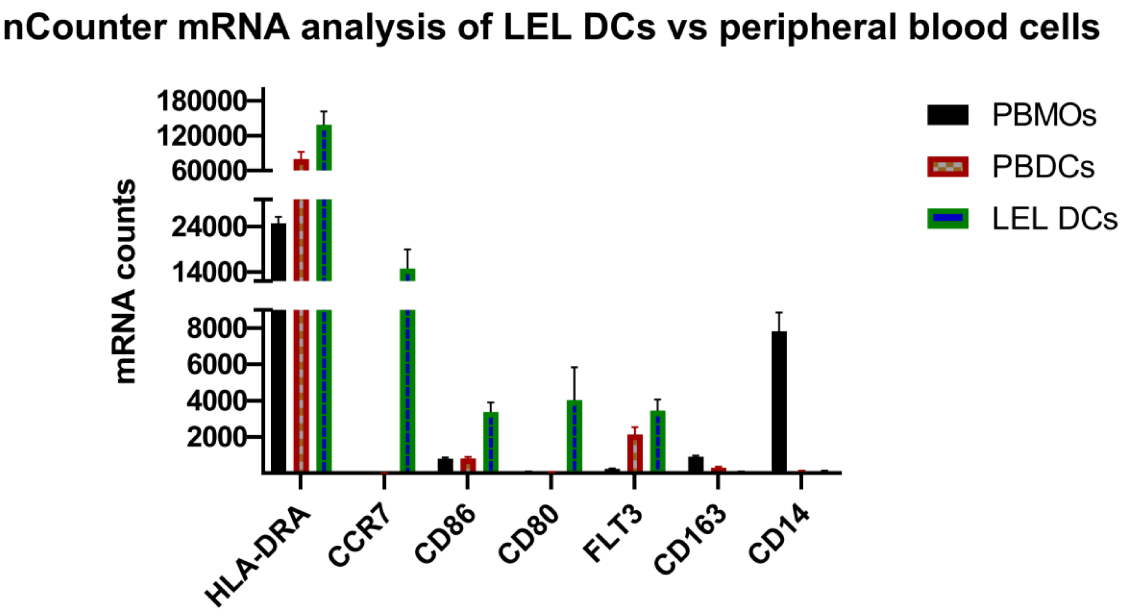

Fig.R7: Nanostring nCounter® mRNA analysis of LEL mDCs vs peripheral blood cells. This graph shows the mRNA expression profile of common genetic markers for DCs, monocytes and macrophages. Compared are dendritic cells (PBDCs) and monocytes (PBMOs) from peripheral blood versus dendritic cells (LEL DCs) from intestinal tissue acquired with the LEL model. Each group had a sample size of 4 individuals.

3.3.2 Assessment of the conventional DC subtype of LEL mDCs

Dendritic cells can be categorized into different conventional DC (cDC) subgroups. The gene expression data from the nCounter® analysis was used together with the cell surface marker information from the cell sorting process and compared to cDC classification from two different publications in table R8. Except for the expression of CD141 and the non-existence of CD209 mRNA the LEL mDCs share the majority of their features with cDC2 DCs. The cDC1 subtype is connected to $CD8^+$ cytotoxic T cell induction, whereas the cDC2 subtype induces Treg and Th17 cells (Sun, Nguyen, and Gommerman 2020).

Publication 1						
Identifier	**DCsubytpe (literature)**					**Experimental data**
	pDC	**cDC1**	**cDC2**	**DN DC**		**LEL mDC**
CD11c	-	+	+	+		++
CD1c		-	+	-		+*
XCR1		+	-	-		-
CD123	+	-	-	-		?
Publication 2						
Identifier	**DC subtype (literature)**					**Experimental data**
		cDC1	**cDC2**			**LEL mDC**
CD103		+	+			+
SIRPα		-	+			?
CD1c		-	+			+*
CD141		+	-			+*
CD209		-	+			-
IRF4		-	+			+++
IRF8		+	-			-
BCL6		+	-			-
BLIMP1		-	+			++
CD26		+	-			-
CD101		-	+			?

Table R8: cDC classification of LEL mDCs. Identification of cDC subgroups is based on human intestinal dendritic cells. A prerequisite for all cells is that they are CD45+, and negative for CD3-, CD14-, CD16-, CD19-, CD56- and CD64-. Green tiles show according LEL mDC gene expression. *: flowcytometric analysis based data. pDC, plasmatycoid DC; cDC1/2 conventional DC1/2; DN DC, double negative DC (CD1c-/XCR1-)
Publication 1:(Caër and Wick 2020)
Publication 2:(Sun, Nguyen, and Gommerman 2020)

3.3.3 Gene expression differences present in LEL mDCs vs PBDCs

An agglomerative heat cluster map is displayed in figure R9. The LEL mDCs from the four colon samples and the four blood samples are respectively so different in terms of their mRNA expression

profile that they are categorized into two distinct groups by unsupervised cluster analysis. The distribution of genes that are highly statistical significant can be observed with the volcano plot in figure R10, plotting each genes p-value in correlation with its differential expression, resulting in one datapoint for each measured gene. The tables R11 and R12 list the 30 most upregulated (table R11) and the 30 most downregulated (table R12) genes in colonic LEL mDCs from an inflammatory environment compared to peripheral blood mDCs (PBDCs). The tables are ordered by linear fold change with blood DCs mRNA levels serving as base value. The gene expression data were subjected to Ingenuity Pathway Analysis (IPA) to gain insight into the function of resident lamina propria mDCs under inflammatory conditions (based on nCounter® normalized data, calculated with nSolver 4.0.7.0).

As expected for dendritic cells, the top canonical pathways of the IPA analysis show involvement in T helper cell activation (Th1 and Th2) and T helper cell differentiation (table R13). This indicates the involvement of mDCs in orchestrating adaptive immune response mechanisms. In the category of top "Diseases and Disorders" the most likely event connected to this dataset of genes is "Inflammatory response", fitting the circumstance that these cells were acquired using the LEL model (table R14).
On the other hand the top canonical pathways also reveal novel functions which are not associated with typical dendritic cell functions in the first place. One unusual pathway uncovered in this analysis was the "Neuroinflammation Signaling Pathway" (table R13). This hints at a possible function of mDCs staying in contact with cells from the enteric nervous system.
The LEL mDCs have some chemokine mRNAs expressed which are not, or only in fewer amounts, present in PBDCs which are *CCL22*, *CXCL8*, *CCL19* and *CCL24*, making them able to orchestrate cell movement by themselves or influencing cells in their vicinity. LEL mDCs also differentially express mRNAs for the endopeptidases *MMP7*, *MMP10* and *MMP12,* giving them the ability to degrade extracellular matrix proteins or process some molecules into their bioactive form. They also differentially express mRNAs for molecules influencing T cell behavior and development like *IDO1*, *CD274* (PD-L1), or *PDCD1LG2* (PD-L2) (gene expression data: appendix table AX3).

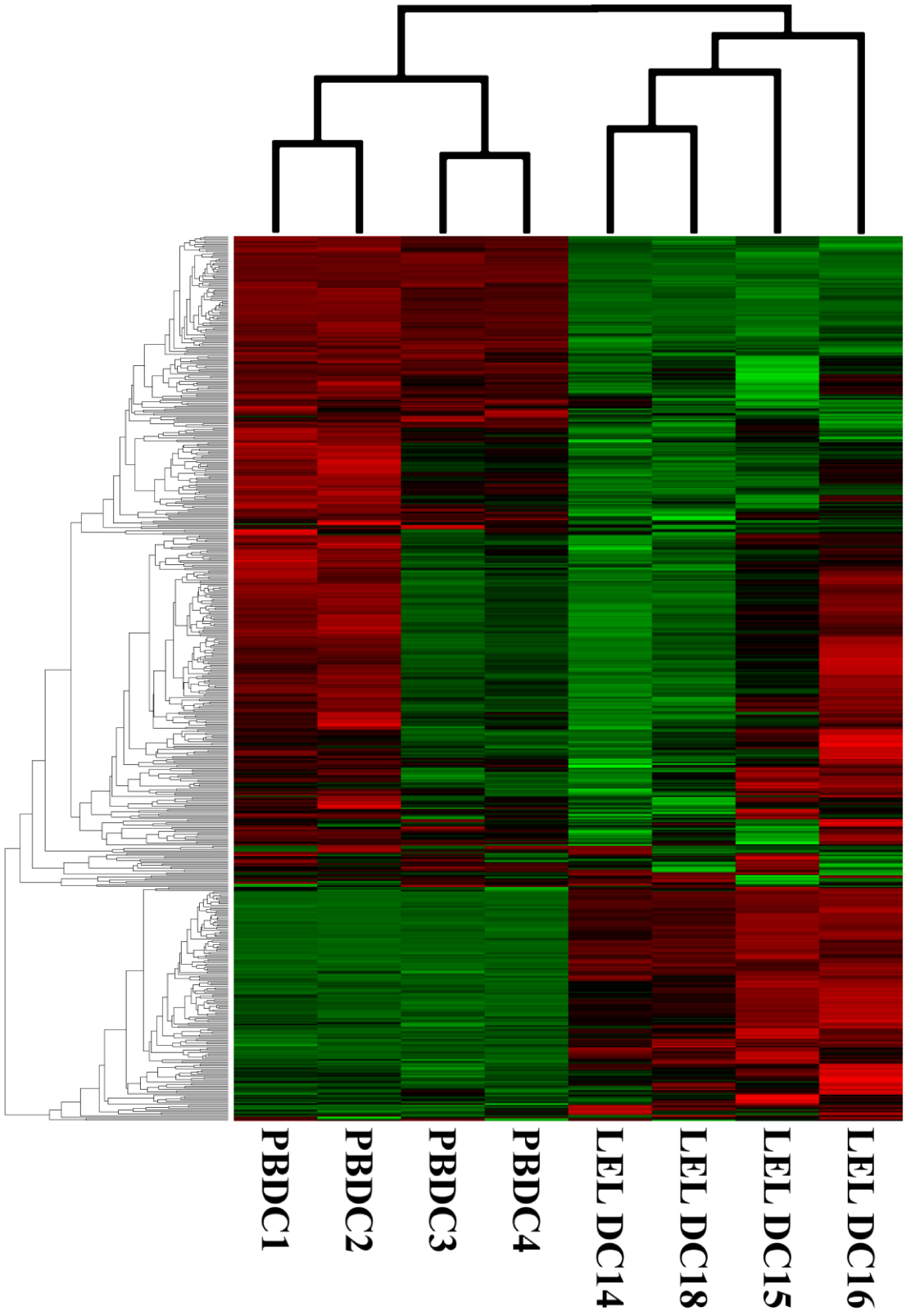

Fig.R9: Agglomerative cluster heat map comparing mRNA expression levels of peripheral blood mDCs versus colonic LEL mDCs (unsupervised). This agglomerative cluster heat map compares the mRNA expression profile of peripheral blood DCs (PBDCs) from four volunteer donors to emigrated colonic LEL mDCs from four patients. The vertical tree structure on top shows the grouping of subjects based on the similarity of upregulated (green) and downregulated (red) genes from the subjects.

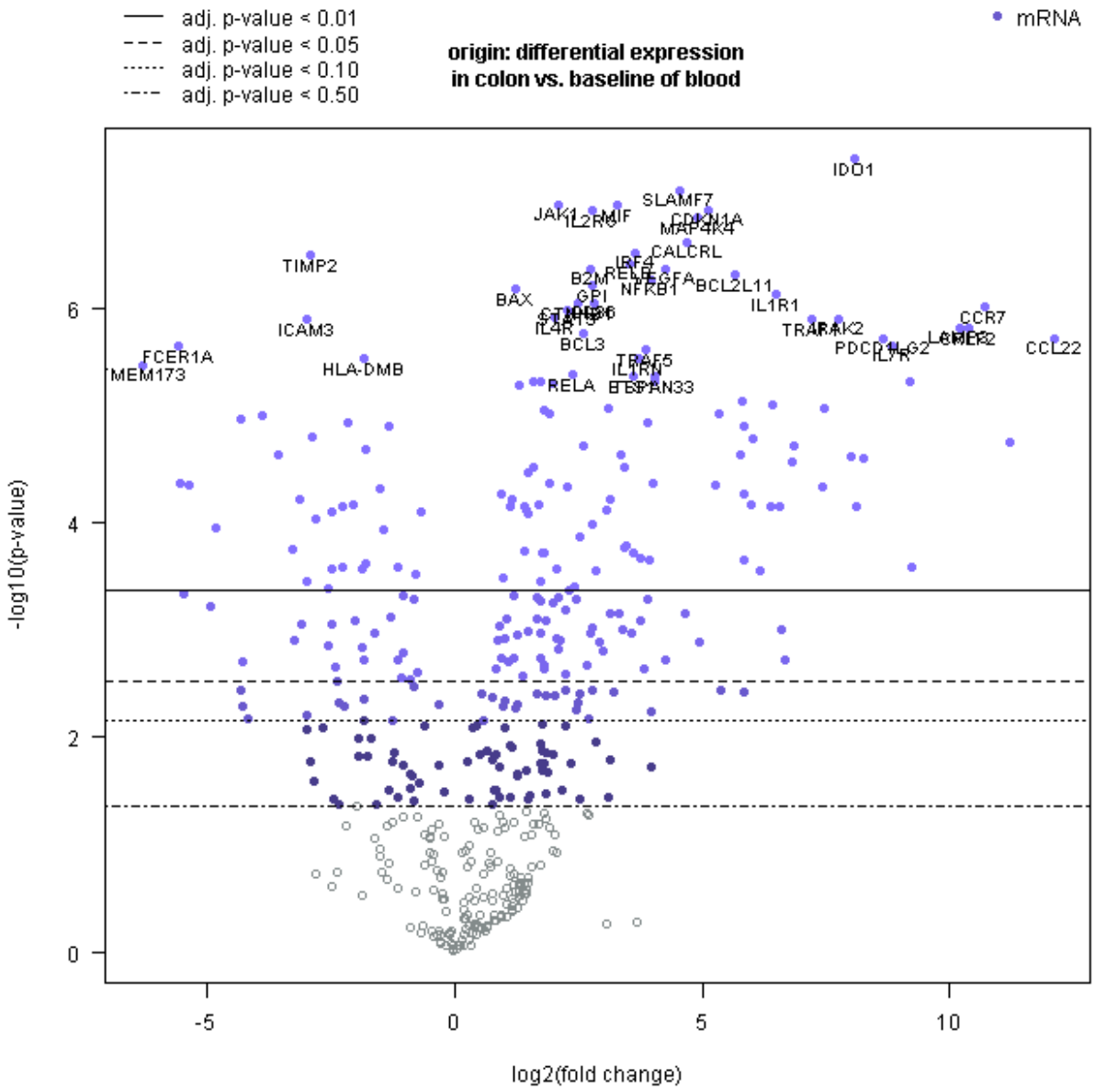

Fig.R10: Volcano plot of mRNA nCounter® data from myeloid PBDCs (basis) vs LEL mDCs. This volcano plot shows the information for each gene on the dataset with its corresponding log2 fold change value on the X-axis and the corresponding –log10 p-value on the Y-axis. Horizontal lines indicate p-value cutoffs (values according to the upper legend). Genes at the top are highly significant. Genes that fall to either side from 0 are differentially expressed.

Symbol	Entrez gene name	probe.ID	Linear fold change	p-value	Location	Type(s)
CCL22	C-C motif chemokine ligand 22	NM_002990.3	4460	1,93E-06	Extracellular Space	cytokine
MMP12	matrix metallopeptidase 12	NM_002426.3	2360	1,77E-05	Extracellular Space	peptidase
CCR7	C-C motif chemokine receptor 7	NM_001838.2	1670	9,90E-07	Plasma Membrane	G-protein coupled receptor
CRLF2	cytokine receptor like factor 2	NM_022148.3	1360	1,55E-06	Plasma Membrane	transmembrane receptor
LAMP3	lysosomal associated membrane protein 3	NM_014398.3	1170	1,52E-06	Plasma Membrane	other
MMP7	matrix metallopeptidase 7	NM_002423.3	602	2,60E-04	Extracellular Space	peptidase
CXCL8	C-X-C motif chemokine ligand 8	NM_000584.2	583	4,79E-06	Extracellular Space	cytokine
IL7R	interleukin 7 receptor	NM_002185.2	452	2,22E-06	Plasma Membrane	transmembrane receptor
PDCD1LG2	programmed cell death 1 ligand 2	NM_025239.3	400	1,91E-06	Plasma Membrane	enzyme
IL2RA	interleukin 2 receptor subunit alpha	NM_000417.1	307	2,47E-05	Plasma Membrane	transmembrane receptor
ANGPTL4	angiopoietin like 4	NR_104213.1	277	7,10E-05	Extracellular Space	other
IDO1	indoleamine 2,3-dioxygenase 1	NM_002164.3	272	4,10E-08	Cytoplasm	enzyme
EBI3	Epstein-Barr virus induced 3	NM_005755.2	259	2,43E-05	Extracellular Space	cytokine
IRAK2	interleukin 1 receptor associated kinase 2	NM_001570.3	216	1,25E-06	Plasma Membrane	kinase
ENO2	enolase 2	NM_001975.2	179	8,77E-06	Cytoplasm	enzyme
CD80	CD80 molecule	NM_005191.3	174	4,68E-05	Plasma Membrane	transmembrane receptor
TRAF1	TNF receptor associated factor 1	NM_005658.3	150	1,28E-06	Cytoplasm	other
SOCS2	suppressor of cytokine signaling 2	NM_003877.3	117	1,95E-05	Cytoplasm	other
CCL24	C-C motif chemokine ligand 24	NM_002991.2	113	2,69E-05	Extracellular Space	cytokine
IL23A	interleukin 23 subunit alpha	NM_016584.2	101	1,92E-03	Extracellular Space	cytokine
CCL19	C-C motif chemokine ligand 19	NM_006274.2	96,5	1,01E-03	Extracellular Space	cytokine
CD274	CD274 molecule	NM_014143.3	95,5	7,15E-05	Plasma Membrane	enzyme
IL1R1	interleukin 1 receptor type 1	NM_000877.2	89,6	7,57E-07	Plasma Membrane	transmembrane receptor
TNFRSF11A	TNF receptor superfamily member 11a	NM_003839.2	86,2	8,02E-06	Plasma Membrane	transmembrane receptor
RAMP1	receptor activity modifying protein 1	NM_005855.2	84,7	7,04E-05	Plasma Membrane	transporter
TNFRSF4	TNF receptor superfamily member 4	NM_003327.2	72,4	2,81E-04	Plasma Membrane	transmembrane receptor
STAT4	signal transducer and activator of transcription 4	NM_003151.2	64,2	1,65E-05	Nucleus	transcrition regulator
LAD1	ladinin 1	NM_005558.3	63,5	6,71E-05	Extracellular Space	other
CLCF1	cardiotrophin like cytokine factor 1	NM_013246.2	58,1	1,28E-05	Extracellular Space	cytokine
TNFRSF9	TNF receptor superfamily member 9	NM_001561.4	57,5	5,40E-05	Plasma Membrane	transmembrane receptor

Table R11: List of the 30 most upregulated genes from the nCounter® mRNA analysis. This list shows the 30 most upregulated genes from the nCounter® mRNA analysis from colonic LEL mDCs versus peripheral blood mDCs. The list is ordered from highest to lowest expression fold change value.

Symbol	Entrez gene name	probe.ID	Linear fold change	p-value	Location	Type(s)
TMEM173	transmembrane protein 173	NM_198282.1	-79,3	3,42E-06	Cytoplasm	other
FCER1A	Fc fragment of IgE receptor Ia	NM_002001.2	-47,8	2,29E-06	Plasma Membrane	transmembrane receptor
CD2	CD2 molecule	NM_001767.3	-45,9	4,34E-05	Plasma Membrane	transmembrane receptor
SELL	selectin L	NR_029467.1	-44,0	4,59E-04	Plasma Membrane	transmembrane receptor
IKBKAP	IkappaB Kinase Complex-Associated Protein	NM_003640.3	-41,1	4,51E-05	Nucleus	scaffold protein
CX3CR1	C-X3-C motif chemokine receptor 1	NM_001337.3	-30,7	6,09E-04	Plasma Membrane	G-protein coupled receptor
IL16	interleukin 16	NM_004513.4	-28,1	1,12E-04	Extracellular Space	cytokine
CSF3R	colony stimulating factor 3 receptor	NM_156038.2	-19,8	1,08E-05	Plasma Membrane	transmembrane receptor
CCND3	cyclin D3	NM_001760.2	-19,7	3,64E-03	Nucleus	kinase
MAP4K1	mitogen-activated protein kinase kinase kinase kinase 1	NM_007181.3	-19,6	5,06E-03	Cytoplasm	kinase
PTPRC	protein tyrosine phosphatase, receptor type C	NM_002838.4	-19,3	1,96E-03	Plasma Membrane	phosphatase
CCR2	C-C motif chemokine receptor 2	NM_001123041.2	-17,9	6,78E-03	Plasma Membrane	G-protein coupled receptor
S100A9	S100 calcium binding protein A9	NM_002965.2	-14,6	1,02E-05	Cytoplasm	other
IFI16	interferon gamma inducible protein 16	NM_005531.1	-11,9	2,35E-05	Nucleus	transctiption regulator
S100A8	S100 calcium binding protein A8	NM_002964.3	-9,6	1,74E-04	Cytoplasm	other
PTPN22	protein tyrosine phosphatase, non-receptor type 22	NM_015967.4	-9,3	1,25E-03	Cytoplasm	phosphatase
PTPN6	protein tyrosine phosphatase, non-receptor type 6	NM_002831.5	-8,8	6,18E-05	Cytoplasm	phosphatase
CD1D	CD1d molecule	NM_001766.3	-8,4	8,99E-04	Plasma Membrane	other
ICAM3	intercellular adhesion molecule 3	NM_002162.3	-7,9	1,28E-06	Plasma Membrane	transmembrane receptor
IFI35	Interferon Induced Protein 35	NM_005533.3	-7,9	6,26E-03	Nucleus	other
POU2F2	POU class 2 homeobox 2	NM_002698.2	-7,9	8,35E-03	Nucleus	transctiption regulator
CD36	CD36 molecule	NM_001001548.2	-7,9	3,50E-04	Plasma Membrane	transmembrane receptor
LILRA2	leukocyte immunoglobulin like receptor A2	NM_006866.2	-7,5	1,67E-02	Plasma Membrane	other
TIMP2	TIMP metallopeptidase inhibitor 2	NM_003255.4	-7,5	3,25E-07	Extracellular Space	other
ARHGDIB	Rho GDP dissociation inhibitor beta	NM_001175.4	-7,3	1,56E-05	Cytoplasm	enzyme
PYCARD	PYD And CARD Domain-Containing Protein	NM_013258.3	-7,2	2,61E-02	Cytoplasm	other
FCGRT	Fc fragment of IgG receptor and transporter	NM_004107.4	-6,9	9,18E-05	Plasma Membrane	transmembrane receptor
PTAFR	Platelet Activating Factor Receptor	NM_000952.3	-6,9	1,85E-01	Plasma Membrane	G-protein coupled receptor
TNFSF12	TNF Superfamily Member 12	NM_003809.2	-6,3	8,14E-03	Plasma Membrane	cytokine
IRF8	interferon regulatory factor 8	NM_002163.2	-5,8	4,15E-04	Nucleus	transctiption regulator

Table R12: List of the 30 most downregulated genes from the nCounter® mRNA analysis. This list shows the 30 most downregulated genes from the nCounter® mRNA analysis from colonic LEL mDCs versus peripheral blood mDCs. The list is ordered from lowest to highest expression fold change value.

Top Canonical Pathways			
Name	**p-value**	**Overlap**	
Th1 and Th2 Activation Pathway	2,54E-86	58,8%	90/153
Altered T and B Cell Signaling in Rheumatoid Arthritis	1,98E-68	80,6%	58/72
Neuroinflammation Signaling Pathway	7,25E-66	39,9%	89/223
T Helper Cell Differentiation	3,70E-65	83,1%	54/65
Th1 Pathway	5,02E-63	60,2%	65/108

Table R13: Top canonical pathways of LEL mDCs. This table shows the top 5 canonical pathways predicted to be active in LEL mDCs based on Ingenuity Pathway Analysis of the dataset of differentially expressed genes.

Top Diseases and Bio Functions		
Name	**p-value range**	**#Molecules**
Diseases and Disorders		
Inflammatory response	4,09E-02 – 3,24E-57	104
Infectious Diseases	4,09E-02 – 3,56E-26	29
Hematological Diseases	4,09E-02 – 2,93E-16	37
Immunological Disease	4,09E-02 – 2,93E-16	57
Cancer	4,09E-02 – 4,95E-10	9
Molecular and Cellular Functions		
Cellular Development	4,09E-02 – 3,57E-84	125
Cellular Growth and Proliferation	4,09E-02 – 3,57E-84	133
Cellular Function and Maintenance	4,09E-02 – 7,46E-66	71
Cellular Movement	4,09E-02 – 5,68E-64	67
Cell-to-Cell Signaling and Interaction	4,09E-02 – 3,24E-57	123
Physiological System Development and Function		
Hematological System Development and Function	4,09E-02 – 3,57E-84	201
Lymphoid Tissue Structure and Development	4,09E-02 – 3,57E-84	152
Immune Cell Trafficking	4,09E-02 – 5,68E-64	110
Cell-Mediated Immune Response	4,09E-02 – 1,10E-59	112
Embryonic Development	4,09E-02 – 7,11E-59	57

Table R14: Top diseases and bio functions of LEL mDCs. This table shows the top 5 diseases and disorders, molecular and cellular functions and physiological system developments and functions predicted to be active in LEL mDCs based on Ingenuity Pathway Analysis of the dataset of differentially regulated genes.

Top Networks		
ID	**Associated Network Functions**	**Score**
1	Hematological System Development and Function, Lymphoid Tissue Structure and Development, Tissue Morphology	15
2	Cell-to-Cell Signaling and Interaction, Hematological System Development and Function, Cellular Movement	15
3	Cell-to-Cell Signaling and Interaction, Cellular Development, Cellular Growth and Proliferation	15
4	Cellular Development, Cellular Growth and Proliferation, Hematological System Development and Function	14
5	Cell-mediated Immune Response, Cellular Development, Cellular Fucntion and Maintenance	9

Table R15: Top Networks of LEL mDCs. This table shows the top 5 associated network functions predicted to be active in LEL mDCs based on Ingenuity Pathway Analysis of the dataset of differentially regulated genes.

3.3.4 mRNA expression levels of IL-12 family subunits in LEL mDCs vs PBDCs

There are several promising drugs for IBD treatment targeting the IL-12 family of cytokines. Some of those drugs, like Ustekinumab (approved in 2009), are targeting the IL-12p40 protein subunit, which is one building block in each of the two heterodimeric cytokines IL-12 and IL-23. Therefore, targeting this specific subunit with Ustekinumab affects both cytokines (IL-12 and IL-23) likewise. Looking at the latest clinical trials regarding treatment options for patients with IBD, there are several therapeutic candidates which target specifically the IL-23p19 subunit of the IL-23 cytokine (IL-23 consists of IL-12p40 and IL-23p19). For instance the monoclonal antibodies Guselkumab or Risankizumab, amongst others, are promising treatment options against IBD (Kashani and Schwartz 2019).On the basis of these facts, it was interesting to see *IL23A*, the gene encoding for the IL-23p19 subunit, in the list of top upregulated genes regarding the analysis from LEL mDCs vs PBDCs (table R11). Two subunit mRNAs of the IL-12 family of cytokines, namely *IL23A* (IL-23p19) and *EBI3*, were markedly higher expressed in colonic LEL mDCs compared to minimal amounts in PBDCs (Fig.R17).

The IL-12 family is a group of heterodimeric cytokines which can form different interleukins due to the ability of a chain pairing promiscuity (Vignali and Kuchroo 2012). There are three alpha chains (p19, p28 and p35) and two beta chains (p40 and EBI3). One alpha chain member binds to one beta chain member building a heterodimer, which makes six possible combinations in total for the IL-12 family of cytokines. Four of those combinations have been known for years, namely: IL-12 (p35 + P40), IL-23 (p19 + p40), IL-27 (p28 + EBI3) and IL-35 (p35 + EBI3) (table R16) (Vignali and Kuchroo

2012). The two missing combinations are IL-39, which consists of the subunits p19 and EBI3, and the combination of p28 and p40 which was referred to as IL-Y, both cytokines which have been described only recently (table R16)(Xiaoqian Wang et al. 2016; Flores et al. 2015).

Remarkably, the mRNAs of the IL-12 family subunits IL-23p19 (*IL23A*) and EBI3 (*EBI3*) were strongly expressed in LEL mDCs, whereas only minor transcript levels of IL-12p40 (*IL12B*), IL12p28 (*IL27*) and IL-12p35 (*IL12A*) were detectable in this cell population. This observation prompted us to investigate whether IL-39 is produced by intestinal mDCs in inflammation, as this mediator could significantly determine inflammatory responses and their modulation by anti-IL-23 therapeutic antibodies. By the time of this discovery there were only two publications observing the combination of IL-23p19 and EBI3, and none of those with respect to intestinal tissues (Ramnath et al. 2015; Xiaoqian Wang et al. 2016).

IL-12 family of cytokines – heterodimer pairing				
		α-chains		
		p19	**p28**	**p35**
β-chains	**p40**	IL-23	IL-12	IL-Y
	EBI3	IL-39	IL-27	IL-35

Table R16: Heterodimer pairing of IL-12 family cytokine subunits. This table shows the different subunits of the IL-12 cytokine family and their respective binding partners resulting in the formation of a variety of different interleukins (Vignali and Kuchroo 2012; Xiaoqian Wang et al. 2016; Flores et al. 2015).

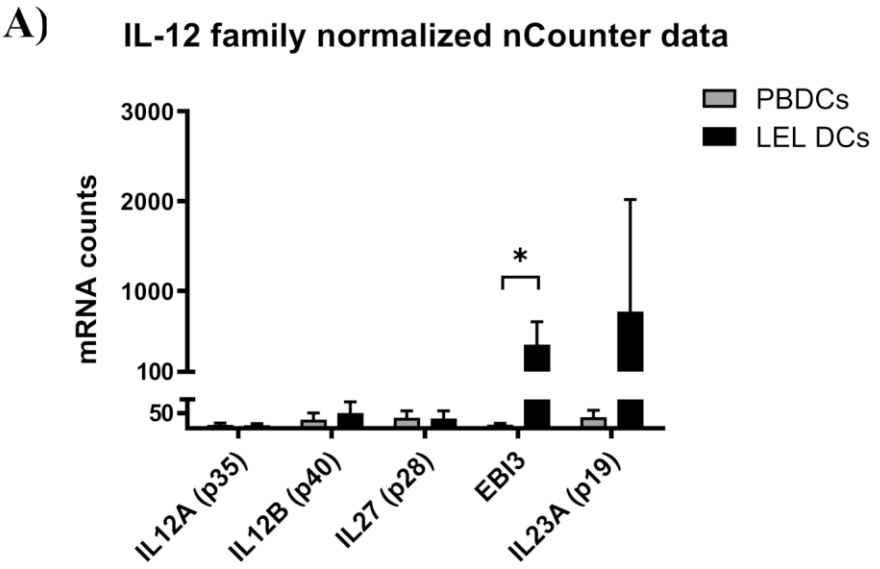

	PBDCs		LELDCs	
	Mean	SD	Mean	SD
IL12A (p35)	11,75	5,91	11	4,70
IL12B (p40)	29	21,68	51,25	36,18
IL27 (p28)	35	22,55	33	25,39
EBI3	13	3,74	404,75	253,02
IL23A (p19)	37,25	22,81	771	1247,70

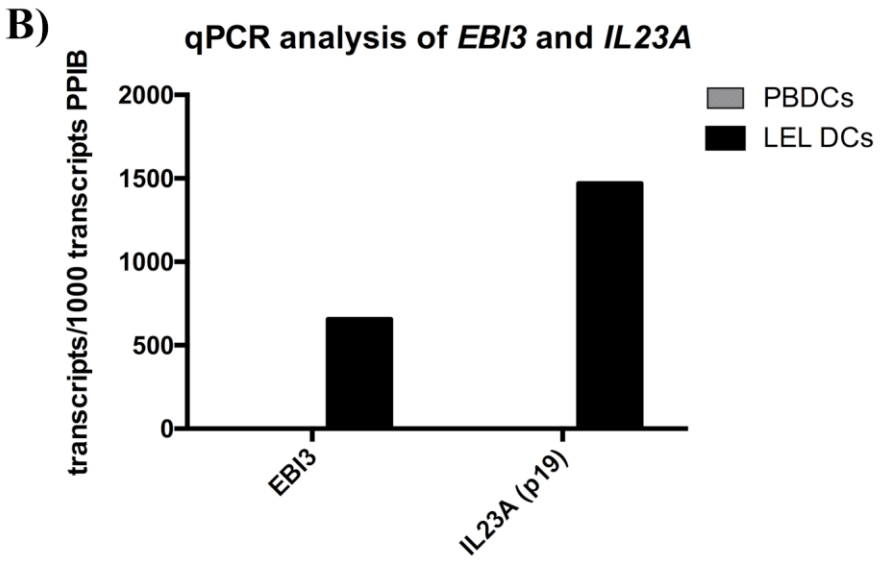

Fig.R17: qPCR and nCounter® mRNA analysis of IL-12 family cytokine subunits. Depicted is the number of mRNA counts from the nCounter® analysis for the different IL-12 cytokine family subunits from mDCs of four blood donors and LEL mDCs from four patients (A). Additional qPCR analysis data from the mDCs of two blood donors and LEL mDCs from one patient were acquired for *EBI3* and *IL23A* (B).

3.4 Protein expression of the IL-12 family members in LEL mDCs and PBDCs

In order to confirm the upregulation of the proteins EBI3 and IL-23p19, as observed via the gene expression data in Fig.R17, protein expression levels from lysed LEL mDCs vs PBDCs were analyzed via SDS-PAGE. As shown in figure R18, the protein expression of EBI3 and IL-23p19 were substantially higher expressed in LEL mDCs compared to PBMCs. The blot displays bands from proteins of dendritic cells from one colonic resection and one voluntary blood donor. As a loading control for equal cell numbers, histone H4 levels were also assessed. Cell lysates from K562 cells (Fig.R18 A, lane 3) and Raji cells (Fig.R18 B, lane 6) were used as positive controls for EBI3 and IL-23p19 expression respectively. In figure R18 A, lane 1 was loaded with 160.000 PBDCs and lane 2 with 130.000 LEL mDCs. The difference in loaded cells is represented by the histone H4 bands showing an approximately 16,5% lower intensity for the colonic LEL mDCs (Fig.R18 A, lane 2). The expression level of EBI3 at ~25kDa was approximately 75,4% higher in colonic LEL mDCs (Fig.R18 A, lane2) compared to PBDCs (Fig.R18 A, lane 1). The K562 cell lysate control showed a band at the same size as EBI3 (~25kDa) (Fig.R18 A, lane3). (The K562 lysate was loaded twice in adjacent pockets and shows therefore 2 bands in lane 3.)

In figure R18 B, lane 4 was loaded with 200.000 PBDCs and lane 5 with 170.000 LEL mDCs. The histone H4 analysis shows an approximately 1,3% higher band intensity for the PBDCs from lane 4 (Fig.R18 B). The expression level of IL-23p19 at ~20kDa was approximately 90,2% higher in colonic LEL mDCs (lane 5) compared to PBDCs (lane 4) (Fig.R18 B). Unexpectedly, the Raji cell lysate showed no respective band for the IL-23p19 control (Fig.R18 B, lane 6). According to the *European Molecular Biology Laboratories Bioinformatics Institute* (EMBL-EBI) database, Raji cells have an expression value of 3 transcripts per million (TPM) of *IL23A* mRNA (www.ebi.ac.uk).Therefore, as an additional clarification for the reliability of the used antibodies for protein detection, a certain amount of recombinant EBI3 and IL-23p19 protein was detected in figure R18 C by the same antibodies used in figure R18 A & B. Densitometric band analysis results for figures R18 A & B are displayed in figure R18 D.

The experiment was done three times and in all three cases the amount of EBI3 and IL-23p19 was elevated or exclusively expressed in dendritic cells under inflammatory conditions from the LEL model, compared to the dendritic cells from blood donors which represent a more quiescent state.

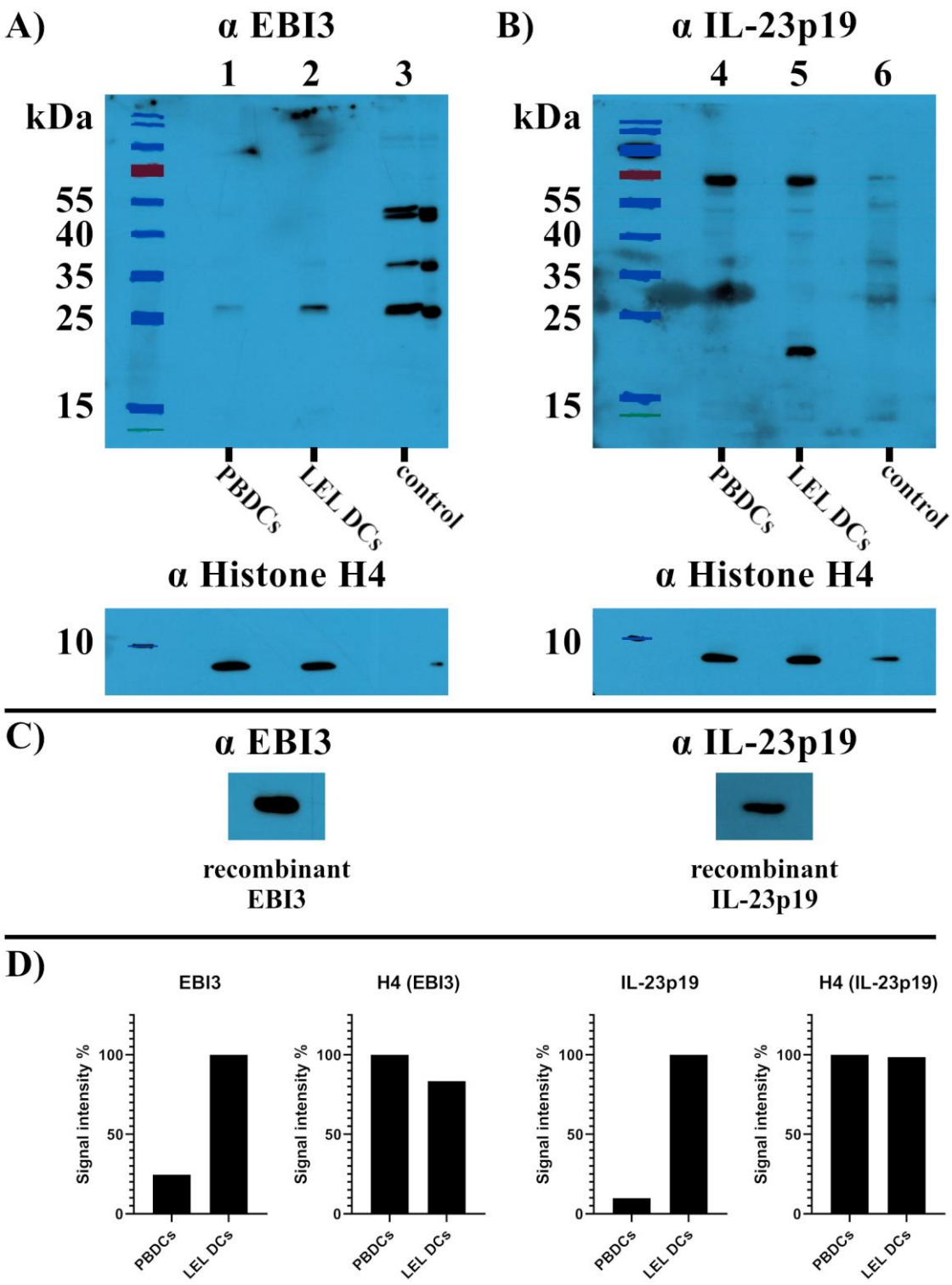

Fig.R18: Protein expression of EBI3 and IL-23p19 in PBDCs vs LEL mDCs. 160.000 blood mDCs (lane 1) and 130.000 colonic LEL mDCs (lane 2) were tested for protein expression of EBI3 (approx. 25.4kDa) (A). 200.000 PBDCs (lane 4) and 170.000 LEL mDCs (lane 5) were tested for protein expression of IL-23p19 (approx. 20.7kDa) (B). K562 (A, lane 3) and Raji (B, lane 6) cell lysates were used as controls for EBI3 and IL-23p19 expression respectively. Antibody validation was done with recombinant proteins for EBI3 and IL-23p19 (20µg each) (C). Section D shows the densitometric analysis of the blots from sections A and B. The results shown are

representative of three individual experiments performed with dendritic cells from three different individuals for each cell type (PBDC/LEL mDC).

According to the Nanostring nCounter® analysis, the amount of mRNA for the IL-12 family subunits p35, p40 and p28 was lower or at background levels compared to EBI3 & IL-23p19 in PBDCs as well as in LEL mDCs (Fig.R17). To test the protein expression levels of the IL-12 subunits, the blot from figure R18 A was incubated with antibodies against IL-12p35 (expected ~24,8kDa; Fig.R19 A), IL-12p40 (expected ~37,2kDa; Fig.R19 B) and IL-27A (expected ~27,5kDa; Fig.R19 C), with a preceding stripping step before each incubation. The functionality of each antibody was tested with the respective recombinant proteins (Fig.R19 D).The signals in lane 3 in figure R19 A and C are unspecifc bands staining the remaining K562 cell lysate. No tested IL-12 family subunit could be detected and all antibodies were able to detect their respective recombinant protein.

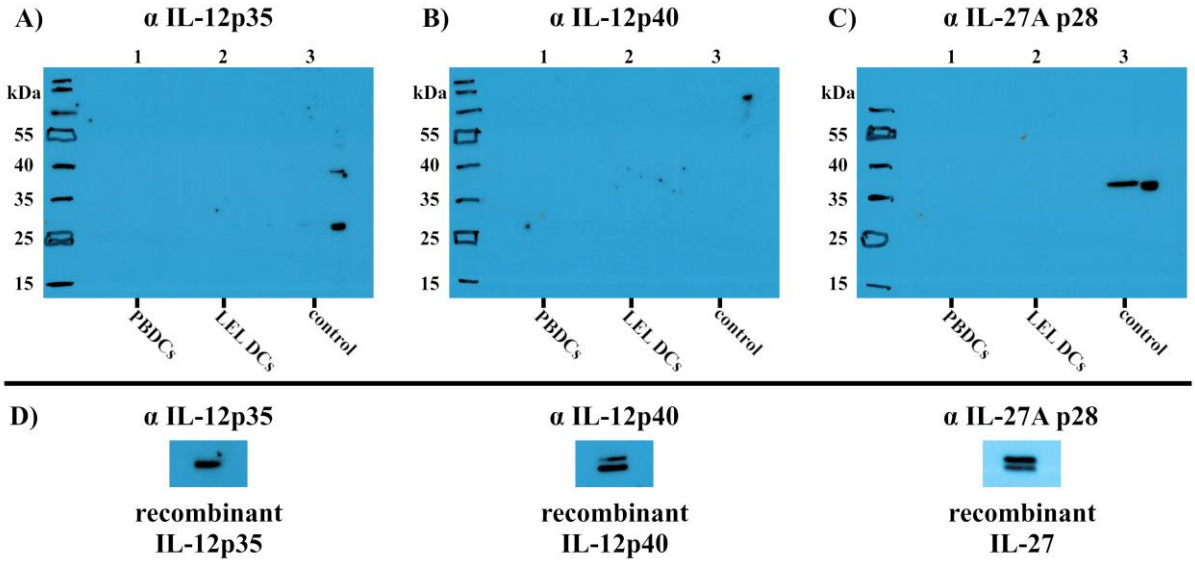

Fig.R19: Protein expression for the IL-12 subunit proteins p35, p40 and p28 in PBDCs vs LEL mDCs. The same blot from figure R18 A, with 160.000 PBDCs (lane 1), 130.000 colonic LEL mDCs (lane 2) and K562 cell lysate (lane 3) was incubated with antibodies against IL-12p35 (A), IL-12p40 (B) or IL-27p28 (C). Each antibody was additionally used to detect 50µg of each respective recombinant protein (D).

3.5 Co-Immunoprecipitation to assess the binding capacities between IL-23p19 and EBI3

In recent publications it was stated that the IL-12 family subunits IL-23p19 and EBI3 can interact with each other, forming a heterodimer cytokine termed IL-39 (Ramnath et al. 2015; Xiaoqian Wang et al. 2016). In order to proof that claim a co-immunoprecipitation (Co-IP) was performed with purified recombinant proteins. The aim of this experiment was to have antibody coupled beads which are directed against one specific protein but are able to retain a second protein through several washing steps due to the protein-protein interaction. For this purpose magnetic beads were coated with the mouse anti human IL-23p19r2 antibody (Fig.R20 A & B). The coated beads were then incubated with 1,5µg of recombinant (r)IL-23p19 (lanes 1 & 5), rEBI3 (lanes 2 & 6) or both together (1,5µg each; lanes 3 & 7)) in PBS. One sample of beads was only incubated with PBS (lanes 4 & 8) without any protein for background determination. The blot in figure R20 A was incubated with anti IL-23p19r2. It was possible to use the identical antibody for coating of the beads and detection of protein on the blotting membrane, because a HRP coupled anti rabbit heavy chain specific secondary antibody was used for detection. This approach ensured that only the heavy chain from the eluted antibody components at 50kDa are visible on the blot with no additional interference from the eluted light chain.

Lanes 1 (rIL-23p19) and 3 (rEBI3+rIL-23p19) in figure R20 A show a band between 20kDa and 25kDa, which represents the eluted rIL-23p19. Lane 1 (rIL-23p19) has a 36,1% stronger signal compared to lane 3 (rEBI3+rIL-23p19). As expected, there is no rIL-23p19 detectable in lane 2 (rEBI3) or 4 (control, PBS). The blot in figure R20 B was incubated with an antibody specific against EBI3. Lane 6 (rEBI3) and 7 (rEBI3+rIL-23p19) show a signal for EBI3 also between 20kDa and 25kDa. With both subunits present in lane 7 (rEBI3+rIL-23p19) the signal was 85,6% higher compared to lane 6 (rEBI3) which shows a slight background signal (Fig.R20 B). Lane 5 (rIL-23p19) and lane 8 (control, PBS) showed no bands at all after incubation with the EBI3 specific mAb (Fig.R20 B).

To assess the amount of unspecific bound proteins to the coated beads the experiment was repeated with isotype antibody coated beads (rabbit IgG MAB1050; figures R20 C & D). In figure R20 C no band is visible for rIL-23p19 in the lanes 1-4, which means that rIL-23p19 does not bind unspecifically to the beads. For rEBI3 in figure R20 D, there is a band visible in lane 6 (rEBI3) and 7 (rEBI3+rIL-23p19), whereas the band in lane 6 (rEBI3) is 35,4% stronger in comparison. This means that the beads are catching some rEBI3 but the amount is reduced when both protein subunits are present. Deduced from this data, the rEBI3 signal in figure R20 B lane 7 is due to the connection of rEBI3 and rIL-23p19. The densitometric analysis for the blots from figure R20 A, B and D are depicted in figure R20 E. The experiment was also performed with (1) cell culture supernatant from rEBI3 and rIL-23p19 double transfected HEK 293F cells, as well as (2) beads coated with a mAb against EBI3, both confirming the

observed results, and additionally showing a connection of both protein subunits after excretion from live cells (data not shown). Using purified recombinant proteins had two major advantages compared to the other approaches with recombinant cell culture supernatants. First, with purified proteins, interferences with other cell culture proteins could be ruled out. The second advantage was the ability to use defined amounts of the recombinant proteins. Overall this data showed that IL-23p19 and EBI3 are indeed forming a heterodimer in an extracellular space.

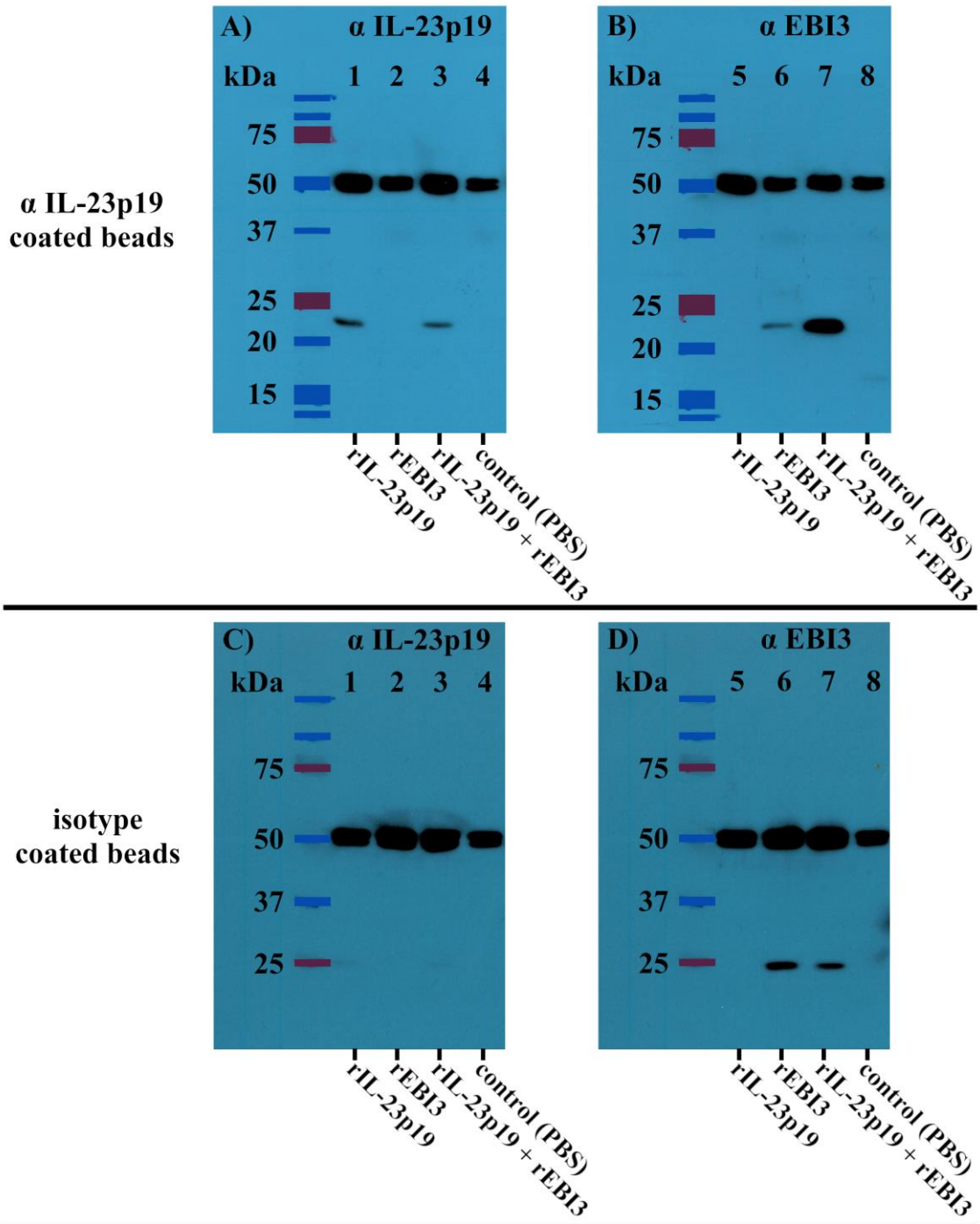
α IL-23p19 coated beads
A)
α IL-23p19
kDa
1 2 3 4
75
50
37
25
20
15
rIL-23p19
rEBI3
rIL-23p19 + rEBI3
control (PBS)
B)
α EBI3
kDa
5 6 7 8
75
50
37
25
20
15
rIL-23p19
rEBI3
rIL-23p19 + rEBI3
control (PBS)
isotype coated beads
C)
α IL-23p19
kDa
1 2 3 4
75
50
37
25
rIL-23p19
rEBI3
rIL-23p19 + rEBI3
control (PBS)
D)
α EBI3
kDa
5 6 7 8
75
50
37
25
rIL-23p19
rEBI3
rIL-23p19 + rEBI3
control (PBS)

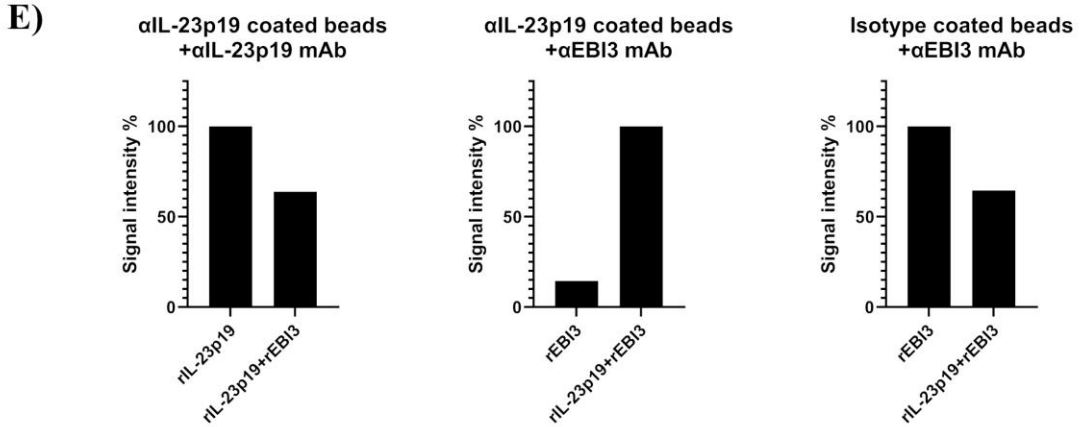
E)
αIL-23p19 coated beads
+αIL-23p19 mAb
Signal intensity %
100
50
0
rIL-23p19
rIL-23p19+rEBI3
αIL-23p19 coated beads
+αEBI3 mAb
Signal intensity %
100
50
0
rEBI3
rIL-23p19+rEBI3
Isotype coated beads
+αEBI3 mAb
Signal intensity %
100
50
0
rEBI3
rIL-23p19+rEBI3

Fig.R20: Co-Immunoprecipitation assay to assess the binding capacities between the proteins EBI3 and IL-23p19. Beads were coated with IL-23p19 specific antibodies (A, B) or with unspecific IgG as control (C, D). The beads were then incubated with recombinant (r) IL-23p19 (lanes 1, 5), recombinant (r) EBI3 (lanes 2, 6), rIL-23p19 + rEBI3 (lanes 3, 7) or PBS (lanes 4, 8). Immunoprecipitated proteins were detected with antibodies directed against IL-23p19 (A, C) or EBI3 (B, D). Section E shows the densitometric analysis from sections A, B and D. A heavy chain specific HRP coupled secondary antibody was used for detection to minimize eluation related antibody interferences. These blots are one representative experiment out of three.

3.6 Establishing a proximity ligation assay to detect IL-23p19 and EBI3 heterodimer formation inside cells

In order to determine whether the shown EBI3 + IL-23p19 interaction could be detected in a cellular environment, a proximity ligation assay (PLA) had to be established. The first step regarding this task was to identify suitable antibodies for immunohistostaining in order to use them later with the PLA.

3.6.1 Detection of IL-23p19 and EBI3 in cell culture via immunofluorescence staining

To find out which antibodies could be used for the PLA assay, HEK cells were either single transfected with plasmids encoding for the proteins IL-23p19 or EBI3, or double transfected with both plasmids simultaneously (more detailed information about the plasmid sequence is displayed in the appendix Figs.AX1/AX2). The transfected cells were then brought onto a microscope slide via the cytospin procedure. In single transfected HEK cells only the antibody specific for the transfected protein could elicit a signal (Fig.R21 A, D).Non-transfected HEK cells were also examined, serving as control cells. Neither IL-23p19 nor EBI3 could be detected in non-transfected cells (Fig.R22 A & B). In double transfected cells, IL-23p19 (Fig.R22 C) and EBI3 (Fig.R22 D) could be detected via the respective antibodies. A double staining with both primary antibodies showed that some cells expressed both proteins (Fig.R22 E; indicated by white arrows). These results show that immunohistochemical detection of EBI3 and IL-23p19 was possible with the antibodies EBI3r and IL-23p19m (antibodies are listet in table M1 (material & methods)).

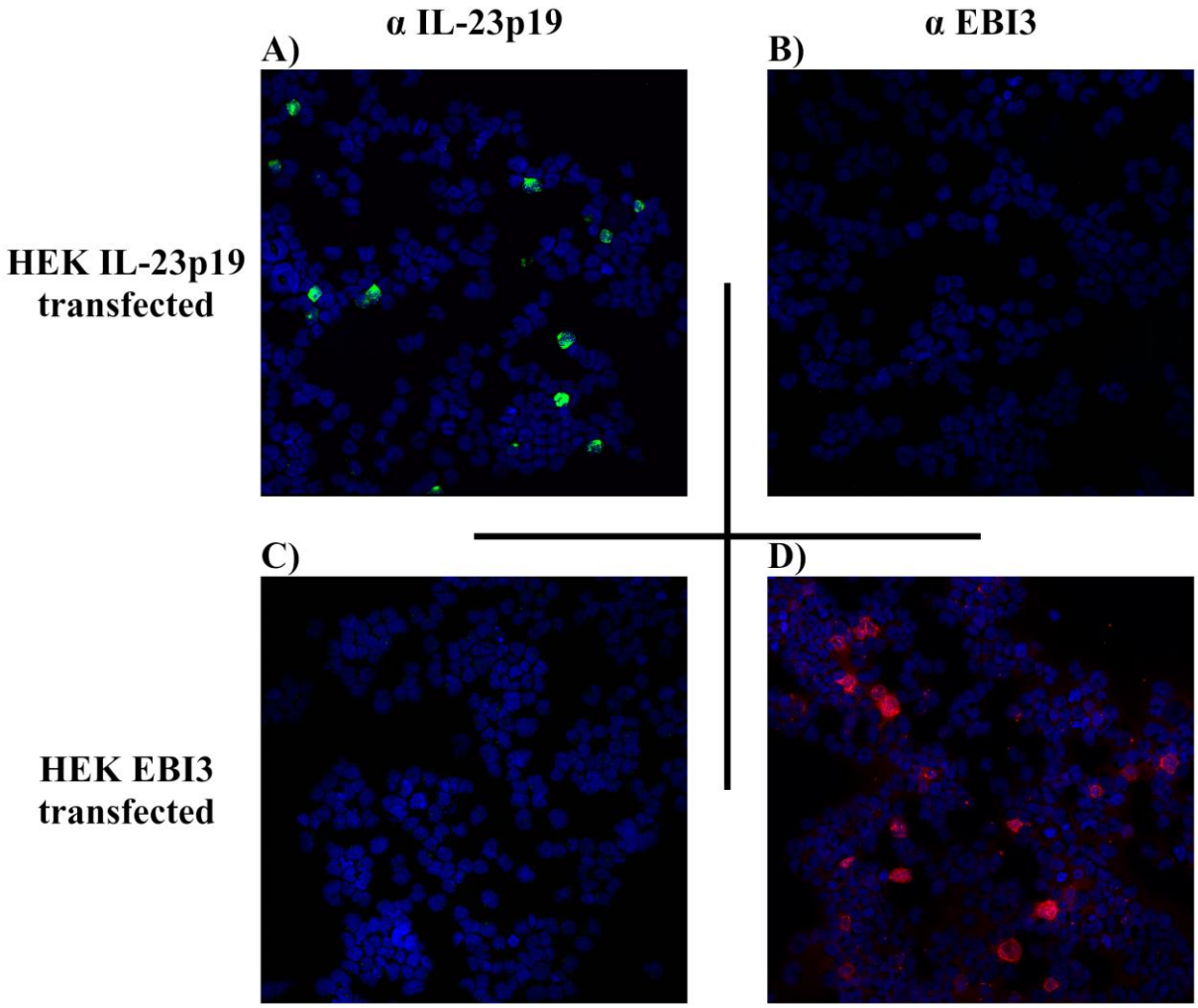

Fig.R21: Antibody specificity determination with single transfected HEK cells. HEK cells were either transfected with plasmids producing IL-23p19 (A, B) or EBI3 (C, D) and then incubated with monoclonal antibodies against IL-23p19 (A, C) or EBI3 (B, D).

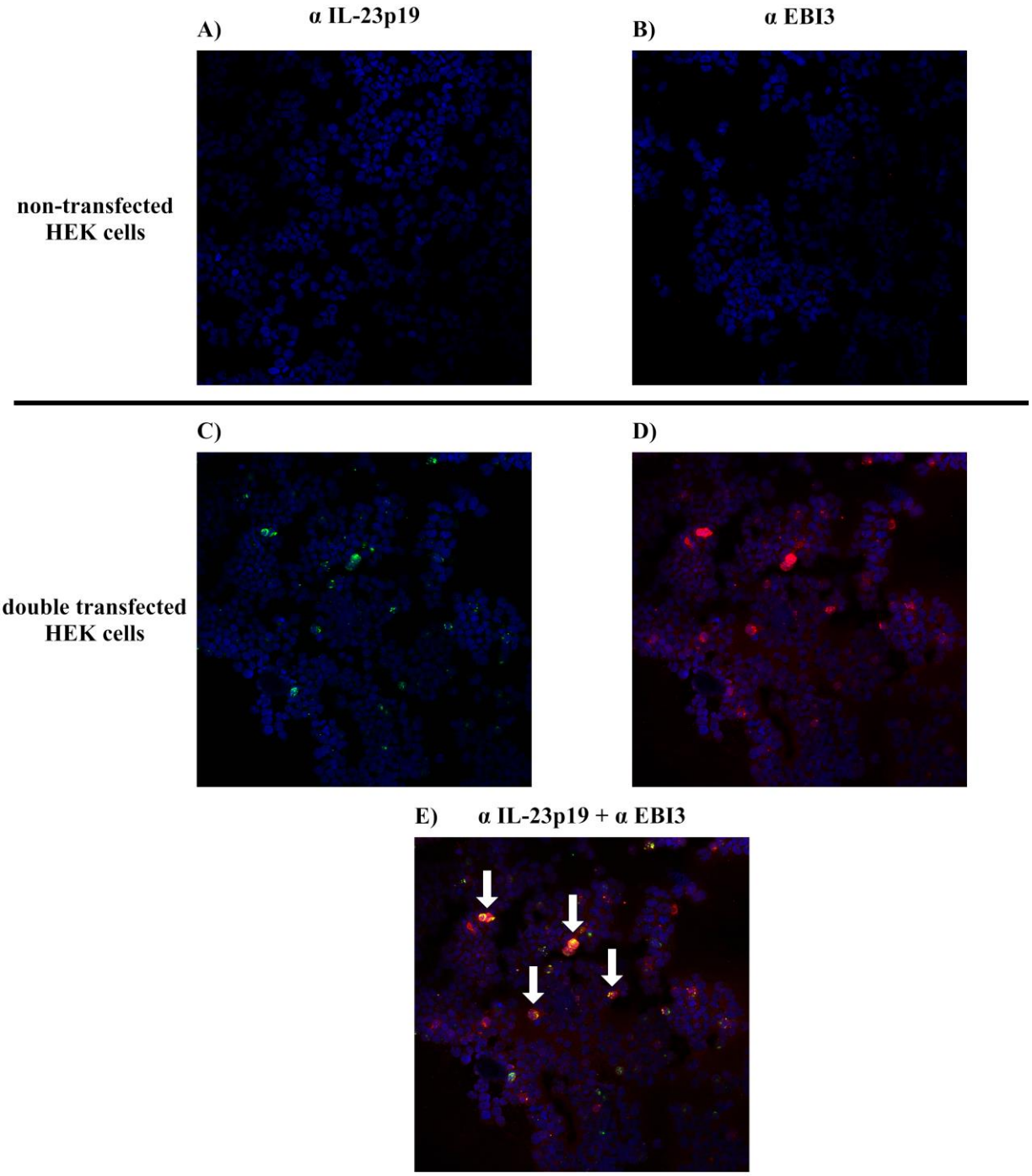

Fig.R22: Immunohistostaining of IL-23p19 and EBI3 in transfected HEK cells. HEK cells were either non-transfected (A, B) or double transfected with plasmids producing IL-23p19 and EBI3 (C, D, E). The cells were then cytospun onto microscope slides. Afterwards they were stained with antibodies directed against IL-23p19 (A, C; green), EBI3 (B, D; red) or both (E). White arrows mark cells which co-express EBI3 + IL-23p19 (E).

3.6.2 Proximity ligation assay for the detection of an IL-23p19/EBI3 heterodimer formation in cell culture cells

For assessment if there is an IL-23p19/EBI3 heterodimer formation in cell culture cells, a Duolink™ proximity ligation assay (PLA) was utilized. In this experiment the proteins EBI3 and IL-23p19 are detected by specific primary antibodies derived from different species (EBI3: rabbit; IL-23p19: mouse)(established in 3.6.1). Specialized PLA probes are then applied, which have an unique DNA sequence attached. The PLA probes, each one directed against the host species of one of the primary antibodies, are able to produce circular DNA, with the help of added enzymes, if the probes are a maximum of 40nm apart (Alam 2018). The produced DNA can then be stained with DNA specific fluorophores.

HEK cells were co-transfected with EBI3 and IL-23p19 encoding plasmids (figures R23 A & C). Control experiments comprised mock transfected cells (figures R23 B & D) as well as single transfections with EBI3 (Fig.R24 E) or IL-23p19 (Fig.R24 F) plasmids.

Further control experiments, assessing the PLA functionality, were made with double transfected HEK cells using only one primary antibody or using only one specialized PLA probe. In both cases no signals above background could be detected (data not shown).

An accumulation of red fluorescently stained DNA dots in cells could only be observed for the double transfected HEK cells with both primary antibodies and both PLA probes present (figures R23 A & C). Control transfections gave only a pattern of scattered red dots which are a normal background phenomenon of the PLA probes in the observed frequency (figures R23 B, D, & R24) (Jalili et al. 2018). This PLA experiment showed that the IL-12 family subgroups IL-23p19 and EBI3 are indeed able to form a heterodimer in cells under the employed conditions.

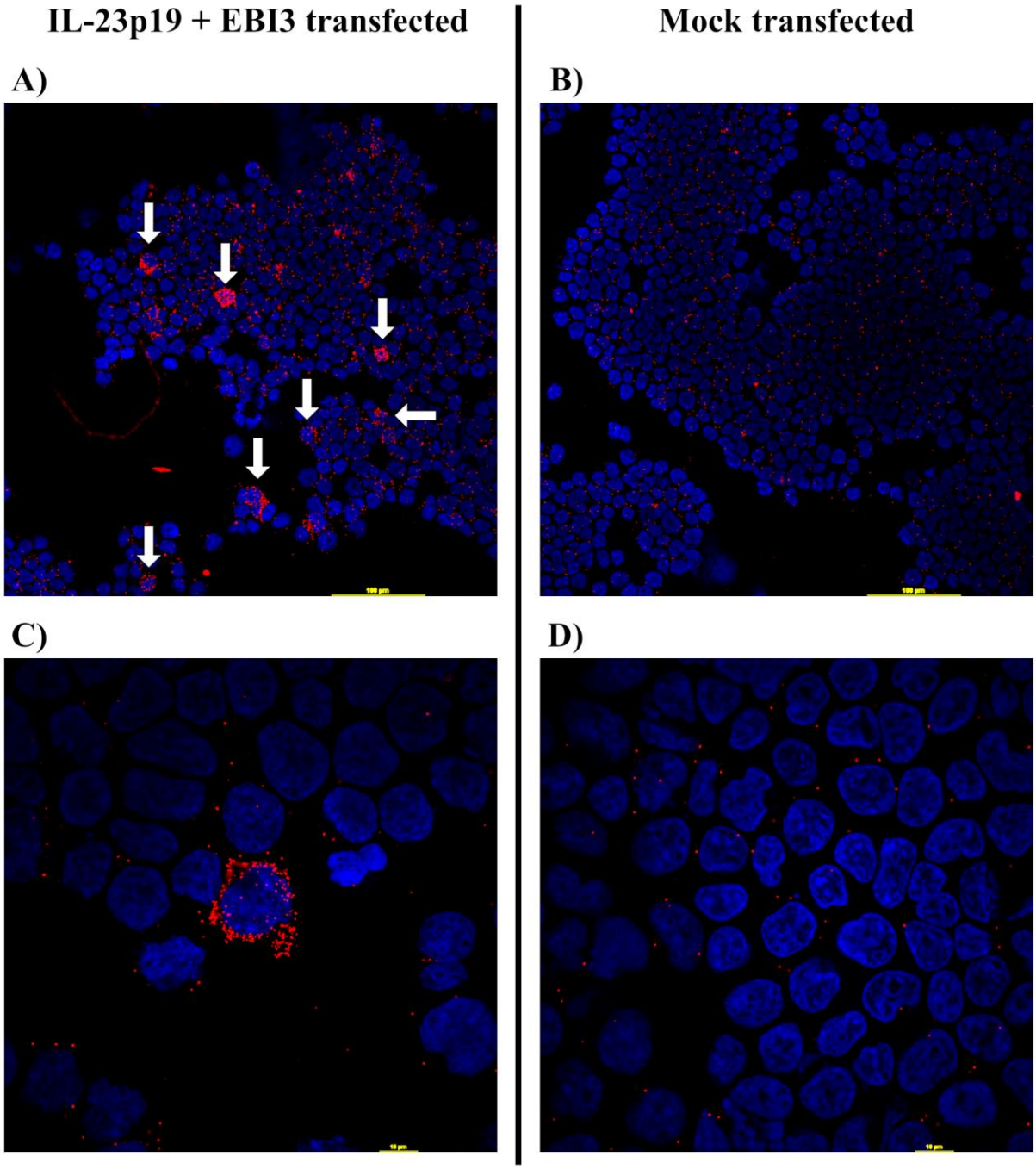

Fig.R23: Proximity ligation assay for IL-23p19 and EBI3 in transfected HEK cells. HEK cells were either double transfected with IL-23p19 + EBI3 (A, C) or as controls: mock transfected (B, D) or single transfected with either EBI3 (Fig.R24 E) or IL-23p19 (Fig.R24 F) plasmids. White arrows indicate accumulations of red fluorescent DNA dots where EBI3 and IL-23p19 proteins are interacting with each other due to close proximity (A). Control transfections show no accumulation of dots beyond a background signal (B, D; Fig.R24 E, F).

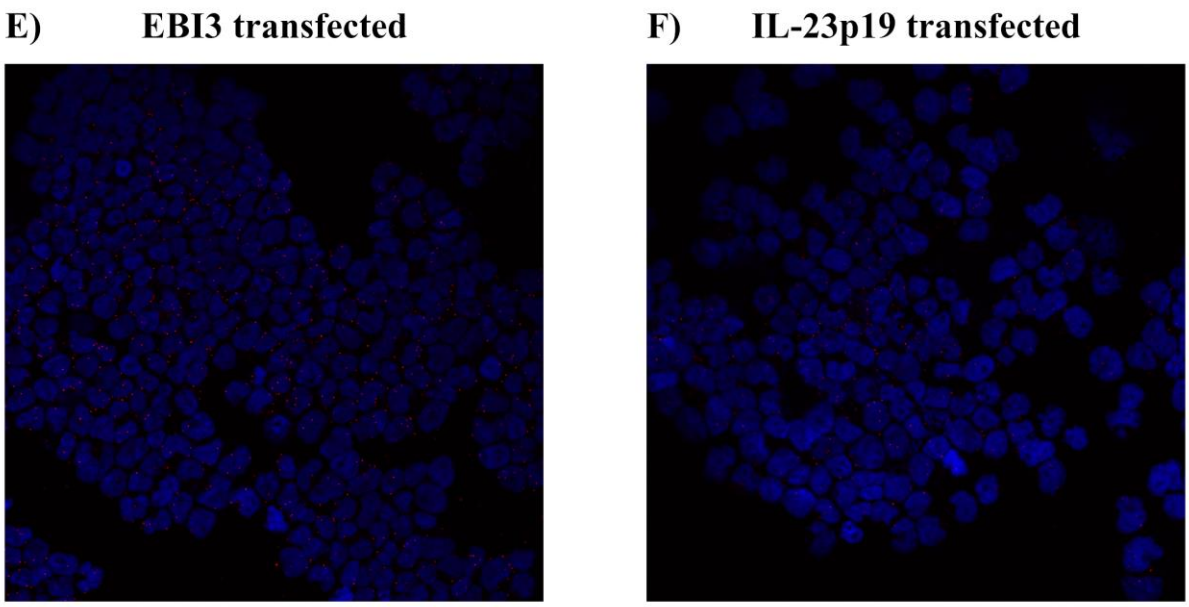

Fig.R24: Proximity ligation assay for IL-23p19 and EBI3 in single transfected cells. HEK cells were either transfected with EBI3 (E) or IL-23p19 (F), followed by a PLA against EBI3 + IL-23p19.

3.7 Analysis of heterodimer formation of IL-23p19 and EBI3 in LEL mDCs using PLA

Having successfully established the PLA technique in HEK cells, it was now applied to investigate the possible heterodimer formation of IL-23p19 and EBI3 in human LEL myeloid dendritic cells.

3.7.1 Immunohistostaining of IL-23p19 and EBI3 in human LEL mDCs

After the walk-out procedure, LEL mDCs were sorted and then cytospun onto a microscope slide. Subsequently, cells were stained with IL-23p19 and EBI3 specific antibodies (Fig.R25 D, E, F). To check if the secondary antibodies exhibit any unspecific binding and therefore generate a background signal, cells were incubated with only the secondary antibodies (Fig.R25 A, B, C.). Note that additionally to the normal block with DCS blocking buffer, cells had been incubated with an Fc block solution (Human BD Fc Block, BD Pharmingen, Cat#: 564220) prior to antibody incubation to inhibit possible Fc receptor binding activities. The stained mDCs from the patient showed a signal for the IL-23p19 antibody (Fig.R25 D) and for the EBI3 antibody (Fig.R25 E) in the same cells (Fig.R25 F). A nearly identical signal in terms of pattern and intensity could be detected for the control staining in which only the secondary antibodies had been applied (Fig.R25 A, B, C). The control staining showed a signal in the channel detecting the wavelength of 488nm (Fig.R25 A), 555nm (Fig.R25 B) and also an

overlay of both signals (Fig.R25 C). This means that the secondary antibodies are unspecifically bound to the LEL myeloid dendritic cells and it is therefore not possible to distinguish if any of the cells in figure R25 D, E, F, show a true staining. Repetition of the experiment with cells from another donor exhibited the same phenomenon (data not shown).

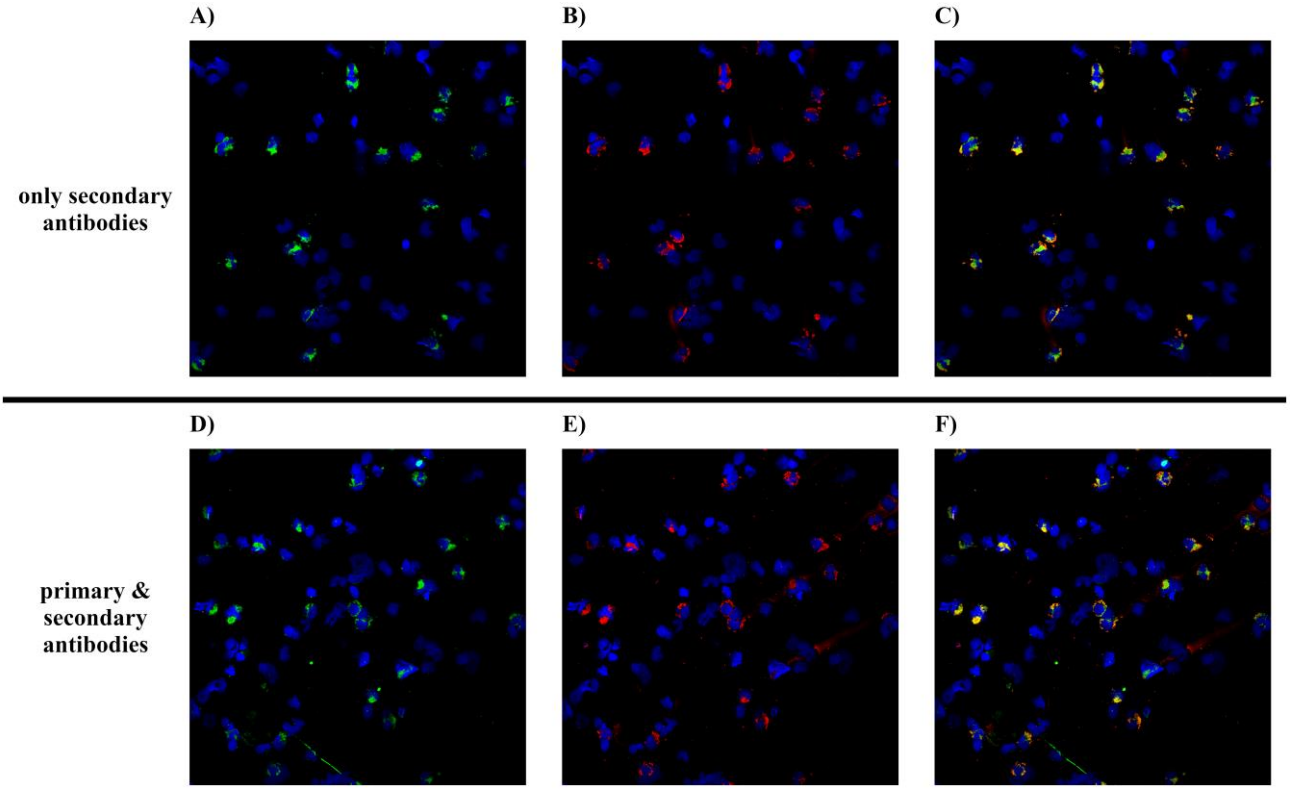

Fig.R25: Immunohistostaining against IL-23p19 and EBI3 in sorted LEL mDCs from patient material. Sorted LEL mDCs were cytospun on a microscope slide and then stained with either primary & secondary antibodies against IL-23p19 and EBI3 (D, E, F) or as a control with secondary antibodies only (A, B, C). The channels show a staining at 488nm (A, D, α IL-23p19), 555nm (B, E, α EBI3) or both wavelengths (C, F). The staining is representative for samples from two individual patients.

3.7.2 Proximity ligation assay for the detection of an IL-23p19/EBI3 heterodimer formation in LEL mDCs

Although the immunohistochemical staining was not successful in patient material, the proximity ligation assay experiment was performed with LEL mDCs analogous to the experiment in HEK cells (see 3.6.2). The main assumption was that the PLA uses specialized secondary antibodies which might not be bound unspecifically by the LEL mDCs. After a walk-out procedure LEL mDCs were cytospun onto a microscope slide and subjected to a PLA staining. As shown in figure R26, a

comparable PLA signal (red dots) could be detected for both setups, being either stained with secondary antibodies only (Fig.R26 A, C) as well as after a normal PLA procedure with primary and secondary antibodies (Fig.R26 B, D). This indicates again, that the secondary antibodies were bound unspecifically to some cells and produced a false positive PLA signal (Fig.R25 A; indicated by white arrows). It was not possible to verify the heterodimer formation of IL-23p19 and EBI3 in LEL mDCs using PLA technology.

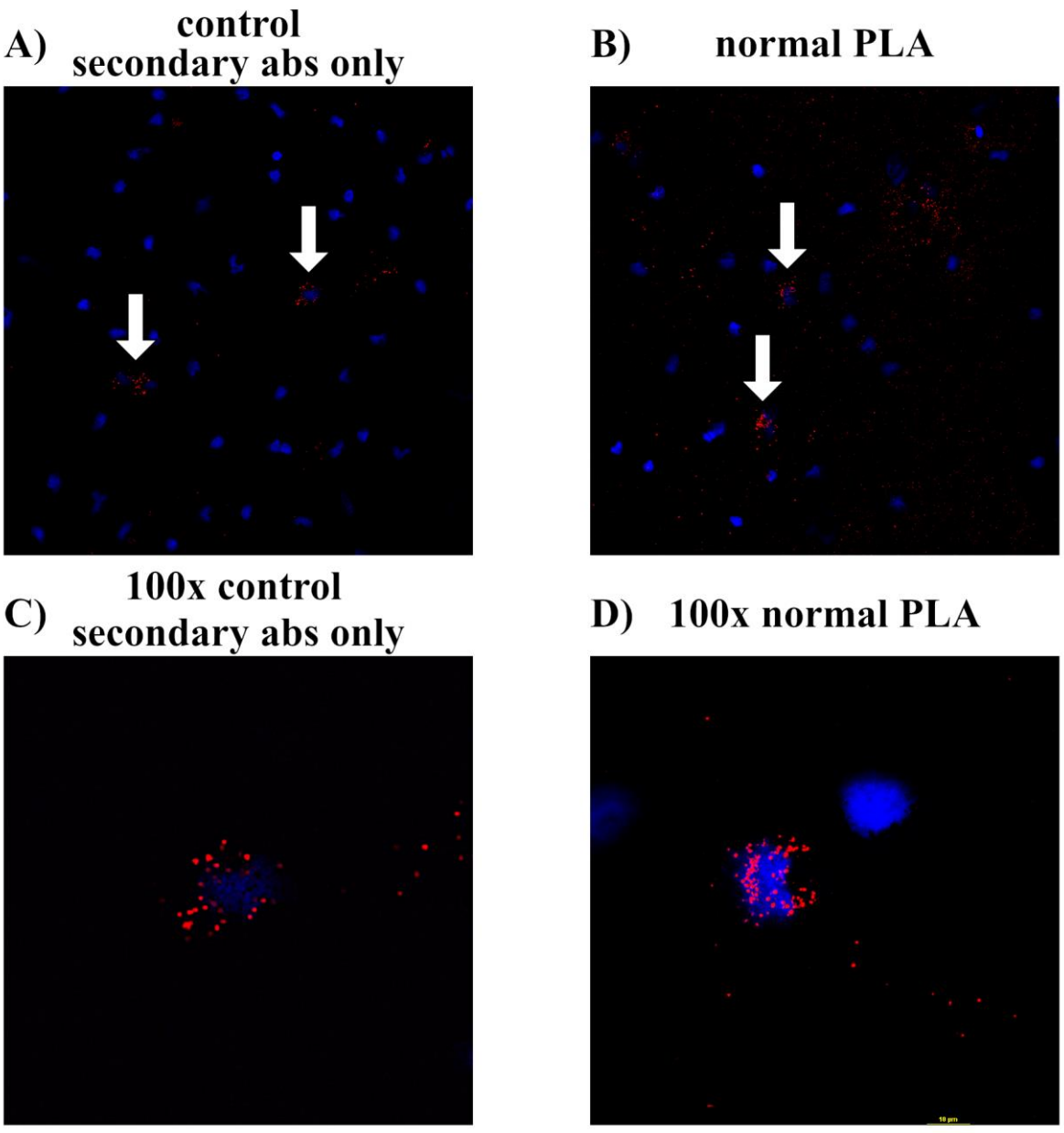

Fig.R26: Proximity ligation assay in LEL mDCs from patient material. Human LEL mDCs were cytospun onto a microscope slide and then tested for EBI3 + IL-23p19 heterodimer formation via PLA. The cells were either incubated with primary and secondary antibodies (B, D) or as a control with secondary antibodies only (A, C). Arrows indicate a positive PLA signal (A, B). Tiles C and D show cells at 100x magnification (A & B were 20x magnified). The staining is representative for samples from two individual patients.

3.8 Opal™ staining technique on colonic formalin fixed paraffin embedded (FFPE) histological slices of patient material

In parallel to the fluorescence analysis of IL-23p19 and EBI3 in LEL mDCs, the expression of both proteins in colonic tissue sections was investigated using the Opal™ multiplex immunofluorescence technology. With this technique it is possible to stain FFPE sections with antibodies of the same host species. Notably, in previous Opal™ tissue stainings, secondary antibodies were observed to have a very low to nonexistent background. Sections of colonic tissue were obtained at different time points during the LEL model and subjected to immunohistological analysis. The time points were: directly after surgery, acquiring complete mucosa (CM); after the third epithelial cell removal step (3.EDTA; (5 hours after CM)); and after 12 hours in culture medium (12h LEL; (17 hours after CM)). Thin slices of those FFPE blocks were produced followed by a staining with several antibodies against IL-23p19 and EBI3 (table M1 (material and methods)). As shown in Fig.R27, the IL-23p19 specific antibody stained epithelial cells and showed a low staining for some cells in the lamina propria in complete mucosa sections (Fig.R27 A, B1, B2). After the removal of epithelial cells, and therefore induction of an inflammatory response, the amount and signal intensity for IL-23p19 protein had risen in cells harbouring in the lamina propria by 9,7% overall (Fig.R28 A, B1, B2; Fig.R30). This trend was continued looking at cells in the lamina propria after 12 hours in culture, having 35,6% higher signal intensity compared to complete mucosa and 25,8% compared to the 3.EDTA time point (Fig.R29 A, B1, B2; Fig.R30). The control stainings did not reveal any unspecific signals at all three time points investigated (Figures R27-29 C, D1, D2). The EBI3 specific antibodies which were used in this experiment did not elicit a coherent or acceptable staining (data not shown). The pictures shown are representative for at least five different patient samples.

So far this experiment showed that IL-23p19 is expressed in epithelial cells and cells of the lamina propria. Moreover the intensity and amount of IL-23p19 signal in lamina propria cells was increased over time after the removal of epithelial cells.

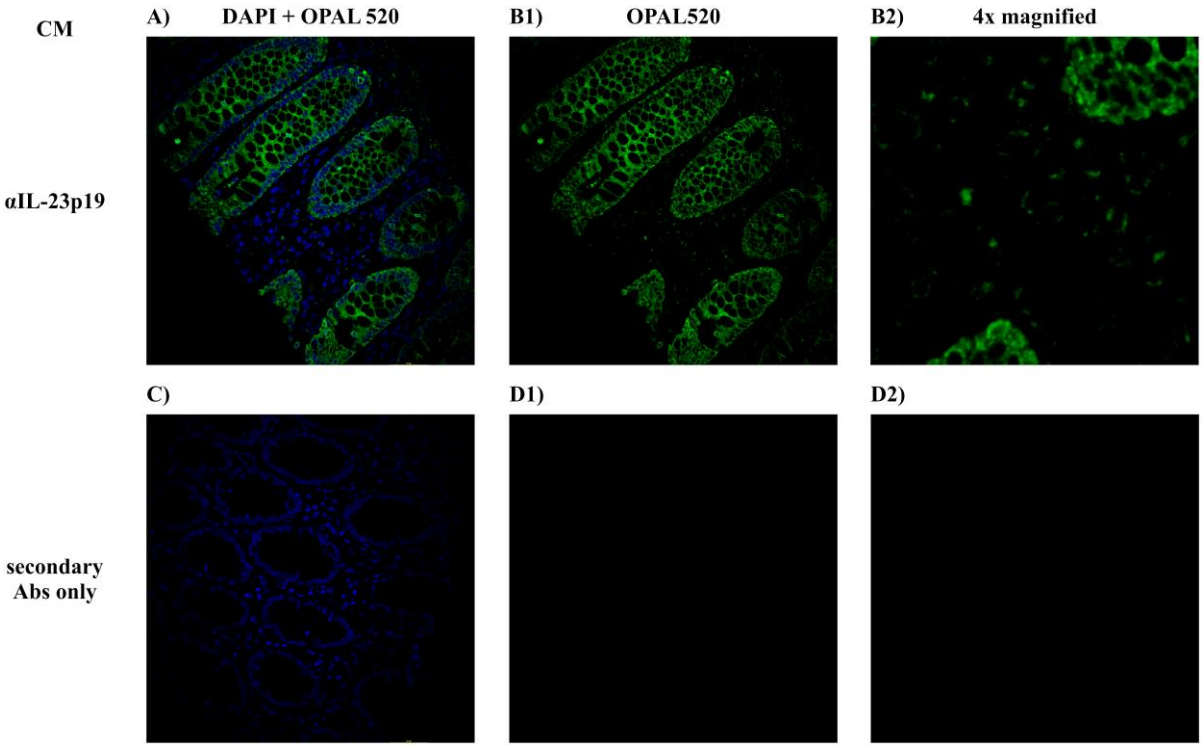

Fig.R27: IL-23p19 expression in the human intestinal mucosa under homeostatic conditions. FFPE sections of normal colonic mucosa were subjected to immunofluorescence staining using an anti IL-23p19 antibody and Opal™ technology (A, B1, B2). Control sections were only treated with secondary antibodies (C, D1, D2). The pictures show an overlay of DAPI and Opal 520 (A, C), only the Opal 520 signal (B1, D1) and a 4x magnification of the Opal 520 signal (B2, D2).

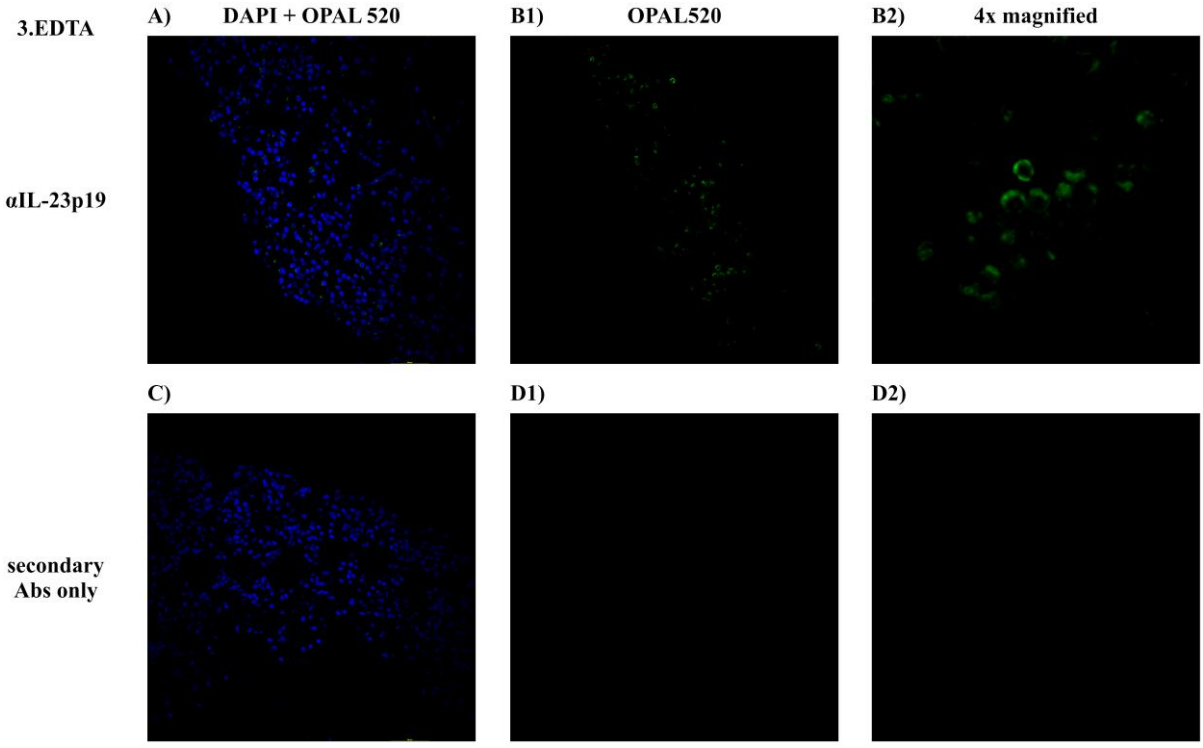

Fig.R28: IL-23p19 expression in lamina propria cells during the induction of an inflammatory response in the LEL model (3.EDTA; 5 hours after CM). FFPE sections of lamina propria tissue after the 3.EDTA step of the LEL model were subjected to immunofluorescence staining using an anti IL-23p19 antibody and Opal™ technology (A, B1, B2). Control sections were only treated with secondary antibodies (C, D1, D2). The pictures show an overlay of DAPI and Opal 520 (A, C), only the Opal 520 signal (B1, D1) and a 4x magnification of the Opal 520 signal (B2, D2).

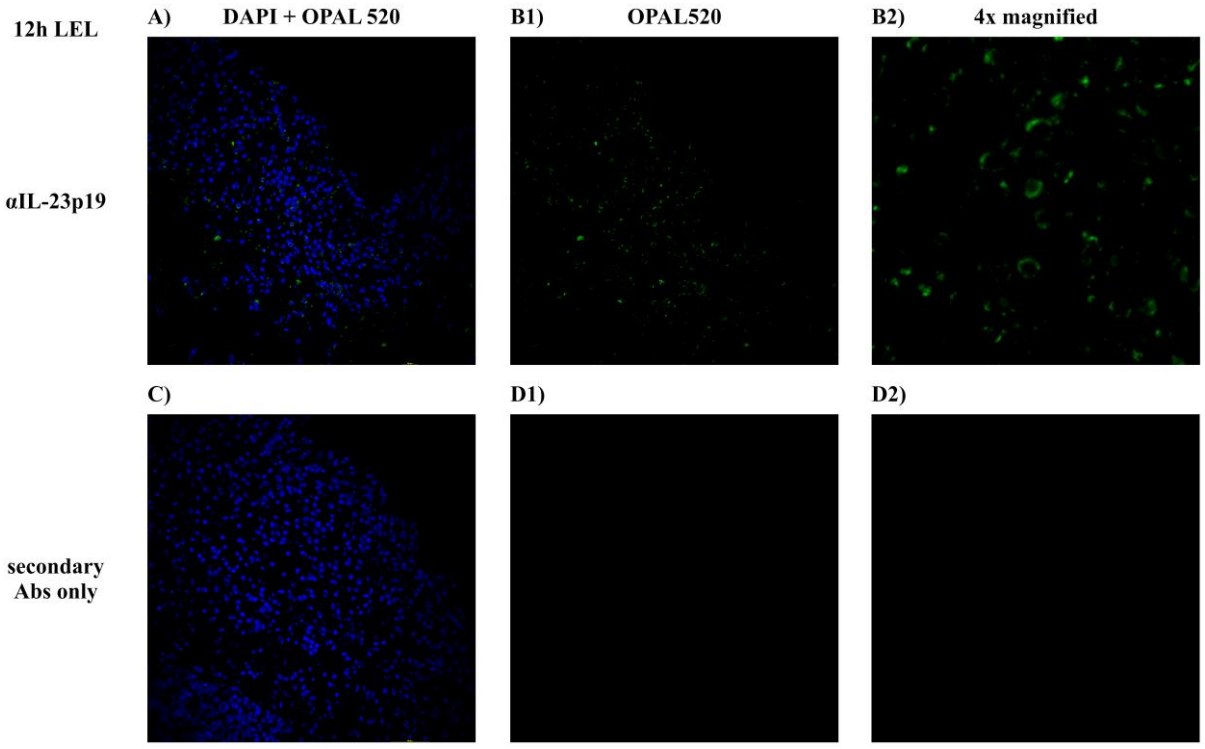

Fig.R29: IL-23p19 expression in lamina propria cells during induction of an inflammatory response in the LEL model (12h LEL; 17 hours after CM). FFPE sections of lamina propria tissue, incubated 12 hours in culture medium after the 3.EDTA step, were subjected to immunofluorescence staining using an anti IL-23p19 antibody and Opal™ technology (A, B1, B2). Control sections were only treated with secondary antibodies (C, D1, D2). The pictures show an overlay of DAPI and Opal 520 (A, C), only the Opal 520 signal (B1, D1) and a 4x magnification of the Opal 520 signal (B2, D2).

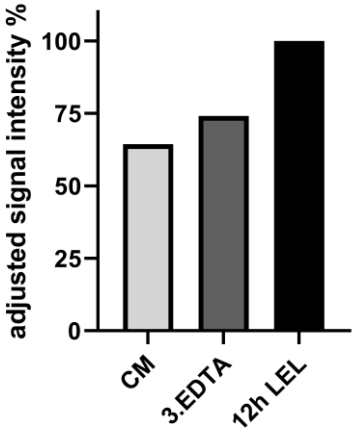

Fig.R30: IL-23p19 fluorescence signal intensities of Opal 520 stained tissue sections. Cell count and overall fluorescence intensity regarding IL-23p19 were calculated for an area of 50µm² of lamina propria for the samples from figures R27 (CM), R28 (3.EDTA) and R29 (12h LEL). The quotient of overall fluorescent signal per cell was calculated and is displayed as adjusted signal intensity %. The highest calculated value represents 100% signal intensity.

3.9 Sandwich ELISA development for the detection of IL-39 protein from patient samples

As an additional approach to investigate IL-39 formation by LEL mDCs, an enzyme linked immunosorbant assay (ELISA) would serve the purpose of IL-39 detection from LEL mDC lysates as well as organ culture supernatants. As commercial IL-39 ELISAs were not available, a sandwich ELISA method for detecting this heterodimeric cytokine needed to be developed. By using a capture antibody directed against one of the subunits and a detection antibody directed against the other subunit, it was intended to detect and quantify the heterodimer formation of IL-23p19 and EBI3. Therefore, the antibodies listed in table M1 (material and methods) were used in all possible combinations to establish a functioning sandwich ELISA. It was assessed whether or not these antibody combinations were able to specifically identify the IL-23p19/EBI3 heterodimer versus solutions containing only one of both subunits. For this purpose, lysates and cell culture supernatants of HEK cells transfected with either IL-23p19-V5 (Fig.AX2 (appendix)), or EBI3-Flag (Fig.AX1 (appendix)) or both plasmids were prepared and tested in the various ELISA configurations. Furthermore, the recognition of commercially available recombinant (r)IL-23p19 (OriGene, TP309680) and rEBI3 (Prospecbio, cyt367) as well as a mixture of both was analyzed by the different antibody combinations. Among the 16 antibody pairs tested, none could be identified to reliably detect the heterodimer only. As an example, figure R31 shows two combinations of capture (c) and

detection (d) antibodies, which are representative for other antibody combinations that elicited measurable signals above background. In figure R31 A, the capture antibody was directed against Ebi3 and the detection antibody against IL-23p19. Except for two samples, namely 1) non-transfected HEK cells (HEK SN), and 2) capture and detection antibodies without target proteins (c+d antibodies); every other sample showed a signal above background. Single transfected EBI3 HEK cell supernatant (ST HEK SN EBI3) and a mixture of single transfected IL-23p19 + single transfected EBI3 supernatant (ST SN Mix 1:1) showed a weak signal. Single transfected IL-23p19 (ST HEK SN IL-23p19), double transfected HEK cells (DT HEK SN) and recombinant EBI3 protein (rEBI3) gave a medium signal. The recombinant protein IL-23p19 (rIL-23p19) or a mixture of both recombinant proteins (rEBI3+rIL-23p19 1:1) exhibited very high signals. The fact that supernatants and samples, which contained only one of the two subunits gave higher or at least similar signal intensities compared to solutions containing both subunits means, that the experiment did not work as intended. The same is true for figure R31 B, where the capture and detection antibodies had switched places. Except for the supernatant from IL-23p19 single transfected HEK cells, every other sample was on a similar level in terms of signal intensity. There may be several causes which can lead to a false positive signal. For example, the capture antibody could bind unspecific to the other IL-39 protein subunit, the proteins could adhere to the ELISA plate or the secondary antibodies could show a species cross reactivity and bind to the capture antibody, amongst others. Several possibilities were explored in the following experiments.

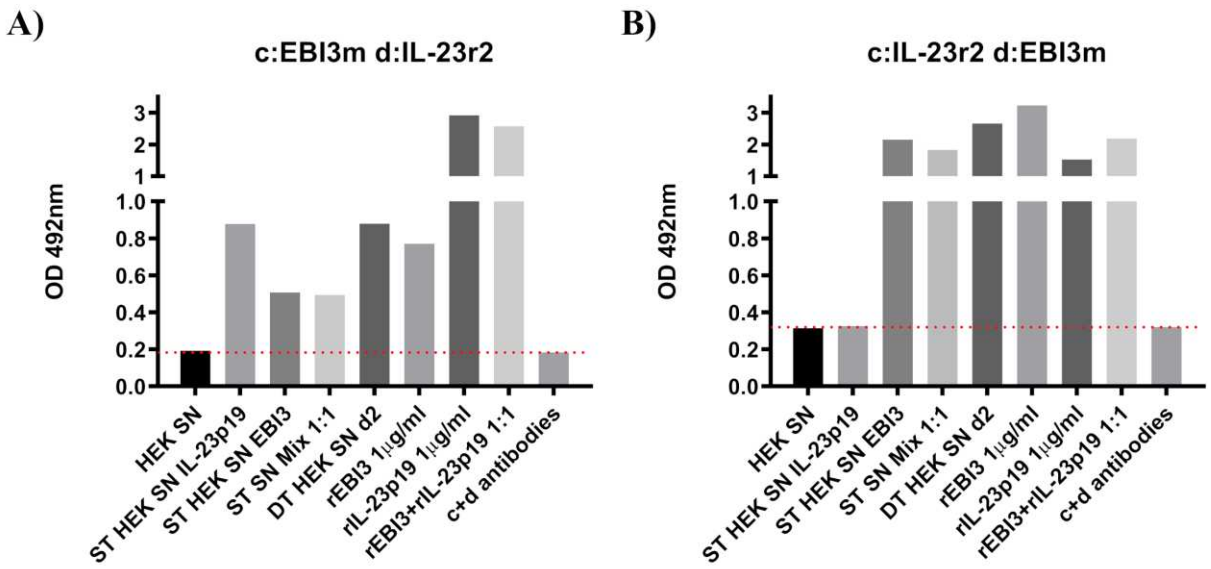

Fig.R31: Sandwich ELISA for the detection of IL-39 presence and amount. ELISA plates were coated with a specific antibody, incubated with protein and control solutions followed by an incubation of a detection

antibody and HRP coupled antibody directed against the host species of the detection antibody. The capture and detection couples were α EBI3m and α IL-23r2 respectively (A) and vice versa (B). The red dotted lines represent the background signal intensity at OD 492nm of samples containing capture and detection antibodies in PBS. ST, single transfected; DT, double transfected; r, recombinant protein; c+d, capture + detection antibodies.

3.9.1 Correlation between protein amount and signal intensity

In order to assess the effects of protein titration on the signal intensity in the IL-39 sandwich ELISA setup, a double transfected HEK cell supernatant containing EBI3 and IL-23p19 was tested. As seen in figure R32, the signal intensity is declining with every titration step. This means that the measured signal is correlating directly with the amount of detectedt proteins and not caused by any other component of the experiment.

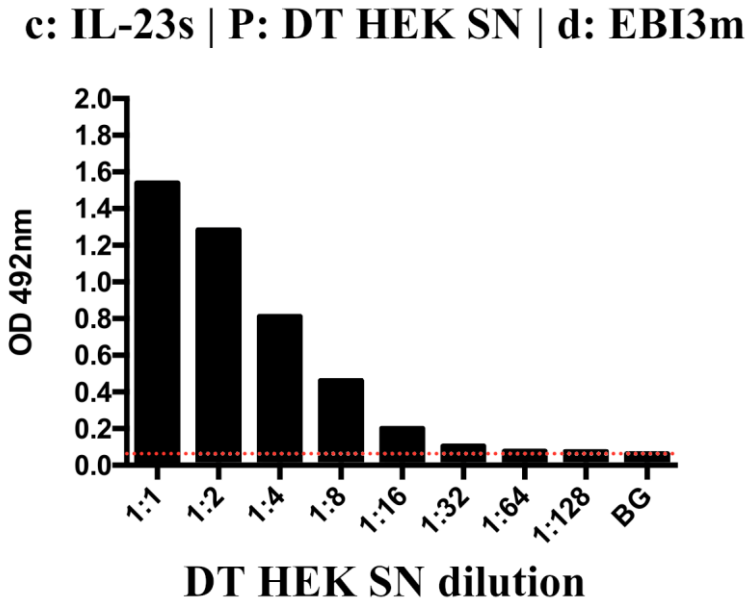

Fig.R32: Titration of double transfected HEK supernatant. The sandwich ELISA setup was used with declining concentrations of double transfected HEK cell supernatant. The signal intensity correlated with the amount of supernatant present in this serial dilution setup.

3.9.2 Influence of coating buffers on ELISA performance

There are different buffers available for the coating of the capture antibody on the ELISA plate. Some antibodies bind better to the plate in PBS (pH 7.4) while others yield better results with carbonate

buffer (pH 9.6) (Cuvelier et al. 1996). If the binding of capture antibody was only a partial of the maximum binding capacity of protein to the ELISA plate, it leaves possible space for unspecific binding of the target proteins. To rule out that the bad performance was due to an unsuitable binding buffer, a test was performed using either PBS or carbonate buffer for the incubation of the capture antibody. Figure R33 shows that there was no observable difference in signal intensity between coating with PBS or carbonate buffer. The very high false positive signal elicited by rEBI3 was unaltered no matter which coating buffer was used.

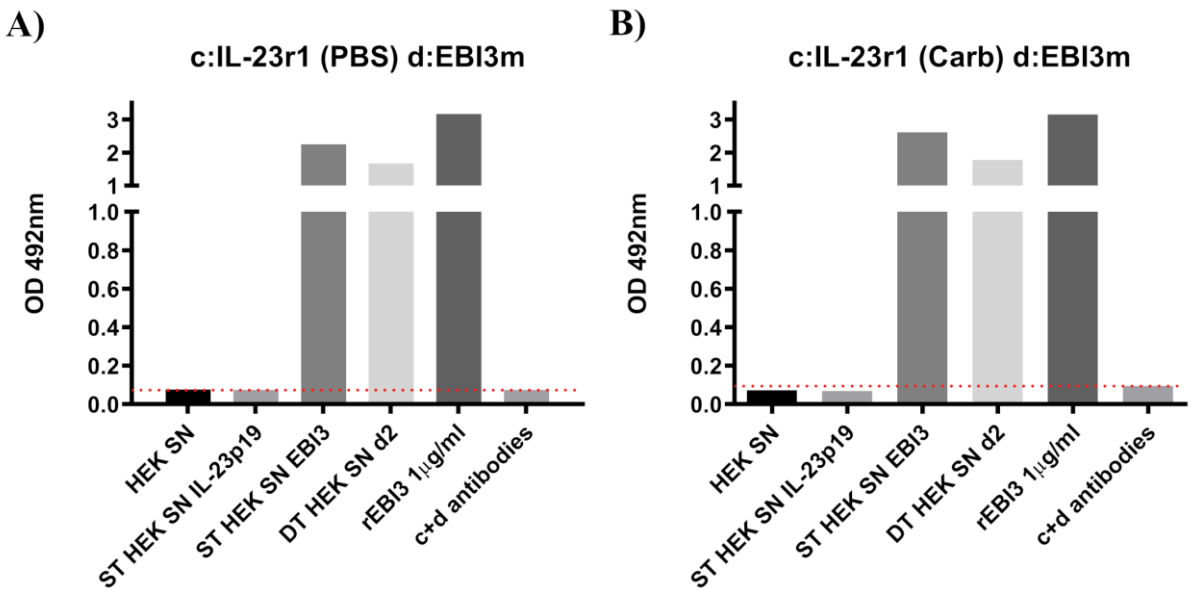

Fig.R33: IL-39 sandwich ELISA using different capture antibody coating solutions. An identical IL-39 sandwich ELISA was performed using either PBS (pH:7,4, A) or carbonate buffer (pH:9,6, B) as coating buffer for the capture antibody IL-23r1. The red dotted lines represent the background signal intensity at OD 492nm of samples containing capture and detection antibodies in PBS. SN, supernatant; ST, single transfected; DT, double transfected; r, recombinant protein; c+d, capture + detection antibodies.

3.9.3 Different blocking strategies to minimize unwanted binding of target proteins

After the incubation with capture antibodies, the remaining binding sites of the plastic wells are usually blocked by some sort of protein or chemical. To determine whether or not a different blocking agent, other than the routinely used bovine serum albumin (BSA), had an influence on minimizing unspecific binding of target protein to the ELISA plate wells, the following experiments were made. The wells of an ELISA plate were coated over night with different blocking agents

namely: 5% BSA, 0,5% non-fat dry milk (NFDM), Pierce Protein free block, 0,1% fish skin gelatin, 5µg/ml human IgG in PBS or in carbonate buffer. The controls were PBS or carbonate buffer only. After the block, the wells were incubated with supernatants from mock (Fig.R35 F, H), IL-23p19 (Fig.R34 A, C), EBI3 (Fig.R34 B, D) or double transfected (Fig.R35 E, G) HEK cell cultures. All setups were then incubated with a detection antibody against EBI3 (EBI3m (Fig.R34 C, D/Fig.R35 G, H)) or IL-23p19 (IL-23p19r2 (Fig.R34 A, B/ Fig.R35 E, F). Throughout all different setups 0,1% fish skin gelatin had the least background followed by 5% BSA. The control samples had always a very high signal when the detection antibody was directed against the incubated target protein (Fig.R34 A, D / Fig.R35 E, G). When the detection antibody was not directed against the incubated protein, the signals for human IgG or 0,5% NFDM were above background levels, which means the detection antibody or HRP coupled antibody were unspecifically bound by the blocking agent (Fig.R34 B, C / Fig.R35 F, H). The halving of signal in figure R34 D from the BSA block, compared to the 0,1% gelatin block, for EBI3 incubated supernatant with EBI3 detection antibody, looked promising for further investigations. Therefore, a sandwich ELISA was performed with one plate being blocked with 5% BSA (Fig.R36 B) and another plate with 0,1% gelatine (Fig.R36 A) and incubated with the same protein mixtures. Despite a small change in signal strength from single transfected EBI3 and double transfected HEK supernatant, there was no major effect of signal reduction visible between both blocking methods. Against the initial observation in terms of blocking efficiency, 0,1% gelatine showed only minimal optical density (OD) intensity differences against the standard BSA blocking method in a normal sandwich ELISA setup (Fig.R36).

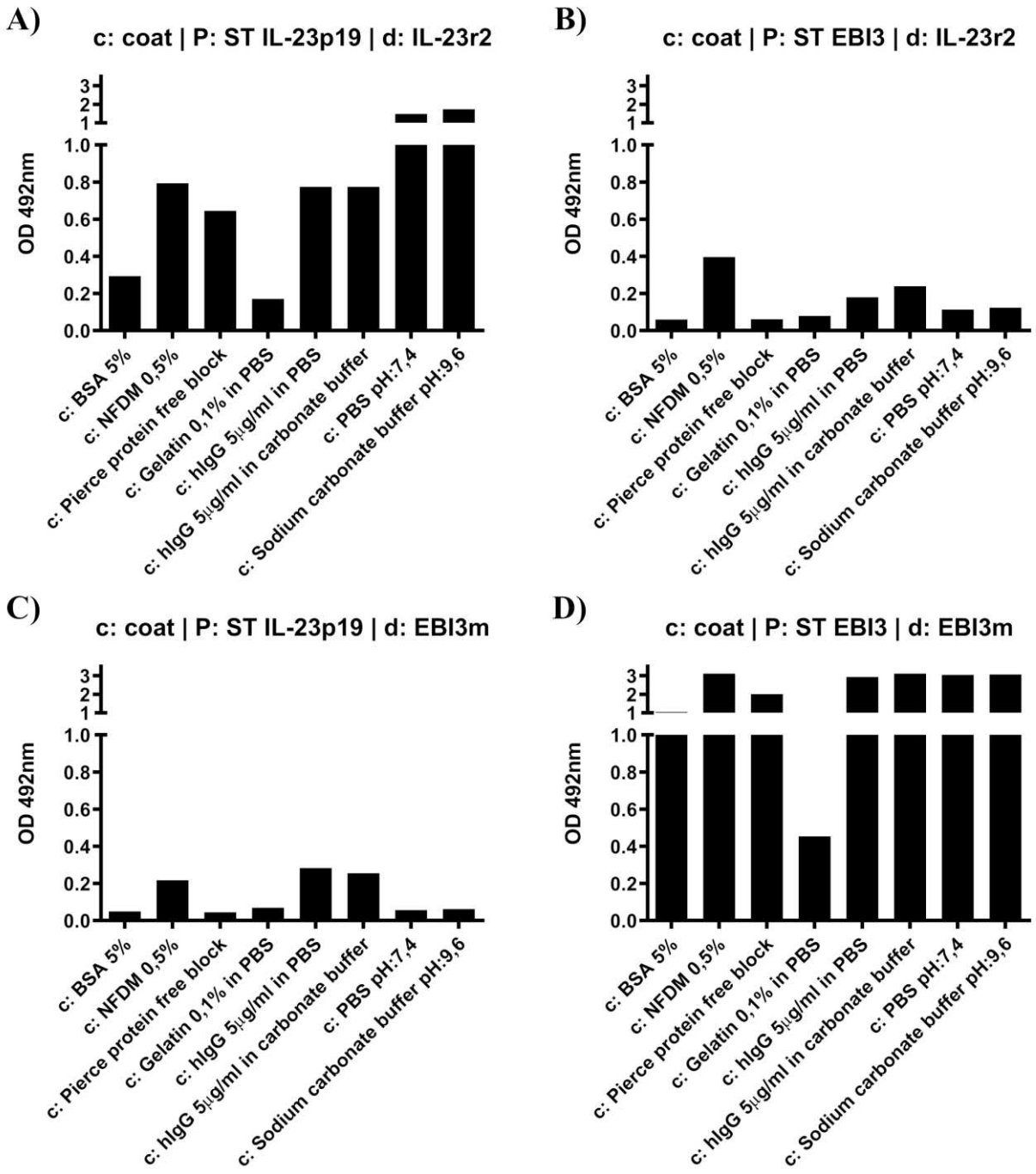

Fig.R34: Different ELISA blocking approaches for the minimization of unwanted protein binding. ELISA plates were coated with different blocking or control agents over night (c, coating). The wells were then incubated with different protein solutions: ST IL23p19 (A, C) or ST EBI3 (B, C). Afterwards, incubation with a specific detection antibody was performed: IL-23r2 (A, B) or EBI3m (C, D). Subsequently, HRP coupled antibodies directed against the detection antibodies' host species were added. Results are indicated as OD measured at 492nm. ST, single transfected; SN, supernatant.

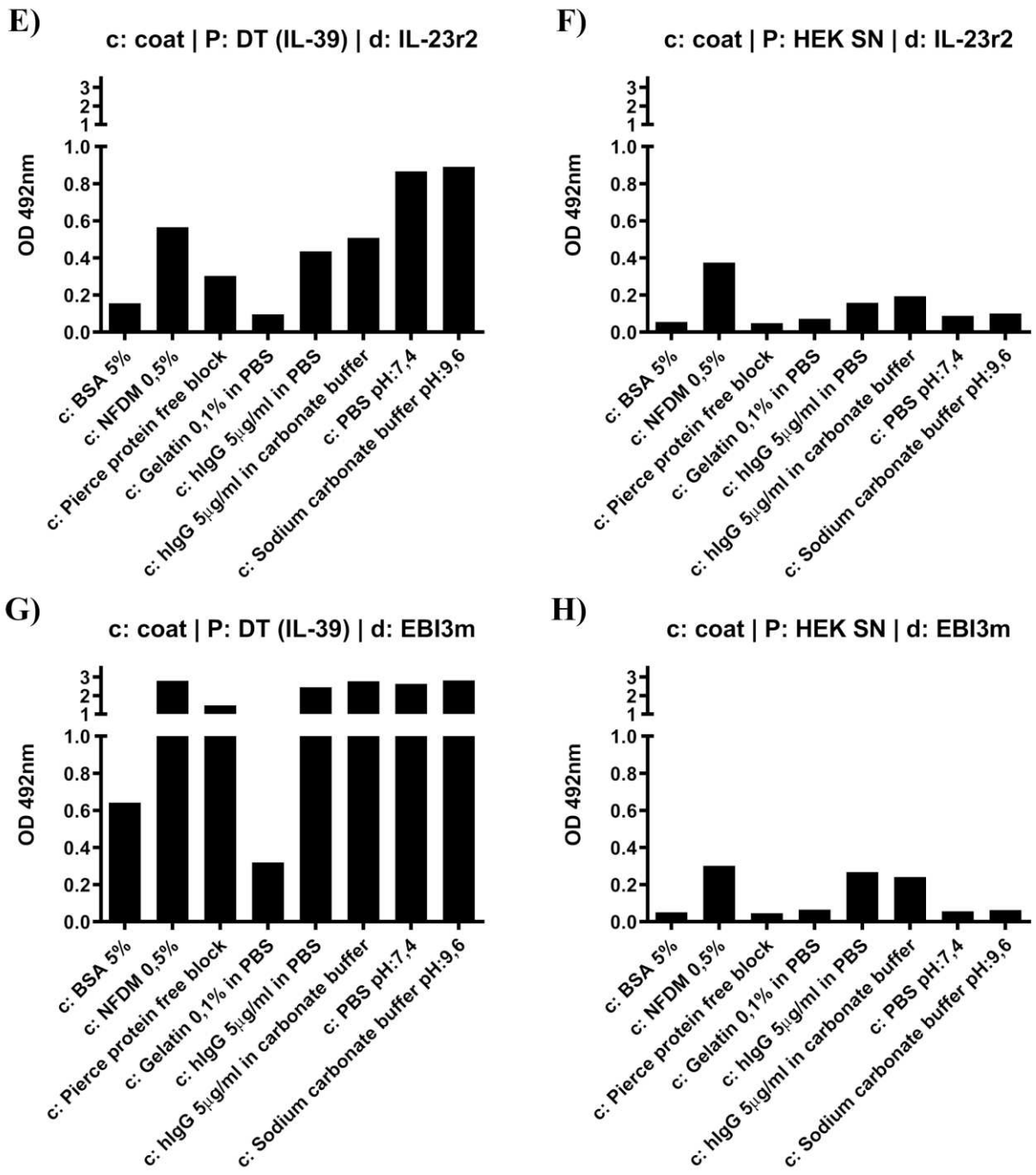

Fig.R35: Continued: Different ELISA blocking approaches for the minimization of unwanted protein binding. ELISA plates were coated with different blocking or control agents over night (c, coating). The wells were then incubated with different protein solutions: DT (IL-39) (E, G) or HEK SN (F, H). Afterwards, incubation with a specific detection antibody was performed: IL-23r2 (E, F) or EBI3m (G, H). Subsequently, HRP coupled antibodies directed against the detection antibodies' host species were added. Results are indicated as OD measured at 492nm. ST, single transfected; SN, supernatant.

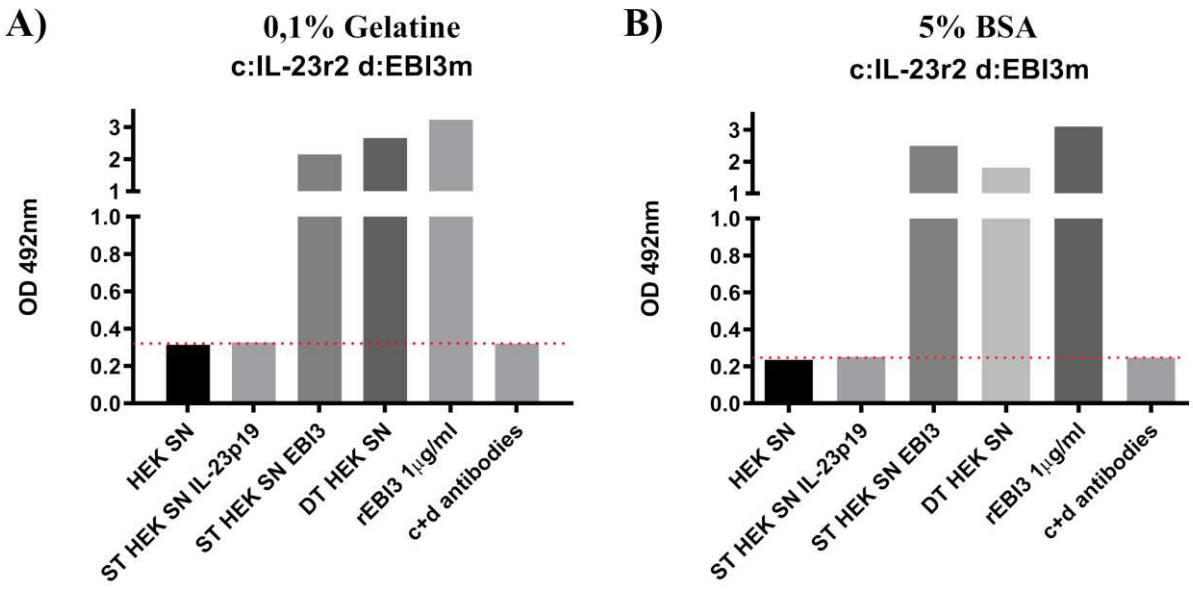

Fig.R36: Effectivity of gelatine vs BSA block in an IL-39 sandwich ELISA. Two identical sandwich ELISAs were performed with different blocking techniques after the capture antibody incubation. One plate was blocked with 0,1% gelatine (A) the other with 5% BSA (B). The red dotted lines represent the background signal intensity at OD 492nm of samples containing capture and detection antibodies in PBS. SN, supernatant; ST, single transfected; DT, double transfected; r, recombinant protein; c+d, capture + detection antibodies

3.9.4 Specificity of HRP coupled secondary antibodies

During the blocking experiments the question arose whether or not the HRP coupled secondary antibodies gave false positive signals. Therefore, wells of 96-well microplates were blocked with 10% BSA followed by incubation with supernatants from control and transfected HEK cells, recombinant proteins, capture and detection antibodies or FreeStyle™ medium (HEK cultivation medium) (Fig.R37). The wells were subsequently incubated with a horseradish peroxidase (HRP) coupled antibody directed against either rabbit (Fig.R37 A) or mouse (Fig.R37 B). A signal could only be measured when a target protein and the respective detection antibody were present. Thus, the secondary antibodies were unlikely to be responsible for high background values due to unspecific binding to the recombinant or cell culture media proteins. The capture and detection antibodies (c+d) also did not bind unspecifically to the ELISA plate and are therefore not responsible for high background signals (Fig.R37). But recombinant proteins could be detected even in the absence of a capture antibody preceded by a 10% BSA block (Fig.R37).

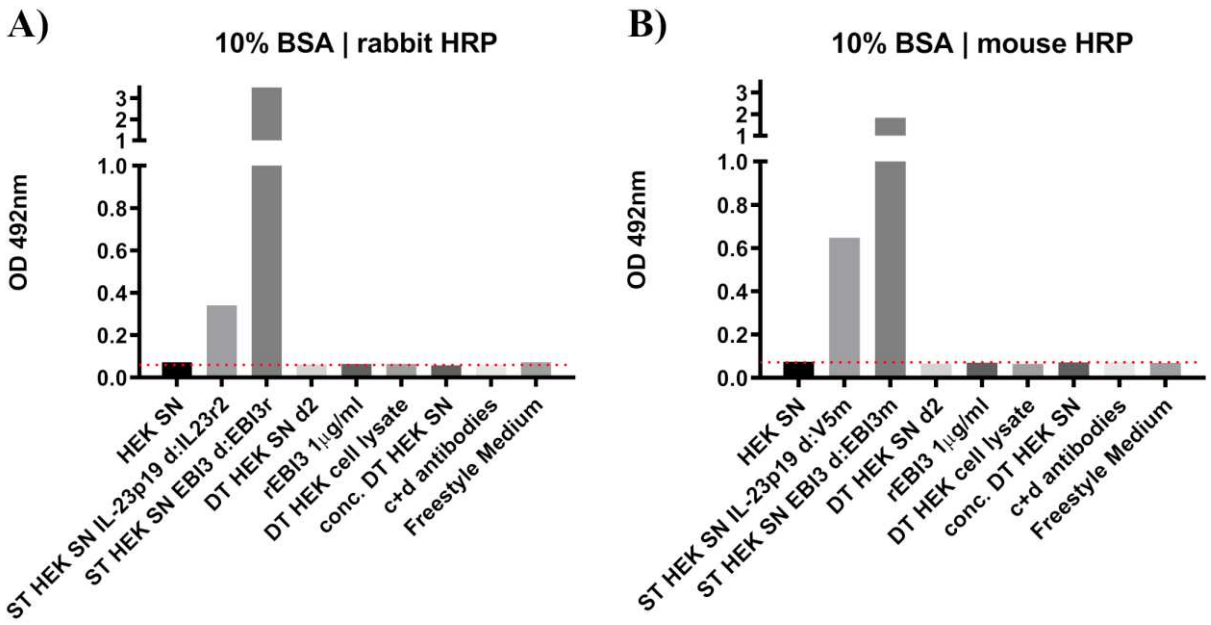

Fig.R37: Evaluation of unspecific HRP coupled secondary antibody binding. ELISA plates were blocked with 10% BSA, coated with different protein and control solutions as indicated under the respective bar (A, B). Two wells were additionally treated with detection antibodies specific for the beforehand incubated protein (d: IL-23r2 or EBI3r (A); V5m or EBI3m (B)). Either rabbit (A) or mouse (B) specific HRP coupled antibodies were added and OD values at 492nm were assessed after the incubation with substrate. SN, supernatant; ST, single transfected; DT, double transfected; r, recombinant protein; c+d, capture + detection antibodies.

3.9.5 Effect of titration of capture and detection antibodies on the IL-39 ELISA performance

In order to find out to which extent the actual measured signals are dependent on the amount of capture and detection antibody used in the ELISAs, the following titration experiments were done. A 96-well microplate was coated with IL-23r2 capture antibody, then incubated with supernatant from either IL-23p19 (Fig.R38 A, B) or EBI3 (Fig.R38 C, D) single transfected, or IL-23p19 + EBI3 double transfected (Fig.R38 E, F) HEK cells, and afterwards incubated with EBI3m detection antibody. For all three combinations both, the capture antibody was titrated from 5µg/ml to 0,0024µg/ml, or the detection antibody was titrated from 2,5µg/ml to 0,02µg/ml. One of the antibodies was always at a constant concentration whilst the other was titrated. Every figure shows the titration data of capture and detection antibodies simultaneously. While the X-axis displays 12 different capture antibody concentrations (Fig.R38 A, C, E) each capture Ab value is displayed with 8 bars. Each of those bars is displaying the data for one detection antibody titration point at this specific capture antibody concentration. Conversely, the detection antibody is titrated with 8 datapoints along the X-axis (Fig.R38 B, D, F) including 12 bars which display the titrated capture antibody data for one specific

detection antibody concentration. Although including two diagrams per approach consists of redundant datasets, both graphs are included to aid the understanding with an additional visual representation.

For the IL-23p19 supernatant, titration of the α IL-23p19 capture antibody has a small declining signal effect from 5µg/ml to 0,31µg/ml and stays constant after that (Fig.R38 A). Since the detection antibody is directed against EBI3, and that protein is not present in figure R38 A and B, the signal is very weak and resembles the background for the capture antibody with the microplate and also IL-23p19 cross reactivity. Titration of the detection antibody has even lesser impact on the signal intensity and stays constant after 0,625µg/ml (Fig.R38 B).

For the samples with the EBI3 supernatant (Fig.R38 C, D), titration of the capture antibody led at first to a small increase in signal intensity and stayed then relatively constant (Fig.R38 C). This indicates that the EBI3 is bound to the microplate independently of the capture antibody concentration. Lowering the amount of the detection antibody on the other hand leads to a decrease in signal intensity (Fig.R38 D). The observed signal correlation with the amount of detection antibody present suggests that the HRP antibody detects a valid EBI3 detection antibody signal without binding unspecifically to other proteins, capture antibody or the ELISA plate.

The double transfected supernatant gives a similar picture compared to the EBI3 single transfected supernatant (Fig.R38 E, F). Regarding the high signal from, somehow sticky, EBI3 supernatant alone, it is not possible to draw further conclusions from the supernatant of double transfected cells. The adherence of EBI3 to the surface is further backed by the observation, that the EBI3 signal intensity is increased with decreasing presence of a capture antibody most prominent in figure R38 E and F.

A)

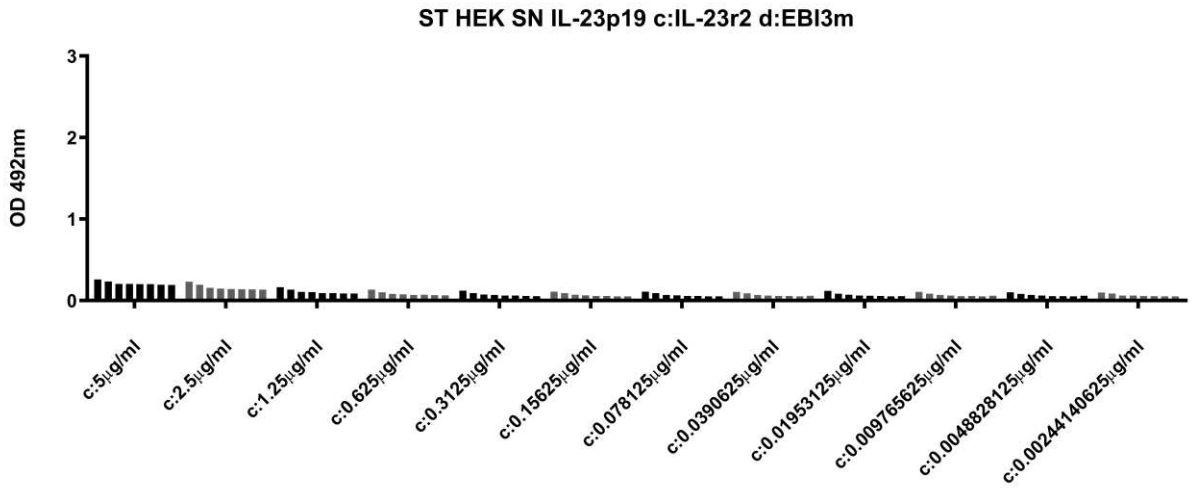

B)

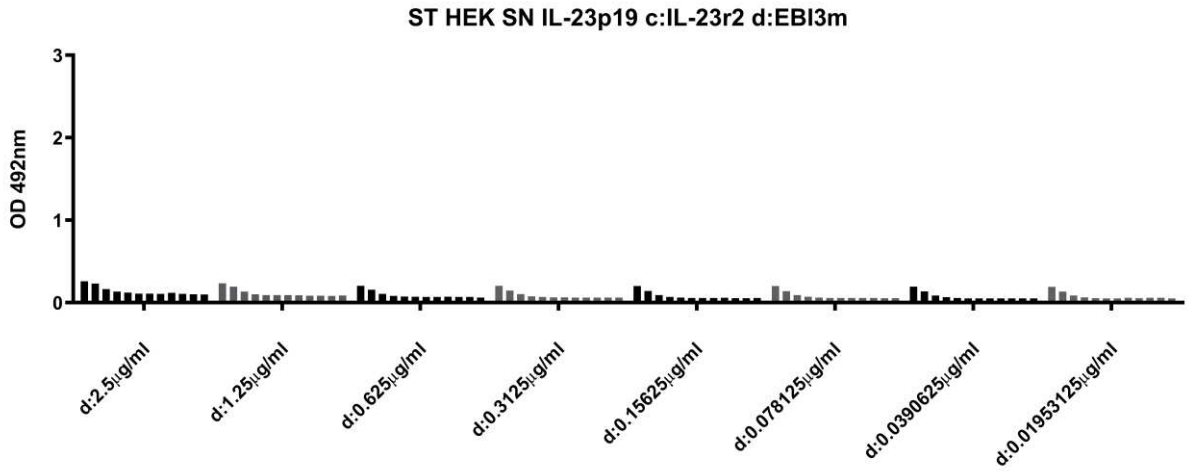

C)

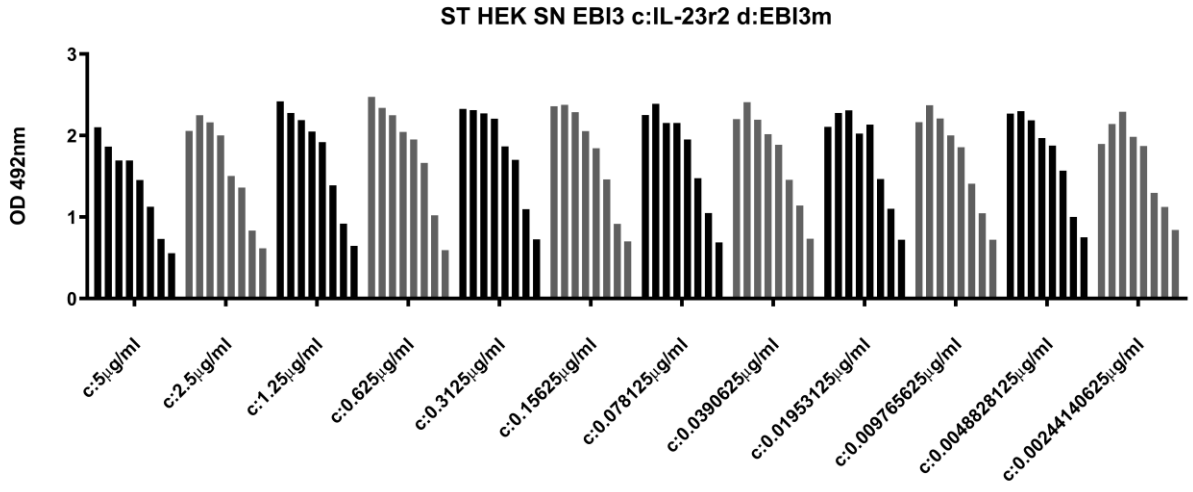

Fig.R38: Please see page after next page for figure legend

D)

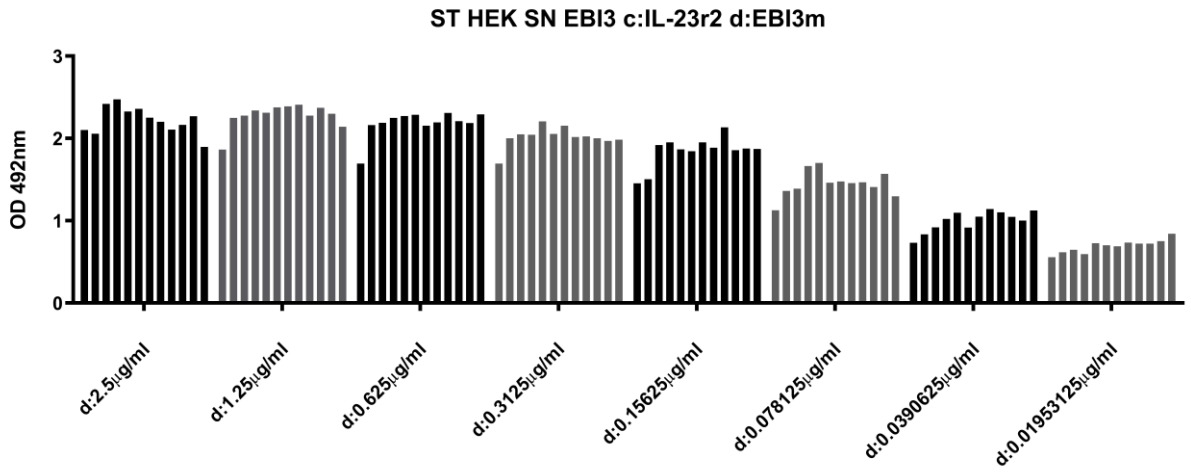

E)

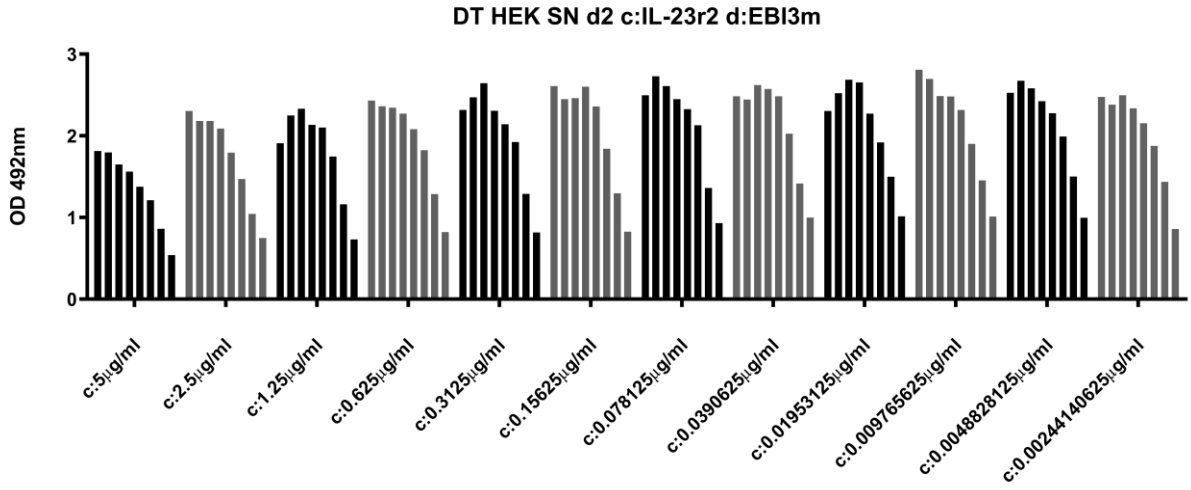

F)

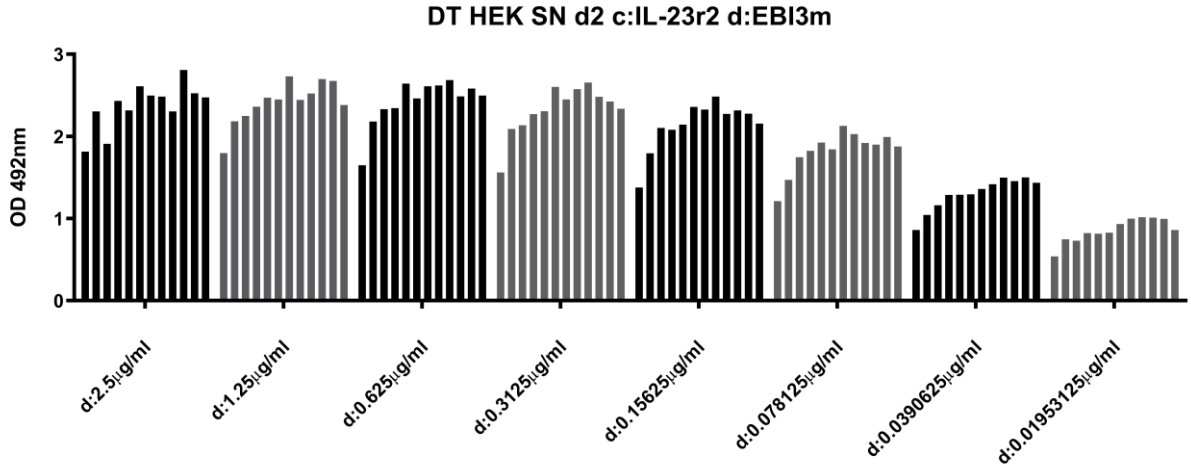

Fig.R38: Please see next page for figure legend

Fig.R38: IL-39 Sandwich ELISA for the assessment of capture and detection antibody efficiency. ELISA plates were coated with α IL-23r2 and blocked with 10% BSA, followed by incubation with IL-23p19 (A, B), EBI3 (C, D) or double transfected (E, F) HEK cell supernatant. The amount of capture antibodies (c:) (A, C, E) or detection antibodies (d:) (B, D, F) were titrated. One data point of a constant capture antibody concentration consists of bars representing the corresponding detection antibody titrations and vice versa. SN, supernatant; ST, single transfected; DT, double transfected.

3.10 Wound healing assay for the assessment of the proliferative potential of rIL-23p19 and rEBI3 on primary human colonic epithelial cells

Regarding the question of what relevance EBI3 and IL-23p19 as a heterodimer could have in a physiological setting, a study from Ramnath et al. suggested that these two subunits could be involved in a wound healing process (Ramnath et al. 2015). They conclude that IL-23p19 and EBI3 are produced in keratinocytes in an IRF6 dependent manner after stimulation of TLR3 or scratch wounds (Ramnath et al. 2017). IRF6 itself is linked to suppression of IFN-β which consequently leads to an increased proliferative potential (Ramnath et al. 2017). Furthermore IL-27 has been reported to facilitate wound healing in keratinocytes and EBI3 is a subunit of the IL-27 heterodimer as well (Yang et al. 2017). As keratinocytes are, like enterocytes, a specialized form of epithelial cells it might be possible that they share mechanistic features.

To test this assumption a wound healing assay with a 2D epithelial monolayer was conducted. Epithelial cells from a donor were grown into organoids, enzymatically processed to receive a solution of mainly single cells, and then grown on a collagen coated culture dish. A special insert was used to achieve two separate cell layers in one culture dish. After removal of the insert a gap of approximately 500µm lies between the two cell layers (Fig.R39 A). The cells were then incubated with a solution containing either recombinant IL-23p19 (OriGene, TP309680), recombinant EBI3 (Prospecbio, cyt367), both subunits or only medium as a control. The cultures were then monitored over a period of 24 hours taking pictures every 2-3 hours. Due to cell proliferation the gap between the layers was narrowed over time (Fig.R39 B) and in the end the gaps from each time point and dish were measured and cell growth rates were calculated (Fig.R39 C, D).

In a first experiment the proteins rEBI3 and the mixture of rEBI3 with rIL-23p19 were given onto the cells in a complete growth medium, which is usually used to grow organoids from epithelial cells (see section 2.4 table “crypt growth medium” (material and methods)). From 3 hours to 14,5 hours there is nearly no difference in the absolute cell growth between the IL-39 and the control sample (Fig.R40 A). Cell growth in the presence of rEBI3 is slowed down to some extend until it catches up to the

control sample after 14,5 hours (Fig.R40 A). Measuring how long it takes for the cells to cover an area of $1{,}56*10^6 \mu m^2$ shows that the rEBI3 sample is a bit slower with approximately 10,7 hours compared to 9 hours and 9,2 hours for the control and IL-39 samples respectively (Fig.R40 B)

In a following experiment all the components from the growth medium had been left out and the recombinant proteins rEBI3, rIL-23p19 or both together were incubated with a basal cell culture medium (advanced DMEM/F12). From 2,4 hours to 24,1 hours the overgrown area of rEBI3 and rIL-39 incubated epithelial cells was always higher compared to the control cells (Fig.R41 A). The rIL-23p19 condition initially reveals a slower epithelial cell growth compared to the control setup until it surpasses the latter condition between 11,8 and 20,2 hours of incubation (Fig.R41 A). Investigating how long it takes for the different groups to cover an area of $1{,}56*10^6 \mu m^2$ shows that the IL-39 treated group is the fastest with 8,5 hours, followed by rEBI3 with 9,7 hours, control and rIL-23p19 with 10,4 hours and 10,6 hours respectively (Fig.R41 B). Another observation was that the control ceased cell growth early although only 73% of the available area were covered, whereas the wells which were incubated with recombinant proteins covered up to 98,5% in the same time period (data not shown).

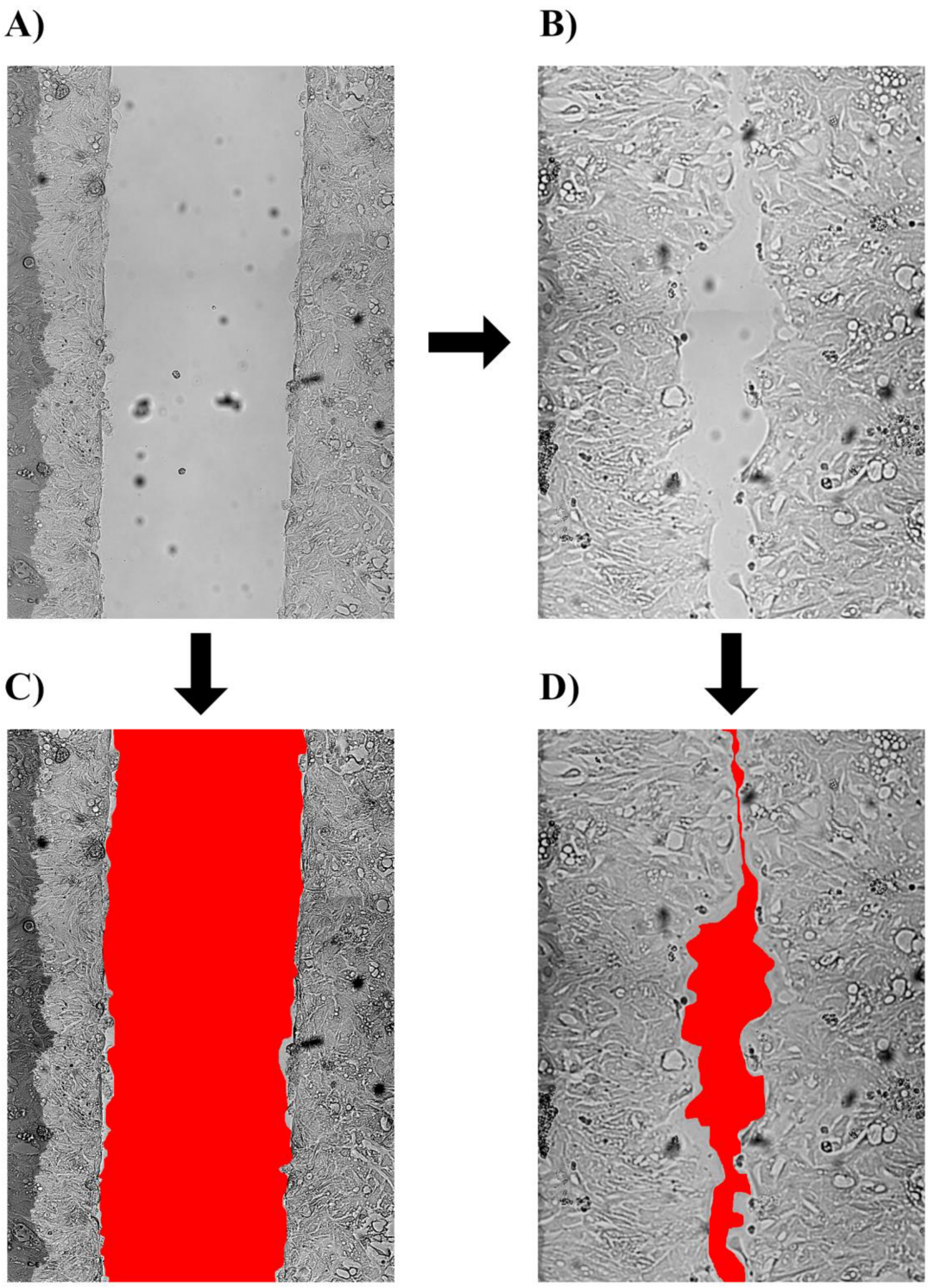

Fig.R39: Technique: Wound healing assay examining the effect of IL-23p19 and EBI3 on epithelial cells. A 2D culture from epithelial cell organoids from patients was grown in a collagen coated 2-well culture dish insert. The insert was removed, leaving a 500µm gap between two cell colonies (A), and cells were treated with different substances in cell culture medium. Cell growth was monitored over time (B) and the gap size was calculated (C, D).

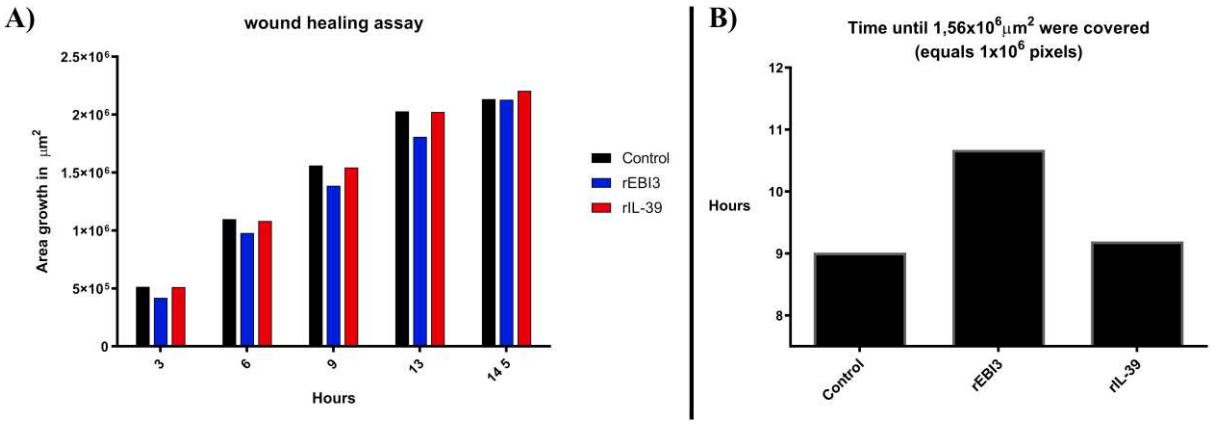

Fig.R40: Effect of rEBI3 and rIL-39 on wound healing in the presence of complete organoid growth medium. Gap sizes of epithelial cell colonies were monitored over time in the presence of rEBI3, rIL-39 or without added protein (control) in a potent cell culture growth medium. The growth area was calculated for each of the different incubated growth media (A) and the time for covering an area of 1,56µm² was assessed (B).

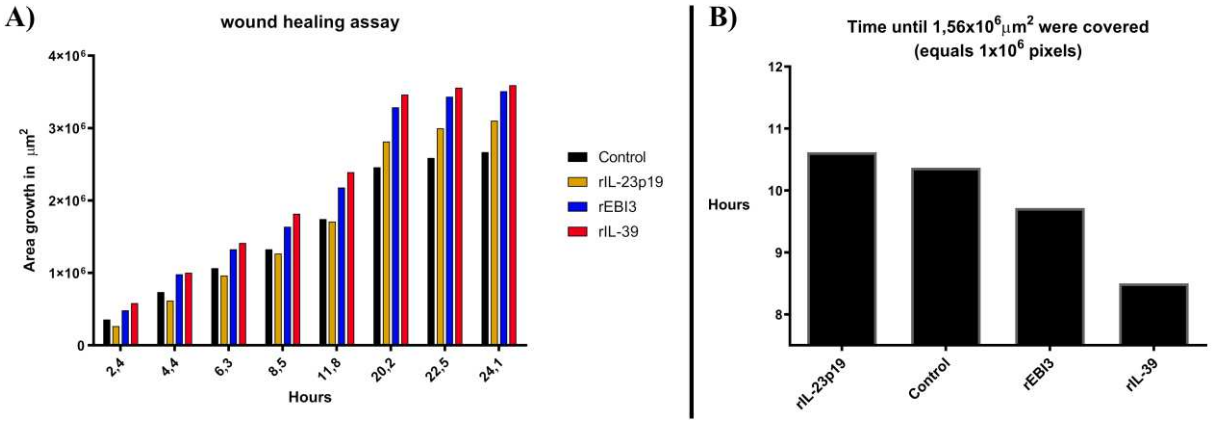

Fig.R41: Effect of rIL-23p19, rEBI3 and rIL-39 on wound healing without the presence of complete organoid growth medium. Gap sizes of epithelial cell colonies were monitored over time in the presence of rIL-23p19, rEBI3, rIL-39 or without added protein (control) in a basic cell culture medium (advanced DMEM/F12). The growth area was calculated for each of the different incubated proteins in basic medium (A) and the time for covering an area of 1,56µm² was assessed (B).

3.11 Characterization of lamina propria dendritic cells in IBD

In the next step we addressed the question if the gathered information about the functional properties of lamina propria mDCs (mLPDCs) under inflammatory conditions, as predicted in the LEL model by gene expression profiling, may also apply to mLPDCs in intestinal inflammation in vivo. For

this purpose, biopsies from inflamed or non-inflamed colonic mucosa of IBD patients or healthy individuals were obtained and transcriptional profiles of isolated mLPDCs were generated.

3.11.1 Composition of immune cell populations in colonic biopsy samples of IBD patients versus healthy individuals

For isolation of mLPDCs, biopsy samples were enzymatically digested; in addition, one group of biopsies from healthy donors was processed with the LEL model and not digested (LEL model, Fig.R42 B). Subsequently, the cell suspensions obtained after disintegration of the tissue or following leukocyte emigration from the tissue were subjected to FACS. The FACS gating strategy of mDCs allowed to determine the composition of immune cells residing in normal vs inflamed colonic mucosa as well as emigrated from the lamina propria in the LEL model.

The amount of cells calculated in the following experiments are always referring to a common denominator of "cell number per 100.000 $CD45^+$ cells". Cell count comparison of the macroscopically non-inflamed biopsy samples from normal colonic mucosa (NC),non-inflamed ulcerative colitis (niUC) and non-inflamed Crohn's disease (niCD) show high similarities regarding the amount of B & T cells (~46.000 cells), granulocytes (~10.700 cells) and mast cells (~3.500 cells) per 100.000 $CD45^+$ cells. The amount of dendritic cells is approximately three times lower in niCD patients (96 cells) compared to NC (274 cells) and niUC (270 cells). NK cells are most prominent in NC (3.076 cells) biopsy tissue with half the amount found in niUC (1.428 cells) and niCD (1.872 cells) patients. Conversely the number of macrophages is two and a half times lower in NC (182 cells) compared to niUC (487 cells) and niCD (436 cells) biopsy samples.

Since the LEL model sample is not from digested material but counting the extravasated cells, these samples serve as a good indicator for the migratory potential of resident lamina propria cells under inflammatory conditions. There are roughly 25% more B & T cells per 100.000 $CD45^+$ cells in the LEL sample (61.844 cells) compared to the NC, niCD and niUC samples. The amount of granulocytes is doubled in the LEL model (20.719 cells) in comparison to NC, niCD and niUC. The amount of mast cells is higher in NC, niCD and niUC (~3500 cells) compared to the LEL model (198 cells). NK cells stay around the same with the LEL model (3090 cells) compared to NC (3076 cells). Macrophages exhibit a higher migratory potential, being nearly doubled in the LEL model (301 cells) compared to NC (182 cells). The highest migratory potential could be observed for dendritic cells which make up for over four times as much cells per 100.000 $CD45^+$ cells in the LEL model (1175 cells) in comparison to NC (273 cells).

In inflamed IBD patient samples, B & T cells are 12,7% higher in inflamed UC (iUC) (53.406 cells) and 14,7% lower in numbers in inflamed CD (iCD) (34.263 cells) tissue compared to their non-inflamed counterparts, niUC and niCD respectively. The amount of granulocytes is raised for both iUC (14.051 cells) and iCD (35.119 cells) under inflammatory conditions compared to niUC (9907 cells) and niCD (10.083 cells). Mast cells are lowered in numbers to 2.853 cells in iUC (20% less than niUC) and 685 cells in iCD (83% less than niCD). NK cell numbers are decreased from ~1600 cells in niUC and niCD to ~600 cells under inflammatory conditions in iUC and iCD patients. For both inflammatory patient groups the amount of macrophages is increased for approximately 1.6 times in iUC (799 cells) and over four times in iCD (2188 cells) patients compared to their non-inflamed counterparts. On the other hand, mDCs are reduced in numbers under inflammatory conditions being 30% lower in iUC and 46% lower in iCD compared to niUC and niCD respectively. It is noteworthy that the data for inflamed Crohn's disease patients is based on a group size of two individuals. Cell numbers depicted in figure R42 are additionally listed in table R43.

According to this data, dendritic cells have by far the most migratory potential under inflammatory conditions comparing the LEL samples with the NC samples. Yet, in iUC and iCD samples the amount of mDCs is lower compared to their non-inflamed counterparts, which may indicate that more cells have extravasated out of the lamina propria. This was also observed for NK cells and could be due to inflammatory processes in macroscopically inflamed regions of iUC and iCD patients.

The differences in cellular composition of the lamina propria leukocyte population between the six conditions analyzed provide further insight and likely represent an important aspect of varying immunological dynamics under homeostatic vs inflamed conditions in NC, CD and UC patients.

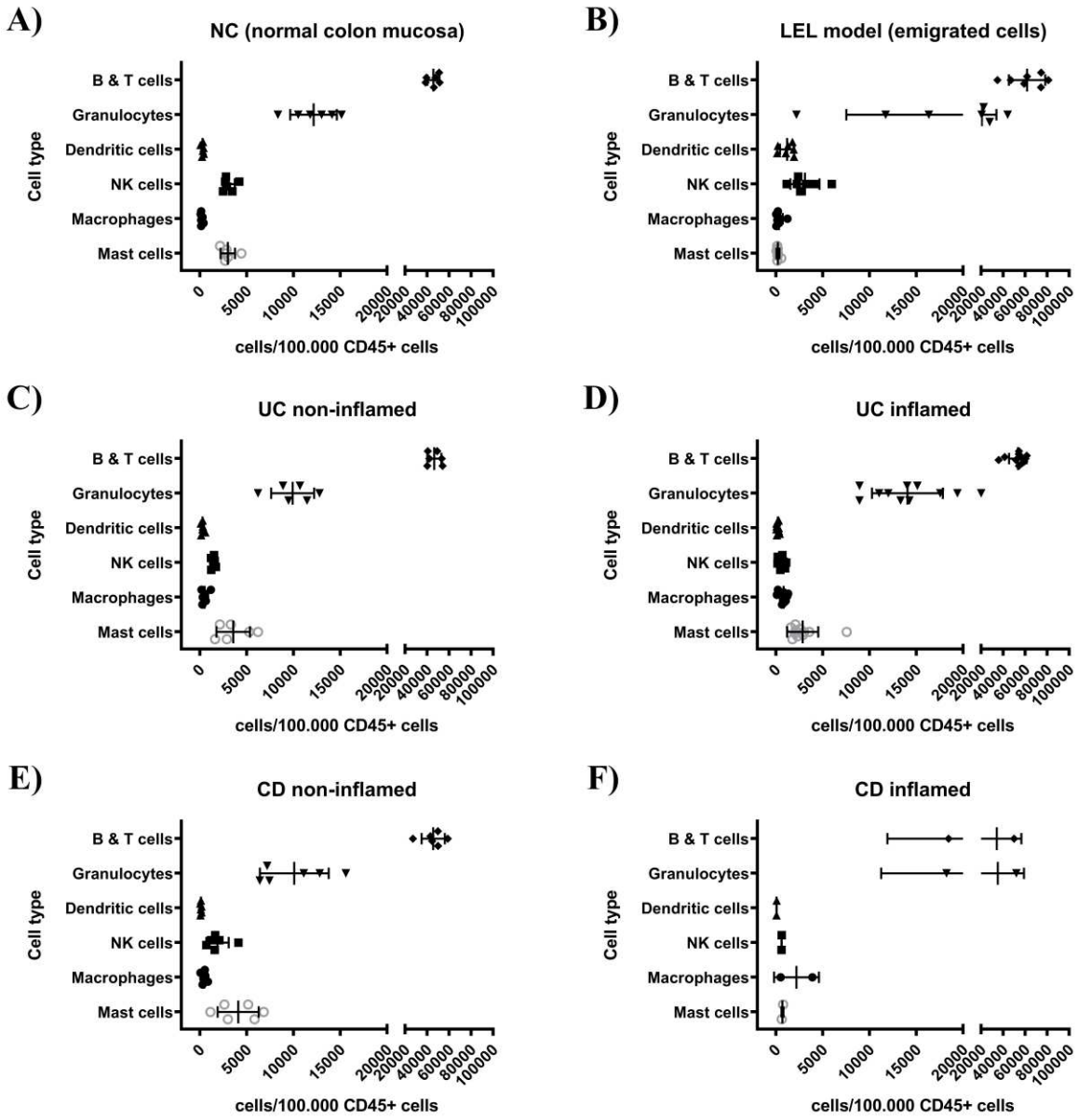

Fig.R42: Immune cell composition in inflamed vs non-inflamed mucosa of IBD patients, normal mucosa of control patients as well as the LEL model. Colonic biopsies of normal mucosa of control patients (A), as well as non-inflamed and inflamed mucosa of patients suffering from ulcerative colitis (UC) (C, D) or Crohn's disease (CD) (E, F), were collected and enzymatically digested prior to flow cytometric analysis. In addition, normal biopsies of control patients were subjected to the LEL model procedure (B) and emigrated cells were analyzed via flow cytometry. Cell types were identified as described in Figs.R2/R3. Shown are the numbers of cells (mean ±SD) per 100.000 $CD45^+$ positive cells for each cell type.

	Macrophages		NK cells		Dendritic cells		Granulocytes		B&T cells		Mast cells		
	Ø#cells	±SD	Ø#cells	±SD	Ø#cells	±SD	Ø#cells	±SD	Ø#cells	±SD	Ø#cells	±SD	n
A) NC	182	118	3076	647	274	132	12142	2488	45726	5516	2970	768	6
B) LEL	301	418	3090	1560	1175	761	20719	13194	61844	16581	198	158	7
C) niUC	488	370	1428	211	270	169	9907	2291	46587	6407	3560	1798	6
D) iUC	799	376	617	309	187	126	14051	3795	53406	7908	2853	1666	11
E) niCD	436	274	1872	1192	96	54	10083	3683	45567	10579	4083	2192	6
F) iCD	2188	2397	601	10	52	10	35119	23874	34263	22348	685	105	2

Table R43: Cell numbers of LEL and digested colon biopsies from normal and IBD patients. Depicted are the cell numbers of the experimental data from Fig.R42. Cell numbers are displayed as: cells per 100.000 $CD45^+$ cells. NC, normal colon mucosa; niUC, non-inflamed ulcerative colitis; niCD, non-inflamed Crohn's disease; LEL, Loss of epithelial layer model; iUC, inflamed ulcerative colitis; iCD, inflamed Crohn's Disease; n, number of patients; Ø#cells, number of cells (arithmetic mean); ±SD, ± standard deviation.

3.11.2 Characterization of dendritic cell subtypes in the colonic mucosa of IBD patients and healthy individuals

Dendritic cells can be categorized into different subtypes based on their expression of blood dendritic cell antigens (BDCA) 1-4 (Dzionek et al. 2000). Most publications distinguish between DCs that express one of the four BDCAs and only recently have scientists also mentioned DCs that are double positive for the BDCAs 1 and 3 also known as CD1c and CD141 respectively (Haniffa et al. 2012; Chu et al. 2012). Inspecting the data of the former flowcytometric analysis, it is revealed that there is not only a difference in the number of mDCs present in the colon tissue of normal vs IBD patients but also that there is a difference in CD1c and CD141 distribution on the surface of these mDCs. With the help of these molecules the mDCs can now be categorized into four different subsets based on their CD1c and CD141 surface expression.

Throughout all analyzed biopsy samples the fraction of CD1c CD141 double positive (DP) mDCs was always the most prominent one. In normal mucosa CD1c CD141 DP mDCs accounted for 51% and were even more abundant in niCD (55%) and niUC (70%) patients (Fig.R44 A, C, B). The LEL model shows that under inflammatory conditions CD1c CD141 DP mDCs were the most motile mDCs representing over 90% of emigrated mDCs (Fig.R44 D). However, in inflamed IBD patients samples the amount rose in iUC patients from 70% to 74%, but declined in iCD patients from 55% to 50,6% overall (Fig.R44 B, C). The next most pronounced fraction were $CD1c^+$ mDCs. In non-inflamed tissues they accounted for 41% in NC, followed by 36% and 24% in niCD and niUC respectively (Fig. R44 A, C,

B). The amount of $CD1c^+$ mDCs was decreased in all cases under inflammatory conditions with 29% in iCD, 10% in iUC and only 3,2% with the LEL model (Fig. R44 F, E, D). mDCs of the $CD141^+$ subtype were only found in smaller numbers under homeostatic conditions representing 2,3% of all mDCs in NC, 2,7% in niUC and 4% in niCD patients (Fig. R44 A, B, C). For all inflammatory conditions the frequency of $CD141^+$ mDCs increased to 5,1% (LEL model), 13% (iUC) and 9,5% (iCD), more than doubling the abundance in all three cases compared to their non-inflammatory counterparts (Fig. R44 D, E, F). Cells that were double negative (DN) (or very low) for CD1c and CD141 decreased in fraction from niUC (3,4%) to iUC (2,5%) (Fig.R44 A, D, B, E), having decreased under inflammatory conditions. But in the case of CD patients the CD1c CD141 DN fraction increased from normal niCD (>5%) to iCD (10,8%) (Fig.R44 C, D). The lowest frequency of CD1c CD141 DN DCs (<1%) was observed among emigrated mDCs in the LEL model. Cell numbers depicted in figure R44 are additionally listed in table R45.

In summary these data show that under inflammatory conditions the amount of CD141 positive mDCs is raised in IBD patients. The CD1c CD141 double positive fraction is more pronounced in IBD patients under homeostatic conditions compared to healthy individuals. This double positive phenotype was also the most motile as demonstrated in the LEL model (Fig.R44 D). The amount of CD1c positive cells was diminished under inflammatory conditions in IBD patients and only in miniscule numbers present after the LEL model. Double negative cells were raised in iCD patients, lowered in iUC and did only emigrate with under 1% in the LEL model.

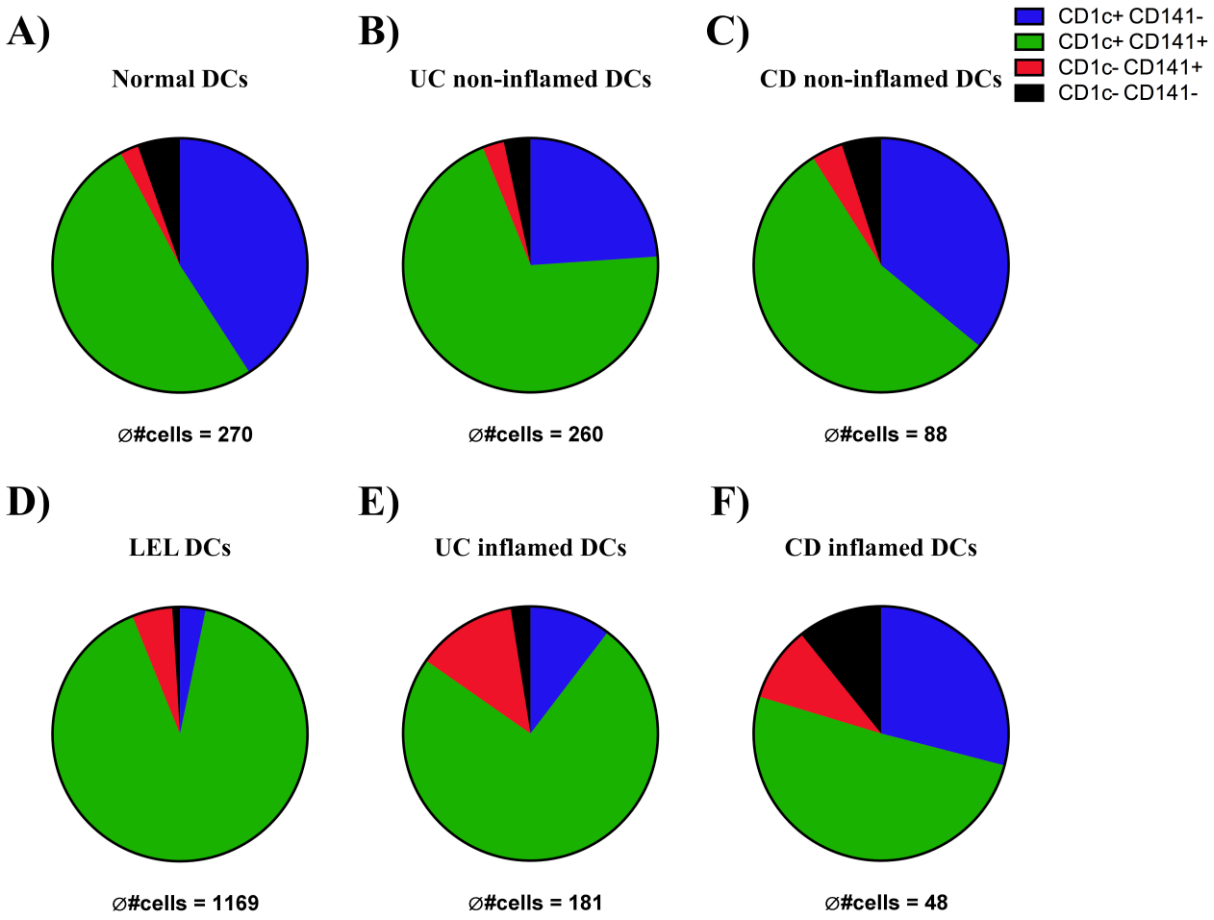

Fig.R44: Subset composition of mLPDC according to their CD1c and CD141 surface expression in the colonic mucosa of IBD patients and healthy individuals. The expression of CD1c and CD141 on mLPDC was determined by flowcytometric analysis. Gating of LPDC among isolated mucosal cells was performed as described before (see Figs.R2/R3). Depicted is the distribution of $CD1c^+$, $CD1c^+$+$CD141^+$, $CD141^+$ and $CD1c^-$+$CD141^-$ mLPDC subtypes in digested biopsies in normal colonic mucosa of healthy individuals (A), non-inflamed mucosa of UC (B) and CD (C) patients as well as inflamed mucosa of UC (E) and CD (F) patients. Additionally the LEL model was utilized depicting the subtypes among emigrated mDCs from NC material (D). Numbers beneath the charts (Ø#cells) represent the arithmetic mean of measured mDCs per 100.000 $CD45^+$ cells across all patients group samples. UC, ulcerative colitis; CD, Crohn's disease; NC, normal colon; LEL, loss of epithelial layer.
$CD1c^+CD141^-$=blue, $CD1c^+CD141^+$=green, $CD1c^-CD141^+$=red, $CD1c^-CD141^-$=black.
Number of patient samples: A: n=6; B: n=6; C: n=6; D: n=7; E: n=11; F: n=2.

	CD1c+ CD141-	CD1c+ CD141+	CD1c- CD141+	CD1c- CD141-	Ø#cells	n
A) NC	40,85%	51,41%	2,34%	5,40%	270	6
B) niUC	23,91%	69,96%	2,72%	3,41%	260	6
C) niCD	35,97%	55,05%	3,96%	5,02%	88	6
D) LEL	3,23%	90,67%	5,11%	0,99%	1169	7
E) iUC	10,34%	74,38%	12,76%	2,51%	181	11
F) iCD	29,05%	50,64%	9,52%	10,80%	48	2

Table R45: Cell percentages for the subset composition of mLPDC according to their CD1c and CD141 surface expression in the colonic mucosa of IBD patients and healthy individuals.. Displayed are the cell percentages for the four different mDC subsets using CD1c and CD141 as discriminator as depicted visually in figure R44.
NC, normal colon mucosa; niUC, non-inflamed ulcerative colitis; niCD, non-inflamed Crohn's disease; LEL, Loss of epithelial layer model; iUC, inflamed ulcerative colitis; iCD, inflamed Crohn's disease; Ø#cells, arithmetic mean of measured mDCs per 100.000 $CD45^+$ cells across all patients group samples.; n, number of patient samples.

3.11.3 Transcriptomic profile of lamina propria mDCs in IBD vs healthy individuals

In order to find out more about possible functional properties of mDCs in IBD patients versus healthy individuals, mDCs were isolated from colonic biopsies and subjected to RNA sequencing. The analysis is comprised of material from inflamed (iUC, iCD) and non-inflamed (niUC, niCD) IBD patients as well as healthy individuals (NC). Due to technical difficulties I was not able to include mDCs from the LEL model into the analysis. It was therefore not possible to identify alterations between the experimentally induced inflammatory mDCs from the LEL model with the inflammatory mDCs from IBD patients.
The mRNA measurement detected a total of 11959 individual expressed genes of which 10535 were found expressed across all groups. The different groups were compared in multiple setups to identify statistical significant differentially expressed (SDE) genes (table R46). Considered as SDE were all transcripts with a p-value<0,05 and a linear fold change of ±1,5. In every dataset were also some novel transcripts identified which are a mixture of long non-coding (lnc)RNAs, pseudogenes, novel proteins and antisense (a)RNAs. Especially aRNAs and lncRNAs are described as regulators of transcriptional processes (Dykes and Emanueli 2017; Eguchi, Itoh, and Tomizawa 1991).

In figure R47 a cluster analysis is shown depicted as dendrogram, comparing the differentially regulated genes in mLPDCs from inflamed IBD versus non-inflamed IBD patients. The mLPDC samples from healthy individuals are also displayed in this analysis and are clustered based on their

expression of genes that are differentially regulated in inflamed IBD versus non-inflamed IBD mDCs. There is a clear separation between inflamed and non-inflamed patient samples. The samples from niUC and niCD patients are mixed, depicting their similarity in gene expression under homeostatic conditions. Regarding this specific analysis of differentially expressed genes, four out of the six samples from healthy individuals are clustering together and are therefore closer related to each other in comparison to the non-inflamed IBD mDCs.

A further cluster analysis of non-inflamed IBD patients mDCs versus healthy individuals mDCs was performed and is shown in figure R48. Based on their differentially expressed genes, healthy individuals are clearly separated from all other IBD samples. The samples from niUC and niCD patients show again a more uniform gene expression and cluster together with no discernible differences. Samples from inflamed IBD DCs were included in this analysis, but only genes differentially expressed between non-inflamed IBD and healthy individual samples were considered, which explains the mingling between non-inflamed and inflamed samples.

Group	#differentially expressed genes (SDE)	#Upregulated SDE genes lfc>+1,5	#Downregulated SDE genes lfc<-1,5	#SDE genes detected in all group samples	#Novel transcript (#antisense)
A) niCD vs NC	727	379	348	691	44 (21)
B) iCD vs NC	1285	536	749	1131	73 (47)
C) iCD vs niCD	983	378	605	809	47 (30)
D) niUC vs NC	722	494	228	700	37 (25)
E) iUC vs NC	1216	766	450	1190	87 (53)
F) iUC vs niUC	731	320	411	251	40 (18)
G) niUC+niCD vs NC	847	644	230	727	47 (29)
H) iUC+iCD vs NC	1438	945	493	1398	111 (75)
I) niUC vs niCD	493	372	121	493	21 (9)
J) iUC vs iCD	845	596	249	709	42 (22)
K) iUC+iCD vs niUC+niCD	1024	485	539	893	62 (39)
L) iUC+iCD+niUC+niCD vs NC	1106	846	260	1090	83 (57)
M) iUC+iCD vs niUC+niCD+NC	1215	624	591	792	94 (58)

Table R46: Numbers of differentially expressed mRNAs over different RNA sequencing group comparisons. From the five examined groups different comparisons were conducted. Displayed are the numbers of differentially expressed genes with a p-value<0,05 and a linear fold change of ±1,5. Values in brackets in the #novel transcript column are novel transcripts which were identified as antisense RNAs for defined genes.
NC, normal colon; niCD, non-inflamed Crohn's disease; iCD, inflamed Crohn's disease; niUC, non-inflamed ulcerative colitis; iUC, inflamed ulcerative colitis; SDE, statistical significant differentially expressed; lfc, linear fold change.

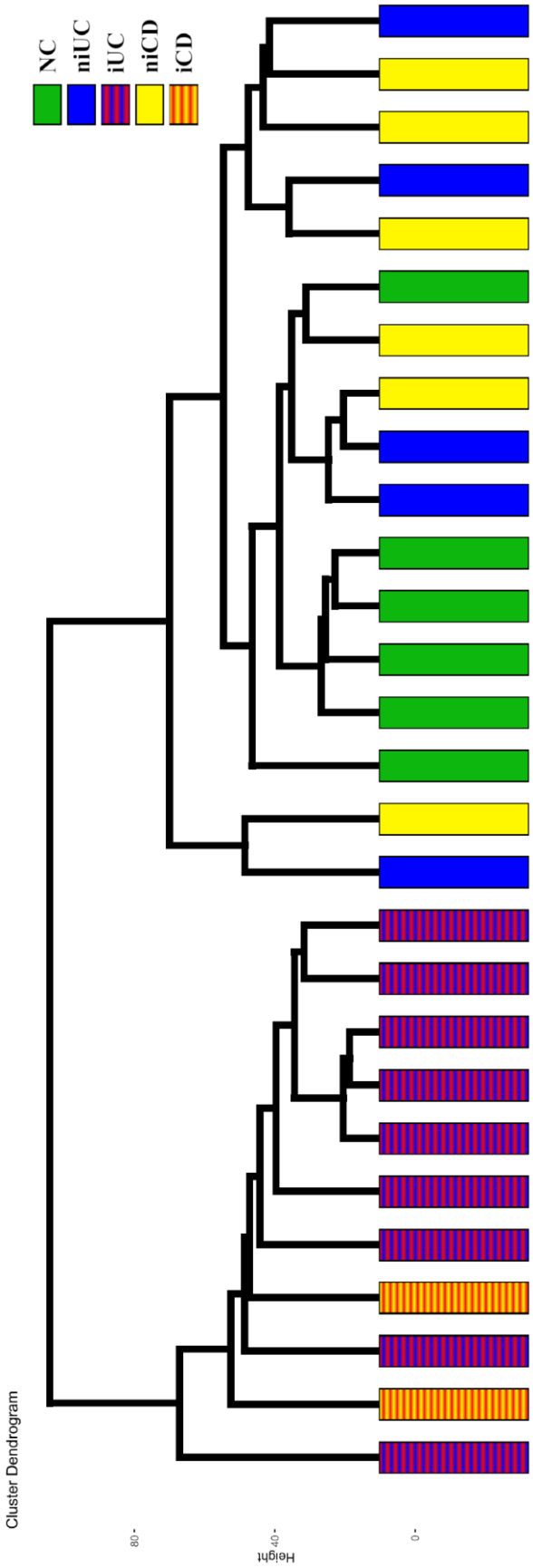

Fig.R47: Cluster analysis of inflamed iUC + iCD mDCs versus non-inflamed niUC + niCD mDCs. This dendrogram of the cluster analysis shows the relationship of gene expression data from inflamed IBD patients mDCs versus non-inflamed IBD patients mDCs. Each colored block represents one patient sample.
NC, normal colon; niUC, non-inflamed ulcerative colitis; iUC, inflamed ulcerative colitis; niCD, non-inflamed Crohn's disease; iCD, inflamed Crohn's disease.

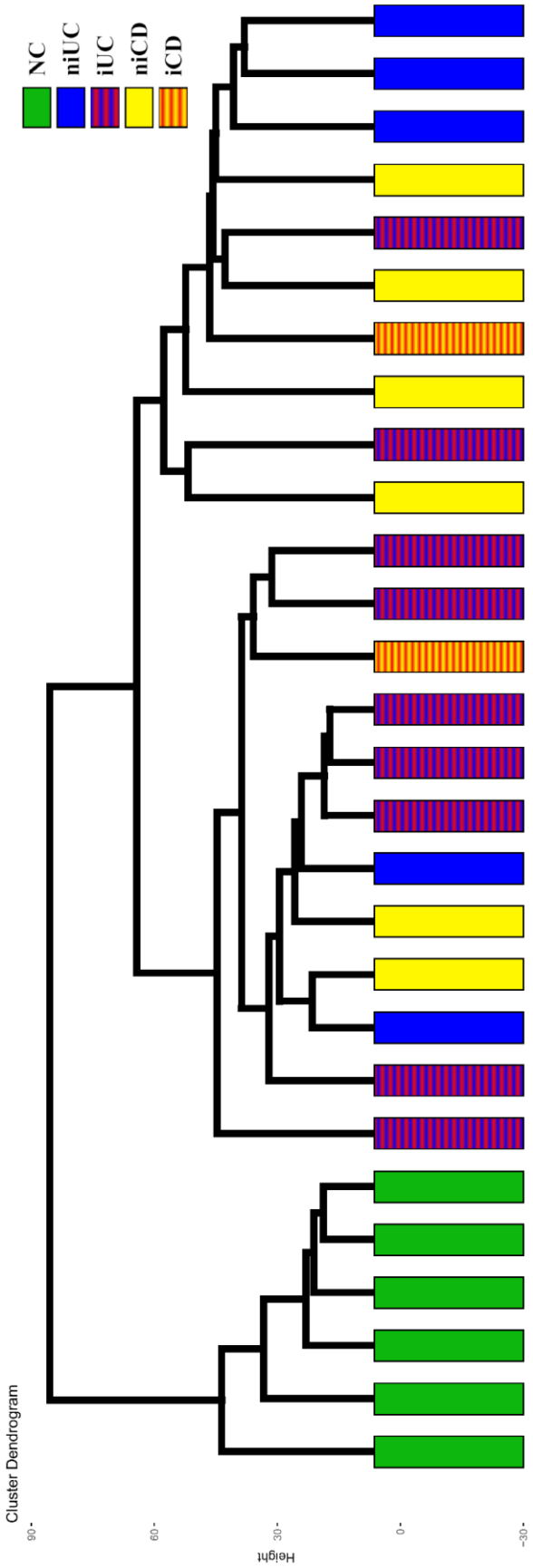

Fig.R48: Cluster analysis of normal colon mDCs versus non-inflamed niUC + niCD mDCs. This dendrogram of the cluster analysis shows the relationship of gene expression data from healthy individuals mDCs (NC) versus non-inflamed IBD patients mDCs (niUC/niCD). Each colored block represents one patient sample.
NC, normal colon; niUC, non-inflamed ulcerative colitis; iUC, inflamed ulcerative colitis; niCD, non-inflamed Crohn's disease; iCD, inflamed Crohn's disease.

3.11.4 Assessment of mDC purity via transcriptomic data

The gene expression profile of the sorted mLPDCs is used to check for a possible contamination against several lamina propria resident cell types. Table R49 lists a set of hallmark genes which are usually used to identify or discriminate the associated cell type. Sorted mLPDCs can be clearly allocated to the DC lineage since identificatory DC genes are preserved. Contamination with other cell types seems to be unlikely according to hallmark gene expression. However, the dataset of non-inflammatory UC patients showed similarities with genetic markers of mast cells.

Cell type	Identifier	Experimental data mLPDCs	Literature
Dendritic cells	**HLA-DR | CCR7 | FLT3 CD1c | CD141 |CD80 | CD86**	**+++ | ++ | + ++ | + | + | ++**	(Caër and Wick 2020)
Macrophages	**CD64 | CD16 | CD14**	**- | - | -**	(Caër and Wick 2020)
T cells	**CD3**	**-**	(Allison and Lanier 1987)
B cells	**CD19 | CD20**	**- | -**	(Sanz et al. 2019)
Plasma cells	**CD138**	**-**	(Sanz et al. 2019)
Plasmablasts	**CD27**	**-**	(Sanz et al. 2019)
NK cells	**CD56 | IL2RB | NKG2D**	**- | - | -**	(Wu, Tian, and Wei 2017)
Basophils	**CD123 | CRTH2 | CD49b**	**- | - | -**	(Chapuy et al. 2014; Yoshimura-Uchiyama et al. 2004)
Epithelial cells	**CD326**	**-**	(Gracz et al. 2013)
Epithelial stem cells	**CD24**	**-**	(Gracz et al. 2013)
Endothelial cells	**CD62P | TIE1 | VWA**	**- | - | -**	(Goncharov et al. 2020; Rodewald and Sato 1996)
Enteric neurons	**UCHL1 | ENO2 | NEFH**	**- | - | -**	(Krammer et al. 1994)
Glia cells	**GFAP**	**-**	(Krammer et al. 1994)
Fibroblasts	**Acta2 | CD90 | MCSP**	**- | - | -**	(Mifflin et al. 2011; Karpus et al. 2019)
Eosinophils	**CCR3**	**-**	(Loktionov 2019)
Neutrophils	**CD66b | CD16 | CD15**	**- | - | -**	(Lakschevitz et al. 2016)
ILCs (1, 2, 3+/-)	**NKp44 | NKp46 | CCR6**	**- | - | -**	(Nagasawa et al. 2019)
Mast cells	**CD117**	**+ (↑niUC)**	(Valent et al. 2010)

Table R49: Cell contamination assessment based on the mLPDCs mRNA expression profile. This list shows the mRNA expression levels of mLPDCs in respect to genetic markers which are typically utilized to identify the listed cell types according to corresponding literature. ↑, significantly upregulated.

Mast cells and dendritic cells share a variety of markers which complicates the identification of possible cell contaminations. Before everything else, the sorting process should omit mast cells not only via the exclusion of CD117 highly positive cells, but they usually do not express HLA-DR or higher levels of CD11c, both highly expressed on mLPDCs (Figs.R2/3) (Teodosio et al. 2015). The transcriptomic data was used to identify gene expression for the niUC vs NC group, investigating molecules which are usually only present in mast cells or needed for identification. Some mast cell specifc genes like *ENPP3* and *TPSB2* are upregulated in sorted cells of niUC patients, but besides *CD117* none of those are statistically significant and therefore not part of further analytical steps. The expression of *HLA-DRA* for instance is unaltered and does not show any signs of significant reduction in base mRNA levels from *HLA-DRA* negative cells. However, this finding should be considered for further interpretations from the niUC dataset.

Gene name	**Linear fold change**	**p-value**	**mRNA base value**	**Expressed in**	
				Mast cells	mDCs
***KIT* (CD117)**	3,29	3,99E-02	162	++	+
***ENPP3* (CD203c)**	14,00	2,50E-01	14	+	-
***MS4A2* (FCεRIB)**	23,84	8,20E-02	172	+	- /+
***ITGA3* (CD49c)**	-	-	-	+	-
TPSB2	20,12	9,54E-02	1864	++	-
HLA-DRA	-1,08	8,15E-01	63751	-	+++
***ITGAX* (CD11c)**	1,60	9,82E-02	2556	dim	++

Table R50: Exploring mRNA expression data for mast cell discrimination in niUC vs NC. This table shows genes that are relevant for the identification of mast cells based upon the dataset of non-inflammatory ulcerative colitis patients versus healthy controls.

3.11.5 Differential gene expression in mLPDCs of IBD patients and healthy individuals

Examining the top 20 significantly differentially expressed genes (up- and downregulated) between different patient groups provided insight into functional aspects of intestinal myeloid DCs. Four DC group comparisons are displayed in tables R51-R54, while the remaining eight comparisons can be found in the appendix (tables AX5-AX12). Surprisingly, among the top upregulated genes, comparing inflamed or non-inflamed IBD samples to normal colon, are genes associated with immunoglobuling production like e.g. *IGKC*, *JCHAIN*, *IGHA1* and *IGLC2* (tables R51-R54). Usually these genes are allocated exclusively to immunoglobulin producing B lineage cells, but recently there were several publications released were they described that heavy and light chain immunoglobulins are expressed in non-B cells such as macrophages extracted from a human tumour environment, and cells in renal tissue (mesengial cells & proximal tubular epithelial cells) (Fuchs et al. 2018; Deng et al. 2020). Sample contamination with B cells, plasma cells or plasmablasts should not occure due to the state of the art sorting strategy, and additionally was not reflected in the transcriptomic data (Fig.R49).

Another interesting find was the expression of genes which are linked to neuronal activity like e.g. axon guidance or neuron to smooth muscle signaling represented by genes like *PRRG4*, *PTPRF* and *P2RX1* (tables R51, R52, R54). Intestinal mDCs might be involved in maintenance of neuronal connections to the lamina propria. This could influence e.g. (1) the connection to the smooth muscle tissue, which is responsible for the peristaltic movement of the bowel, or (2) the brain-gut axis in general (Cryan et al. 2019; Murillo-Rincon et al. 2017; Quigley 2011; De Vadder et al. 2014). A possible contamination with mast cells as seen with figure R50 needs to be considered for the assessment of connections to the nervous system.

Besides that, it is noteworthy that within the top 20 up- and downregulated lists of thirteen different DC group comparisons there are 25 individual novel transcripts found, indicating the possibility for new functions and regulatory processes that can not be allocated yet. The novel transcript *AC009570.2* for instance is the top differentially expressed gene between non-inflamed IBD and normal colon samples and the second most differentially expressed gene in inflamed IBD versus normal colon (tables R51, R52).

After reviewing the data, it becomes apparent that mDCs seem to have more functions beside antigen sampling, T/B cell induction and participation in lymphoid tissue development(Chu et al. 2012; McDonald et al. 2010).

Upregulated	Gene name	Linear Fold Change	p-value	Gene description
1	*IGKC*	463,60	1,24E-07	immunoglobulin kappa constant
2	*AC009570.2*	376,72	5,09E-04	novel transcript
3	*JCHAIN*	190,93	5,86E-05	joining chain of multimeric IgA and IgM
4	*PRRG4*	92,78	1,31E-13	proline rich and Gla domain 4
5	*ALOX15B*	88,01	1,96E-03	arachidonate 15-lipoxygenase type B
6	*TNFRSF11A*	71,18	1,54E-06	TNF receptor superfamily member 11a
7	*TCEA3*	64,90	2,19E-02	transcription elongation factor A3
8	*CASZ1*	56,66	2,73E-06	castor zinc finger 1
9	*TGM2*	55,42	8,52E-09	transglutaminase 2
10	*PIGR*	46,88	9,85E-05	polymeric immunoglobulin receptor
11	*IKZF3*	42,94	3,94E-04	IKAROS family zinc finger 3
12	*ZNF155*	42,10	1,79E-03	zinc finger protein 155
13	*MAP3K9*	42,07	5,11E-03	mitogen-activated protein kinase kinase kinase 9
14	*DLC1*	41,52	1,49E-02	DLC1 Rho GTPase activating protein
15	*PTPRF*	39,74	1,82E-03	protein tyrosine phosphatase receptor type F
16	*EBF4*	38,59	4,96E-07	EBF family member 4
17	*RHEBL1*	36,60	5,14E-03	RHEB like 1
18	*CKAP4*	36,27	2,43E-03	cytoskeleton associated protein 4
19	*LAD1*	35,94	1,96E-06	ladinin 1
20	*WNT5B*	35,40	1,35E-03	Wnt family member 5B
Downregulated	**Gene name**	**Linear Fold Change**	**p-value**	**Gene description**
1	*CD209*	-12,80	6,31E-03	CD209 molecule
2	*LETM2*	-12,66	6,67E-03	leucine zipper and EF-hand containing transmembrane protein 2
3	*FCER1A*	-11,27	2,27E-08	Fc fragment of IgE receptor Ia
4	*PLB1*	-10,59	2,23E-03	phospholipase B1
5	*KLF3P1*	-10,47	2,25E-02	Kruppel like factor 3 pseudogene 1
6	*AL390957.1*	-10,38	2,87E-05	novel transcript
7	*PRAM1*	-10,30	9,37E-04	PML-RARA regulated adaptor molecule 1
8	*AC108134.3*	-9,76	1,02E-02	novel transcript
9	*TRIT1*	-9,33	1,59E-02	tRNA isopentenyltransferase 1
10	*SDS*	-9,09	2,22E-07	serine dehydratase
11	*GUCY1B1*	-8,99	3,57E-03	guanylate cyclase 1 soluble subunit beta 1
12	*AC243960.3*	-8,75	1,30E-03	novel transcript
13	*ELAVL4*	-8,49	7,01E-04	ELAV like RNA binding protein 4
14	*NFKBIL1*	-8,32	3,65E-03	NFKB inhibitor like 1
15	*AC087239.1*	-8,24	1,00E-02	novel transcript
16	*IGF1*	-8,18	2,64E-03	insulin like growth factor 1
17	*CTSZ*	-7,80	7,78E-04	cathepsin Z
18	*AC024145.1*	-7,62	1,48E-02	novel transcript to ITPR2
19	*CXCL10*	-7,48	3,14E-02	C-X-C motif chemokine ligand 10
20	*LINC02029*	-7,41	5,31E-03	long intergenic non-protein coding RNA 2029

Table R51: Top 20 up- and downregulated genes from iUC+iCD mDCs vs NC mDCs

Upregulated	Gene name	Linear Fold Change	p-value	Gene description
1	*AC009570.2*	794,38	9,10E-05	novel transcript
2	*IGKC*	560,90	4,99E-08	immunoglobulin kappa constant
3	*JCHAIN*	397,59	4,66E-06	joining chain of multimeric IgA and IgM
4	*HDC*	58,29	2,48E-03	histidine decarboxylase
5	*IGHA1*	56,63	3,51E-04	immunoglobulin heavy constant alpha 1
6	*IKZF3*	53,83	1,70E-04	IKAROS family zinc finger 3
7	*RETREG1*	50,43	4,51E-05	reticulophagy regulator 1
8	*TNFRSF11A*	33,64	7,55E-05	TNF receptor superfamily member 11a
9	*PTPRF*	27,13	5,19E-03	protein tyrosine phosphatase receptor type F
10	*CASZ1*	26,58	1,40E-04	castor zinc finger 1
11	*CRAMP1*	26,27	1,47E-05	cramped chromatin regulator homolog 1
12	*DLC1*	25,43	3,45E-02	DLC1 Rho GTPase activating protein
13	*CKAP4*	22,16	8,92E-03	cytoskeleton associated protein 4
14	*TGM2*	21,41	1,14E-05	transglutaminase 2
15	*KANK1*	19,44	4,60E-05	KN motif and ankyrin repeat domains 1
16	*HEG1*	17,39	4,72E-03	heart development protein with EGF like domains 1
17	*DDR1*	17,04	6,80E-03	discoidin domain receptor tyrosine kinase 1
18	*PRRG4*	17,00	3,87E-06	proline rich and Gla domain 4
19	*P2RX1*	15,06	3,75E-03	purinergic receptor P2X 1
20	*MYO7B*	14,99	8,41E-04	myosin VIIB
Downregulated	**Gene name**	**Linear Fold Change**	**P-value**	**Gene description**
1	*CTSZ*	-25,72	1,12E-07	cathepsin Z
2	*CDT1*	-10,85	2,73E-03	chromatin licensing and DNA replication factor 1
3	*PRKCH*	-5,39	4,27E-03	protein kinase C eta
4	*APH1A*	-5,29	5,26E-04	aph-1 homolog A, gamma-secretase subunit
5	*HNRNPA0*	-4,92	5,47E-05	heterogeneous nuclear ribonucleoprotein A0
6	*AC092053.2*	-4,66	1,01E-03	novel transcript, antisense CSRNP1
7	*AC004837.4*	-4,65	4,48E-02	novel transcript
8	*SNORD3A*	-4,56	1,20E-03	small nucleolar RNA, C/D box 3A
9	*NFKBIL1*	-4,54	3,67E-02	NFKB inhibitor like 1
10	*RSAD2*	-4,26	1,89E-02	radical S-adenosyl methionine domain containing 2
11	*UNC93B1*	-3,99	1,25E-02	unc-93 homolog B1, TLR signaling regulator
12	*AL158834.2*	-3,94	1,38E-02	novel transcript
13	*PES1*	-3,88	1,20E-02	pescadillo ribosomal biogenesis factor 1
14	*AL031602.2*	-3,79	3,02E-02	novel transcript, antisense to RNF19B
15	*SOCS3*	-3,70	1,17E-04	suppressor of cytokine signaling 3
16	*SLC16A3*	-3,70	2,93E-04	solute carrier family 16 member 3
17	*LMNB1*	-3,68	1,04E-02	lamin B1
18	*AC109326.1*	-3,67	2,09E-03	TEC
19	*RCC1L*	-3,64	2,95E-02	RCC1 like
20	*UBE2S*	-3,63	4,69E-04	ubiquitin conjugating enzyme E2 S

Table R52: Top 20 up- and downregulated genes from niUC + niCD mDCs vs NC mDCs

Upregulated	Gene name	Linear Fold Change	p-value	Gene description
1	*CCL19*	33,43	1,09E-03	C-C motif chemokine ligand 19
2	*IGLC2*	19,02	5,04E-03	immunoglobulin lambda constant 2
3	*ALOX15B*	17,23	1,53E-02	arachidonate 15-lipoxygenase type B
4	*BLOC1S4*	13,82	1,20E-03	biogenesis of lysosomal organelles complex 1 subunit4
5	*MUC1*	12,93	1,42E-04	mucin 1, cell surface associated
6	*S1PR1*	7,95	2,22E-03	sphingosine-1-phosphate receptor 1
7	*TGFA*	7,56	2,58E-04	transforming growth factor alpha
8	*FSCN1*	7,50	2,72E-08	fascin actin-bundling protein 1
9	*NPFFR1*	7,40	3,27E-03	neuropeptide FF receptor 1
10	*SLC6A12*	7,27	2,45E-02	solute carrier family 6 member 12
11	*LAD1*	6,70	2,27E-03	ladinin 1
12	*TCF7*	6,54	1,31E-02	transcription factor 7
13	*TBC1D13*	6,35	2,48E-03	TBC1 domain family member 13
14	*RCC1L*	6,31	2,26E-04	RCC1 like
15	*SLC9A6*	6,26	2,76E-03	solute carrier family 9 member A6
16	*CD200*	6,15	2,69E-03	CD200 molecule
17	*MMD*	5,85	1,29E-03	monocyte to macrophage differentiation associated
18	*PERP*	5,81	3,90E-02	p53 apoptosis effector related to PMP22
19	*FAM114A1*	5,81	1,59E-02	family with sequence similarity 114 member A1
20	*GZMB*	5,62	4,79E-03	granzyme B
Downregulated	**Gene name**	**Linear Fold Change**	**p-value**	**Gene description**
1	*TPSD1*	-27,38	2,31E-02	tryptase delta 1
2	*ELAVL4*	-9,26	3,05E-05	ELAV like RNA binding protein 4
3	*FCER1A*	-9,25	1,01E-09	Fc fragment of IgE receptor Ia
4	*GUCY1B1*	-9,25	4,95E-04	guanylate cyclase 1 soluble subunit beta 1
5	*IGHA1*	-7,97	2,80E-02	immunoglobulin heavy constant alpha 1
6	*ADRB2*	-7,33	7,83E-03	adrenoceptor beta 2
7	*PLB1*	-7,19	2,53E-03	phospholipase B1
8	*RAB33A*	-7,11	7,78E-03	RAB33A, member RAS oncogene family
9	*LHFPL6*	-7,00	1,61E-02	LHFPL tetraspan subfamily member 6
10	*RRP9*	-6,95	7,77E-03	ribosomal RNA processing 9, U3 small nucleolar RNA binding protein
11	*AL390957.1*	-6,29	1,12E-04	novel transcript
12	*DNASE1L3*	-6,15	1,13E-07	deoxyribonuclease 1 like 3
13	*MTRNR2L8*	-6,09	2,27E-04	MT-RNR2 like 8
14	*C1QC*	-5,91	5,38E-05	complement C1q C chain
15	*TRIT1*	-5,76	2,52E-02	tRNA isopentenyltransferase 1
16	*GHRL*	-5,61	1,40E-04	ghrelin and obestatin prepropeptide
17	*FLYWCH2*	-5,61	3,71E-05	FLYWCH family member 2
18	*SDS*	-5,59	1,52E-06	serine dehydratase
19	*GINS2*	-5,21	4,27E-02	GINS complex subunit 2
20	*CD1E*	-5,05	1,33E-05	CD1e molecule

Table R53: Top 20 up- and downregulated genes from iUC + iCD mDCs vs niUC + niCD mDCs

Upregulated	Gene name	Linear Fold Change	p-value	Gene description
1	*CCL19*	21,98	1,31E-03	C-C motif chemokine ligand 19
2	*IGLC2*	21,01	1,15E-03	immunoglobulin lambda constant 2
3	*PIGR*	10,12	1,91E-03	polymeric immunoglobulin receptor
4	*S1PR1*	9,81	1,96E-04	sphingosine-1-phosphate receptor 1
5	*LAD1*	9,40	1,87E-04	ladinin 1
6	*ECE1*	8,69	3,88E-05	endothelin converting enzyme 1
7	*PRRG4*	8,19	2,44E-05	proline rich and Gla domain 4
8	*CD200*	7,13	3,07E-04	CD200 molecule
9	*FSCN1*	5,83	1,14E-07	fascin actin-bundling protein 1
10	*IL32*	5,10	2,23E-03	interleukin 32
11	*STARD10*	5,05	4,27E-03	StAR related lipid transfer domain containing 10
12	*MMD*	4,78	1,56E-03	monocyte to macrophage differentiation associated
13	*ZNF366*	4,34	1,37E-05	zinc finger protein 366
14	*MYH11*	4,25	9,66E-05	myosin heavy chain 11
15	*TBC1D4*	4,19	5,64E-05	TBC1 domain family member 4
16	*PHF23*	4,15	2,27E-04	PHD finger protein 23
17	*ITPR3*	4,00	1,30E-02	inositol 1,4,5-trisphosphate receptor type 3
18	*GZMB*	3,92	1,42E-02	granzyme B
19	*CBLB*	3,79	3,00E-04	Cbl proto-oncogene B
20	*SLC25A25*	3,77	6,07E-04	solute carrier family 25 member 25
Downregulated	**Gene name**	**Linear Fold Change**	**p-value**	**Gene description**
1	*TPSD1*	-19,42	2,44E-02	tryptase delta 1
2	*FCER1A*	-9,96	2,16E-12	Fc fragment of IgE receptor Ia
3	*SDS*	-6,83	3,95E-09	serine dehydratase
4	*ADRB2*	-6,38	5,81E-03	adrenoceptor beta 2
5	*DNASE1L3*	-5,84	9,68E-09	deoxyribonuclease 1 like 3
6	*IGF1*	-5,81	9,50E-04	insulin like growth factor 1
7	*CCL2*	-5,47	4,50E-03	C-C motif chemokine ligand 2
8	*CD1E*	-5,02	1,27E-06	CD1e molecule
9	*C1QC*	-4,73	1,27E-04	complement C1q C chain
10	*GHRL*	-4,67	1,94E-04	ghrelin and obestatin prepropeptide
11	*PTX3*	-4,64	4,44E-03	pentraxin 3
12	*CD36*	-4,64	4,43E-07	CD36 molecule
13	*HELLPAR*	-4,48	1,17E-03	HELLP associated long non-coding RNA
14	*CD207*	-4,46	1,17E-04	CD207 molecule
15	*FLYWCH2*	-4,43	1,45E-04	FLYWCH family member 2
16	*HCAR2*	-4,36	2,30E-04	hydroxycarboxylic acid receptor 2
17	*AL355881.1*	-4,35	4,51E-04	novel transcript, antisense to SGK1
18	*AL109615.2*	-4,26	1,69E-03	novel transcript
19	*ITGAM*	-4,22	1,96E-04	integrin subunit alpha M
20	*CACNA2D3*	-4,18	9,66E-04	calcium voltage-gated channel auxiliary subunit alpha2delta 3

Table R54: Top 20 up- and downregulated genes from iUC + iCD mDCs vs niUC + niCD + NC mDCs

3.11.6 Gene Ontology analysis of IBD patients and healthy individuals mDCs

Multiple gene ontology (GO) analyses were made between the five different patient groups of analyzed mLPDCs. To gain insight into general functional properties of mDCs in the lamina propria, a GO term analysis was done investigating the top 10% of of all non-differentially expressed genes with the highest base mRNA amount from genes present across all five sample groups (unsupervised) (table AX4 (appendix)). As expected, the majority of found GO terms have to do with described functions of mDCs like antigen processing and presentation, Treg cell differentiation, regulation of T cell mediated cytotoxicity, memory T cell induction, B-cell mediated immunity, and tissue homeostasis. Moreover, general tasks of intestinal mDCs seem also to include functions related to growth, anatomical structure homeostasis and humoral immune response (table AX4 (appendix)).

Additional GO term analyses were conducted, considering statistical significant differentially expressed up- and downregulated genes separately, comparing the five patient groups mLPDCs data in thirteen different combinatorial setups (table R55). According to a study from Hong et al. it is more powerful to analyze up- and downregulated differentially expressed genes in gene ontology analyses separately compared to a combined approach (Hong et al. 2014). The GO terms identified cover novel aspects of intestinal mLPDCs with the most prominent ones being neuronal development, neuronal signaling and epithelial cell maintenance. Neuronal processes were upregulated when comparing mLPDCs from inflamed or non-inflamed IBD mucosa against mLPDCs from normal mucosa of healthy individuals (table R55, F, G, L). Notably, neurons are distributed in great numbers throughout the whole intestinal tissue and dendrites are reaching out until closely beneath the epithelial cell layer (Rao and Gershon 2016). Therefore, it might be possible that tissue resident intestinal mDCs are managing repair and structural framework guidance processes for their environment including neuronal cell maintenance. Processes regarding epithelial differentiation were also predicted to be upregulated in inflamed IBD mLPDCs when compared to mLPDCs in non-inflamed IBD or healthy individuals (table R55, C, E, F). Inflammatory sites of IBD patients are known to be impaired regarding the epithelial barrier integrity accompanied by loss of epithelial cells (Mankertz and Schulzke 2007), and intestinal mLPDCs seem to be involved in epithelial differentiation/proliferation and therefore wound healing processes in IBD.

A)

niCD vs NC upregulated

GO term	Description	P-value	FDR q-value	Enrichment (N, B, n, b)
GO:1903034	regulation of response to wounding	9,07E-04	1,00E+00	4,91 (314,5,64,5)

niCD vs NC downregulated

GO term	Description	P-value	FDR q-value	Enrichment (N, B, n, b)
GO:0051128	regulation of cellular component organization	9,30E-05	3,78E-01	1,41 (279,50,178,45)

B)

iCD vs NC upregulated

GO term	Description	P-value	FDR q-value	Enrichment (N, B, n, b)
GO:0003008	system process	1,40E-04	6,74E-01	6,04 (460,29,21,8)
GO:0045745	positive regulation of G protein-coupled receptor signaling pathway	1,99E-04	4,78E-01	65,71 (460,2,7,2)
GO:0044057	regulation of system process	3,77E-04	6,04E-01	4,57 (460,13,62,8)
GO:0008277	regulation of G protein-coupled receptor signaling pathway	4,00E-04	4,80E-01	13,53 (460,8,17,4)
GO:0007600	sensory perception	7,18E-04	6,90E-01	10,57 (460,6,29,4)
GO:1903522	regulation of blood circulation	7,27E-04	5,82E-01	4,11 (460,6,112,6)

iCD vs NC downregulated

GO term	Description	P-value	FDR q-value	Enrichment (N, B, n, b)
GO:0006950	response to stress	3,20E-04	1,00E+00	1,14 (652,151,525,139)

C)

iCD vs niCD upregulated

GO term	Description	P-value	FDR q-value	Enrichment (N, B, n, b)
GO:0030855	epithelial cell differentiation	9,70E-04	1,00E+00	53,17 (319,4,3,2)

iCD vs niCD downregulated

GO term	Description	P-value	FDR q-value	Enrichment (N, B, n, b)
GO:0030258	lipid modification	2,86E-04	1,00E+00	3,84 (537,12,105,9)
GO:0001889	liver development	8,03E-04	1,00E+00	7,36 (537,4,73,4)

D)

niUC vs NC upregulated

GO term	Description	P-value	FDR q-value	Enrichment (N, B, n, b)
GO:0006956	complement activation	2,43E-04	1,00E+00	59,43 (416,2,7,2)
GO:0072376	protein activation cascade	2,43E-04	5,59E-01	59,43 (416,2,7,2)
GO:0001895	retina homeostasis	3,73E-04	5,71E-01	19,50 (416,4,16,3)
GO:0043207	response to external biotic stimulus	5,63E-04	6,46E-01	13,87 (416,20,6,4)
GO:0046189	phenol-containing compound biosynthetic process	6,37E-04	5,85E-01	37,82 (416,2,11,2)
GO:0043270	positive regulation of ion transport	7,61E-04	5,83E-01	8,99 (416,5,37,4)
GO:0009607	response to biotic stimulus	8,77E-04	5,75E-01	12,61 (416,22,6,4)

niUC vs NC downregulated

GO term	Description	P-value	FDR q-value	Enrichment (N, B, n, b)
	no GO Term with p-value > 1,0E-03			

E)

iUC vs NC upregulated

GO term	Description	P-value	FDR q-value	Enrichment (N, B, n, b)
GO:0001503	ossification	1,47E-04	8,21E-01	106,50 (639,2,6,2)
GO:0045616	regulation of keratinocyte differentiation	1,47E-04	4,11E-01	106,50 (639,2,6,2)
GO:0045604	regulation of epidermal cell differentiation	3,50E-04	6,50E-01	71,00 (639,3,6,2)
GO:0051271	negative regulation of cellular component movement	3,69E-04	5,15E-01	5,35 (639,11,76,7)
GO:0001894	tissue homeostasis	5,78E-04	6,45E-01	26,62 (639,9,8,3)
GO:0040013	negative regulation of locomotion	8,91E-04	8,28E-01	4,90 (639,12,76,7)
GO:0016338	calcium-independent cell-cell adhesion via plasma membrane cell-adhesion molecules	9,32E-04	7,43E-01	31,95 (639,2,20,2)
GO:0001667	ameboidal-type cell migration	9,56E-04	6,67E-01	3,31 (639,7,193,7)

iUC vs NC downregulated

GO term	Description	P-value	FDR q-value	Enrichment (N, B, n, b)
GO:0019935	cyclic-nucleotide-mediated signaling	5,51E-05	2,69E-01	12,96 (363,4,28,4)
GO:0008015	blood circulation	8,04E-05	1,96E-01	25,93 (363,3,14,3)
GO:0007263	nitric oxide mediated signal transduction	6,25E-04	1,00E+00	12,96 (363,3,28,3)
GO:0019932	second-messenger-mediated signaling	9,53E-04	1,00E+00	7,20 (363,9,28,5)
GO:0034764	positive regulation of transmembrane transport	9,85E-04	9,61E-01	15,12 (363,4,18,3)

F)

iUC vs niUC upregulated

GO term	Description	P-value	FDR q-value	Enrichment (N, B, n, b)
GO:0045595	regulation of cell differentiation	1,86E-04	7,83E-01	6,91 (266,33,7,6)
GO:0030856	regulation of epithelial cell differentiation	4,26E-04	8,95E-01	44,33 (266,2,6,2)
GO:0045682	regulation of epidermis development	4,26E-04	5,96E-01	44,33 (266,2,6,2)
GO:0045616	regulation of keratinocyte differentiation	4,26E-04	4,47E-01	44,33 (266,2,6,2)
GO:0045604	regulation of epidermal cell differentiation	4,26E-04	3,58E-01	44,33 (266,2,6,2)
GO:1901617	organic hydroxy compound biosynthetic process	4,26E-04	2,98E-01	44,33 (266,2,6,2)
GO:0030334	regulation of cell migration	4,59E-04	2,76E-01	8,64 (266,22,7,5)
GO:0018958	phenol-containing compound metabolic process	4,60E-04	2,42E-01	59,11 (266,3,3,2)
GO:0022610	biological adhesion	4,76E-04	2,22E-01	2,33 (266,17,94,14)
GO:0007155	cell adhesion	4,76E-04	2,00E-01	2,33 (266,17,94,14)
GO:0061549	sympathetic ganglion development	5,96E-04	2,28E-01	38,00 (266,2,7,2)
GO:0061548	ganglion development	5,96E-04	2,09E-01	38,00 (266,2,7,2)
GO:2000145	regulation of cell motility	6,06E-04	1,96E-01	8,26 (266,23,7,5)
GO:0030335	positive regulation of cell migration	7,66E-04	2,30E-01	11,69 (266,13,7,4)
GO:2000147	positive regulation of cell motility	7,66E-04	2,15E-01	11,69 (266,13,7,4)
GO:0051272	positive regulation of cellular component movement	7,66E-04	2,01E-01	11,69 (266,13,7,4)
GO:1901615	organic hydroxy compound metabolic process	8,79E-04	2,17E-01	19,00 (266,7,6,3)
GO:0098609	cell-cell adhesion	8,95E-04	2,09E-01	2,83 (266,8,94,8)
GO:0040012	regulation of locomotion	9,99E-04	2,21E-01	7,60 (266,25,7,5)

iUC vs niUC downregulated

GO term	Description	P-value	FDR q-value	Enrichment (N, B, n, b)

GO:0003013	circulatory system process	4,14E-04	1,00E+00	14,71 (353,3,24,3)
G)				
niUC+niCD vs NC upregulated				
GO term	**Description**	P-value	FDR q-value	Enrichment (N, B, n, b)
GO:0099536	synaptic signaling	1,16E-06	5,55E-03	10,83 (509,6,47,6)
GO:0099537	trans-synaptic signaling	1,16E-06	2,77E-03	10,83 (509,6,47,6)
GO:0098916	anterograde trans-synaptic signaling	1,16E-06	1,85E-03	10,83 (509,6,47,6)
GO:0007268	chemical synaptic transmission	1,16E-06	1,39E-03	10,83 (509,6,47,6)
GO:0050900	leukocyte migration	6,56E-05	6,31E-02	43,63 (509,7,5,3)
GO:0009617	response to bacterium	8,71E-05	6,97E-02	42,42 (509,9,4,3)
GO:0006910	phagocytosis, recognition	1,28E-04	8,78E-02	113,11 (509,3,3,2)
GO:0050864	regulation of B cell activation	1,33E-04	8,00E-02	38,18 (509,10,4,3)
GO:0007267	cell-cell signaling	1,37E-04	7,33E-02	6,32 (509,12,47,7)
GO:0043207	response to external biotic stimulus	2,78E-04	1,33E-01	16,29 (509,25,5,4)
GO:0032501	multicellular organismal process	2,98E-04	1,30E-01	2,05 (509,69,101,28)
GO:1903034	regulation of response to wounding	3,22E-04	1,29E-01	4,54 (509,6,112,6)
GO:0099024	plasma membrane invagination	3,75E-04	1,38E-01	84,83 (509,4,3,2)
GO:0010324	membrane invagination	3,75E-04	1,29E-01	84,83 (509,4,3,2)
GO:0006956	complement activation	3,75E-04	1,20E-01	84,83 (509,4,3,2)
GO:0006959	humoral immune response	3,75E-04	1,12E-01	84,83 (509,4,3,2)
GO:0006958	complement activation, classical pathway	3,75E-04	1,06E-01	84,83 (509,4,3,2)
GO:0006911	phagocytosis, engulfment	3,75E-04	1,00E-01	84,83 (509,4,3,2)
GO:0072376	protein activation cascade	3,75E-04	9,47E-02	84,83 (509,4,3,2)
GO:0050853	B cell receptor signaling pathway	3,75E-04	9,00E-02	84,83 (509,4,3,2)
GO:0009607	response to biotic stimulus	3,76E-04	8,60E-02	15,08 (509,27,5,4)
GO:0002673	regulation of acute inflammatory response	4,45E-04	9,72E-02	67,87 (509,3,5,2)
GO:0023052	signaling	6,27E-04	1,31E-01	5,41 (509,14,47,7)
GO:0035024	negative regulation of Rho protein signal transduction	6,35E-04	1,27E-01	17,35 (509,4,22,3)
GO:0008037	cell recognition	6,75E-04	1,30E-01	67,87 (509,5,3,2)
GO:0045216	cell-cell junction organization	7,95E-04	1,47E-01	7,49 (509,4,68,4)
niUC+niCD vs NC downregulated				
GO term	**Description**	P-value	FDR q-value	Enrichment (N, B, n, b)
	no GO Term with p-value > 1,0E-03			
H)				
iUC+iCD vs NC upregulated				
GO term	**Description**	P-value	FDR q-value	Enrichment (N, B, n, b)
GO:0060401	cytosolic calcium ion transport	2,08E-04	1,00E+00	6,71 (778,5,116,5)
GO:0060402	calcium ion transport into cytosol	2,08E-04	6,41E-01	6,71 (778,5,116,5)
GO:0002673	regulation of acute inflammatory response	2,27E-04	4,68E-01	10,10 (778,4,77,4)
GO:0016477	cell migration	2,56E-04	3,96E-01	3,22 (778,47,77,15)
GO:0032501	multicellular organismal process	2,88E-04	3,55E-01	1,97 (778,113,119,34)
GO:0003008	system process	4,38E-04	4,51E-01	2,53 (778,44,133,19)

iUC+iCD vs NC downregulated				
GO term	**Description**	P-value	FDR q-value	Enrichment (N, B, n, b)
GO:0043901	negative regulation of multi-organism process	6,66E-05	3,36E-01	4,17 (403,11,79,9)
GO:0019935	cyclic-nucleotide-mediated signaling	4,79E-04	1,00E+00	14,93 (403,3,27,3)
GO:0050830	defense response to Gram-positive bacterium	6,73E-04	1,00E+00	9,21 (403,5,35,4)
GO:0061061	muscle structure development	9,63E-04	1,00E+00	31,00 (403,2,13,2)
GO:0007517	muscle organ development	9,63E-04	9,72E-01	31,00 (403,2,13,2)
I)				
niUC vs niCD upregulated				
GO term	**Description**	P-value	FDR q-value	Enrichment (N, B, n, b)
GO:0010469	regulation of signaling receptor activity	1,11E-04	4,82E-01	26,75 (321,4,9,3)
GO:0045599	negative regulation of fat cell differentiation	5,84E-04	1,00E+00	53,50 (321,2,6,2)
niUC vs niCD downregulated				
GO term	**Description**	P-value	FDR q-value	Enrichment (N, B, n, b)
GO:0032502	developmental process	3,58E-04	8,47E-01	1,70 (101,31,44,23)
GO:0032501	multicellular organismal process	4,23E-04	5,01E-01	4,42 (101,16,10,7)
GO:0009617	response to bacterium	4,58E-04	3,62E-01	7,21 (101,4,14,4)
GO:0048869	cellular developmental process	5,24E-04	3,10E-01	1,73 (101,18,55,17)
GO:0048856	anatomical structure development	5,51E-04	2,61E-01	1,49 (101,21,68,21)
J)				
iUC vs iCD upregulated				
GO term	**Description**	P-value	FDR q-value	Enrichment (N, B, n, b)
GO:0120031	plasma membrane bounded cell projection assembly	8,30E-04	1,00E+00	5,20 (525,5,101,5)
GO:0030031	cell projection assembly	8,30E-04	1,00E+00	5,20 (525,5,101,5)
iUC vs iCD downregulated				
GO term	**Description**	P-value	FDR q-value	Enrichment (N, B, n, b)
GO:0051928	positive regulation of calcium ion transport	6,09E-04	1,00E+00	49,75 (199,2,4,2)
GO:0051924	regulation of calcium ion transport	6,09E-04	1,00E+00	49,75 (199,2,4,2)
K)				
iUC+iCD vs niUC+niCD upregulated				
GO term	**Description**	P-value	FDR q-value	Enrichment (N, B, n, b)
GO:0002673	regulation of acute inflammatory response	7,44E-05	3,45E-01	134,00 (402,2,3,2)
GO:0030449	regulation of complement activation	7,44E-05	1,73E-01	134,00 (402,2,3,2)
GO:2000257	regulation of protein activation cascade	7,44E-05	1,15E-01	134,00 (402,2,3,2)
GO:0002920	regulation of humoral immune response	7,44E-05	8,63E-02	134,00 (402,2,3,2)
GO:0043506	regulation of JUN kinase activity	1,24E-04	1,15E-01	80,40 (402,2,5,2)
GO:0043507	positive regulation of JUN kinase activity	1,24E-04	9,58E-02	80,40 (402,2,5,2)
GO:0007257	activation of JUN kinase activity	1,24E-04	8,22E-02	80,40 (402,2,5,2)
GO:0050900	leukocyte migration	1,48E-04	8,55E-02	33,50 (402,12,3,3)
GO:0031294	lymphocyte costimulation	1,61E-04	8,28E-02	15,31 (402,7,15,4)
GO:0031295	T cell costimulation	1,61E-04	7,45E-02	15,31 (402,7,15,4)

GO:0006814	sodium ion transport	4,68E-04	1,97E-01	8,04 (402,4,50,4)
GO:0035725	sodium ion transmembrane transport	4,68E-04	1,81E-01	8,04 (402,4,50,4)
GO:0098662	inorganic cation transmembrane transport	4,95E-04	1,76E-01	2,57 (402,14,134,12)
GO:0098660	inorganic ion transmembrane transport	4,95E-04	1,64E-01	2,57 (402,14,134,12)
GO:0098655	cation transmembrane transport	4,95E-04	1,53E-01	2,57 (402,14,134,12)
GO:0070613	regulation of protein processing	6,05E-04	1,75E-01	67,00 (402,4,3,2)
GO:1903317	regulation of protein maturation	6,05E-04	1,65E-01	67,00 (402,4,3,2)
GO:0042102	positive regulation of T cell proliferation	6,99E-04	1,80E-01	11,91 (402,9,15,4)
GO:0008037	cell recognition	7,64E-04	1,86E-01	67,00 (402,6,2,2)
GO:0006935	chemotaxis	8,60E-04	1,99E-01	10,44 (402,7,22,4)
GO:0050920	regulation of chemotaxis	8,60E-04	1,90E-01	10,44 (402,7,22,4)
GO:0042330	taxis	8,60E-04	1,81E-01	10,44 (402,7,22,4)

iUC+iCD vs niUC+niCD downregulated

GO term	Description	P-value	FDR q-value	Enrichment (N, B, n, b)
GO:0002673	regulation of acute inflammatory response	2,74E-04	1,00E+00	3,84 (461,7,120,7)

L)

iUC+iCD+niUC+niCD vs NC upregulated

GO term	Description	P-value	FDR q-value	Enrichment (N, B, n, b)
GO:0099536	synaptic signaling	2,32E-05	1,35E-01	8,08 (686,11,54,7)
GO:0099537	trans-synaptic signaling	2,32E-05	6,76E-02	8,08 (686,11,54,7)
GO:0098916	anterograde trans-synaptic signaling	2,32E-05	4,51E-02	8,08 (686,11,54,7)
GO:0007268	chemical synaptic transmission	2,32E-05	3,38E-02	8,08 (686,11,54,7)
GO:0007267	cell-cell signaling	3,10E-05	3,61E-02	6,78 (686,15,54,8)
GO:0023052	signaling	1,31E-04	1,28E-01	4,40 (686,19,82,10)
GO:0007154	cell communication	4,84E-04	4,03E-01	3,46 (686,28,85,12)
GO:0030324	lung development	5,05E-04	3,68E-01	8,37 (686,4,82,4)
GO:0051271	negative regulation of cellular component movement	8,81E-04	5,71E-01	2,39 (686,10,287,10)
GO:0003008	system process	9,24E-04	5,39E-01	3,18 (686,39,72,13)

iUC+iCD+niUC+niCD vs NC downregulated

GO term	Description	P-value	FDR q-value	Enrichment (N, B, n, b)
GO:0002673	regulation of acute inflammatory response	2,74E-04	1,00E+00	3,84 (461,7,120,7)

M)

iUC+iCD vs niUC+niCD+NC upregulated

GO term	Description	P-value	FDR q-value	Enrichment (N, B, n, b)
GO:0042102	positive regulation of T cell proliferation	1,49E-04	7,54E-01	3,59 (520,8,145,8)
GO:0030335	positive regulation of cell migration	1,93E-04	4,89E-01	11,82 (520,20,11,5)
GO:2000147	positive regulation of cell motility	1,93E-04	3,26E-01	11,82 (520,20,11,5)
GO:0040017	positive regulation of locomotion	2,73E-04	3,45E-01	11,26 (520,21,11,5)
GO:0030334	regulation of cell migration	2,84E-04	2,87E-01	8,34 (520,34,11,6)
GO:0051272	positive regulation of cellular component movement	3,59E-04	3,02E-01	10,74 (520,22,11,5)
GO:0098662	inorganic cation transmembrane transport	3,78E-04	2,73E-01	2,34 (520,21,169,16)
GO:0098660	inorganic ion transmembrane transport	3,78E-04	2,39E-01	2,34 (520,21,169,16)
GO:0050920	regulation of chemotaxis	4,39E-04	2,47E-01	12,38 (520,7,24,4)

GO:0002673	regulation of acute inflammatory response	4,89E-04	2,47E-01	43,33 (520,2,12,2)
GO:0030449	regulation of complement activation	4,89E-04	2,25E-01	43,33 (520,2,12,2)
GO:2000257	regulation of protein activation cascade	4,89E-04	2,06E-01	43,33 (520,2,12,2)
GO:0002920	regulation of humoral immune response	4,89E-04	1,90E-01	43,33 (520,2,12,2)
GO:1903522	regulation of blood circulation	5,42E-04	1,96E-01	2,17 (520,12,240,12)
GO:0043506	regulation of JUN kinase activity	6,08E-04	2,05E-01	65,00 (520,4,4,2)
GO:0043507	positive regulation of JUN kinase activity	6,08E-04	1,92E-01	65,00 (520,4,4,2)
GO:0007257	activation of JUN kinase activity	6,08E-04	1,81E-01	65,00 (520,4,4,2)
GO:2000145	regulation of cell motility	6,67E-04	1,87E-01	7,27 (520,39,11,6)
GO:1903039	positive regulation of leukocyte cell-cell adhesion	7,29E-04	1,94E-01	2,20 (520,14,219,13)
GO:0040012	regulation of locomotion	9,39E-04	2,37E-01	6,92 (520,41,11,6)
GO:0072507	divalent inorganic cation homeostasis	9,99E-04	2,41E-01	2,60 (520,13,169,11)
GO:0072503	cellular divalent inorganic cation homeostasis	9,99E-04	2,30E-01	2,60 (520,13,169,11)
iUC+iCD vs niUC+niCD+NC downregulated				
GO term	**Description**	P-value	FDR q-value	Enrichment (N, B, n, b)
GO:0040014	regulation of multicellular organism growth	1,21E-04	6,44E-01	13,52 (490,5,29,4)
GO:0019935	cyclic-nucleotide-mediated signaling	1,81E-04	4,80E-01	12,25 (490,5,32,4)
GO:0032720	negative regulation of tumor necrosis factor production	3,62E-04	6,40E-01	4,45 (490,6,110,6)
GO:1903556	negative regulation of tumor necrosis factor superfamily cytokine production	3,62E-04	4,80E-01	4,45 (490,6,110,6)
GO:0007263	nitric oxide mediated signal transduction	4,90E-04	5,20E-01	15,31 (490,3,32,3)

Table R55: GO term analysis comparing different setups of sample groups. A GOrilla GO term analysis was conducted comparing the differentially expressed up- and downregulated genes across different setups of sample groups. NC, normal colon; niUC, non-inflamed ulcerative colitis; iUC, inflamed ulcerative colitis; niCD, non-inflamed Crohn's disease; iCD, inflamed Crohn's disease; N, total number of genes; B, total number of genes associated with a specific GO term; n, number of differentially expressed genes tested for enrichment; b, number of detected genes belonging to the respective GO term; Enrichment: (b/n)/(B/N)
GOrilla tool: (Eden et al. 2009)

Gene name	Base mean mRNA	Non-inflamed UC vs normal colon		Non-inflamed CD vs normal colon		Inflamed UC vs normal colon		Inflamed CD vs normal colon	
		lfc	p-value	lfc	p-value	lfc	p-value	lfc	p-value
LAD1	140	5,24	5,72E-02	5,52	6,15E-02	26,30	4,02E-05	79,43	3,43E-04
CTSK	44	-2,25	6,74E-01	39,28	6,28E-02	64,63	1,56E-02	10,46	3,76E-01
ALOX15B	30	2,43	6,09E-01	8,52	2,35E-01	84,00	4,87E-03	106,86	5,05E-02
PTPRF	47	34,36	1,04E-02	18,53	4,36E-02	43,48	2,90E-03	23,29	1,03E-01
SLC12A4	32	16,87	3,74E-03	12,71	1,28E-02	12,21	5,25E-03	17,85	3,42E-02
P2RX1	73	26,17	1,37E-04	1,45	6,83E-01	6,27	1,94E-02	18,05	1,62E-02
ALS2	19	15,53	1,09E-02	5,86	1,19E-01	13,26	9,18E-03	17,46	5,68E-02
SLC6A12	68	1,82	6,20E-01	1,13	9,23E-01	6,00	1,04E-01	33,25	3,94E-02
IGHA1	1168	299,10	2,19E-05	6,48	1,85E-01	69,95	5,36E-04	1,78	7,61E-01
JCHAIN	2988	389,62	6,52E-05	407,47	1,25E-04	232,17	6,55E-05	5,58	4,16E-01
CD200	81	-1,89	4,23E-01	2,98	1,88E-01	21,80	5,45E-03	7,44	5,32E-03

Table R56: Selection of significantly expressed differentially regulated genes associated with epithelial cell proliferation, neuronal processes, immunoglobulin production and cell modulation. Green tiles represent statistical significant differentially regulated genes (p-value < 0,05, cutoff lfc ±1,5). UC, ulcerative colitis; CD, Crohn's disease; lfc, linear fold change.

3.11.7 Differential gene expression comparison in groups of inflamed and non-inflamed IBD patients

Investigation of the preceding GO term analysis (table R55) reveals that there seem to be major differences in the gene expression profiles of significant differentially regulated genes in UC and CD patients, independent of the activation status.

Under non-inflammatory conditions, when compared to mLPDCs from normal colon, niCD samples have 727 significant differentially expressed genes (SDE) and niUC samples have 722 SDE genes (Fig.R57). Yet, only 251 of these SDE genes are shared between both comparisons, resulting in a difference of approximately 65%. Non-inflamed UC and niCD patients themselves show a set of 493 SDE genes, when comparing both sample groups. A total of 1942 SDE genes is present between all three comparisons shown in figure R56 of which 1463 SDE genes are unique, and 449 combined SDE genes are shared between dual comparisons which contain 2 SDE genes (table AX13 (appendix)) that are present in all three comparisons.

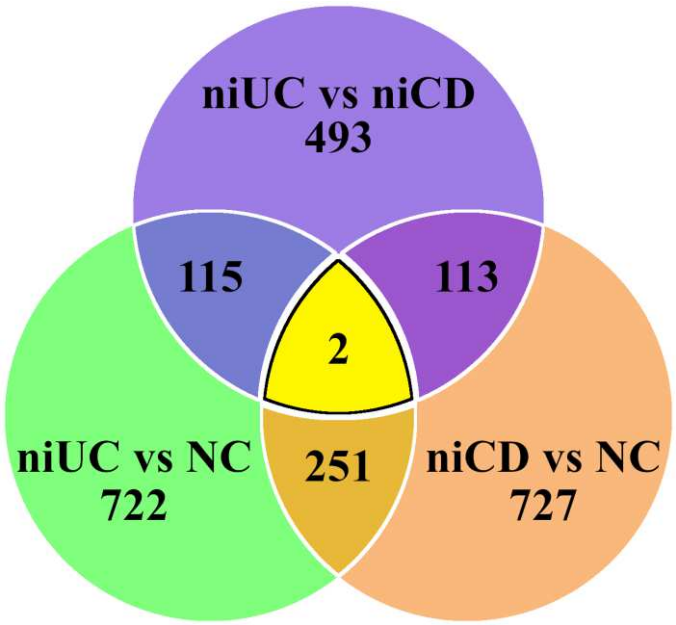

Fig.R57: Significant differential gene expression comparison between niUC, niCD and healthy individuals mLPDCs. This Venn diagram shows the relationship of shared significant differentially expressed genes in numbers of different mLPDC comparisons, containg samples of niUC, niCD patients and healthy individuals. niUC, non-inflamed ulcerative colitis; niCD, non-inflamed Crohn's disease; NC, normal colon.

A similar trend can be observed for the same type of comparison under inflammatory conditions (Fig.R58). Inflamed UC and iCD patients mLPDCs share 412 SDE genes when compared to non-inflamed mLPDCs from healthy individuals. This results in a difference of approximately 67% of SDE genes in these two comparisons. A difference of 845 SDE genes can be observed between iUC and iCD patients mLPDCs. A total of 3346 SDE genes is present between all three comparisons of which 2312 SDE genes are unique, and 1034 combined SDE genes are shared between dual comparisons which contain 37 SDE genes (table AX14 (appendix)) that are present in all three comparisons.

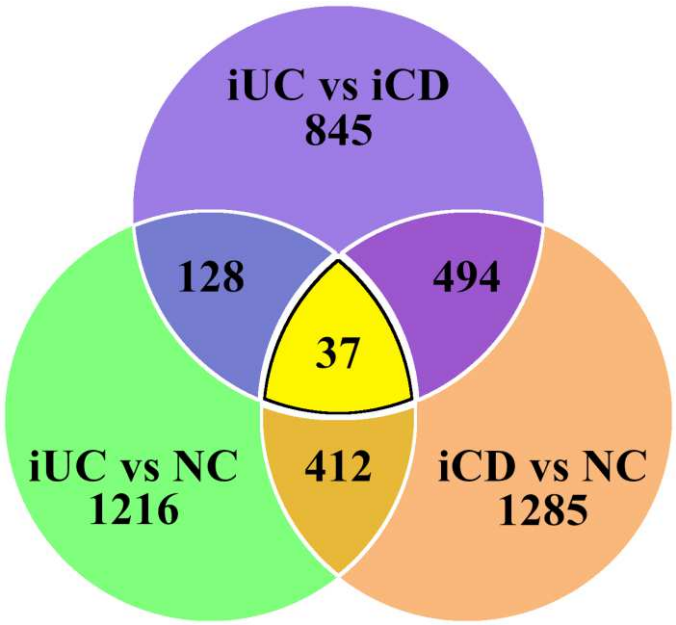

Fig.R58: Significant differential gene expression comparison between iUC, iCD and healthy individuals mLPDCs. This Venn diagram shows the relationship of shared significant differentially expressed genes in numbers of different mLPDC comparisons, containg samples of iUC, iCD patients and healthy individuals. iUC, inflamed ulcerative colitis; iCD, inflamed Crohn's disease; NC, normal colon.

The two Venn diagrams (Figs. R57/R58) reveal that the majority of mLPDC SDE genes differ when comparing IBD patients as well as CD or UC against healthy individuals. This could be shown for inflammatory as well as under non-inflammatory conditions. The level of disparity represented in differential gene expression profiles of mLPDCs of the individual patient groups might be a cause or effect of varying pathological manifestations due to the underlying disease status.

3.11.8 Revisiting: LEL mDC nCounter® data in comparison to the mRNA sequencing dataset from IBD patients and healthy individuals

In section 3.3 the gene expression of LEL mDCs and PBDCs was compared against each other. Due to the nature of the LEL model, and rise in inflammatory mediators in the culture environment, it is assumed that this technique represents an inflammatory process (Schröder-Braunstein et al. 2014). Since the LEL mDCs were compared to DCs from peripheral blood some of the observed differences might be due to the environment mLPDCs are residing in independent from their activation status. Therefore, the information gathered from the nCounter® dataset, more precisely the top 30 differentially expressed genes between LEL mDCs and PBDCs (as seen in table R11), were compared for IBD patients against healthy individuals mLPDCs via their mRNA sequencing data (table R59).

Some of the genes in the aforementioned dataset do not seem to be differentially regulated in IBD patients when compared against normal colon mLPDCs. Genes like *CCL22, CCR7, IL7R, IRAK2* and *CD274* amongst others are upregulated in lamina propria mDCs, compared to PBDCs, probably due to their local environment and independently of an ongoing inflammation. Since the information on inflammatory cells is now based on data of IBD patients, and the LEL mDCs were generated from healthy individuals, differences in gene expression could be attributed to the underlying disease. It is noteworthy that also applied methods of cell extraction could lead to a change in the gene expression profile.

The gene expression for *CD80*, *LAD1, EBI3* and *CXCL8* is significantly differentially regulated in inflammatory IBD patients mLPDCs. TNFRSF11A and TNFRSF4 are significantly upregulated not only under inflammatory but under non-inflammatory conditions as well. Traf1 and TNFRSF9 are significantly differentially regulated, but only in non-inflamed IBD.

A trend towards differential regulation can be seen for *PDCD1LG2, CCL19* and *MMP12*, although not statistical significant within this dataset. *CRLF2, MMP7, ANGPTL4, ENO2* and *CCL24* were not detected using this experimental setup.

Expression of *IL23A* and *EBI3*, which were studied more closely after the nCounter® analysis, were present in all measured groups of mLPDCs. The amount of *IL23A* mRNA is nearly equal expressed in all mLPDC samples. Compared to NC samples, iUC have the same amount of *IL23A* transcripts, and niUC, niCD and iCD mDCs have up to twice as much measured transcripts compared to NC samples. But a statistical significance is not given according to the observed p-values. For *EBI3* expression on the other hand, there is a statistical significant increased amount of *EBI3* in iCD samples compared to NC. Dendritic cells taken from macroscopically inflamed regions from patients with iCD have a ~9,6 times higher *EBI3* mRNA amount compared to mLPDCs from healthy individual biopsy samples. Since this phenomenon was only observed for one group of IBD patients it is of interest if the absence or presence of *EBI3* in mLPDCs correlates with a poor or good prognosis on disease progression.

Gene name	Base mean mRNA	Non-inflamed UC vs normal colon		Non-inflamed CD vs normal colon		Inflamed UC vs normal colon		Inflamed CD vs normal colon	
		lfc	p-value	lfc	p-value	lfc	p-value	lfc	p-value
CCL22	5436	-1,10	8,92E-01	-1,97	3,43E-01	1,35	6,25E-01	-1,52	6,63E-01
MMP12	1066	1,71	4,46E-01	1,68	4,83E-01	-2,24	2,09E-01	-4,88	1,12E-01
CCR7	7566	-1,05	9,10E-01	-1,26	5,89E-01	1,09	8,13E-01	1,58	4,30E-01
CRLF2	-	-	-	-	-	-	-	-	-
LAMP3	1107	-1,12	8,22E-01	-1,19	7,42E-01	1,40	4,63E-01	2,58	1,81E-01
MMP7	-	-	-	-	-	-	-	-	-
CXCL8	17584	-1,41	4,01E-01	-1,63	2,56E-01	-2,09	4,97E-02	-3,22	4,50E-02
IL7R	1406	-1,08	9,19E-01	1,05	9,52E-01	2,96	1,00E-01	2,69	3,34E-01
PDCD1LG2	27	-1,50	7,14E-01	-10,02	6,36E-02	2,63	3,37E-01	15,64	7,61E-02
IL2RA	316	-1,04	9,61E-01	-2,97	1,55E-01	-1,05	9,41E-01	1,70	6,07E-01
ANGPTL4	-	-	-	-	-	-	-	-	-
IDO1	1811	-1,26	6,04E-01	1,84	1,97E-01	2,16	5,99E-02	3,12	7,31E-02
EBI3	353	1,20	7,40E-01	1,35	6,05E-01	2,41	8,41E-02	9,60	4,11E-03
IRAK2	576	1,04	9,04E-01	-1,13	7,38E-01	1,29	4,17E-01	-1,45	4,44E-01
ENO2	-	-	-	-	-	-	-	-	-
CD80	342	2,11	1,98E-01	1,47	5,27E-01	4,65	3,72E-03	7,93	1,16E-02
TRAF1	1639	-1,30	4,05E-01	-2,06	3,00E-02	-1,21	5,06E-01	-1,13	7,88E-01
SOCS2	103	-1,15	8,23E-01	-2,87	1,08E-01	-1,12	8,39E-01	2,96	2,16E-01
CCL24	-	-	-	-	-	-	-	-	-
IL23A	418	2,08	2,63E-01	1,95	3,30E-01	1,03	9,60E-01	1,71	5,63E-01
CCL19	110	-4,50	3,14E-01	-1,61	7,61E-01	8,44	1,16E-01	36,09	8,73E-02
CD274	840	-1,15	8,37E-01	-2,79	1,36E-01	-1,17	7,95E-01	1,12	9,06E-01
IL1R1	696	-1,37	3,12E-01	-1,16	6,47E-01	-1,02	9,51E-01	-3,92	1,92E-03
TNFRSF11A	32	56,65	2,07E-05	5,99	7,71E-02	71,81	1,27E-06	67,95	9,75E-04
RAMP1	429	-2,25	8,06E-02	-1,36	5,22E-01	-1,27	5,73E-01	2,70	1,29E-01
TNFRSF4	184	10,94	7,65E-10	7,43	9,16E-07	11,54	7,60E-12	26,76	1,39E-09
STAT4	293	1,38	3,68E-01	-1,08	8,29E-01	1,53	1,89E-01	1,91	1,97E-01
LAD1	140	5,24	5,72E-02	5,52	6,15E-02	26,30	4,02E-05	79,43	3,43E-04
CLCF1	125	1,19	8,09E-01	-1,13	8,77E-01	2,23	2,26E-01	2,36	4,02E-01
TNFRSF9	391	3,37	1,81E-02	1,25	6,79E-01	1,57	3,38E-01	4,00	5,63E-02

Table R59: Top 30 upregulated LEL mDC genes explored within the RNA seq datasets of IBD patients against normal colon. Green tiles represent statistical significant differentially regulated genes (p-value < 0,05). UC, ulcerative colitis; CD, Crohn's disease; lfc, linear fold change.

4.0 Discussion

Dendritic cells are the bridge between the innate and the adaptive immune system and are key players in orchestrating the outcomes of the immune response to invading organisms and pathogens. Understanding the behavior of those cells under certain conditions might lead to a deeper understanding of why inflammations are not resolved in patients suffering from chronic inflammatory bowel diseases like Crohn's disease or ulcerative colitis. Studies addressing the function of intestinal dendritic cells so far are mainly covering their contribution to a homeostatic equilibrium. This includes antigen uptake and transport to secondary lymphoid structures for presentation, leading to the induction of adaptive immune responses by regulating the allocation and maintenance of T cell subsets (Bekiaris, Persson, and Agace 2014; Bernardo, Chaparro, and Gisbert 2018) and inducing class switching to IgA antibodies in B cells (Tezuka and Ohteki 2019). All of these processes are happening in response to the commensal microbiota, food antigens and unwanted invading pathogens (Kim et al. 2018). Local roles of human myeloid dendritic cells in the intestine besides antigen sampling, especially under acute inflammatory conditions, are rarely investigated or published.

The aim of this study was to gain insight into the local functions of human myeloid dendritic cells residing in the intestinal mucosa under inflammatory versus homeostatic conditions. For this purpose, gene expression profiling of isolated mDCs was employed and sets of differentially expressed genes were subsequently subjected to bioninformatic predictions of biological functions.

4.1 Cell sorting strategy

At first the development of a reliable identification and sorting strategy of intestinal DCs needed to be developed. These mononuclear phagocytes (MNPs) are not so easily distinguishable from other MNPs, namely macrophages, present in the lamina propria, as they share some features and are closely related to each other. Another important factor is that, for a long time, the scientific community had no definitive agreement on the classification of those cell types as they might be mixed up depending on the strategy used to identify them, which makes older publications inaccurate in some cases.

In this study, the identification of cells via flow cytometric analysis was based on the guidelines elaborated at the Flow Immunophenotyping Technical Meeting at NIH (FITMaN) in 2011 (Maecker, McCoy, and Nussenblatt 2012). Additionally, to overcome the non-uniformity in MNP categorization between different scientific groups, Ginhoux, Guillams and Naik released a book in 2016 collecting

scientific works from 2007 to 2016 entitled “Dendritic Cell and Macrophage Nomenclature and Classification” (Ginhoux, Guilliams, and Naik 2016). In line with these guidelines the FACS panel was designed for a proper identification of intestinal mucosal DCs among the emigrated cells. A mixture of several cell surface markers is necessary to identify this cell type and dendritic cells themselves are a heterogeneous group. One phenotype of DCs stood clearly out, as it was a large population present after the LEL model. Target cells were CD45+, CD3-, CD19-, CD20-, CD66b-, CD56-, CD117-,CD326-, CD14- , CD64-/int, had a high expression of HLA-DR++, CD11c+ and were double positive for CD1c+ and CD141+.

To distinguish DCs from other granular cells after the LEL model, CD66b and CD117 were used. CD66b is a marker for granulocytes, which is present on eosinophils and neutrophils in a resting state and increases after activation of the cell (Yoon, Terada, and Kita 2007; Skubitz, Campbell, and Skubitz 1996). CD117 is expressed during all stages of mast cell development (Valent et al. 2010) and could be found in the piece of digested lamina propria (Fig.R4 A) but only a nearly negligible amount could be found after the LEL procedure (Fig.R2 F). For the discrimination from epithelial cells, CD326 was included into the panel (Trzpis et al. 2007).

4.2 The LEL model, inducing an acute inflammatory environment

In order to address the function of colonic DCs during an acute inflammatory response, the LEL model was utilized (Schröder-Braunstein et al. 2014). In this model, an inflammatory reaction is induced in lamina propria cells by ablation of epithelial cells from healthy colonic mucosa via ETDA treatment (Bull and Bookman 1977). The presence of gut epithelial cells (and their mucus) for maintaining homeostasis is vital, as they segregate contents of the lumen, like microbial and nutritional antigens, from the immune cells inside the lamina propria. Both of those sides are interacting with the epithelial cells, which in turn release mediators in both directions to keep the homeostatic balance in the intestinal mucosa (Okumura and Takeda 2017). It was shown that immune cell derived cytokines are influencing intestinal epithelial cells and in parallel, epithelial cells release mediators contributing to immune homeostasis (Kulkarni, Pathak, and Lal 2017). So when the epithelial cells are missing, some important mediators contributing to the maintenance of mucosal homeostasis might be missing, which may promote the inflammatory processes in the LEL model. In fact, extracellular vesicles derived from epithelial cells have been shown to maintain immune homeostasis in the intestine of mice by inducing regulatory T cells and immunosuppressive DCs (Jiang et al. 2016). One could argue that, because of the excision of the tissue and incubation in cell culture medium, some bacteria and bacterial agents are coming in direct contact with immune cells,

mimicking an invasion and leading to the observed immune response. The cell culture medium is admittedly filled with five different bacteriostatic and bactericidal agents (see section 2.4 table "Walk-Out medium" (Material and Methods)) and is changed regularly during the experiment, but for the first 20 minutes minimum everything resides in the same liquid, leaving some time for interaction and possible initial activation of immune cells. However, as shown in a previous study, incubation of mucosal tissue in the culture medium without the removal of the epithelium did not induce an inflammatory response (Schröder-Braunstein et al. 2014). The loss of epithelial cells leads to the phenomenon of initializing the inflammatory response, making it possible for us to examine the cells in this early acute state of inflammation. The advantage of the LEL model, in respect to activated dendritic cells, lies in the fact that this cell type is migrating out of the tissue and can be collected from the culture medium/culture dish, after a few hours of organ culture, without the need of a lengthy isolation procedure.

A study from Mahida et al. showed that after the removal of intestinal epithelium, lymphocytes are actively migrating through basement membrane pores onto the now exposed luminal surface of the lamina propria (Mahida et al. 1997). The same research team could also show that this phenomenon was present in untreated samples of IBD patients. Due to the disease, there were ulcered regions devoid of epithelial cells with migratory lymphocytes coming out of the basement membrane pores (McAlindon et al. 1998). This migratory activity leads to the departure of mDCs from the lamina propria and is replicated with the LEL model. The analysis of those mDCs might unravel new local functions besides antigen sampling and induction of adaptive immune responses.

4.3 Gene expression profiling of migratory mDC in the LEL model

On the search for local functions of mDCs during acute inflammation, gene expression profiling of LEL mDCs was performed employing Nanostring nCounter® mRNA analysis. The advantage of this method is that every molecule of mRNA which is detected is originated from the cell itself, which means that there is no artificial bias introduced as this method forgoes a preceding RNA, more precise, cDNA amplification used in other gene expression profiling techniques (Geiss et al. 2008). The downside, compared to e.g. RNA sequencing, is that the nCounter® technology relies on specific probes for each RNA, limiting the readout to approximately 600 genes in this case. A predefined codeset entitled "human immunology v2" was used for the analysis, and the 579 different predetermined probes were complemented by 30 additional personalized probes based on a former dataset of LEL mononuclear cells. The LEL mDC samples from four patients were compared to DCs from peripheral blood of four healthy donors, which were sorted in the exact same fashion. The idea

behind that was to acquire mDCs which were as quiescent as possible. Enzymatically digesting a piece of lamina propria with subsequent mLPDC isolation requires several hours, most likely resulting in some sort of cell activation. Furthermore, attempts to sort “resting” mDCs from intestinal mucosa, following enzymatic digestion, were not successful due to the low fraction of mDCs in the resulting cell solution. The comparison of LEL mDCs and mPBDCs allowed to identify tissue-specific and/or inflammation-induced genes expressed by resident intestinal mDCs, providing insight into the local function of these cells.

4.3.1 Categorization of cell type and activity status from LEL mDCs versus PBDCs

The nCounter mRNA expression data makes it possible to confirm the categorization of the sorted LEL mDCs, PBDCs and PBMOs (Fig.R7).

The cytokine receptor FLT3 is present on hematopoietic and myeloid progenitor cells and upon stimulation with FLT3 ligand, those cells expand into FLT3 positive DCs (Karsunky et al. 2003). This is in line with the observation that the amount of FLT3 transcripts was high in PBDCs and LEL mDCs and negligibly low in PBMOs. The surface molecule CD14, which was only expressed by PBMOs, is a PRR found predominantly on monocytes and macrophages (Grage-Griebenow, Flad, and Ernst 2001). CD14 is also expressed by some tissue DCs but hints at a monocyte derived origin and these cells were excluded in this study (Collin, McGovern, and Haniffa 2013).

The scavenger receptor CD163 is expressed on monocytes and macrophages and was also absent from the LEL mDC mRNA profile (Buechler et al. 2000).

HLA-DR was present on all 3 groups (PBMO, PBDC and LEL mDC), which is a MHC class II cell surface receptor (Brooks and Moore 1988), constitutively present on B-cells, monocytes, macrophages and DCs (Trombetta and Mellman 2005)and is increased on the cell surface due to inflammatory stimuli (Cella et al. 1997). The number of HLA-DR transcripts on LEL DCs was nearly doubled in comparison to PBDCs indicating cell activation of LEL mDCs. CD80 and CD86 are both upregulated in DCs upon CD40 cross-linking, activating dendritic cells (Caux et al. 1994). CD86 was substantially higher expressed in LEL mDCs compared to PBMOs or PBDCs, and CD80 was exclusively found in LEL mDCs indicating again an activated phenotype of LEL mDCs.

The chemokine receptor CCR7 was only expressed on LEL mDCs. CCR7 is required for migration of DCs inside the lamina propria. Upon activation CCR7 is increased and DCs can enter mesenteric lymph nodes in a CCR7 dependent manner (Jang et al. 2006). It was also shown that lymphocytes re-expressed CCR7 to leave MLNs suggesting that this receptor is needed for general migration purposes (Genua, Sgambato, and Danese 2015). The macrophage specific marker CD64 (*FCGR1A*) was

also not present in LEL mDCs as seen in the appendix table AX3. The gene expression profile in section 3.3.1 shows that the sorted cells are indeed DCs and are not contaminated by monocytes or macrophages. Moreover, LEL mDCs have an activated phenotype compared to DCs extracted from peripheral blood.

4.3.2 Definition of the cDC subtype of LEL mDCs

Dendritic cells in colonic tissue can be categorized into plasmacytoid pDCs, which are CD11c negative and three DC types which are all CD11c positive; these are conventional DCs with the subgroups cDC1 (CD1c-, XCR+), cDC2 (CD1c+, XCR-) and DN DCs(CD1c-, XCR-) (Caër and Wick 2020). Dendritic cell categorization is no easy task and still a matter of debate with conflicting classifications depending on which research group is making the analysis (Caër and Wick 2020). Therefore, two recent classification strategies for human intestinal cDCs from separate publications are listed in table R8, comparing it to gene expression and surface marker levels of the LEL mDCs. In accordance with the gene expression profile and the gating strategy, the sorted LEL mDCs are most probably categorized as cDC2 or a subset of those (Segura 2016; Caër and Wick 2020; Guilliams et al. 2016). Just recently, a study by Brown et al. revealed via single cell analysis, that there are at least two distinct DC populations within the cDC2 subset (Brown et al. 2019). The simultaneous expression of CD1c and CD141 in LEL mDCs is unusal regarding most publications, which make a clear cut between DCs by the expression of the different Blood Dendritic Cell Antigens (BDCA1 = CD1c, BDCA2 = CD303, BDCA3 = CD141, BDCA4 = CD304) (Dzionek et al. 2000). Only a few publications have also mentioned a co-expression of CD1c and CD141 in non-lymphoid tissue DCs (Haniffa et al. 2012; Chu et al. 2012). One of the published CD1c CD141 double positive DC subsets was able to suppress inflammatory reactions in the skin (Chu et al. 2012). Since LEL mDCs are also most probably belonging to the cDC2 subset, an anti-inflammatory behavior is highly likely. Functionally, cDC1 are important for cytotoxic CD8 T cell priming, while cDC2 induce T cells into the Th17 and Treg phenotype (Sun, Nguyen, and Gommerman 2020).

4.3.3 Bioinformatic analysis of the nCounter dataset of LEL mDCs vs PBDCs

The ingenuity pathway analysis (IPA) gave some complementary information on possible functions for the LEL mDCs based on their gene expression profile. The advantage of an IPA analysis is that it takes the exact fold change and p-values into account for the assessment of cellular functions and pathways. The IPA analysis revealed canonical functional properties of LEL mDCs related to their

participation in adaptive immune responses such as: T helper cell differentiation and Th1 and Th2 activation pathways. Surprisingly, the canonical signaling pathway regarding neuroinflammation was also listed, which might hint at a new functional aspect of intestinal mDCs. It is now believed that the gut microbiota and interacting immune cells could be involved in neurodegenerative disorders like Alzheimer's and Parkinson's disease (Baizabal-Carvallo and Alonso-Juarez 2020; Cerovic, Forloni, and Balducci 2019).

As expected the top disease with most associated molecules was "Inflammatory response", given the fact that the LEL mDCs are collected from an inflammatory environment. The uncovered cellular functions include cell-to-cell signaling, cellular development, growth and proliferation, maintenance and movement, which are all logical aspects of known dendritic cell functions.

The subitem "physiological system development and function" revealed participation in "lymphoid tissue structure and development". It was shown in a murine model, that DCs are important in the formation of lymphoid tissue in the intestine (McDonald et al. 2010). It is therefore possible, that the investigated intestinal mDCs are involved in lymphoid tissue formation.

It is noteworthy that the IPA analysis is limited to the fact that a predefined nCounter codeset is used. This means that functional aspects outside of the ~600 investigated genes remain uncovered and the IPA analysis underlies a bias by default. However, uncovered pathways and functional aspects give still valuable insight but are not displaying a complete feature set of mDCs.

4.3.4 Functional aspects regarding top differentially expressed genes

Having a closer look at the lists of up- and downregulated genes in LEL mDCs (tables R11/R12) compared to peripheral blood DCs, the LEL mDCs seem to have some unique functional features based on their activated state and/or local environment they reside in. The following is an analysis based on an excerpt of the lists of top 30 differentially expressed genes of LEL mDCs.

Chemokines

Chemokines are by definition cytokines which act as chemotactic signals for cells bearing the appropriate receptor, inducing directed cell migration (chemotaxis) (Hughes and Nibbs 2018). Among the top 30 upregulated genes are four chemokine mRNAs differentially expressed, which are *CCL22*, *CXCL8*, *CCL19* and *CCL24*; with very high mRNA amounts for *CCL22* and *CXCL8* and lower amounts for *CCL19* and *CCL24*. In comparison blood DCs have a really low mRNA expression of *CXCL8* and only background values for the other three remaining chemokines.

Cells which express the chemokine receptor CCR4 on their surface, predominantly Treg cells and Th2 cells, are affected by CCL22 (Yoshie and Matsushima 2015). In a murine model CCL22 was shown to be important in the communication between DCs and Tregs in lymph nodes (Rapp et al. 2019). $CCL22^{-/-}$ deficient mice suffered from DSS induced colitis at DSS concentrations where WT mice were still without symptoms. Under steady state conditions in the lymph node, CCL22 was exclusively expressed by DCs, and its receptor CCR4 was only found on Treg cells. Treg migration into this area was attributed to the aforementioned fact, but $CCL22^{-/-}$ deficient mice showed no difference in Treg distribution in the lymph node. In models of dermal inflammation CCR4 was also expressed by Th2 cells migrating to sites of inflammation, but the severity of inflammation was worsened in $CCR4^{-/-}$ mice (Lehtimäki et al. 2010). Therefore the expression of CCL22 by DCs could influence Treg (and Th2) homing to their location inducing tolerogenic actions. In a recent publication CCL22 mRNA was shown to be increased in activated DCs from Crohn's disease lesions investigated via singe cell analysis (J. C. Martin et al. 2019).

LEL mDCs themselves express CCR7, which is the chemokine receptor for both, CCL19 and CCL21. They also express CCL19, and an autocrine expression of CCL19 in human monocyte derived DCs blocked their migration towards weaker signals of CCL21, which is a chemotactic factor maturing DCs are following into lymphatic tissues (Hansen et al. 2016). Besides the fact that in the LEL model mDCs are migrating out of the tissue, and therefore most likely not towards a lymphatic tissue derived signal, their CCL19 expression is further evidence of a lymph node independent migration.
T helper cell subsets Th1, Th17 and Treg also express the chemokine receptor CCR7. This receptor has been shown to be important in the regulation of balance regarding these T helper subsets in an inflammatory intestinal environment in mice (McNamee et al. 2015). However, since CCL21 expression was not measured in the LEL mDC mRNA dataset, it is not possible to draw conclusions about the chemotactic potential these mDCs could have on the mentioned T helper subsets. The interplay of CCL19 and CCL21 was shown to be important in directed T cell migration and a weak signal of CCL19 in combination with a high signal of CCL21 led to T cells migrating away from the CCL19 source (Nandagopal, Wu, and Lin 2011). Different CCL19 to CCL21 ratios led to distinct migratory effects and it is therefore of upmost importance to know the balance of CCL19 and CCL21 in the environment before making assumptions. In a recent publication CCL19 mRNA was shown to be increased in activated DCs from Crohn's disease lesions investigated via singe cell analysis (J. C. Martin et al. 2019).

The receptors for CXCL8, namely CXCR1 and CXCR2 are expressed by mononuclear cells, epithelial cells, and lymphocytes in germinal centres in non-inflamed intestinal tissue. In ulcerative colitis patients under inflammatory conditions, CXCR1 expression is increased on macrophages, epithelial

cells, and additionally found on B and T cells outside of germinal centres (Williams et al. 2000). CXCL8 is known as a chemotactic factor for neutrophils, promoter of angiogenesis, proliferative and survival factor of endothelial cells (Waugh and Wilson 2008). On top of that it has been shown to induce migration and proliferation in human intestinal epithelial cell culture cells, indicating to be important for wound healing processes in the intestinal epithelium (Sturm et al. 2005; A. Li, Varney, and Singh 2001). Goblet cells in the intestinal epithelium are secreting mucus components to build up a thick gel like layer, or in the large intestine a double layer, of heavily glycosylated proteins to shield the intestinal tissue from contents of the intestinal lumen and invading pathogens (Johansson and Hansson 2016). If the intestinal epithelium is now damaged, mucus components come in contact with the underlying lamina propria. It has been shown that in response to the mucin MUC2, a key component of the mucus, human monocyte derived dendritic cells were activated with increased surface expression of CD83 and CD86 accompanied by an increase in CXCL8 (IL-8) production (Melo-Gonzalez et al. 2018). These findings link the CXCL8 production from LEL mDCs to a possible recruitment of neutrophils and proliferative and survival factor of intestinal epithelial cells in response to wounding.

CCL24 is a chemoattractant for eosinophils, mast cells, basophils and Th2 cells (Zimmerman et al. 2008). CCR3 is the receptor for several cytokines with CCL24 being one of them (Kulkarni, Pathak, and Lal 2017). The expression level of CCR3 in the colon of UC and CD patients was, independently of the IBD activation status, significantly increased compared to biopsies from normal controls (Manousou et al. 2010). The CCL24 serum levels, amongst other CCR3 ligands, were also increased in IBD patients linking this receptor-chemokine axis to the diseases. Injection of CCL24 into human skin showed a dose dependent infiltration of eosinophils, basophils, neutrophils and macrophages (Menzies-Gow et al. 2002). Dendritic cells from human skin explants have been shown to express CCR3 and monocyte derived DCs were migrating towards CCL24 in a CCR3 dependent manner (Beaulieu et al. 2002). Two human colonic epithelial cell culture lines have been shown to express CCR3 ligands including CCL24 (Manousou et al. 2010). Scientific publications regarding the CCL24 expression in intestinal dendritic cells seems to be lacking at the moment. With regard to the LEL mDC data on CCR3 and CCL24 expression, LEL mDCs could accumulate a variety of innate immune cells in conjunction with and in close proximity to the intestinal epithelium.

Matrix Meatlloproteinases (MMPs)

Among the differentially expressed mRNAs were also the matrix metalloproteinases MMP12, MMP10 and MMP7, which are endopeptidases giving the DCs the ability to degrade extracellular

matrix proteins or process bioactive molecules (Page-McCaw, Ewald, and Werb 2007). So far, 25 MMPs are known and described to be important in inflammatory and wound healing processes (Fingleton 2017; Sengupta and MacDonald 2007). The majority of publications covering MMPs in intestinal tissues refer to macrophages, neutrophils, epithelial cells and mesenchymal cells. Information on intestinal DCs expressing MMPs is scarce to non-existent. When human monocytes transitioned into moDCs they began to express MMPs, which were upregulated upon activation (Kis-Toth et al. 2013). Roles of MMPs are manifold as every molecule has its unique set of functions. Regarding the three upregulated MMPs in intestinal LEL mDCs, MMP7 and MMP10 were found to be increased at ulcer edges in IBD patients, and macrophages in the vicinity expressed high levels of MMP12 (Sengupta and MacDonald 2007).

MMPs are linked to IBDs as they are known to be upregulated under inflammatory conditions and have been shown to be involved in fibrosis, angiogenesis, epithelial barrier function and wound healing (O'Sullivan, Gilmer, and Medina 2015).

The role of MMP12 seems to be multifarious and not easy to pinpoint to a specific function. One study showed that MMP12 was used by murine macrophages to disrupt the bacterial cell wall after ingestion, killing them (Houghton et al. 2009). Another murine study showed that MMP12 cleaved corneal injury induced CCL2 and led therefore to a reduced infiltration of inflammatory macrophages (M. Wolf et al. 2019). In accordance with the previous study CCL2 inhibition was shown to protect mice from trinitrobenzene sulfonic acid (TNBS)-induced colitis due to a reduced leukocyte infiltration (Bhatia et al. 2008). The MMP12 expression in LEL mDCs could hence suggest a role for these cells in bacterial clearance as well as regulation of macrophage infiltration at sites of inflammation.

In a murine model of colitis and dysplasia, the absence of MMP10 was associated with increased disease severity (Koller et al. 2012). MMP10 was predominantly produced by infiltrating cells in the lamina propria and critical for the resolution of the disease and wound healing. This indicates a possible contribution of LEL mDCs in wound healing processes after injury.

In the light of MMP10, MMP7 is also known to be associated with wound healing processes. In a mouse model experiment with $MMP7^{-/-}$ deficient mice, it was shown that MMP7 was needed to prevent an uncontrolled influx of neutrophils (Swee et al. 2008). Additionally, the re-epithelialization after injury was increased in the presence of MMP7. Another function for MMP7 in respect to DSS induced colitis in mice was the production of cryptdins (α-defensins) out of procryptdins. These cryptdins inhibited the IL-1β release from LPS-activated monocytes which is a pro-inflammatory mediator (Shi et al. 2007). LEL mDCs show again a mRNA profile with possible contributions to wound healing through a potential direct impact on epithelial cells and cell type orchestration of their environment.

Miscellaneous molecules

The tryptophan catabolite enzyme indoleamine 2,3 dioxygenase-1 (IDO1) mRNA was also highly expressed in LEL mDCs. Expression of IDO1 has been described in a subset of human intestinal dendritic cells before (Matteoli et al. 2010). Furthermore, an increase in IDO1 expression in the lamina propria could be observed in IBD patients and under inflammatory conditions (A. M. Wolf et al. 2004; Ferdinande et al. 2008). The IDO1 expression was also increased by pro-inflammatory cytokines like IL-1β, which mRNA is also present in LEL mDCs (Barceló-Batllori et al. 2002). In a mouse experiment they showed that IDO1 expression by DCs induced Treg conversion and proliferation, while blocking Th1 and Th17 generation, hence limiting gut inflammation (Matteoli et al. 2010). The induction of IDO1 in epithelial and lamina propria DCs in another murine study has been shown to reduce the severity of colitis (Ciorba et al. 2010). Based on these findings, LPDCs might be involved in the local control of acute inflammatory responses in the intestinal mucosa.

More hints on the regulation of T cell subsets by intestinal dendritic cells during an acute intestinal inflammatory response gave the increased mRNA expression for the molecules PD-L1 (*CD274*) and PD-L2 (*PDCD1LG2*). Both ligands play important roles in the regulation of adaptive and innate immune cells with a focus on T cell regulation (Versteven et al. 2018). The activation and infiltration of cytotoxic $CD8^+$ T cells is inhibited by PD-L1 (Carter et al. 2002) while iTreg proliferation and function are increased (Francisco et al. 2009). The role for PD-L2 is not yet established in detail but it has been shown that it is necessary to sustain CD4 T cell memory in mice (Ellis et al. 2010). The upregulation of both molecules in LEL mDCs suggests that mucosal dendritic cells may be important for controlling intestinal inflammation by suppression of cytotoxic $CD8^+$ T cell responses as well as supporting the formation of a memory phenotype in $CD4^+$ T cells.

Genes with low expression in LEL mDCs but high expression in PBDCs

Focussing on the list of genes showing low expression in LEL mDCs but high expression in PBDCs, it comprises genes shown to be promoting intestinal inflammation.

IL-16 for instance is a chemoattractant for $CD4^+$ T cells and shown to be upregulated in IBD patients (Seegert et al. 2001). Another study showed that in a mouse model IL-16 aggravated DSS induced colitis in conjunction with an increased polarization of macrophages into the pro-inflammatory M1 phenotype (Zhu et al. 2018).

The stimulator of interferon genes (STING), encoded by the *TMEM173* gene, senses bacterially-derived cyclic dinucleotides and triggers the production of pro-inflammatory cytokines and type I

interferons by macrophages, leading to an increase in disease severity in DSS induced colitis in mice (G. R. Martin et al. 2019). In bone marrow derived DCs it was shown that STING was important for the activation of DCs in response to mycobacterium tuberculosis DNA, resulting in IFN-β and IL-12 production as well as CD40 and CD86 expression (Marinho et al. 2018).

CCR2 was shown to be a mediator of adaptive immune responses during Aspergillus fumigatus infection in mice, as depletion of CCR2 inhibited antigen transport to the lymph nodes resulting in abolished $CD4^+$ T cell priming (Hohl et al. 2009). On top of that it has been shown, that CCR2 positive and CCR2 negative DC subsets exist in the human lamina propria and that murine CCR2 positive DCs are allocated to an inflammatory phenotype driving mucosal Th17 cytokine production (Scott et al. 2015). The chemokine receptor CCR2 is clearly linked to inflammatory conditions and seems to be needed for the entry to inflammatory sites by peripheral blood derived cells and is also an important factor for antigen transport into the lymph node. Lack of this receptor further supports an important role for lamina propria DCs in the regulation of intestinal inflammation.

The interferon gamma inducible protein 16 (*IFI16*) is a pattern recognition receptor for ssDNA and dsDNA (Unterholzner et al. 2010; Hurst et al. 2019), which mediates IFN-β production by activating STING following viral infection or DNA damage (Dunphy et al. 2018). Furthermore, it is part of an inflammasome which can react to conserved pathogenic antigens, promotes pyroptotic cell death and is necessary for the processing of e.g. pro-IL-1β into its active form IL-1β before release (Aguilera, Darby, and Melgar 2014). It has been shown that a higher amount of *IFI16* mRNA is correlated with active and inactive IBD versus control patients resulting in the presence of CASP1 in the inflamed mucosa (Vanhove et al. 2015). Low expression of *IFI16* and *TMEM173* in LEL mDCs may suggest a limited capability to activate cell death and secretion of IL-1β under inflammatory conditions, further supporting the notion of a local regulatory function in acute inflammation. LEL mDCs express a considerable amount of IL-1β mRNA, but since the *IFI16* gene seems to be downregulated there might be no release of active IL-1β by these cells under the specific acute inflammatory LEL conditions.

In line with the already discussed beneficial effects of MMPs for wound healing processes, a positive correlation for anti-TNF-α induced low serum levels of tissue inhibitor of matrix metalloproteinases 2 (TIMP2) in IBD patients with remission status could be shown (Carbone et al. 2018). The amount of TIMP2 mRNA is in the range of background transcript levels in LEL mDCs and therefore most likely no active inhibition of MMPs via TIMP2 is taking place.

For the lowly expressed genes it is not so obvious to deduce functions, as some of the features may be present in other cell types and this observation counts only for mDCs and not necessarily for the whole lamina propria environment.

Based on their gene expression profile as characterized in this study, LEL mDCs seem to have a regulatory phenotype, promoting tissue repair e.g. by promoting epithelial cell propagation and survival. Furthermore, they express genes favoring Treg differentiation and maintenance as well as $CD8^+$ cytotoxic T cell inhibition. If these DCs were able to induce $CD4^+$ Th cells the overall cytokine profile for signal 3 shows only TGFβ expression which induces Th3 cells (Martinez-Sanchez et al. 2018). Th3 are a type of regulatory cell involved in oral tolerance induction (Gol-Ara et al. 2012).

These results in the LEL model suggest that human resident lamina propria mDCs – or at least subgroups of them – locally contribute to wound repair and the control of the inflammatory response.

4.4 Analysis of IL-39 expression and function in intestinal mDCs under acute inflammatory conditions in the LEL model

4.4.1 Expression of IL-12 family members in LEL mDCs

Revisiting the list of upregulated genes (table R11), the simultaneous expression of two IL-12 family member mRNAs, namely *IL23A* and *EBI3*, was striking because transcript levels of the other IL-12 family members, these two proteins usually heterodimerize with, could only be detected at background levels. The IL-12 family of cytokines show a chain pairing promiscuity between α and β chains, forming different interleukins with 6 possible heterodimeric combinations as well as different receptor pairings on the cell surface. There are three α chains (IL-12p35, IL-23p19, IL-27p28) and two β chains (IL-12p40, EBI3) resulting in the following six possible combinations: IL-12 (p35/p40), IL-23 (p19/p40), IL-Y (p28/p40), IL-27 (p28/EBI3), IL-35 (p35/EBI3), IL-39 (p19/EBI3) (Hideaki Hasegawa et al. 2016). The interleukins IL-Y and IL-39 have only been discovered recently, and at the time of the observation in the transcript profile of LEL mDCs there were only two publications addressing IL-39 formation and function (Ramnath et al. 2015; Xiaoqian Wang et al. 2016). The majority of research has focused on the functional analysis of the other four heterodimers, demonstarating that the latter interleukins could exert pro-inflammatory as well as anti-inflammatory properties. IL-12, for instance, is produced by APCs after encountering microbial pathogens and has pro-inflammatory properties as it facilitates Th1 differentiation and IFN-γ production by T cells and NK cells (Ma and Trinchieri 2001). IL-35, on the other hand, is an anti-inflammatory cytokine and was shown to be produced by Treg

cells, being critical for proper Treg functions and resolution of inflammation induced symptoms in a murine model (Collison et al. 2007). This shows that although IL-12 and IL-35 share the same subunit Il-12/IL-35-p35 they possess contrasting functions depending on their heterodimeric pairing partner and receptor combination.

IL-23p19 is a current objective of IBD research as it was shown to be elevated in CD and UC patients with increased levels correlating with disease severity (Schmidt et al. 2005; Z. Liu et al. 2011). There are several clinical trials ongoing with monoclonal antibodies targeting the IL-23p19 subunit in IBD patients; first results are promising but the underlying pharmacodynamics remain poorly understood (Hanžel and D'Haens 2020). As IL-39 is a relatively new cytokine all possible explanations for IL-23p19 inhibition and resulting influence on the disease status neglect this molecule completely so far. There was even one publication which stated that IL-23p19$^{-/-}$ deficient mice have an overproduction of IL-12p35/p40 and are more prone to colitis development, indicating that IL-23p19 could have a role in contributing to a homeostatic outcome (Becker et al. 2006).

EBI3 has also been reported to be elevated in the intestines of IBD patients under inflammatory conditions (Gehlert, Devergne, and Niedobitek 2004). In a mouse model it was shown that EBI3 was able to suppress IL-17 production, and EBI3$^{-/-}$ deficient mice experienced an increased infiltration of inflammatory cells to sites of infection. These observations indicate that EBI3 acts in an anti-inflammatory manner (Tong et al. 2010). This notion is further supported by the observation that blockade of EBI3 induced antitumor specific cytotoxic T lymphocytes in colorectal cancer, and thereby reduced tumor growth (Liang et al. 2016).

Functional properties of IL-39, IL-23p19 or EBI3 are not easy to pinpoint as they are involved in a vast array of molecular processes either as individual molecule or in conjunction with different binding partners. As already stated both molecules, IL-23p19 and EBI3, are part of different cytokines, depending on their binding partner, and may even exert immunmodulatory functions on their own. Therefore it is not accurately possible to pinpoint the effects of the presented research to one or two pathways alone, as they may be involved in quite more processes which research has not covered yet.

The first publication describing a heterodimer formation of IL-23p19 and EBI3 was from Ramnath et al., which showed that keratinocytes upregulated IL-23p19 and EBI3 after TLR3 stimulation, proposing that this cytokine heterodimer could contribute to dermal wound healing processes (Ramnath et al. 2015). The second study which addressed IL-39 showed that activated B cells were producing both IL-39 subunits and that IL-39 contributes to expansion of pathogenic B cells in Lupus-like mice aggravating disease severity (Xiaoqian Wang et al. 2016). The same group also released a study revealing that IL-39 produced by these B cells can mediate expansion of neutrophils in the spleen of mice (X. Wang et al. 2016). Furthermore, a study by Manning et al. demonstrated that IL-39

had a positive effect on the pancreatic cancer cell line MiaPiaCa-2 in terms of cell survival and proliferative activity (Manning et al. 2018).

Overall, information on IL-39 is scarce and in terms of the intestinal environment non-existent. Therefore it was of great interest to explore this newly discovered cytokine and its traits in intestinal DCs under acute inflammatory conditions.

4.4.2 Analysis of protein expression of IL-23p19 and EBI3 in the LEL model including LEL mDCs

In order to determine whether the mRNA expression pattern of IL-12 family members, as observed in LEL mDCs employing nCounter® analysis, could be verified on the protein level, immunoblot analysis of LEL mDCs and PBDCs was performed (Figs.R18/R19). Using antibodies against all IL-12 family subunits confirmed a high expression of IL-23p19 and EBI3 in LEL mDCs compared to miniscule amounts of both proteins in PBDCs. The positive control for IL-23p19 did not elicit a signal although Raji cells have *IL23A* mRNA, according to the European Molecular Biology Laboratories Bioinformatics Institute (EMBL-EBI) database (www.ebi.ac.uk/gxa). Either the amount of lysed cells was not sufficient for signal generation or the specific cells used did not express IL-23p19, since the antibody could reliably detect recombinant IL-23p19. The remaining IL-12 family member proteins IL-12p35, IL-12p40 and IL-27p28 could not be detected in either sample group. Again, the functionality of all three antibodies was shown with the detection of their respective recombinant proteins. Thus, the immunoblot results confirmed the observed mRNA transcript level patterns from the nCounter® mRNA analysis.

4.4.3 Expression of IL-23p19 and EBI3 in tissue sections acquired during the LEL model

In line with its high expression in isolated LEL mDCs, an upregulation of IL-23p19 could be detected in lamina propria cells in sections of colonic tissue samples. The immunofluorescence (IF) staining was performed at three different time points during the LEL model. These timepoints were: prior to treatment (healthy complete mucosa (CM)) (Fig.R27), after induction of an intestinal inflammatory response by EDTA mediated removal of mucus and epithelial cells (3.EDTA) (Fig.R28), and after subsequent incubation in cell culture medium for 12 hours (12h LEL) (Fig.R29). Under homeostatic conditions (CM) IL-23p19 was detectable in crypt epithelial cells and some cells in the lamina propria. After the loss of epithelial cells and induction of an inflammatory response (3.EDTA) the number and

intensity of IL-23p19 positive cells had risen from CM over 3.EDTA to 12h LEL in lamina propria residing cells. A study from Wetzel et al. from 2020 showed that IL-23p19 is expressed in human colon epithelial cell culture cells without additional stimulation (Wetzel et al. 2020). This finding was further backed up by a publication from Macho-Fernandez et al. from 2014, where they could see IL-23p19 expression in epithelial cells in a murine model, as well as an increase of IL-23p19 in lamina propria epithelial cells, DCs and macrophages after DSS induced colitis (Macho-Fernandez et al. 2015). The authors also note, that IL-23 release promoted mucosal wound healing.

The expression of EBI3 was also investigated with several available antibodies, but so far none of the tested antibodies gave a valid IF staining. The overall availability of good and valid anti IL-23p19 and anti EBI3 antibodies was in general in need of improvement, and this experiment should be repeated in the future with certified antibodies against EBI3 in FFPE sections. Notably, according to the previous mentioned study from Wetzel et al. EBI3 protein was also expressed in low levels in primary human colon epithelial cells and upregulated after cell stimulation (Wetzel et al. 2020).

Taken together, these findings support the notion that IL-23p19 and EBI3 produced by lamina propria dendritic cells play an important role in lamina propria cell regulation during the induction of an inflammatory response.

4.4.4 Heterodimer detection of IL-23p19 with EBI3 in different setups

The heterodimerization of IL-23p19 and EBI3 could be shown with a co-immunoprecipitation (co-IP) assay (Fig.R20). A considerable amount of rEBI3 protein could only be recovered from anti IL-23p19 coated beads if rIL-23p19 itself was present in the incubated solution. Background binding of rEBI3 to coated beads was minimal as shown with isotype control coated beads. The blot showed bands at 50kDa because a heavy chain specific secondary antibody was used for the detection of protein on the PVDF membrane, minimizing interferences of otherwise occurring light chain bands at 25kDa from the eluation process.

Ramnath et al. came to the same conclusion that both proteins are interacting with each other in a similar co-IP experiment with transfected cells (Ramnath et al. 2015).

However, one study from Detry et al. from 2019 showed that EBI3 and IL-23p19 are not heterodimerizing and they also said that alpha subunits are not secreted by HEK 293T cells without their cognate beta partner (not shown) (Detry et al. 2019). The expression of α or β subunits without their respective binding partner from human cells might be inducible (Müller et al. 2019). On the contrary, EBI3 and IL-23p19 single proteins (derived from human sequence information) could be

detected from cell culture supernatants by ELISA in our lab, contributing to the notion that transfected HEK cells can secrete IL-12 subunits without their respective binding partner.
Moreover all of their cytokines carry multiple tags (FLAG, HIS, V5) for the analysis which could be an inhibiting factor for normal protein function and therefore inhibitor of heterodimer formation (Majorek et al. 2014; Debeljak et al. 2006). In our experminetal setup only rIL-23p19 carried a c-myk/DDK tag and rEBI3 was tag free (missing the first 20 amino acids). Therefore both proteins are detected at an approximate similar kDa value.
The performed co-IP experiment showed that rIL-23p19 and rEBI3 are able to form a heterodimer even in the absence of an intracellular environment, meaning that even if both subunits are not expressed by the same cell type they can interact with each other in the extracellular space.

In order to detect IL-23p19, EBI3 or IL-39 in cells, a cytospin immunohistostaining was established. It was possible to clearly discriminate single and double transfected cells from each other and non-transfected cells (Figs.R21/R22). A proximity ligation assay (PLA) was established based on this technique, showing that IL-23p19 and EBI3 heterodimerize to IL-39 inside double transfected cells (Fig.R23). Control experiments with single transfected cells or using only one of the two probes or primary antibodies in double transfected cells remained negative for every setup tested.

Taken together, the toolset for the detection of IL-23p19 and EBI3 as well as detection and heterodimer formation of IL-39 in cells was established. However, this data is based on overexpression experiments with high protein concentrations, therefore these results needed to be validated under physiological conditions.

After establishing the immunofluorescent staining and PLA techniques for IL-39 in cytospun HEK293T cells, both techniques had been used to verify IL-39 expression and subunit connection in human LEL mDCs. Although Human LEL mDCs had been fixed, blocked and permeabilized the same way as HEK cells, the staining showed an unspecific binding of secondary antibodies to the cells, generating a signal without the presence of primary antibodies directed against the target proteins (Fig.R25). Since DCs have phagocytic abilities and are professional APCs they carry a variety of receptors to catch particles (MacPherson et al. 2004; Sallusto et al. 1995; Lundberg et al. 2014). The nCounter® analysis of LEL mDCs shows that there are mRNAs expressed for several Immunoglobulin receptors (*FCER1G*, *FCGR2A*, *FCGR2A/C*, *FCGRT;* table AX3 (appendix)), and it is known that unspecific binding of antibodies to cells could be a side effect of Fc receptor binding (Smith and Chattopadhyay 2016). But additional treatment with an Fc blocking solution (BD biosciences) did not reduce unspecific binding in cytospun LEL mDCs. To further rule out Fc receptor interference, staining could be performed using conjugated F(ab) or $F(ab')_2$ fragments instead of whole conjugated secondary antibodies.

When performing the PLA with human LEL mDCs, the problem from the immunofluorescent (IF) staining carried over, which is no surprise given the nature of the experimental setup using secondary antibodies as probes. Even in the absence of primary antibodies, using only the secondary antibody probes, accumulation of red fluorescent dots could be detected in some cells (Fig.R26). The PLA was performed with a commercially available kit and there are no probes available without the Fc part to test if this could circumvent the unspecific binding. Perhaps another kind of cell fixation could help to overcome this problem in future experiments.

In addition, attempts were made to detect heterodimers of IL-23p19 and EBI3 from supernatants or cell extracts via sandwich ELISA. But despite a vast array of efforts to overcome false positive signals of heterodimer formation it was not possible to establish a functional sandwich ELISA. Supernatants from transfected HEK cells or recombinant protein solutions served as basis for the assay development. Several combinations of capture and detection antibodies had been tested to find the most potent duo detecting IL-23p19 and EBI3 proteins. But one major problem was that solutions with only one protein subunit of IL-39 gave high OD measurements despite using a sandwich ELISA setup (Fig.R31). The problem was not confined to byproducts in HEK cell supernatants because it occurred also with recombinant proteins in PBS. Incomplete adsorption of capture antibody to the plastic surface was ruled out using either PBS (pH:7,4) or corbonate-bicarbonate buffer (pH:9,4) for microplate coating (Cuvelier et al. 1996), which did not alter the unspecific signal (Fig.R33). Choosing the right blocking reagent can have a huge impact on ELISA performance, minimizing unspecific binding of the target protein to the microplate plastic surface (Vogt et al. 1987). Although 0,1% gelatin was the superior blocking agent compared to the standard 5% BSA, a side by side comparison revealed only minor differences, not being able to reduce the unspecific background in a desirable magnitude (Figs.R34-R36).

Eliminating the uncertainty if the peroxidase coupled secondary antibodies could contribute to the high OD values, generating false positive signals, both secondary antibodies were incubated on several pre-incubated supernatants or protein solutions. Only when the specific detection antibody was present did the secondary HRP coupled antibody bind and generate a signal (Fig.R37). Contribution of false positive signals from unspecific binding of secondary antibodies could therefore be excluded.

To explore to which extent the binding of the target proteins is really based on the presence of capture and detection antibodies, a series of titration experiments were performed (Fig.R38). Capturing IL-23p19 followed by an anti EBI3 detection antibody gave a very low background signal which was diminished with decreasing capture antibody concentrations. No critical cross reactivity of the EBI3 detection antibody, with the IL-23p19 specific capture antibody or IL-23p19 protein could be observed. On the other hand, in the same setup using an IL-23p19 specific capture antibody but

incubating with EBI3 protein followed by detection of EBI3 gave a strong optical density (OD) signal. Lowering the concentration of the capture antibody increased the OD value, which means that the EBI3 protein was binding unspecifically to the microplate plastic surface. ELISAs had shown that the EBI3 detection antibody elicited only measurable signals when EBI3 protein was present. Titration of the detection antibody lowered the signal intensity and was therefore a real effect of binding to EBI3 protein. Using double tranfected cell supernatant in the same setup gave an even stronger signal after lowering the amount of capture antibody. This effect could be due to a varying amount of EBI3 in single versus double transfected cell supernatants.

Taken together all the control experiments showed, that EBI3 protein has a strong adherent affinity to the plastic surface of the ELISA microplates independently of cross reactions to capture, detection or secondary peroxidase coupled antibodies. Even different blocking techniques could not overcome the strong adherent effect observed.

4.4.5 Exploring possible functions of IL-23p19, EBI3 and IL-39

The few available studies on IL-39 have also addressed possible functions of this cytokine. As already mentioned, a study from Wang et al. found out that IL-39 had some effects on neutrophils in mice leading to their expansion and some sort of differentiation (X. Wang et al. 2016). Another study by Bridgewood et al. stated contradictory results as they did not observe any effects on blood leukocytes after IL-39 incubation (Bridgewood et al. 2019). But one major flaw of the study by Bridgewood was that they used a chimeric IL-39 (R&D Systems, #9990-IL) which was covalently bound via a disulfide bridge and additionally linked to the Fc part of human IgG1, adding over 230 amino acids to the only 377 amino acids from both subunits combined. The natural binding dynamics of both subunits, which do not build up a disulfide bond, could be disrupted and is therefore not suited to make a definitive conclusion.

The following research publications did not focus on IL-39, but observed IL-23p19 and EBI3 regulation under certain conditions. The first publication that observed TLR3 induced IL-23p19 and EBI3 expression in keratinocytes linked the production of both subunits to possible wound healing mechanisms (Ramnath et al. 2015). Two cell lines of human intestinal epithelial cells (HT29, Caco2) have been shown to produce IL-12p35, IL-23p19 and EBI3 but not IL-12p40 or IL-27p28 which means they could potentially produce IL-35 and IL-39 but not IL-12, IL-23, IL-27 or IL-Y, giving further evidence for a possible important role of IL-39 in epithelial cell regulation (Maaser et al. 2004). Furthermore, human epithelial colon cells, generated from healthy tissue, showed the same expression profile with EBI3, IL-23p19 and IL-12p35 with an increase in production of those subunits after stimulation (Wetzel et al. 2020). Epithelial cells in other body compartments are also able to

upregulate EBI3 and IL-23p19 as shown e.g. for oral epithelial cells in response to autocrine IL-36γ as induced by bacterial Porphyromonas gingivalis antigen (Scholz et al. 2018). The authors also linked EBI3 and IL-23p19 upregulation to possible wound healing mechanisms with both subunits being stimulated by signaling through the epidermal growth factor receptor (EGFR).

IL-23p19 and EBI3 expression has also been linked to psoriasis, an inflammatory disease of the skin with hyperproliferative keratinocytes (Di Meglio, Villanova, and Nestle 2014). Patients with psoriasis were shown to have a decreased expression of EBI3 and an increased expression of IL-23p19 in keratinocytes compared to healthy individuals (T. Li et al. 2018; X. Chen et al. 2006). The subunit IL-12p40 is also expressed which leads to IL-23 formation and is relevant for the encountered hyperplasia (Lindroos et al. 2011). An additional finding of the same study was that IL-6 signaling is important for the epidermal hyperplasia. Interstingly , it was reported that EBI3 can bind to IL-6 and mediate trans signaling to a gp130-gp130 receptor pair without the need of IL-6R or soluble IL-6R (Chehboun et al. 2017). Moreover it was shown by Aden et al. that deletion of IL-6R in mice did not interrupt intestinal epithelial proliferation or wound healing. Additionally, proliferation of intestinal organoids was induced via IL-6 trans signaling but not classical IL-6 signaling (K. Aden et al. 2016). Maybe this is one regulatory key factor in psoriasis and epithelial cell proliferation in general that has not been scientifically explored. IL-23p19 and EBI3 might not act together but might be influenced by each other. The EBI3 binding to IL-23p19 could also influence the intrinsic effects of IL-23p19 or inhibit IL-23 formation, as well as inducing effects as IL-39 heterodimer to epithelial cells. As it was shown in patients with psoriasis administration of guselkumab, an anti IL-23p19 specific monoclonal antibody, ameliorates disease severity (Wechter, Cline, and Feldman 2018). The already mentioned lower level of EBI3 in patients with psoriasis could therefore be a contributing factor to unregulated IL-23p19 signaling with all its side effects.

Both receptors for IL-23p19 and EBI3 (IL-23R and gp130 respectively) are expressed by colonic epithelial cells (Ernst et al. 2014; Konrad Aden et al. 2016). Besides its impact on the intestinal environment, gp130 was shown to be important for the repair in bronchial epithelial cells, and also affecting their migratory potential (Kida et al. 2008). Epithelial IL-23R was critical for protection of inflammation in a murine model of intestinal inflammation (Konrad Aden et al. 2016).

Given these results, IL-23p19, EBI3 or IL-39 may be involved either directly, indirectly or both in epithelial cell regulation.

In addition, DCs are now recognized to be participating in wound healing processes (Strbo, Yin, and Stojadinovic 2014; Brazil et al. 2019) and e.g. have been shown to accelerate cellular proliferation in burn wounds (Vinish et al. 2016).

This lead to the next experiment exploring the direct wound healing capabilities of IL-39 on primary human epithelial cells. A 2D layer of human colon epithelial cells with a defined gap of 500µm between two compartments of cells was generated, followed by incubation with IL-39, Ebi 3, IL-23p19 and a control solution. When these proteins were incubated in advanced DMEM devoid of any additional growth inducing supplements, cells treated with rIL-39 closed the gap faster compared to samples incubated with rEBI3, control solution or rIL-23p19 in that order (Fig.R41). The experiment could not be repeated due to time constraints and availability of suitable patient material, but this preliminary result shows that effects of IL-39 or EBI3/IL-23p19 on epithelial cells should be further investigated.

In summary, under acute inflammatory conditions the phenotype of CD1c CD141 double positive mDCs was the most abundant of emigrated DCs using the LEL model. Gene expression analysis clearly showed that the sorted cells could be attributed to the DC faction of cells. Furthermore the gene expression profile hinted at a more regulatory and anti-inflammatory rather than pro-inflammatory phenotype. The IL-12 family member subunits of IL-23p19 and EBI3 were highly expressed in these cells without any other IL-12 family member in parallel, hinting at a possible connection to the newly discovered IL-39 cytokine. The subunits of IL-39 namely IL-23p19 and EBI3 could be shown to form the heterodimer IL-39 in cells as well as in an extracellular space. Unfortunately it was not possible to confirm these data in primary cells from humans due to unexpected technical issues specifically with this type of APCs. But first experiments regarding the function of IL-39 look promising towards having a regulatory role in epithelial cell proliferation or wound healing processes backed up by recent scientific publications. IBD patients seem also have an altered amount of those regulatory DCs present in the tissue which might be interesting to investigate in further experiments.

4.5 Gene expression profiling of myeloid LPDCs in intestinal homeostasis and IBD

In order to determine whether genes highly expressed in LEL mDCs during the onset of inflammation are also present in mLPDCs in intestinal inflammation in vivo, a RNA sequencing (RNAseq) analysis of lamina propria mDCs was conducted. Therefore, colonic biopsy samples from healthy individuals as well as colonic biopsy samples from inflamed and non-inflamed regions of IBD patients were gathered and mLPDCs extracted via tissue digestion. Subsequently, the transcriptome of the mLPDCs from the different patient groups was determined. Biopsy material was used for this analysis due to the limited availability of surgical specimens of IBD patients.

Since DCs are rare in the tissue only a small amount of cells can be recovered from biopsy samples. Therefore RNAseq was done on a sample size of around 100 cells per patient, a cell number that would not have been sufficient for gene expression analysis using the nCounter® technique. There are some positive and negative aspects that come along with the change in technique. The negative aspect is that RNAseq relies on the artificial amplification of mRNA, introducing uncertainty about the precise physiological amount of mRNA present in a cell due to a possible unequal amplificication, whereas nCounter® detects cell-derived mRNA molecules without preceding amplification. However, the positive aspect is that without a fixed probe set, a more diverse set of genes can be uncovered. The latter is especially helpful in finding new and important aspects of cell functions and biological processes.

For all following analyses, a p-value <0,05 and a fold change of ±1,5 was considered to be statistical significant differentially expressed. The false discovery rate (FDR) was neglected since fewer replicates than twelve per group in RNAseq experiments have shown to give inadequate FDR measurements (Schurch et al. 2016).

4.5.1 Intestinal dendritic cell subset composition in intestinal inflammation and homeostasis

The amount of dendritic cells recovered from biopsies of normal mucosa of healthy individuals was significantly higher compared to biopsies of inflamed mucosa of IBD patients. The lower mLPDC numbers in inflamed IBD samples may be related to the phenomenon of leukocyte emigration out of the lamina propria through basal membrane pores at sites where epithelial cells are missing (McAlindon et al. 1998), as observed in the LEL model. Moreover, reduced recruitment of DCs into the intestinal mucosa or increased apoptosis may contribute to the low numbers in IBD and thereby restrain the regulatory function of DCs in mucosal inflammation (Hitoshi Hasegawa and Matsumoto 2018) as predicted by the results of this thesis. Supporting this hypothesis, the deletion of a specific DC subset exacerbated DSS induced colitis in mice (Muzaki et al. 2016), emphasizing on the regulatory role of DCs in the intestine. Remarkably, mLPDC numbers were reduced in non-inflamed mucosa of CD but not UC patients when compared to normal mucosa of healthy individuals (table R43). The consistently lower mLPDC numbers in the colonic mucosa of CD vs UC patients, independent of the inflammation state, as well as in comparison to healthy mucosa may hint at a pathogenetically relevant differential regulation of this cell population in these diseases.

As already mentioned, $CD141^+$ or $CD1c^+$ DCs belong to the cDC1 or cDC2 phenotype respectively. The CD141 CD1c double positive (DP) dendritic cells, detected in the intestinal mucosa, likely belong to the cDC2 subtype in accordance with their gene expression profile. According to a study by

MacDonald et al. the majority of dendritic cells in human blood are plasmacytoid DCs and cDC1 DCs, both accounting for approximately 18% of Lin^- $HLA\text{-}DR^+$ cells, followed by cDC2 DCs with 2,7% (MacDonald et al. 2002). In contrast as analyzed in this study, in colonic tissues the cDC2 phenotype was always the most prominent one under homeostatic and inflammatory conditions. In non-inflamed tissues cDC2 cells, classified as $CD1c^+$ and CD1c CD141 DP, made up over 91% of Lin^- $HLA\text{-}DR^{++}$ $CD33^+$ mDCs, whereas in inflamed tissues between 80-85%. The CD1c CD141 DP mLPDCs had the most migratory capacity as seen with the LEL model biopsies (Fig.R44). Another explanation for the enrichment of CD1c CD141 DP DCs could be a change in phenotype under inflammatory conditions, as shown for murine respiratory cDC2 cells which acquired features from cDC1 DCs and macrophages under inflammatory conditions (Bosteels et al. 2020). A similar high amount of cDC2 DCs in colonic tissue compared to cDC1 DCs was described by Granot et al. who reported a cDC2:cDC1 DC ratio of 4:1 in human colonic tissues (Granot et al. 2017).

Functional aspects of conventional DCs in the human intestine are not fully explored yet, especially in IBD patients. Two recent publications made single cell analyses from either CD patients inflamed vs non-inflamed ileums (J. C. Martin et al. 2019) or UC patients colonic biopsies from inflamed or non-inflamed sites versus healthy individuals (Smillie et al. 2019), and reviewed possible traits of LPDCs, amongst other cells, based on their gene expression profile. The study from Martin et al. found four different types of LPDCs being cDC1, cDC2, inflammatory DCs and a fourth DC subset expressing langerin (J. C. Martin et al. 2019). They identified activated DCs as the main drivers of activation and coordination of adaptive immune responses in the inflamed CD tissues. Moreover, based on the receptor and cytokine profile of activated macrophages and activated DCs, they suspect that these cell types are influencing each other in a directed manner (J. C. Martin et al. 2019). The second single cell study by Smillie et al. linked anti-TNF resistance in some patients to expression of Oncostatin M (OSM) in cDC2 and inflammatory monocytes (Smillie et al. 2019; West et al. 2017).

As already mentioned cDC1 are associated with induction of cytotoxic CD8+ T cells (shown in a murine model (Hildner et al. 2008)) and cDC2 with induction of Treg cells (Matsuno et al. 2017). In general, lamina propria derived DCs from IBD patients are more reactive towards bacterial PAMPs compared to healthy control LPDCs (Baumgart et al. 2009). In healthy colonic tissues cDC2 have the ability to induce regulatory T cells, yet in UC patients equivalent cells did not induce Treg but Th1, Th2 and Th17 cells, which lead the authors to assume that these DCs are involved in UC pathogenesis (Matsuno et al. 2017). There is also a report about a special kind of langerin expressing anti-inflammatory cDC2 subset in the ileum, which is significantly decreased in numbers in CD patients, and its absence proposed to be responsible for a pro-inflammatory environment (Doyle et al. 2021).

When comparing the experimental data on mLPDC subset compositions, differences can be observed between normal colonic mucosa of healthy individuals and inflamed and non-inflamed mucosa of IBD patients. Importantly, the mLPDC subset composition in inflamed as well as non-inflamed mucosa differs between UC and CD patients, further supporting the notion that a differential regulation of the dendritic cell compartment may contribute to the pathogenesis of these diseases.

Interestingly, the mDC subset distribution in non-inflamed mucosa of CD patients is, in contrast to the non-inflamed UC state, very similar to that of normal healthy mucosa, which may e.g. reflect a lower inflammatory state of the colonic mucosa in macroscopically non-inflamed mucosa in CD vs UC. Remarkably, the total number of mDCs in non-inflamed CD is only ~1/3 of that of normal mucosa. As there are no considerable changes observed in the composition of leukocyte subsets when compared to normal gut, and furthermore those changes which can be observed are similar between non-inflamed UC and non-inflamed CD, these results may indicate that differential regulation of mDCs may be involved in the pathogenesis of CD. This notion is further supported by the combined observations that (1) DC subset compositions in inflamed CD and UC are considerably different, and (2) the changes observed in UC are more similar to that observed in the LEL model, which reflects a “regular” inflammatory response of mucosal cells of normal individuals. However, due to the low number of replicates (n=2) for the inflamed CD subgroup, the latter observations needs to be confirmed in further experiments analyzing inflamed colonic tissue of CD patients. Due to the manifestation of the disease only a part of CD patients experience inflammations in the colon (Mills and Stamos 2007), which lead to the low number of available inflamed CD replicates.

All in all the reduced amount of overall mDCs in inflamed IBD patient material and the more pronounced CD141 positive and CD1c CD141 double negative fractions might be important factors as to why UC and CD homeostasis regulation might be disturbed in those individuals.

This finding is partly backed up by a publication by Magnusson et al., which showed that $CD1c^+$ and $CD141^+$ cDC subsets are decreased in numbers in the colon of inflamed CD and UC patients (Magnusson et al. 2016). Additionally a specific subset of DCs expressing aldehyde dehydrogenase (ALDH) was reduced in UC patients independent of inflammation (Magnusson et al. 2016).

In order to gain deeper insight into the differential regulation of mLPDCs in IBD, it would be interesting to apply the LEL model to mucosa of niCD and niUC patients. Comparing mLPDC subset composition and transcriptomes under the same experimental conditions with the ones observed in the LEL model applied to normal mucosa may help to identify pathophysiologically relevant dysregulations in mLPDCs in the two disease entities.

4.5.2 Predicting functional properties of mLPDCs in IBD patients versus healthy individuals based on transcriptomic analysis

The hierarchical cluster analysis showed that mDCs gathered from healthy individuals are distinct from mDCs of IBD patients (Fig.R48). Another hierarchical clustering revealed that the mDCs of IBD patients are separated into inflamed and non-inflamed conditions (Fig.R47). In between inflamed or non-inflamed IBD patient samples was no clear distinction between mDCs from niCD and niUC or iCD and iUC detectable. In line with these findings it has been reported that although there are genetic differences between CD and UC patients, the majority of risk alleles is shared between both groups (Ellinghaus et al. 2015). The cluster analysis could not make out any major differences between mDCs of either IBD subgroup.

The gathered mDC mRNA sequencing data were subjected to multiple gene ontology analyses. The bioinformatical tool of choice used for this approach was “GOrilla”, as it incorporates the ranking of genes into the analysis, generating a list of possible biological functions considering the relative amount of differentially expressed mRNAs (Eden et al. 2009). Analysis of the top 10% of non-differentially expressed genes between all five groups, ordered by their base amount of detected mRNA across all samples, revealed prominent features these mDCs share between each other (table AX4 (appendix)). Besides a variety of RNA and protein regulatory GO terms, this approach revealed general mDC involvement in MHC class II antigen processing and presentation, T cell regulation (regulatory, cytotoxic and memory T cells), regulation of cell mediated cytotoxicity and humoral immune response. Interestingly, GO terms for developmental growth and anatomical structure homeostasis were also predicted as basic functionalities. The mentioned features seem therefore to be present in intestinal mDCs independent of the disease or inflammation status.

Although the majority of expressed genes between UC and CD patients mLPDCs is similar, the differentially expressed genes between UC and NC or CD and NC mLPDCs differ substantially. Under non-inflamed conditions UC and CD patients mLPDCs share approximately 35% of statistical significant differentially expressed genes with healthy individuals mLPDCs (Fig.R57). This trend is continued under inflammatory conditions, where UC and CD patients mLPDCs share 33% of SDE genes when compared to healthy individuals mLPDCs (Fig.R58). These differing gene expression profiles hint at different properties the mLPDCs from different patient groups inherit under non-inflammatory as well as inflammatory conditions. This is another hint that the divergent manifestations of the diseases are maybe in part attributable to differences in the mLPDC cell compartment.

Before going further into detail about the differentially regulated genes in biopsies from IBD patients and healthy individuals, a comparison between upregulated genes in the nCounter® LEL DCs vs PBDCs dataset is explored within the mRNA Seq dataset. Taking the list of the top 30 upregulated genes from LEL mDCs vs PBDCs and looking at the exact same genes in IBD patients versus NC, it becomes apparent that not all differences found with the nCounter® analysis can be attributed to the inflammatory process initiated by the LEL model (table R59). Genes like *CCL22*, *MMP12*, *CCR7* and *LAMP3* amongst others, are not differentially regulated between mLPDCs from NC versus inflamed or non-inflamed IBD patients. This means that the differences in these genes found within the nCounter® analysis are describing functional properties of DCs resident to the lamina propria independently of the inflammatory state of the environment. This includes (1) a possible contribution in epithelial differentiation, angiogenesis or neutrophil recruitment via CXCL8; (2) Treg conversion, proliferation and maintenance through IDO1, CCL22 and PD-L1; (3) and utilizing MMP12 to degrade bacterial cell components or limit macrophage infiltration among others.
Another observation is that *CRLF2*, *MMP7*, *ANGPTL4*, *ENO2* and *CCL24* mRNAs could not be found in the RNAseq dataset. A possible explanation could be that these genes were upregulated in the nCounter™ dataset due to the experimental conditions of the LEL model, having an inflammation in a sort of “sterile” environment were most of the microbiota has been removed beforehand. Another possible explanation could be that the LEL model is mimicking an acute inflammatory response, whereas the biopsy samples are taken from regions with prolonged inflammation.
Genes like *CD80* and *LAD1* amongst others, could be shown to be indeed induced by the inflammatory state. Whereas *TNFRSF11A* and *TNFRSF4* were not only differentially regulated under inflammatory conditions but also in IBD patients from macroscopically non-inflamed biopsy samples compared to NC.

The LEL model is therefore helpful in identifying possible targets of inflammatory reactions. In this specific case it has to be considered that the compared cell types were taken from different sources in the body, and the received differentially expressed data is a mixture of inflammatory induced gene expression and general traits of mDCs resident to the lamina propria which are not present in circulating DCs.

Following analyses with differentially expressed genes across all groups and group combinations were made to reveal differences in abilities under certain conditions and diseases. There were two major findings predicted by the GO term analysis connecting mLPDCs to (1) epithelial proliferation and wound healing, as well as (2) participation in neuronal communication/regulation (table R55).

Epithelial cell maintenance

The first prediction of GO terms which stood out was that, under inflammatory conditions of IBD patients, mDCs seem to regulate epithelial cell differentiation. This phenomenon was also proposed as possible function of LEL mDCs in the previous nCounter® analysis. Most studies on wound healing capabilities in intestinal tissues of animal experiments focus on macrophages (Ruder and Becker 2020; Xue and Falcon 2019). Since intestinal DCs and macrophages are closely related to each other and many studies show DC involvement in wound healing processes, like e.g. in the skin or corneal tissue, it is not unlikely that intestinal DCs may have an impact on intestinal epithelial repair as well (Vinish et al. 2016; Mölzer et al. 2019).

The significant and distinct upregulation of ladinin (*LAD1*) under inflammatory conditions in IBD patients as well as in the LEL model might be connected to mLPDC interaction with the epithelium. Ladinin is a component of the intestinal basement membrane, a layer of extracellular matrix, which serves as an anchor for epithelial cells with the underlying connective tissue (Marinkovich et al. 1996). So far, functional aspects of ladinin expression by intestinal dendritic cells have not yet been described. Since this component is anchoring epithelial cells to the basement membrane, maybe mLPDCs express this gene to anchor themselves to the basement membrane or establish a connection with epithelial cells. They might also contribute to the reconstitution of basement membrane mass to help epithelial cells cover up lesions in the epithelial cell layer. The expression of *LAD1* was recently described to be vital for the migration of human colon cancer cells (SW620, Caco-2 (both epithelial cell lines)) (Moon et al. 2020) as well as the migration and proliferation of mammary cells (Roth et al. 2018).

Another indicator for induction of epithelial cell proliferation by mLPDCs was the expression of Cathepsin K (CTSK), which was significantly upregulated in iUC vs NC and, although not statistical significant but with a similar trend, in iCD and niCD vs NC. Exogenous CTSK has been shown to be inducing proliferation in human epithelial colorectal cancer cells (R. Li et al. 2019). Additionally, administered CTSK has been shown to have anti-inflammatory properties in DSS induced colitis in mice (Sina et al. 2013). Moreover, mice deficient in CTSK had an abnormal organization of colonic intercellular junction proteins, leading to a suggested impairment in intestinal barrier integrity (Arampatzidou et al. 2012).

Another factor possibly attributing to intestinal epithelial barrier integrity is the upregulation of *ALOX15B* in inflamed IBD patients mLPDCs. The Arachidonate 15-Lipoxygenase type B (ALOX15B) is an enzyme which can convert Arachidonic acid (AA) into 15-Hydroxyeicosatetraenoic acid (15-HETE). A publication from Pochard et al. established a link with reduced intestinal 15-HETE availability in CD patients resulting in an increased permeability of the intestinal barrier (Pochard et al. 2016). This

means that high levels of 15-HETE are promoting intestinal barrier integrity as shown with epithelial cell lines and in animal experiments (Pochard et al. 2016).
The reported accumulation of mononuclear cells on the basement membrane after removal of epithelial cells (Mahida et al. 1997) and the observed migratory potential of mLPDCs in the LEL model in combination with the gene expression profile hints at mLPDCs to be involved in propagation of intestinal epithelial cells and therefore barrier function integrity and wound healing.

Neuronal connection

Another observation was that mDCs from non-inflamed IBD patients were predicted to be involved in synaptic signaling. Furthermore iUC mDCs displayed GO terms for ganglion and sympathetic ganglion development when compared to niUC mDCs.
A study with a murine model by Guseva et al. established a direct link between serotonin signaling and intestinal inflammation regulation through dendritic cells (Guseva et al. 2014). A review by Yoo et al. shows the manifold interactions how the enteric nervous system influences the intestinal barrier and resident immune cells including dendritic cells (Yoo and Mazmanian 2017).
Additionally, research has accumulated evidence that dendritic cells in the skin, lymphoid organs and the intestine are modulated by neurotransmitters derived from the sympathetic nervous system (Takenaka, Guereschi, and Basso 2017). Although a study by Muller et al. was focused on intestinal macrophages showing that they are interacting with enteric neurons participating in regulation of peristaltic activity (Muller et al. 2014), similar modes of action might be possible for dendritic cells since both cell types are closely related to each other. The mDCs might therefore be influenced by mutual cell signaling with neuronal cells in IBD patients. This observation could be e.g. (1) a countermeasure towards inflammation induced tissue damage restoring the local environment, or (2) a cause contributing to the chronic inflammatory state.

Some of the genes responsible for the predicted GO term regarding neuronal signaling are themselves linked to certain functional aspects of dendritic cells like e.g. *SLC12A4* and *P2RX1.* The solute carrier protein encoded by the *SLC12A4* gene was shown to be important for the uptake of dead cells from phagocytes (Perry et al. 2019). The purinergic receptor P2X1 (*P2RX1*) was shown to function as a danger signal receptor, boosting activation of dendritic cells in the presence of ATP (Di Virgilio 2005). Therefore it is necessary to investigate the findings from the predicted GO terms with further experimental tests to confirm the verisimilitude of the predictions.

Nonetheless, further evidence for a close interaction between mLPDC and the enteric nervous system is provided by the list of top differentially expressed genes. One example is that under

inflammatory conditions mDCs expressed the gene *SLC6A12*, which is a transporter for the neurotransmitter γ-aminobutyric acid (GABA) (Bala et al. 2013). GABA has been shown to have a direct effect in inhibition of the release of pro-inflammatory cytokines from PBMCs (Bhandage et al. 2018). In this way neuronal cells in the lamina propria might have a direct impact on regulation of inflammatory processes in the intestinal tissue. This finding should be explored in more detail and could potentially be used to alter inflammatory reactions in the intestine of patients.

It is noteworthy, that in the dataset of niUC vs NC were signs of a possible minor mast cell contamination. CD117 was found to be statistically significant differentially upregulated in niUC compared to NC (table R50). A higher CD117 level alone is not enough evidence for mast cell contamination, since CD117 was also found to be expressed on dendritic cells and regulated under certain conditions (Ray et al. 2010; Simonetti et al. 2019). Genes which are usually not associated with dendritic cells like *ENPP3*, *MS4A2* or *TPSB2* were found to be enriched in the niUC dataset but not statistical significant. The ectonucleotide pyrophosphatase/phosphodiesterase 3 (ENPP3) found to be expressed in mast cells or basophils (Tsai et al. 2015) was upregulated in niUC compared to NC in half of the niUC patients. Mast cells are known to interact with intestinal neuronal cells (Buhner and Schemann 2012) and therefore every result coming from this dataset regarding neuronal interactions should be observed carefully. Since the analyses were only made with significantly differentially expressed genes and mast cell specific or related genes were excluded beforehand due to high p-values, the contamination effects in the analysis might be close to non-existent. The aforementioned publications showing that macrophages, mast cells as well as dendritic cells are in a mutual influenced relationship with nerve cells or neurotransmitters makes it even harder to tell if a observed neuronal related gene transcript is a contamination, derived from another cell type.
The gating from the cell sorting process should not have allowed mast cells to contaminate the sample. The exclusion of CD117 high cells in combination with including only cells expressing very high amounts of HLA-DR and CD11c are features not present on mast cells. However, inflammatory mast cells from patients with systemic mastocytosis have an increased expression of HLA-DR and CD11c but should still be easily distinguishable from DCs due to lower levels of the mentioned surface markers (Teodosio et al. 2015). Inspection of the patients medical records revealed no signs of systemic mastocytosis whatsoever. Expression of *HLA-DRA* and *CD11c* was also not altered in niUC vs NC although a larger contamination with mast cells should decrease the amount of both transcripts (table R50). The gene *MS4A2* is to be considered as absent on DCs (present on basophils and mast cells), but high transcript levels were found to be expressed in cDC2 cells in porcine lymphatic tissue (Auray et al. 2020), which might hint at a possibility being expressed under certain conditions in human cDC2 as well.

Further tests need to be conducted confirming the observed GO terms for neuronal signaling in mLPDCs and rule out that some observations might stem from a possible cell contamination.

Top differentially regulated genes

Examination of the 20 most significantly up- and downregulated genes, when comparing the five analyzed groups in different combinations, revealed further insight into novel functional properties of intestinal mLPDCs:

Immunoglobulins in mLPDCs

Surprisingly, genes for heavy and light immunoglobulin chains were found among the top differentially expressed genes between control subjects and IBD patients. Immunoglobulin chains were significantly upregulated in inflamed as well as non-inflamed UC patients compared to healthy individuals. The applied cell sorting strategy should have excluded B cells, plasmaplasts or plasma cells via CD19, CD20, lower levels of HLA-DR on antibody secreting cells or absence of CD33. The mRNA sequencing mLPDC dataset was checked for possible contaminations, but no mRNA for CD19, CD20 (B cells), CD27 (plasmablasts) or CD138 (plasma cells) could be found in the dataset (table R49) (Sanz et al. 2019).

A publication from Macosko et al. stated that in single cell studies contaminations with ambient RNA are common as result from cell damage due to the experimental handling (Macosko et al. 2015). Since this analysis was done with approximately 100 cells per patient, the contamination with ambient RNA might still be a factor that needs to be taken into account. However, since significant upregulation was only found in UC patients it is to be questioned why contamination would only be higher in UC patients. Another single cell study from Smillie et al. experienced also an increased presence of *IGHA1* in cell preparations from the lamina propria, but they used this specific gene as an exclusion marker stating that only B lineage cells express it (Smillie et al. 2019). But looking at their gene expression dataset reveals that *IGHA1* is indeed distributed amongst cell preparations from colonic material, but for instance the light chain gene *IGLC2* was found highly expressed in activated DCs but not every other cell type that showed contamination with *IGHA1* (Smillie et al. 2019)(supplementary material).

The mRNA for the J-chain protein was also found to be upregulated in mLPDCs from IBD patients compared to healthy individuals (tables R51/R52). In 2008 a publication was released showing that a subset of murine splenic dendritic cells expressed the j-chain protein (Källberg and Leanderson 2008), substantiating the former observation.

So far, immunoglobulin production was only attributed to the B cell compartment (or degenerated (cancer) cells), but recently studies were published describing immunoglobulin production in other cell types than B cells. Two studies showed that immunoglobulins were expressed in tumor-associated macrophages from different sites, circulating monocytes, as well as ex-vivo differentiated macrophages (Fuchs et al. 2018; Busch et al. 2019). Moreover they identified the expression of heavy and light chain immunoglobulin genes via single cell analysis of tumor-associated macrophages from human colon cancer patients (Fuchs et al. 2018). Other cell types which have been found to express immunoglobulin genes, were epithelial cells, mesangial cells and podocytes in renal tissue (Deng et al. 2020; 2021).

The expression of immunoglobulins in macrophages showed a restricted repertoire in V(D)J combinations compared to B cells (Busch et al. 2019). They could also show immunoglobulin expression in macrophages from B cell deficient mice (Fuchs et al. 2018).

The functional aspect of Immunoglobulin gene expression in intestinal mDCs of IBD patients is a subject that needs further investigation. Possible functional aspects could be that mDCs use immunoglobulins as additional cell surface receptor. However, BCR signal transduction molecules CD79A and CD79B were not expressed by the mDCs. Therefore, they either use different signaling molecules or do not use their immuniglobulins as a receptor. But comparison of non-inflamed IBD patients versus healthy individuals revealed the GO term “B-cell receptor signaling pathway”, hinting at intracellular processes connected to BCR related downstream signaling molecules. Immunoglobulin expression on the cell surface could also act as a kind of more specialized PRR, catching invading pathogens followed by ingestion and presentation.

Further immunregulatory properties

The CD200 molecule mRNA was statistical significant differentially increased in IBD patients mLPDCs under inflammatory conditions (table R56). Interactions of CD200 with CD200R1 were identified as inhibitory, limiting inflammatory mediator expression (Vaine and Soberman 2014). The receptor for CD200, namely CD200R1, was shown to be present on murine intestinal macrophages (Bain and Mowat 2012). Maybe the mDCs express CD200 to regulate to some extent resident macrophages present in the lamina propria. Moreover, overexpression of the CD200 molecule in transgenic mice protected them from DSS induced colitis and lead to an increase in Treg cells (Z. Chen et al. 2016). A connection between IBD and CD200/CD200R1 expression levels on peripheral blood mDCs in humans was observed, proposing that those molecules correlated with the Treg and Th17 balance in IBD patients (Elshal et al. 2015). The increase of CD200 on mDCs under inflammatory conditions might therefore regulate macrophage activity in the vicinity and influence specific T cell accumulation.

The gene expression profile revealed also a plethora of novel transcripts being statistical significant differentially expressed between IBD patients and healthy individuals mLPDCs. Some of these molecules are protein coding and might therefore uncover new targets relevant for inflammation regulatory processes. Other molecules are so called long non-coding RNAs (lncRNAs), exhibiting functional properties as ribonucleic acid, acting e.g. as antisense strand inhibiting protein translation. lncRNAs have just recently be reviewed to be potential biomarkers for IBD and partake in several regulatory processes like for example influence the intestinal barrier integrity amongst others (Lin et al. 2020).

IL23A and EBI3 in IBD

In line with the observations in mLPDC in the LEL model, transcript levels of *EBI3* and *IL23A* could be detected in all samples of mLPDCs.

Regarding the expression of *IL23A* and *EBI3* in mLPDC in IBD, mRNA levels for *EBI3* were significantly increased in mDCs of inflamed CD samples compared to non-inflamed CD or healthy individuals. Levels of *IL23A* mRNA stayed constant across all groups. It is not possible to further deduce relevance of *EBI3* expression in relation to the disease status from this dataset. But since increased *EBI3* mRNA expression is clearly linked to an inflammatory environment, further experiments investigating functional aspects of this cytokine in intestinal tissues should be performed. The initial tests on EBI3s capacity to induce epithelial cell proliferation are supported by the beforehand predicted potential of mLPDCs involvement in epithelial cell proliferation.

RNAseq observations summary

In summary, transcriptomic and flowcytometric analysis of intestinal mDCs from IBD patients and healthy individuals revealed that this cell population represents a mixture of cDC1 and cDC2 cells, with the majority belonging to the cDC2 subgroup based on the surface expression of CD1c and CD141 (see 3.11.2) as well as the mRNA profile (table AX15 (appendix)). GO term analysis of non-differentially and highly expressed mRNAs revealed that these mDCs have general functionalities inducing T cells (regulatory, cytotoxic, memory), cell mediated cytotoxicity and humoral immune responses (table AX4 (appendix)). Features previously found within the nCounter® analysis of the LEL model, like tissue remodeling via MMPs seem to be conserved across the analyzed mLPDCs independent of their underlying disease or activity status. An involvement of mLPDC in epithelial cell proliferation and therefore wound healing processes seem to be likely. Furthermore, in IBD patients,

GO terms and highly differentially expressed genes were found to be involved in neuronal signaling and development, having intestinal mLPDCs being influenced by neuronal signaling and/or vice versa. Moreover a set of genes for immunoglobulin production was found to be upregulated in IBD patients compared to healthy individuals. Intestinal mLPDCs are well known to be important contributors to maintenance of a homeostatic environment via regulating inflammatory processes through orchestration of the adaptive immune response. The performed sequencing analysis predicts possible new functional aspects of how intestinal mDCs partake in local processes besides antigen processing and adaptive immune response induction in secondary lymphoid organs. Moreover, a distinct differentially regulatory gene expression profile was observed comparing ulcerative colitis and Crohn's disease patients mLPDCs with each other or against mLPDCs from healthy individuals. This was observed under inflammatory as well as non.inflammatory conditions.

4.5.3 Future experiments

In order to validate the via GO term or differential expression predicted contributions of mLPDCs in the intestinal environment further experiments need to be conducted. First of all protein expression should be assessed under different activation states of mLPDCs using immunohistochemistry or mass spectrometry. Functional assays need to follow examining the wound healing capabilities via scratch assays or effects on organoid growth in direct contact with mLPDCs. Involvement in processes regarding neuronal interaction could be observed with co-cultures, assessing mLPDC and neuronal gene expression in absence or presence of both cell types simultaneously. Antibody production could be investigated via ImageStream® technology combining the flowcytometric analysis with microscopy features. Moreover the observed differential expression of genes in UC and CD patients when compared to NC should be observed more closely as well. Functional differences of mLPDCs, which are important regulators of immune homeostasis, might uncover novel individual strategies ameliorating intestinal inflammation in UC or CD patients.

5.0 Appendix

5.1 Plasmids used for the transfection of HEK cells

Plasmids for EBI3 and IL-23p19 were each enriched in a bacterial cell culture and sequenced after the extraction from the cells (figures AX1 A & AX2 A). The plasmids hEBI3 pEF6-Flag (MJS_003) and hIL23p19 pEF6-V5 (MJS_004) were kind gifts from Matthew Sweet (Addgene plasmids # 72491 & # 72492)). Translating the nucleotide sequence of the open reading frame into an amino acid sequence with the ExPASy tool and blasting this sequence via the NCBI blastp suite gave a 100% sequence homology for human EBI3 (Fig.AX1 B) and for human IL-23p19 (Fig.AX2 B) for the respective plasmids. Plasmid sequencing was done by eurofins genomics and plasmid maps were generated with SnapGene (Version 4.3.11) (ExPASy tool: https://web.expasy.org/translate/; blastp suite: https://blast.ncbi.nlm.nih.gov/Blast.cgi).

A)

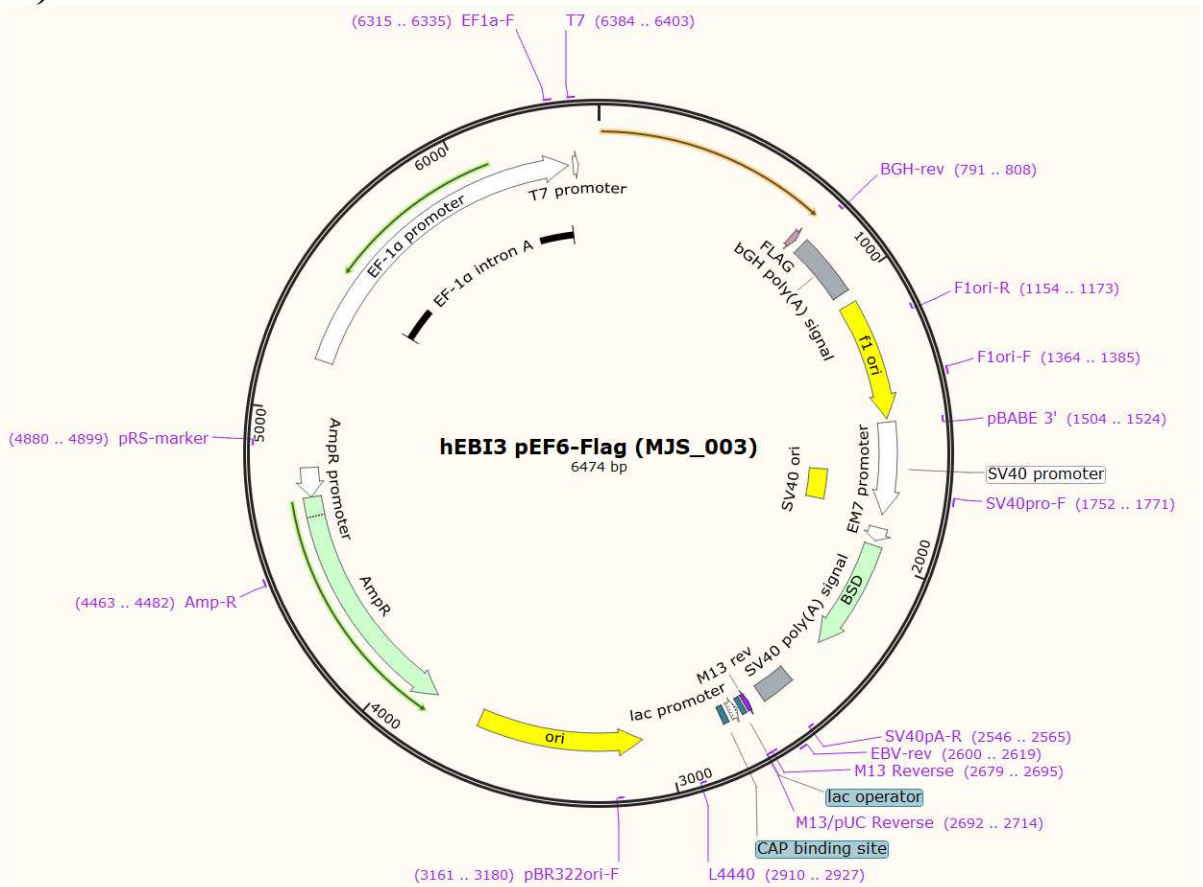

B)

Epstein-Barr virus induced gene 3 [Homo sapiens]

Sequence ID: ABK41923.1 **Length:** 229 **Number of Matches:** 1

See 1 more title(s) See all Identical Proteins(IPG)

Range 1: 1 to 229 GenPept Graphics ▼ Next Match ▲ Previous Match

Score	Expect	Method	Identities	Positives	Gaps
466 bits(1200)	1e-165	Compositional matrix adjust.	228/229(99%)	229/229(100%)	0/229(0%)

```
Query  1    MTPQLLLALVLWASCPPCSGRKGPPAALTLPRVQCRASRYPIAVDCSWTLPPAPNSTSPV  60
            MTPQLLLALVLWASCPPCSGRKGPPAALTLPRVQCRASRYPIAVDCSWTLPPAPNSTSPV
Sbjct  1    MTPQLLLALVLWASCPPCSGRKGPPAALTLPRVQCRASRYPIAVDCSWTLPPAPNSTSPV  60

Query  61   SFIATYRLGMAARGHSWPCLQQTPTSTSCTITDVQLFSMAPYVLNVTAVHPWGSSSSFVP  120
            SFIATYRLGMAARGHSWPCLQQTPTSTSCTITDVQLFSMAPYVLNVTAVHPWGSSSSFVP
Sbjct  61   SFIATYRLGMAARGHSWPCLQQTPTSTSCTITDVQLFSMAPYVLNVTAVHPWGSSSSFVP  120

Query  121  FITEHIIKPDPPEGVRLSPLAERQLQVQWEPPGSWPFPEIFSLKYWIRYKRQGAARFHRV  180
            FITEHIIKPDPPEGVRLSPLAERQLQVQWEPPGSWPFPEIFSLKYWIRYKRQGAARFHRV
Sbjct  121  FITEHIIKPDPPEGVRLSPLAERQLQVQWEPPGSWPFPEIFSLKYWIRYKRQGAARFHRV  180

Query  181  GPIEATSFILRAVRPRARYYVQVAAQDLTDYGELSDWSLPATATMSLGK  229
            GPIEATSFILRAVRPRARYY+QVAAQDLTDYGELSDWSLPATATMSLGK
Sbjct  181  GPIEATSFILRAVRPRARYYIQVAAQDLTDYGELSDWSLPATATMSLGK  229
```

Fig.AX1: Plasmid schematic and open reading frame translation of hEBI3 pEF-FLAG. Map of the EBI3 producing plasmid (A). ORF translation into an amino acid sequence and blast against the human genome showing that the ORF encodes for EBI3 protein (B).

A)

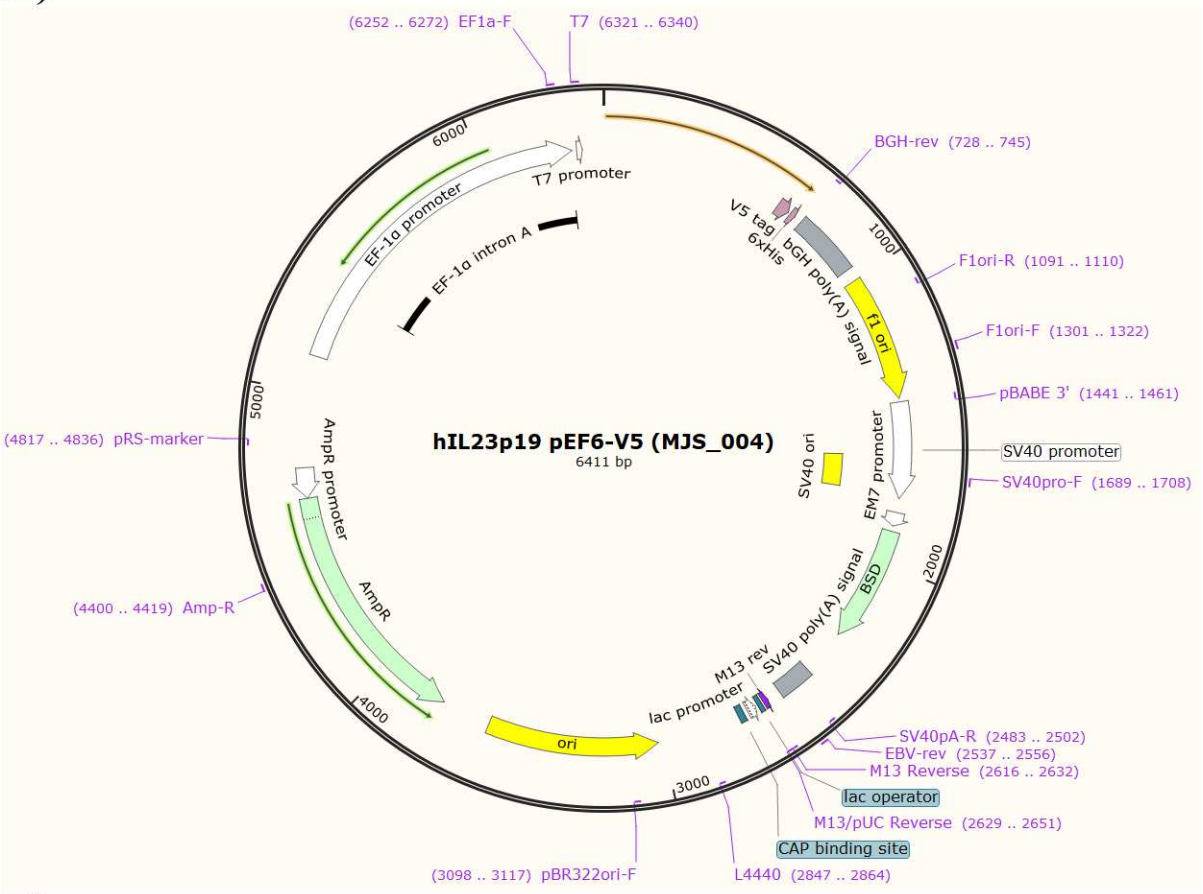

B)

interleukin-23 subunit alpha precursor [Homo sapiens]

Sequence ID: NP_057668.1 **Length:** 189 **Number of Matches:** 1

See 11 more title(s) See all Identical Proteins(IPG)

Range 1: 1 to 189 GenPept Graphics ▼ Next Match ▲ Previous Match

Score	Expect	Method	Identities	Positives	Gaps
381 bits(978)	1e-132	Compositional matrix adjust.	189/189(100%)	189/189(100%)	0/189(0%)

```
Query  1    MLGSRAVMLLLLLPWTAQGRAVPGGSSPAWTQCQQLSQKLCTLAWSAHPLVGHMDLREEG  60
            MLGSRAVMLLLLLPWTAQGRAVPGGSSPAWTQCQQLSQKLCTLAWSAHPLVGHMDLREEG
Sbjct  1    MLGSRAVMLLLLLPWTAQGRAVPGGSSPAWTQCQQLSQKLCTLAWSAHPLVGHMDLREEG  60

Query  61   DEETTNDVPHIQCGDGCDPQGLRDNSQFCLQRIHQGLIFYEKLLGSDIFTGEPSLLPDSP  120
            DEETTNDVPHIQCGDGCDPQGLRDNSQFCLQRIHQGLIFYEKLLGSDIFTGEPSLLPDSP
Sbjct  61   DEETTNDVPHIQCGDGCDPQGLRDNSQFCLQRIHQGLIFYEKLLGSDIFTGEPSLLPDSP  120

Query  121  VGQLHASLLGLSQLLQPEGHHWETQQIPSLSPSQPWQRLLLRFKILRSLQAFVAVAARVF  180
            VGQLHASLLGLSQLLQPEGHHWETQQIPSLSPSQPWQRLLLRFKILRSLQAFVAVAARVF
Sbjct  121  VGQLHASLLGLSQLLQPEGHHWETQQIPSLSPSQPWQRLLLRFKILRSLQAFVAVAARVF  180

Query  181  AHGAATLSP  189
            AHGAATLSP
Sbjct  181  AHGAATLSP  189
```

Fig.AX2: Plasmid schematic and open reading frame translation of hIL23p19 pEF6-V5. Map of the IL-23p19 producing plasmid (A). ORF translation into an amino acid sequence and blast against the human genome showing that the ORF encodes for IL-23p19 protein (B).

5.2 Nanostring nCounter® mRNA gene expression dataset (PBDCs vs LEL DCs)

Probe Name	Accession #	PBDC1	PBDC2	PBDC3	PBDC4	LEL DC14	LEL DC15	LEL DC16	LEL DC18
ABCB1	NM_000927.3	20	80	17	61	69	19	11	36
ADA	NM_000022.2	176	191	171	207	1474	1142	349	502
AGRN	NM_198576.2	26	74	29	53	636	677	575	540
AHR	NM_001621.3	3561	3343	6012	5279	4515	1244	3099	2229
AICDA	NM_020661.1	5	13	5	16	12	14	8	6
AIRE	NM_000383.2	16	65	16	68	75	21	12	33
ANGPTL4	NR_104213.1	8	6	10	4	93	177	196	128
APP	NM_000484.3	929	763	875	776	280	226	103	117
ARG1	NM_000045.2	18	97	18	80	80	85	56	83
ARG2	NM_001172.3	7	27	8	22	42	14	14	25
ARHGDIB	NM_001175.4	3721	3230	4203	3758	262	77	129	188
ATG10	NM_001131028.1	80	113	87	133	77	39	39	74
ATG12	NM_004707.2	74	120	67	101	82	40	22	59
ATG16L1	NM_198890.2	223	289	256	244	85	33	6	48
ATG5	NM_004849.2	339	370	409	416	199	113	156	139
ATG7	NM_001136031.2	221	278	248	265	136	109	72	96
ATM	NM_000051.3	29	58	20	31	42	6	8	26
B2M	NM_004048.2	54292	47297	57762	50985	117152	89490	108904	86311
B3GAT1	NM_018644.3	7	26	2	21	24	4	4	11
BATF	NM_006399.3	54	90	83	72	56	58	8	25
BATF3	NM_018664.2	477	131	825	955	129	66	9	98
BAX	NM_138761.3	903	860	925	973	858	501	576	618
BCAP31	NM_005745.7	690	622	732	660	278	164	290	246
BCL10	NM_003921.2	834	751	786	779	405	184	227	291
BCL2	NM_000657.2	153	169	176	258	324	379	153	209
BCL2L11	NM_138621.4	91	101	89	76	1717	603	1119	1425
BCL3	NM_005178.2	273	380	294	293	641	489	525	515

BCL6	NM_001706.2	568	519	781	811	176	101	81	123
BID	NM_001196.2	50	80	35	65	52	12	21	25
BLNK	NM_013314.2	165	154	171	136	7	20	17	18
BST1	NM_004334.2	182	171	170	208	49	5	6	24
BST2	NM_004335.2	458	453	476	454	222	45	106	54
BTK	NM_000061.1	670	686	760	666	176	110	118	137
BTLA	NM_181780.2	163	193	160	212	184	100	32	142
C14orf166	NM_016039.2	1621	1681	1845	1701	665	317	326	382
C1QA	NM_015991.2	18	58	20	58	62	39	29	41
C1QB	NM_000491.3	32	85	19	82	162	26	27	41
C1QBP	NM_001212.3	1242	1232	1334	1117	222	129	116	144
C1R	NM_001733.4	11	27	11	10	20	3	6	6
C1S	NM_001734.2	13	54	20	47	29	12	7	27
C2	NM_000063.3	9	36	8	22	24	11	4	17
C3	NM_000064.2	6	28	12	27	34	14	87	22
C4A/B	NM_007293.2	26	172	32	101	89	22	9	73
C4BPA	NM_000715.3	16	40	12	37	32	21	12	28
C5	NM_001735.2	45	64	69	91	58	17	14	28
C6	NM_000065.2	26	106	29	78	84	30	17	54
C7	NM_000587.2	51	31	47	54	40	38	45	51
C8A	NM_000562.2	12	71	9	42	49	18	6	40
C8B	NM_000066.2	10	40	7	31	43	14	3	17
C8G	NM_000606.2	21	57	18	53	46	14	7	28
C9	NM_001737.3	20	83	15	79	98	19	13	49
CALCRL	NM_005795.3	304	278	341	275	3147	1202	2571	1997
CAMP	NM_004345.3	13	57	12	44	39	8	3	20
CARD9	NM_052813.4	138	190	156	186	41	16	13	26
CASP1	NM_001223.3	2426	1970	2412	2236	1674	431	879	865
CASP10	NM_032977.3	21	40	17	53	42	16	8	25
CASP2	NM_032982.2	393	427	431	330	123	46	81	122
CASP3	NM_032991.2	158	138	141	152	303	143	263	134

CASP8	NM_001228.4	1180	1264	1361	1112	173	69	58	101
CCBP2	NM_001296.3	18	47	18	50	45	11	4	28
CCL11	NM_002986.2	17	73	11	55	65	19	12	39
CCL13	NM_005408.2	20	64	17	51	78	8	13	37
CCL15	NM_032965.3	17	63	10	58	77	16	8	38
CCL16	NM_004590.2	8	72	14	48	61	12	1	24
CCL18	NM_002988.2	13	52	9	43	67	11	8	36
CCL19	NM_006274.2	27	70	22	57	1281	2397	28	224
CCL2	NM_002982.3	3	18	4	16	24	5	1	12
CCL20	NM_004591.1	10	67	11	52	113	1294	126	105
CCL22	NM_002990.3	11	52	14	41	37707	30844	24790	21968
CCL23	NM_145898.1	3	23	5	12	20	4	5	8
CCL24	NM_002991.2	11	21	6	21	161	267	317	261
CCL26	NM_006072.4	8	18	7	22	27	4	3	21
CCL3	NM_002983.2	50	145	113	165	129	107	14	75
CCL4	NM_002984.2	42	178	48	146	172	89	24	118
CCL5	NM_002985.2	66	74	91	69	58	35	20	25
CCL7	NM_006273.2	9	3	1	5	1	5	2	4
CCL8	NM_005623.2	4	59	4	50	46	8	1	25
CCND3	NM_001760.2	855	901	1017	833	48	7	11	31
CCR1	NM_001295.2	148	287	254	600	75	19	25	70
CCR10	NM_016602.2	17	59	15	49	47	14	9	40
CCR2	NM_001123041.2	715	839	1139	826	60	10	2	27
CCR5	NM_000579.1	300	312	360	231	33	16	31	51
CCR6	NM_031409.2	162	311	325	269	179	100	117	180
CCR7	NM_001838.2	15	36	12	41	9238	11072	8897	6555
CCR8	NM_005201.2	16	56	9	31	49	9	2	27
CCRL1	NM_016557.2	23	165	17	110	293	99	133	167
CCRL2	NM_003965.4	73	171	113	135	205	72	106	131
CD14	NM_000591.2	113	150	163	171	107	19	30	81
CD160	NM_007053.2	16	67	12	62	59	13	3	32

CD163	NM_004244.4	288	433	412	391	68	21	15	57
CD164	NM_006016.4	1956	1473	1903	1814	426	268	239	303
CD19	NM_001770.4	23	46	14	56	52	10	13	23
CD1A	NM_001763.2	94	143	89	82	39	8	2	26
CD1D	NM_001766.3	902	1382	1863	1870	63	26	39	113
CD2	NM_001767.3	127	112	163	129	12	6	6	9
CD209	NM_021155.2	30	64	46	57	72	19	21	49
CD22	NM_001771.2	178	209	178	199	69	30	3	79
CD24	NM_013230.2	45	125	28	100	146	39	7	55
CD244	NM_016382.2	429	475	572	473	24	21	67	28
CD247	NM_198053.1	9	35	9	34	36	14	8	23
CD27	NM_001242.4	27	60	16	54	64	8	7	40
CD274	NM_014143.3	14	76	14	41	1468	727	591	697
CD276	NM_001024736.1	11	66	17	52	65	24	13	45
CD28	NM_001243078.1	8	38	9	32	34	9	4	26
CD34	NM_001025109.1	11	18	4	9	18	12	4	12
CD36	NM_001001548.2	1214	1383	1579	1257	84	21	87	52
CD3D	NM_000732.4	11	49	12	55	58	9	12	27
CD3E	NM_000733.2	23	30	13	26	28	10	16	28
CD3EAP	NM_012099.1	41	113	53	99	92	15	3	34
CD4	NM_000616.4	1132	1027	1228	1094	97	19	101	102
CD40	NM_001250.4	85	160	87	190	2373	3226	940	1089
CD40LG	NM_000074.2	8	69	11	54	35	17	16	65
CD44	NM_001001392.1	2374	2821	2468	2277	4169	4805	2010	1373
CD45R0	NM_080921.3	1670	1382	2060	2072	836	241	693	698
CD45RA	NM_002838.4	323	98	145	81	19	6	11	5
CD45RB	ENST00000367367.1	1032	746	911	717	259	54	102	144
CD46	NM_172350.1	1449	1316	1647	1486	606	321	318	457
CD48	NM_001778.2	2592	2099	2984	1533	490	146	152	185
CD5	NM_014207.2	241	220	192	140	196	110	162	293

CD53	NM_001040033.1	3551	3536	4036	3565	3151	1024	1784	2024
CD55	NM_000574.3	33	93	21	67	74	23	6	38
CD59	NM_000611.4	478	460	328	415	925	797	1143	416
CD6	NM_006725.3	28	75	16	64	47	34	26	54
CD7	NM_006137.6	8	1	4	2	3	2	3	1
CD70	NM_001252.2	21	66	18	40	110	42	31	56
CD74	NM_001025159.1	133174	121679	137308	117319	72799	52121	80794	82577
CD79A	NM_001783.3	20	25	16	20	15	7	10	14
CD79B	NM_021602.2	75	106	60	93	89	36	20	52
CD80	NM_005191.3	26	105	17	72	3908	2837	836	2422
CD81	NM_004356.3	480	330	409	331	633	347	433	364
CD82	NM_002231.3	16	33	19	30	53	45	7	12
CD83	NM_004233.3	872	924	1856	2985	23654	20929	12489	18689
CD86	NM_175862.3	899	1082	1067	1055	2528	2198	1740	1792
CD8A	NM_001768.5	4	46	1	40	40	6	4	19
CD8B	NM_004931.3	12	82	15	65	99	15	15	41
CD9	NM_001769.2	99	1	8	2	59	51	207	131
CD96	NM_005816.4	7	10	8	3	8	8	18	5
CD99	NM_002414.3	1895	1802	2047	1671	755	479	403	245
CDH5	NM_001795.3	7	62	8	38	56	12	1	23
CDKN1A	NM_000389.2	302	380	375	373	4043	2248	3787	3886
CEACAM1	NM_001712.3	9	61	15	28	61	24	10	35
CEACAM6	NM_002483.4	13	55	12	40	46	19	2	21
CEACAM8	NM_001816.3	15	102	17	72	78	23	11	55
CEBPB	NM_005194.2	641	757	1205	1631	724	323	630	516
CFB	NM_001710.5	43	97	51	82	106	188	74	115
CFD	NM_001928.2	63	117	66	81	36	55	67	72
CFH	NM_001014975.2	10	50	5	33	48	37	13	32
CFI	NM_000204.3	17	50	12	42	65	8	4	31
CFP	NM_002621.2	1809	2167	2526	2050	1420	722	1250	1374
CHUK	NM_001278.3	306	352	254	278	93	48	57	66

CIITA	NM_000246.3	1505	1343	1571	1256	432	279	310	321
CISH	NM_145071.2	25	71	23	59	106	26	34	41
CLCF1	NM_013246.2	41	67	30	60	721	1092	456	499
CLEC4A	NM_194448.2	1307	1257	1429	1283	247	60	58	98
CLEC4E	NM_014358.2	35	84	57	71	58	30	12	30
CLEC5A	NM_013252.2	20	8	13	13	31	20	56	27
CLEC6A	NM_001007033.1	18	40	21	50	30	7	4	16
CLEC7A	NM_197954.2	560	440	656	798	84	16	31	52
CLU	NM_001831.2	7	62	10	46	57	11	6	40
CMKLR1	NM_004072.1	32	101	17	70	99	24	14	39
CR1	NM_000651.4	84	113	66	123	88	33	9	43
CR2	NM_001006658.1	1	5	8	7	2	1	3	3
CRADD	NM_003805.3	30	96	34	74	69	65	23	50
CRLF2	NM_022148.3	13	58	20	36	9815	9040	8805	8855
CSF1	NM_000757.4	9	26	3	19	32	9	6	12
CSF1R	NM_005211.2	71	126	92	87	30	22	17	30
CSF2	NM_000758.2	8	30	3	17	37	21	2	15
CSF2RB	NM_000395.2	548	519	478	541	602	424	410	393
CSF3R	NM_156038.2	517	533	643	532	26	12	22	13
CTGF	NM_001901.2	21	64	21	40	109	100	126	109
CTLA4-TM	NM_005214.3	8	21	12	26	40	3	12	21
CTLA4_all	NM_005214.3	32	63	50	109	74	15	18	53
CTNNB1	NM_001098210.1	2175	2059	2464	2035	4178	2779	4130	2961
CTSC	NM_001814.4	1591	1500	1826	1771	365	147	405	298
CTSG	NM_001911.2	7	57	16	31	42	15	6	29
CTSS	NM_004079.3	9474	7143	10028	8222	2002	820	1327	625
CUL9	NM_015089.2	89	128	94	96	53	31	22	40
CX3CL1	NM_002996.3	15	32	5	23	54	31	35	65
CX3CR1	NM_001337.3	1252	977	1209	1081	45	12	3	22
CXCL1	NM_001511.1	120	116	153	173	272	1326	224	121
CXCL10	NM_001565.1	22	70	28	56	160	21	16	31

CXCL11	NM_005409.4	25	76	23	63	81	18	23	52
CXCL12	NM_000609.5	6	8	8	6	3	3	11	12
CXCL13	NM_006419.2	8	6	5	5	42	23	25	16
CXCL2	NM_002089.3	29	63	21	89	310	914	101	114
CXCL9	NM_002416.1	26	85	29	72	423	50	85	69
CXCR1	NM_000634.2	4	62	14	54	58	16	3	29
CXCR2	NM_001557.2	61	90	52	82	72	27	6	36
CXCR3	NM_001504.1	80	100	53	107	66	39	36	94
CXCR4	NM_003467.2	10282	10560	17329	20898	5855	4480	12290	7998
CXCR6	NM_006564.1	9	59	9	56	67	8	6	18
CYBB	NM_000397.3	1335	1282	1588	1691	168	42	73	87
CYP27B1	NM_000785.3	28	54	9	52	164	299	30	56
DEFB1	NM_005218.3	11	63	12	49	67	8	5	28
DEFB103A	NM_001081551.2	27	106	14	84	129	47	25	71
DEFB103B	NM_018661.3	21	62	9	42	78	15	4	31
DEFB4A	NM_004942.2	12	154	15	93	156	22	10	49
DPP4	NM_001935.3	44	33	41	32	19	27	27	11
DUSP4	NM_057158.2	28	63	54	143	334	174	270	388
EBI3	NM_005755.2	17	8	13	14	394	766	232	227
EDNRB	NM_003991.2	5	42	4	30	38	10	1	30
EGR1	NM_001964.2	32	65	84	145	67	16	2	34
EGR2	NM_000399.3	28	80	39	169	111	56	83	121
ENO2	NM_001975.2	14	39	18	49	1491	1235	665	1244
ENTPD1	NM_001098175.1	326	373	322	336	374	142	306	543
EOMES	NM_005442.2	20	15	6	9	5	7	9	10
ETS1	NM_005238.3	86	80	42	66	262	229	199	208
FADD	NM_003824.2	12	12	14	25	24	9	8	7
FAS	NM_000043.3	38	62	33	49	52	23	9	19
FCAR	NM_133280.1	8	44	12	21	35	15	8	16
FCER1A	NM_002001.2	9438	8823	11458	8371	68	38	107	51
FCER1G	NM_004106.1	3076	2510	2912	2836	395	236	508	417

FCGR1A/B	NM_000566.3	12	65	16	41	50	10	2	35
FCGR2A	NM_021642.3	598	549	761	721	262	112	193	125
FCGR2A/C	NM_201563.4	2128	2070	3176	2347	1780	223	640	486
FCGR2B	NM_001002273.1	859	972	1008	1109	632	156	949	551
FCGR3A/B	NM_000570.4	17	123	10	84	156	21	9	47
FCGRT	NM_004107.4	2750	2467	3295	2629	136	58	187	117
FGF11	NM_004112.2	43	118	36	99	982	318	830	967
FKBP5	NM_001145775.1	1481	1573	2143	1691	236	206	210	251
FLT3	NM_004119.2	3004	1921	3198	2508	2932	1450	2484	1772
FN1	NM_212482.1	1	2	3	2	1	2	1	1
FOXP3	NM_014009.3	7	60	11	63	29	12	9	40
FYN	NM_002037.3	1062	1167	1045	968	580	225	327	417
GATA3	NM_001002295.1	9	39	11	21	24	11	9	16
GBP1	NM_002053.1	318	448	419	426	2202	619	184	440
GBP5	NM_052942.3	19	22	15	31	357	19	72	22
GFI1	NM_005263.2	31	78	29	62	91	51	56	53
GNLY	NM_006433.2	13	31	14	24	30	22	12	26
GP1BB	NM_000407.4	21	73	31	60	52	9	2	29
GPI	NM_000175.2	499	584	623	518	1468	891	847	1224
GPR183	NM_004951.3	3703	3036	5254	6764	13038	9671	11159	11761
GSDMB	NM_001042471.1	105	120	121	131	122	164	94	179
GZMA	NM_006144.2	15	33	5	40	45	17	6	23
GZMB	NM_004131.3	195	77	6	60	105	43	63	50
GZMK	NM_002104.2	11	65	11	48	57	10	2	30
HAMP	NM_021175.2	4	4	3	4	1	1	4	1
HAVCR2	NM_032782.3	625	705	741	706	536	74	264	306
HFE	NM_139011.2	29	66	34	68	42	12	8	20
HLA-A	NM_002116.5	3908	3688	5186	3909	5157	3383	4285	3241
HLA-B	NM_005514.6	8471	7407	8901	7179	7400	6896	5920	5324
HLA-C	NM_002117.4	1575	2116	528	1439	2451	1428	1346	892
HLA-DMA	NM_006120.3	4549	4356	5116	4166	1121	841	1087	1500

HLA-DMB	NM_002118.3	3644	3126	3846	3498	402	218	241	340
HLA-DOB	NM_002120.3	429	345	345	472	1287	1891	201	1168
HLA-DPA1	NM_033554.2	48124	38682	54179	39839	30371	17407	30248	29147
HLA-DPB1	NM_002121.4	65425	46098	57900	55001	45903	28465	31642	37288
HLA-DQA1	NM_002122.3	31540	38192	3	2	2	6356	10141	17102
HLA-DQB1	NM_002123.3	8760	10497	4	9	9	1768	2440	5591
HLA-DRA	NM_019111.3	109350	74746	110287	102414	106542	57042	89000	90964
HLA-DRB1	NM_002124.2	8509	7662	6664	6900	6143	1318	3712	18776
HLA-DRB3	NM_022555.3	21672	15775	22732	17795	16108	6609	12530	16531
HRAS	NM_005343.2	31	49	37	47	40	20	20	33
ICAM1	NM_000201.2	471	558	479	461	1499	1793	716	829
ICAM2	NM_000873.3	191	226	229	251	88	17	11	40
ICAM3	NM_002162.3	1582	1477	1740	1622	126	44	55	63
ICAM4	NM_001039132.1	47	70	54	72	65	22	12	31
ICAM5	NM_003259.3	8	27	9	35	54	34	10	40
ICOS	NM_012092.2	8	68	7	43	51	14	6	25
ICOSLG	NM_015259.4	207	351	203	228	474	171	161	462
IDO1	NM_002164.3	268	160	198	309	21853	18064	18448	11851
IDO2	NM_194294.2	19	56	17	35	96	75	44	72
IFI16	NM_005531.1	775	829	887	817	51	15	31	28
IFI35	NM_005533.3	135	119	100	108	25	12	10	7
IFIH1	NM_022168.2	205	227	195	213	237	110	73	116
IFIT2	NM_001547.4	74	85	70	125	73	5	8	38
IFITM1	NM_003641.3	643	1243	487	649	119	54	52	69
IFNA1/13	NM_024013.1	6	78	15	59	78	25	3	45
IFNA2	NM_000605.3	9	51	9	41	50	10	4	21
IFNAR1	NM_000629.2	66	111	56	84	90	28	47	85
IFNAR2	NM_000874.3	851	1122	1017	990	1012	684	1121	917
IFNB1	NM_002176.2	10	94	10	59	73	13	3	32
IFNG	NM_000619.2	5	65	4	35	50	11	2	34
IFNGR1	NM_000416.1	2624	2558	3705	3472	1191	713	856	1256

IGF2R	NM_000876.1	73	66	62	77	87	128	105	104
IKBKAP	NM_003640.3	129	128	122	109	12	10	7	6
IKBKB	NM_001556.1	327	237	397	342	250	186	78	172
IKBKE	NM_014002.2	43	127	62	71	65	10	17	55
IKBKG	NM_003639.2	170	261	192	230	187	143	116	144
IKZF1	NM_006060.3	241	290	286	232	327	123	114	141
IKZF2	NM_016260.2	20	61	13	39	67	32	28	32
IKZF3	NM_183232.2	6	34	11	46	33	13	1	21
IL10	NM_000572.2	5	14	8	19	18	15	8	11
IL10RA	NM_001558.2	3648	3299	3789	3287	4409	4167	3316	3112
IL11RA	NM_147162.1	29	80	35	61	45	10	3	21
IL12A	NM_000882.2	11	4	18	14	8	9	9	18
IL12B	NM_002187.2	11	52	10	43	78	86	13	28
IL12RB1	NM_005535.1	64	133	100	128	86	24	12	50
IL13	NM_002188.2	17	86	16	61	100	41	6	53
IL13RA1	NM_001560.2	2929	2595	3131	2421	3418	1428	3611	2858
IL15	NM_172174.1	22	66	40	72	139	136	51	78
IL16	NM_004513.4	1965	1719	2050	1802	75	15	17	25
IL17A	NM_002190.2	5	3	7	3	3	7	10	10
IL17B	NM_014443.2	11	20	4	19	22	18	8	15
IL17F	NM_052872.3	11	83	11	61	66	14	3	27
IL18	NM_001562.2	515	676	726	395	147	51	34	119
IL18R1	NM_003855.2	411	370	503	723	295	117	216	128
IL18RAP	NM_003853.2	49	57	52	95	82	18	21	30
IL19	NM_013371.3	5	22	3	20	18	10	6	15
IL1A	NM_000575.3	11	32	11	33	74	61	6	33
IL1B	NM_000576.2	521	519	686	1027	1146	1016	170	444
IL1R1	NM_000877.2	29	31	32	25	556	424	717	472
IL1R2	NM_173343.1	372	284	419	510	238	73	337	147
IL1RAP	NM_002182.2	102	132	119	111	330	72	124	240
IL1RL1	NM_016232.4	8	40	10	26	29	45	9	22

IL1RL2	NM_003854.2	11	44	16	31	71	12	40	38
IL1RN	NM_000577.3	138	231	156	221	811	727	553	645
IL2	NM_000586.2	12	67	13	45	49	18	10	32
IL20	NM_018724.3	17	70	13	51	69	23	13	28
IL21	NM_021803.2	9	71	10	42	56	11	2	23
IL21R	NM_021798.2	19	51	15	46	102	64	22	50
IL22	NM_020525.4	16	66	4	34	59	21	4	28
IL22RA2	NM_181310.1	3	2	2	8	18	5	3	12
IL23A	NM_016584.2	22	67	17	43	324	2633	30	97
IL23R	NM_144701.2	16	44	5	37	66	18	6	21
IL26	NM_018402.1	10	54	10	38	52	19	5	25
IL27	NM_145659.3	20	49	12	59	60	19	5	48
IL28A	NM_172138.1	21	169	27	117	114	28	7	64
IL28A/B	NM_172139.2	7	42	12	33	37	8	3	14
IL29	NM_172140.1	2	17	4	12	14	8	5	12
IL2RA	NM_000417.1	17	58	9	40	3142	2828	1744	987
IL2RB	NM_000878.2	26	73	26	68	63	59	52	83
IL2RG	NM_000206.1	1627	1457	1630	1655	3774	2673	3110	3193
IL3	NM_000588.3	7	52	9	35	43	2	2	18
IL4	NM_000589.2	16	43	5	20	28	12	1	23
IL4R	NM_000418.2	371	331	437	321	696	341	378	345
IL5	NM_000879.2	13	91	15	52	78	10	7	44
IL6	NM_000600.1	8	4	1	10	36	221	11	16
IL6R	NM_000565.2	1091	1245	1229	1057	542	563	399	543
IL6ST	NM_002184.2	348	373	368	423	448	200	146	381
IL7	NM_000880.2	35	102	35	86	68	1	1	22
IL7R	NM_002185.2	22	79	21	57	6120	4342	5042	4219
IL8	NM_000584.2	93	88	209	441	32604	52576	25330	16302
IL9	NM_000590.1	6	8	5	18	20	4	3	8
ILF3	NM_001137673.1	1560	1568	1756	1427	527	309	267	423
IRAK1	NM_001569.3	241	320	271	237	105	84	45	83

IRAK2	NM_001570.3	21	20	17	18	715	894	596	534
IRAK3	NM_007199.1	154	163	195	163	47	14	7	39
IRAK4	NM_016123.1	182	301	232	240	99	41	49	69
IRF1	NM_002198.1	309	362	411	323	1105	1077	350	385
IRF3	NM_001571.5	31	35	20	29	22	8	10	5
IRF4	NM_002460.1	796	963	939	962	3357	2940	3326	3157
IRF5	NM_002200.3	410	404	418	372	151	92	275	119
IRF7	NM_001572.3	192	268	141	198	224	81	76	114
IRF8	NM_002163.2	1421	1252	1255	1129	170	66	39	44
IRGM	NM_001145805.1	4	44	8	22	36	11	3	15
ITGA2B	NM_000419.3	26	75	19	53	60	9	9	44
ITGA4	NM_000885.4	595	640	591	580	189	153	77	139
ITGA5	NM_002205.2	1179	1096	1176	884	346	358	401	290
ITGA6	NM_000210.1	14	61	12	44	36	12	7	26
ITGAE	NM_002208.4	212	229	194	214	231	128	244	242
ITGAL	NM_002209.2	813	923	929	899	104	30	21	100
ITGAM	NM_000632.3	136	203	219	218	67	18	15	40
ITGAX	NM_000887.3	5885	6764	7495	6175	881	317	390	734
ITGB1	NM_033666.2	712	694	732	667	640	356	580	589
ITGB2	NM_000211.2	4914	5499	4960	4991	870	775	561	923
ITLN1	NM_017625.2	6	45	10	49	49	16	12	29
ITLN2	NM_080878.2	9	77	12	43	57	17	1	53
JAK1	NM_002227.1	940	862	999	1010	1474	1049	1119	1042
JAK2	NM_004972.2	2025	2169	2210	2135	496	160	177	279
JAK3	NM_000215.2	292	287	395	370	180	138	129	140
KCNJ2	NM_000891.2	21	113	23	72	128	30	6	54
KIR3DL1	NM_013289.2	6	24	5	31	21	8	1	20
KIR3DL2	NM_006737.2	11	83	21	66	75	23	16	48
KIR3DL3	NM_153443.3	23	55	11	53	57	7	4	45
KIR_Activating_Subgroup_1	NM_001083539.1	8	20	15	12	10	8	8	7

KIR_Activating_Subgroup_2	NM_014512.1	14	100	16	87	98	16	1	58
KIR_Inhibiting_Subgroup_1	NM_014218.2	4	27	7	18	39	14	6	19
KIR_Inhibiting_Subgroup_2	NM_014511.3	1	18	10	7	12	6	8	5
KIT	NM_000222.2	66	70	74	87	67	19	39	59
KLRAP1	NR_028045.1	24	18	23	14	2	8	2	7
KLRB1	NM_002258.2	3	5	4	2	15	11	10	3
KLRC1	NM_002259.3	12	50	11	46	57	12	6	29
KLRC2	NM_002260.3	9	93	17	60	48	15	8	28
KLRC3	NM_007333.2	3	8	6	17	15	16	12	11
KLRC4	NM_013431.2	20	48	17	23	37	6	7	31
KLRD1	NM_002262.3	4	7	7	2	7	7	6	8
KLRF1	NM_016523.1	27	69	18	68	56	17	5	30
KLRF2	NM_001190765.1	1	1	2	4	1	1	1	2
KLRG1	NM_005810.3	59	10	31	16	4	13	10	6
KLRG2	NM_198508.2	14	50	9	48	55	17	6	35
KLRK1	NM_007360.1	18	51	14	23	36	10	8	13
LAD1	NM_005558.3	16	86	28	61	600	885	666	714
LAG3	NM_002286.5	7	30	11	21	48	10	33	28
LAIR1	NM_002287.3	119	151	87	138	135	69	44	103
LAMA5	NM_005560.3	4	52	14	34	36	14	13	24
LAMP3	NM_014398.3	23	70	15	58	14691	11180	9738	10851
LCK	NM_005356.2	14	43	7	28	50	19	11	37
LCP2	NM_005565.3	2194	2270	2625	2603	324	81	141	128
LEF1	NM_016269.3	2	2	4	4	3	4	5	4
LIF	NM_002309.3	17	57	18	52	65	15	44	70
LILRA1	NM_006863.1	238	300	275	255	56	11	6	28
LILRA2	NM_006866.2	441	422	443	459	68	12	10	29

LILRA3	NM_006865.3	21	85	37	41	274	140	91	173
LILRA4	NM_012276.3	61	19	26	29	21	4	2	14
LILRA5	NM_181879.2	713	808	939	862	1218	372	276	585
LILRA6	NM_024318.2	45	107	43	75	69	10	9	24
LILRB1	NM_001081637.1	259	286	302	304	96	28	15	97
LILRB2	NM_005874.1	719	898	878	858	459	181	119	276
LILRB3	NM_006864.2	230	324	284	289	38	13	19	31
LILRB4	NM_001081438.1	573	489	605	584	346	207	170	206
LILRB5	NM_001081442.1	8	39	8	49	44	4	4	26
LITAF	NM_004862.3	1965	1656	1763	1239	2468	2642	1091	1367
LTA	NM_000595.2	14	63	16	51	69	15	5	40
LTB4R	NM_181657.3	266	358	306	313	75	24	17	44
LTB4R2	NM_019839.4	200	286	224	233	53	11	8	27
LTBR	NM_002342.1	471	492	493	460	95	52	81	80
LTF	NM_002343.2	12	94	13	81	69	20	8	47
LY96	NM_015364.2	316	252	320	260	74	27	49	51
MAF	NM_005360.4	9	58	10	41	31	4	4	35
MALT1	NM_006785.2	1094	1240	984	1055	4826	2365	4527	6943
MAP4K1	NM_007181.3	866	859	950	847	53	3	5	27
MAP4K2	NM_004579.2	152	205	194	168	65	46	30	46
MAP4K4	NM_004834.3	255	180	300	264	2500	2275	1871	1608
MAPK1	NM_138957.2	1542	1642	1713	1401	629	492	556	557
MAPK11	NM_002751.5	12	70	12	44	49	11	5	35
MAPK14	NM_001315.1	785	802	835	799	215	126	104	133
MAPKAPK2	NM_004759.3	267	261	272	259	156	152	116	105
MARCO	NM_006770.3	44	89	43	66	29	6	3	16
MASP1	NM_139125.3	9	36	5	20	31	10	2	27
MASP2	NM_139208.1	16	40	12	37	30	16	3	26
MBL2	NM_000242.2	4	18	4	7	7	1	5	7
MBP	NM_002385.2	355	328	415	380	82	20	91	55
MCL1	NM_021960.3	9285	9281	10645	9860	4514	2492	2554	3371

MERTK	NM_006343.2	11	11	29	14	7	12	10	4
MIF	NM_002415.1	471	346	388	407	1762	833	957	1018
MME	NM_000902.2	11	37	9	37	45	9	2	26
MMP10	NM_002425.1	13	10	10	11	15	947	476	57
MMP12	NM_002426.3	1	10	4	5	1483	291	1900	1504
MMP7	NM_002423.3	12	22	10	19	652	4207	151	117
MR1	NM_001531.2	102	95	83	116	118	27	30	46
MRC1	NM_002438.2	93	139	583	169	1775	263	1014	816
MS4A1	NM_152866.2	19	24	15	36	34	5	8	22
MSR1	NM_002445.3	33	102	39	60	53	7	13	18
MUC1	NM_001018017.1	11	12	9	12	35	26	48	44
MX1	NM_002462.2	886	2127	642	1248	279	43	115	82
MYD88	NM_002468.3	2299	2374	2811	2681	263	96	178	183
NAV1	NM_001167738.1	118	132	115	148	214	238	206	194
NCAM1	NM_000615.5	20	75	7	60	82	14	5	36
NCF4	NM_000631.4	173	158	173	174	69	24	23	36
NCR1	NM_004829.5	9	4	2	9	17	18	10	9
NEFH	NM_021076.3	15	34	17	31	95	593	20	31
NFATC1	NM_172389.1	121	135	105	111	111	117	67	88
NFATC2	NM_012340.3	596	744	733	603	92	72	37	49
NFATC3	NM_004555.2	482	468	490	387	105	84	62	91
NFIL3	NM_005384.2	298	251	436	518	1450	563	1588	1005
NFKB1	NM_003998.2	359	390	372	382	2619	1788	1123	1313
NFKBIZ	NM_001005474.1	447	271	1026	970	944	1637	364	513
NLRP3	NM_001079821.2	632	772	807	713	140	71	78	194
NOD1	NM_006092.1	139	213	129	190	292	225	50	116
NOD2	NM_022162.1	586	729	659	638	283	111	115	244
NOS2	NM_000625.4	23	62	8	45	50	22	26	57
NOTCH1	NM_017617.3	69	103	51	59	51	37	36	43
NT5E	NM_002526.2	33	75	28	62	55	41	36	69
PAPLN	NM_173462.3	20	62	16	43	122	128	183	82

PAX5	NM_016734.1	18	69	21	64	66	24	10	54
PDCD1	NM_005018.1	16	90	13	65	74	34	25	84
PDCD1LG2	NM_025239.3	11	14	15	12	958	472	418	445
PDCD2	NM_144781.2	103	213	128	185	128	33	27	86
PDGFB	NM_033016.2	15	41	5	44	116	74	53	81
PDGFRB	NM_002609.3	19	79	18	50	65	19	6	53
PECAM1	NM_000442.3	1305	1214	1644	1320	61	43	217	105
PIGR	NM_002644.2	28	89	17	65	71	13	8	33
PLA2G2A	NM_000300.2	16	87	12	58	104	15	6	47
PLA2G2E	NM_014589.1	6	43	12	32	28	10	5	19
PLAU	NM_002658.2	53	83	37	65	100	72	42	46
PLAUR	NM_001005376.1	573	527	517	494	238	60	102	102
PLOD1	NM_000302.2	201	223	243	197	86	33	58	71
PLOD2	NM_182943.2	7	13	6	7	32	26	65	35
PML	NM_002675.3	262	384	279	329	317	246	94	178
POU2F2	NM_002698.2	425	397	457	345	54	10	15	28
PPARG	NM_015869.3	16	24	3	16	34	8	14	23
PPBP	NM_002704.2	10	22	97	11	19	8	4	6
PRDM1	NM_001198.3	122	185	85	135	663	564	659	514
PRF1	NM_005041.3	31	60	16	58	71	23	15	56
PRKCD	NM_006254.3	1534	1425	1634	1306	185	170	121	152
PSMB10	NM_002801.2	610	619	621	537	380	230	143	170
PSMB5	NM_001130725.1	304	354	330	360	300	197	152	164
PSMB7	NM_002799.2	1376	1098	1431	1281	436	284	330	272
PSMB8	NM_004159.4	1253	1436	1290	1127	539	338	122	192
PSMB9	NM_002800.4	1152	1173	1003	1223	876	333	96	260
PSMC2	NM_002803.3	672	638	726	666	238	126	161	190
PSMD7	NM_002811.3	1072	975	1107	1006	581	286	300	344
PTAFR	NM_000952.3	448	381	599	417	209	1	23	110
PTGER4	NM_000958.2	246	242	292	308	230	170	227	232
PTGS2	NM_000963.1	1744	1634	3035	4215	1164	2831	440	429

PTK2	NM_005607.3	212	169	253	199	69	21	21	38
PTPN2	NM_002828.2	470	516	583	552	526	240	284	347
PTPN22	NM_015967.4	525	397	580	492	45	12	15	34
PTPN6	NM_002831.5	1990	2300	2301	2079	139	36	58	106
PTPRC_all	NM_080921.2	7541	6159	8238	6798	2055	529	1386	1731
PYCARD	NM_013258.3	207	205	247	212	47	7	4	15
RAF1	NM_002880.2	410	463	573	427	300	161	367	269
RAG1	NM_000448.2	15	61	12	43	54	12	5	32
RAG2	NM_000536.3	19	78	13	57	68	12	9	31
RAMP1	NM_005855.2	12	48	29	67	688	412	1344	625
RARRES3	NM_004585.3	135	111	159	189	119	36	18	21
RELA	NM_021975.2	137	131	144	127	218	189	176	204
RELB	NM_006509.2	126	123	130	121	438	364	408	358
RORC	NM_001001523.1	9	33	8	30	27	13	17	22
RUFY3	NM_001130709.1	440	356	497	443	329	237	161	240
RUNX1	NM_001754.4	168	202	284	186	122	111	57	91
S100A8	NM_002964.3	1373	1960	1669	1026	59	23	69	67
S100A9	NM_002965.2	3956	5564	5067	3363	121	54	85	136
S1PR1	NM_001400.3	9	41	5	25	151	59	102	153
SELE	NM_000450.2	6	31	6	31	45	23	10	13
SELL	NR_029467.1	3229	2109	2916	2605	67	16	6	29
SELPLG	NM_003006.3	59	89	37	85	52	11	18	25
SERPING1	NM_000062.2	46	131	56	81	170	26	64	51
SH2D1A	NM_001114937.2	1	5	4	5	6	45	14	8
SIGIRR	NM_021805.2	204	252	274	256	55	16	8	37
SKI	NM_003036.2	278	313	321	294	124	38	52	79
SLAMF1	NM_003037.2	7	22	9	10	39	66	4	11
SLAMF6	NM_001184714.1	8	20	1	16	22	7	4	10
SLAMF7	NM_021181.3	192	201	158	162	1400	916	1282	1030
SLC2A1	NM_006516.2	107	129	103	129	144	123	67	105
SMAD3	NM_005902.3	321	386	419	443	330	53	81	155

SMAD5	NM_005903.5	214	221	201	222	79	25	29	47
SOCS1	NM_003745.1	15	46	14	42	456	689	167	158
SOCS2	NM_003877.3	30	112	30	74	2161	2687	1177	1245
SOCS3	NM_003955.3	204	135	268	302	757	1076	330	473
SPP1	NM_000582.2	12	41	20	39	120	31	261	81
SRC	NM_005417.3	101	127	86	124	472	362	176	248
STAT1	NM_007315.2	544	762	543	582	1514	235	267	275
STAT2	NM_005419.2	1080	1302	1119	933	587	241	247	284
STAT3	NM_139276.2	685	858	821	769	1696	921	820	1039
STAT4	NM_003151.2	46	63	24	47	964	996	302	532
STAT5A	NM_003152.2	383	473	487	434	971	1394	227	283
STAT5B	NM_012448.3	315	285	329	319	337	622	100	146
STAT6	NM_003153.3	2136	2218	2604	1882	984	825	958	980
SYK	NM_003177.3	1655	1656	1939	1726	252	111	213	209
TAGAP	NM_054114.3	1135	984	1192	839	119	32	39	77
TAL1	NM_003189.2	18	97	20	81	84	16	5	39
TAP1	NM_000593.5	232	236	213	225	504	293	139	219
TAP2	NM_000544.3	171	266	193	180	263	307	46	172
TAPBP	NM_003190.4	1114	1302	1217	1161	864	592	624	632
TBK1	NM_013254.2	213	243	222	233	234	139	145	157
TBX21	NM_013351.1	45	58	23	66	91	54	29	60
TCF4	NM_003199.1	225	224	181	182	122	38	83	68
TCF7	NM_003202.2	10	109	16	73	153	68	34	107
TFRC	NM_003234.1	348	385	304	337	752	561	1341	557
TGFB1	NM_000660.3	1045	1192	1158	1075	179	72	78	104
TGFBI	NM_000358.2	1861	1797	1825	1442	240	58	219	107
TGFBR1	NM_004612.2	317	399	286	324	491	317	297	284
TGFBR2	NM_001024847.1	1033	934	1135	873	186	74	249	168
TGM2	NM_004613.2	13	24	48	14	35	28	62	36
THY1	NM_006288.2	5	53	7	53	29	7	9	21
TICAM1	NM_014261.1	168	152	161	167	184	129	73	94

TIGIT	NM_173799.2	37	59	35	59	49	21	16	41
TIMP2	NM_003255.4	429	486	477	467	30	24	26	29
TIRAP	NM_148910.2	39	72	67	58	38	29	31	39
TLR1	NM_003263.3	807	789	923	810	184	34	103	139
TLR2	NM_003264.3	481	494	655	594	234	107	98	169
TLR3	NM_003265.2	83	112	79	105	69	9	6	30
TLR4	NM_138554.2	209	306	232	249	60	26	25	51
TLR5	NM_003268.3	151	244	246	237	67	18	19	43
TLR7	NM_016562.3	56	80	46	69	23	9	10	19
TLR8	NM_016610.2	324	429	472	366	431	284	859	537
TLR9	NM_017442.2	34	46	25	33	58	14	8	30
TMEM173	NM_198282.1	504	667	674	558	6	14	12	10
TNF	NM_000594.2	36	54	26	57	120	43	30	58
TNFAIP3	NM_006290.2	715	669	916	1174	3088	4628	1441	1511
TNFAIP6	NM_007115.2	21	18	26	17	20	47	34	29
TNFRSF10C	NM_003841.3	54	125	63	110	75	22	26	35
TNFRSF11A	NM_003839.2	4	10	22	19	182	198	190	145
TNFRSF13B	NM_012452.2	1	1	1	1	2	1	1	5
TNFRSF13C	NM_052945.3	22	68	18	54	46	5	2	40
TNFRSF14	NM_003820.2	297	283	307	273	292	259	190	164
TNFRSF17	NM_001192.2	32	58	15	54	65	14	12	46
TNFRSF1B	NM_001066.2	710	840	861	551	591	754	808	565
TNFRSF4	NM_003327.2	9	43	7	24	372	509	158	211
TNFRSF8	NM_152942.2	36	90	47	79	82	16	14	33
TNFRSF9	NM_001561.4	19	40	13	45	396	532	281	238
TNFSF10	NM_003810.2	201	229	253	289	124	17	7	23
TNFSF11	NM_003701.2	17	18	18	21	11	17	14	7
TNFSF12	NM_003809.2	351	236	316	353	38	8	33	19
TNFSF13B	NM_006573.4	1282	1199	1201	1143	1420	348	3586	2175
TNFSF15	NM_001204344.1	19	94	45	105	90	44	5	48
TNFSF4	NM_003326.2	30	91	30	87	205	67	86	189

TNFSF8	NM_001244.3	117	100	99	93	37	16	1	17
TOLLIP	NM_019009.2	274	336	269	287	201	117	143	181
TP53	NM_000546.2	916	988	971	879	92	51	33	89
TRAF1	NM_005658.3	49	103	52	71	3775	3405	1426	2133
TRAF2	NM_021138.3	43	137	71	118	220	110	122	137
TRAF3	NM_145725.1	161	245	178	216	340	143	199	222
TRAF4	NM_004295.2	104	148	86	133	320	351	88	146
TRAF5	NM_004619.3	50	56	83	73	266	194	233	292
TRAF6	NM_145803.1	190	267	161	244	331	186	132	219
TSPAN33	NM_178562.3	599	492	853	737	3430	3945	2915	1923
TYK2	NM_003331.3	993	1120	1166	960	468	460	410	390
UBE2L3	NM_198157.1	397	386	358	337	161	67	62	107
VCAM1	NM_001078.3	4	14	8	21	39	10	24	20
VEGFA	NM_001025366.1	336	527	441	628	3853	1922	2367	2715
VTN	NM_000638.3	12	58	14	39	58	7	12	40
XBP1	NM_005080.2	315	272	295	253	264	281	118	142
XCL1	NM_002995.1	16	94	9	56	74	16	8	38
XCR1	NM_005283.2	107	114	33	91	69	45	13	39
ZAP70	NM_001079.3	10	51	8	53	43	13	4	25
ZBTB16	NM_006006.4	1	1	9	7	17	29	2	19
ZEB1	NM_001128128.1	72	105	62	77	108	100	56	69
sCTLA4	NM_001037631.1	20	36	43	50	30	39	37	33
ABCF1	NM_001090.2	199	193	231	198	67	33	32	32
ALAS1	NM_000688.4	87	101	130	84	155	179	299	133
EEF1G	NM_001404.4	18528	16107	19398	18494	10593	7031	9320	8672
G6PD	NM_000402.2	257	275	280	226	196	179	177	144
GAPDH	NM_002046.3	17464	16736	18669	17082	26971	19468	20725	23491
GUSB	NM_000181.1	310	268	295	261	51	37	61	85
HPRT1	NM_000194.1	508	509	534	548	652	387	743	340
OAZ1	NM_004152.2	8524	8528	9293	8058	3341	2627	2937	2510
POLR2A	NM_000937.2	501	604	505	479	357	266	245	297

PPIA	NM_021130.2	333	295	377	327	103	51	49	52
RPL19	NM_000981.3	19762	18988	22219	21078	9530	5897	7201	5942
TBP	NM_001172085.1	320	291	319	337	141	65	75	96
TUBB	NM_178014.2	596	719	541	542	834	833	482	592
NEG_A	ERCC_00096.1	11	14	14	10	11	15	22	18
NEG_B	ERCC_00041.1	4	10	2	5	8	7	4	7
NEG_C	ERCC_00019.1	6	2	8	5	6	7	6	5
NEG_D	ERCC_00076.1	11	7	6	3	5	4	9	10
NEG_E	ERCC_00098.1	17	13	18	10	13	9	21	22
NEG_F	ERCC_00126.1	11	14	9	7	11	11	10	7
NEG_G	ERCC_00144.1	3	4	2	7	5	3	1	1
NEG_H	ERCC_00154.1	4	5	12	1	11	20	6	11
POS_A	ERCC_00117.1	16433	16628	16470	14114	15237	11423	14975	10829
POS_B	ERCC_00112.1	4232	4438	4181	3549	4010	3066	4062	2759
POS_C	ERCC_00002.1	1243	1211	1127	1045	1163	850	1055	777
POS_D	ERCC_00092.1	316	331	313	267	310	270	323	203
POS_E	ERCC_00035.1	67	67	76	60	62	45	59	33
POS_F	ERCC_00034.1	45	39	48	44	39	36	56	30

Table AX3. Gene expression data from the nCounter analysis of LEL mDCs vs PBDCs

5.3 GO term analysis of the top 10% of non-differentially expressed genes across all mLPDC sample groups

GO term	Description	P-value	FDR q-value	Enrichment (N, B, n, b)
GO:0006614	SRP-dependent cotranslational protein targeting to membrane	1.21E-10	7.29E-7	3.01 (582,34,159,28)
GO:0019083	viral transcription	1.21E-10	3.65E-7	3.01 (582,34,159,28)
GO:0006412	translation	1.66E-10	3.34E-7	2.89 (582,38,159,30)
GO:0043043	peptide biosynthetic process	1.66E-10	2.51E-7	2.89 (582,38,159,30)
GO:0000184	nuclear-transcribed mRNA catabolic process, nonsense-mediated decay	5.16E-10	6.25E-7	2.87 (582,37,159,29)
GO:0006402	mRNA catabolic process	5.28E-10	5.32E-7	2.72 (582,43,159,32)
GO:0000956	nuclear-transcribed mRNA catabolic process	5.65E-10	4.88E-7	2.77 (582,41,159,31)
GO:0043604	amide biosynthetic process	7.67E-10	5.8E-7	2.59 (582,40,180,32)
GO:0006518	peptide metabolic process	1.55E-9	1.04E-6	2.41 (582,48,181,36)
GO:0045047	protein targeting to ER	1.65E-9	9.98E-7	2.85 (582,36,159,28)
GO:0006413	translational initiation	5.13E-9	2.82E-6	2.68 (582,41,159,30)
GO:0034655	nucleobase-containing compound catabolic process	5.23E-9	2.64E-6	2.40 (582,56,160,37)
GO:0070972	protein localization to endoplasmic reticulum	5.38E-9	2.5E-6	2.72 (582,39,159,29)
GO:0006613	cotranslational protein targeting to membrane	5.41E-9	2.34E-6	2.77 (582,37,159,28)
GO:0072599	establishment of protein localization to endoplasmic reticulum	5.41E-9	2.18E-6	2.77 (582,37,159,28)
GO:0006401	RNA catabolic process	1.03E-8	3.91E-6	2.55 (582,46,159,32)
GO:0006612	protein targeting to membrane	1.55E-8	5.51E-6	2.65 (582,40,159,29)
GO:0006605	protein targeting	1.8E-8	6.06E-6	2.44 (582,51,159,34)
GO:0072594	establishment of protein localization to organelle	2,00E-08	6.38E-6	2.34 (582,58,159,37)
GO:0090150	establishment of protein localization to membrane	2.73E-8	8.24E-6	2.49 (582,47,159,32)
GO:1901566	organonitrogen compound biosynthetic process	3.16E-8	9.11E-6	2.25 (582,63,160,39)
GO:0046700	heterocycle catabolic process	4.05E-8	1.11E-5	2.27 (582,61,160,38)
GO:0044271	cellular nitrogen compound biosynthetic process	4.21E-8	1.11E-5	2.20 (582,89,128,43)
GO:1901361	organic cyclic compound catabolic process	8.2E-8	2.07E-5	2.23 (582,62,160,38)
GO:0072657	protein localization to membrane	8.74E-8	2.12E-5	2.35 (582,53,159,34)
GO:0044270	cellular nitrogen compound catabolic process	1.05E-7	2.45E-5	2.24 (582,60,160,37)
GO:0019439	aromatic compound catabolic process	2.17E-7	4.86E-5	2.21 (582,61,160,37)
GO:0043603	cellular amide metabolic process	3.22E-7	6.96E-5	2.12 (582,56,181,37)
GO:0034645	cellular macromolecule biosynthetic process	1.01E-6	2.1E-4	2.18 (582,77,128,37)
GO:0009059	macromolecule biosynthetic process	1.49E-6	3,00E-04	2.13 (582,81,128,38)
GO:0001895	retina homeostasis	2.45E-6	4.78E-4	26.45 (582,4,22,4)
GO:0048519	negative regulation of biological process	5.55E-6	1.05E-3	1.32 (582,298,171,116)
GO:0006955	immune response	6.62E-6	1.21E-3	3.25 (582,81,42,19)

GO:0019883	antigen processing and presentation of endogenous antigen	7.85E-6	1.4E-3	33.26 (582,10,7,4)
GO:0060333	interferon-gamma-mediated signaling pathway	8.2E-6	1.42E-3	10.42 (582,17,23,7)
GO:0051235	maintenance of location	8.48E-6	1.42E-3	13.43 (582,13,20,6)
GO:0033365	protein localization to organelle	9.07E-6	1.48E-3	1.96 (582,73,159,39)
GO:0016032	viral process	1.02E-5	1.63E-3	1.78 (582,99,162,49)
GO:0044403	symbiont process	1.02E-5	1.59E-3	1.78 (582,99,162,49)
GO:0034613	cellular protein localization	1.03E-5	1.56E-3	1.87 (582,84,159,43)
GO:0070727	cellular macromolecule localization	1.03E-5	1.53E-3	1.87 (582,84,159,43)
GO:0009057	macromolecule catabolic process	1.04E-5	1.5E-3	1.93 (582,76,159,40)
GO:0010605	negative regulation of macromolecule metabolic process	1.19E-5	1.68E-3	1.49 (582,180,171,79)
GO:1901576	organic substance biosynthetic process	1.33E-5	1.83E-3	1.49 (582,112,251,72)
GO:0042493	response to drug	1.43E-5	1.93E-3	2.12 (582,44,181,29)
GO:0006959	humoral immune response	1.45E-5	1.9E-3	7.39 (582,15,42,8)
GO:0010629	negative regulation of gene expression	1.5E-5	1.93E-3	1.67 (582,125,159,57)
GO:0006886	intracellular protein transport	1.51E-5	1.9E-3	1.93 (582,74,159,39)
GO:0009892	negative regulation of metabolic process	1.62E-5	2,00E-03	1.47 (582,187,171,81)
GO:0051651	maintenance of location in cell	1.93E-5	2.33E-3	16.17 (582,9,20,5)
GO:0044249	cellular biosynthetic process	2.31E-5	2.74E-3	1.48 (582,113,251,72)
GO:0009058	biosynthetic process	2.31E-5	2.68E-3	1.48 (582,113,251,72)
GO:0002504	antigen processing and presentation of peptide or polysaccharide antigen via MHC class II	3.31E-5	3.78E-3	11.41 (582,17,18,6)
GO:0002495	antigen processing and presentation of peptide antigen via MHC class II	3.31E-5	3.71E-3	11.41 (582,17,18,6)
GO:0019886	antigen processing and presentation of exogenous peptide antigen via MHC class II	3.31E-5	3.64E-3	11.41 (582,17,18,6)
GO:0044419	interspecies interaction between organisms	4.07E-5	4.39E-3	1.67 (582,114,162,53)
GO:0002483	antigen processing and presentation of endogenous peptide antigen	8.51E-5	9.03E-3	5.36 (582,8,95,7)
GO:0051100	negative regulation of binding	8.51E-5	8.87E-3	43.65 (582,8,5,3)
GO:0044265	cellular macromolecule catabolic process	8.7E-5	8.92E-3	2.06 (582,70,125,31)
GO:0002250	adaptive immune response	1.11E-4	1.11E-2	6.53 (582,31,23,8)
GO:0019221	cytokine-mediated signaling pathway	1.16E-4	1.15E-2	3.11 (582,88,34,16)
GO:1901575	organic substance catabolic process	1.33E-4	1.3E-2	1.65 (582,96,180,49)
GO:0050790	regulation of catalytic activity	1.85E-4	1.77E-2	1.34 (582,150,266,92)
GO:0002684	positive regulation of immune system process	1.87E-4	1.77E-2	3.19 (582,111,23,14)
GO:0006880	intracellular sequestering of iron ion	2.13E-4	1.98E-2	64.67 (582,2,9,2)
GO:0051238	sequestering of metal ion	2.13E-4	1.95E-2	64.67 (582,2,9,2)
GO:0097577	sequestering of iron ion	2.13E-4	1.92E-2	64.67 (582,2,9,2)
GO:0016064	immunoglobulin mediated immune response	2.2E-4	1.95E-2	24.25 (582,4,18,3)
GO:0019724	B cell mediated immunity	2.2E-4	1.93E-2	24.25 (582,4,18,3)
GO:0048002	antigen processing and presentation of peptide antigen	2.31E-4	2,00E-02	5.95 (582,34,23,8)

GO:0002478	antigen processing and presentation of exogenous peptide antigen	2.31E-4	1.97E-2	5.95 (582,34,23,8)
GO:0043382	positive regulation of memory T cell differentiation	2.48E-4	2.09E-2	83.14 (582,2,7,2)
GO:0002469	myeloid dendritic cell antigen processing and presentation	2.48E-4	2.06E-2	83.14 (582,2,7,2)
GO:0002468	dendritic cell antigen processing and presentation	2.48E-4	2.03E-2	83.14 (582,2,7,2)
GO:0002491	antigen processing and presentation of endogenous peptide antigen via MHC class II	2.48E-4	2,00E-02	83.14 (582,2,7,2)
GO:0045589	regulation of regulatory T cell differentiation	2.48E-4	1.98E-2	83.14 (582,2,7,2)
GO:0045591	positive regulation of regulatory T cell differentiation	2.48E-4	1.95E-2	83.14 (582,2,7,2)
GO:0032829	regulation of CD4-positive, CD25-positive, alpha-beta regulatory T cell differentiation	2.48E-4	1.93E-2	83.14 (582,2,7,2)
GO:0032831	positive regulation of CD4-positive, CD25-positive, alpha-beta regulatory T cell differentiation	2.48E-4	1.9E-2	83.14 (582,2,7,2)
GO:0051704	multi-organism process	2.49E-4	1.89E-2	1.50 (582,153,162,64)
GO:0001916	positive regulation of T cell mediated cytotoxicity	2.9E-4	2.17E-2	31.18 (582,8,7,3)
GO:0019884	antigen processing and presentation of exogenous antigen	2.92E-4	2.15E-2	5.78 (582,35,23,8)
GO:0051606	detection of stimulus	3.15E-4	2.29E-2	2.93 (582,13,168,11)
GO:0002480	antigen processing and presentation of exogenous peptide antigen via MHC class I, TAP-independent	3.27E-4	2.36E-2	6.13 (582,5,95,5)
GO:0048589	developmental growth	3.43E-4	2.44E-2	2.90 (582,13,170,11)
GO:0045824	negative regulation of innate immune response	4.06E-4	2.86E-2	5.25 (582,7,95,6)
GO:0050778	positive regulation of immune response	4.13E-4	2.87E-2	3.53 (582,86,23,12)
GO:0001914	regulation of T cell mediated cytotoxicity	4.8E-4	3.3E-2	27.71 (582,9,7,3)
GO:0001912	positive regulation of leukocyte mediated cytotoxicity	4.8E-4	3.27E-2	27.71 (582,9,7,3)
GO:0031343	positive regulation of cell killing	4.8E-4	3.23E-2	27.71 (582,9,7,3)
GO:0040007	growth	5.34E-4	3.55E-2	2.27 (582,14,238,13)
GO:0046638	positive regulation of alpha-beta T cell differentiation	6.08E-4	4,00E-02	3.02 (582,8,193,8)
GO:0009056	catabolic process	6.36E-4	4.14E-2	1.62 (582,103,160,46)
GO:0043380	regulation of memory T cell differentiation	6.98E-4	4.49E-2	55.43 (582,3,7,2)
GO:0045655	regulation of monocyte differentiation	6.98E-4	4.45E-2	55.43 (582,3,7,2)
GO:0045657	positive regulation of monocyte differentiation	6.98E-4	4.4E-2	55.43 (582,3,7,2)
GO:0051262	protein tetramerization	6.98E-4	4.35E-2	55.43 (582,3,7,2)
GO:0046598	positive regulation of viral entry into host cell	6.98E-4	4.31E-2	55.43 (582,3,7,2)
GO:0002753	cytoplasmic pattern recognition receptor signaling pathway	7.23E-4	4.42E-2	6.30 (582,6,77,5)

GO:0070423	nucleotide-binding oligomerization domain containing signaling pathway	7.23E-4	4.37E-2	6.30 (582,6,77,5)
GO:0035872	nucleotide-binding domain, leucine rich repeat containing receptor signaling pathway	7.23E-4	4.33E-2	6.30 (582,6,77,5)
GO:0031341	regulation of cell killing	8.29E-4	4.92E-2	3.29 (582,15,118,10)
GO:0019882	antigen processing and presentation	8.77E-4	5.15E-2	5.06 (582,40,23,8)
GO:0001894	tissue homeostasis	8.91E-4	5.18E-2	11.76 (582,9,22,4)
GO:0060249	anatomical structure homeostasis	9,00E-04	5.19E-2	8.82 (582,15,22,5)
GO:0060255	regulation of macromolecule metabolic process	9.5E-4	5.42E-2	1.23 (582,323,171,117)

Table AX4: GO terms from the top 10% non-differentially expressed genes with the highest base mean mRNA amount; unsupervised NC, CD, UC, iUC, iCD. This list contains the GO terms for all processed samples from the mLPDC RNA sequencing analysis with p-values greater than 1,0E-03. GO terms were computed using the top 10% mRNAs with the highest base mean value that were not differentially expressed between all samples. This method gives an overview about the top functions across all sample groups these mDCs inherit in the lamina propria environment. N, total number of genes; B, total number of genes associated with a specific GO term; n, number of differentially expressed genes tested for enrichment; b, number of detected genes belonging to the respective GO term; Enrichment: (b/n)/(B/N)(GOrilla tool: (Eden et al. 2009))

5.4 Top 20 differentially expressed up- and downregulated genes comparing groups of IBD patients and healthy individuals

Upregulated	Gene name	Linear Fold Change	pvalue	Gene description
1	AC009570.2	929,49	9,53E-04	novel transcript
2	JCHAIN	407,47	1,25E-04	joining chain of multimeric IgA and IgM
3	RETREG1	67,53	3,34E-04	reticulophagy regulator 1
4	NSUN5P1	44,51	5,68E-04	NSUN5 pseudogene 1
5	CRAMP1	41,49	1,69E-05	cramped chromatin regulator homolog 1
6	WDR24	39,59	3,82E-03	WD repeat domain 24
7	AL096701.3	39,21	1,67E-03	novel transcript
8	CKAP4	33,04	1,46E-02	cytoskeleton associated protein 4
9	FANCF	29,88	4,83E-02	FA complementation group F
10	SPATA5	27,28	2,52E-03	spermatogenesis associated 5
11	KANK1	26,06	2,33E-04	KN motif and ankyrin repeat domains 1
12	NSG1	21,16	2,09E-02	neuronal vesicle trafficking associated 1
13	TGM2	18,61	4,28E-04	transglutaminase 2
14	PTPRF	18,53	4,36E-02	protein tyrosine phosphatase receptor type F
15	MYOM1	18,13	1,30E-02	myomesin 1
16	THEM6	18,12	3,80E-02	thioesterase superfamily member 6
17	CASZ1	16,01	7,06E-03	castor zinc finger 1
18	DNASE2	14,79	1,28E-03	deoxyribonuclease 2, lysosomal
19	ATP6V0A1	14,15	3,10E-04	ATPase H+ transporting V0 subunit a1
20	MINDY3	14,07	3,56E-02	MINDY lysine 48 deubiquitinase 3
Downregulated	**Gene name**	**Linear Fold Change**	**pvalue**	**Gene description**
1	CDT1	-53,54	4,52E-05	chromatin licensing and DNA replication factor 1
2	ACOX3	-46,78	1,47E-03	acyl-CoA oxidase 3, pristanoyl
3	RRAGB	-40,79	7,33E-03	Ras related GTP binding B
4	RETSAT	-31,46	1,06E-05	retinol saturase
5	POC1B-AS1	-26,34	4,40E-03	POC1B antisense RNA 1
6	ZNF701	-25,02	1,96E-04	zinc finger protein 701
7	RTTN	-24,10	1,74E-02	rotatin
8	NRP1	-23,88	3,87E-03	neuropilin 1
9	UQCC1	-23,34	1,32E-04	ubiquinol-cyt c reductase complex assembly factor 1
10	CTSZ	-22,74	1,86E-05	cathepsin Z
11	GPRC5A	-21,48	1,19E-02	G protein-coupled receptor class C group 5 member A
12	CCL20	-21,41	5,58E-05	C-C motif chemokine ligand 20
13	AC040970.1	-20,33	2,18E-02	novel transcript
14	MGME1	-20,19	3,38E-03	mitochondrial genome maintenance exonuclease 1
15	GAS2L1	-20,03	1,07E-03	growth arrest specific 2 like 1
16	LBH	-18,76	4,36E-02	LBH regulator of WNT signaling pathway
17	PLAC9	-18,67	7,73E-03	placenta associated 9
18	ZNF124	-18,43	3,12E-03	zinc finger protein 124
19	GCLM	-18,08	1,72E-06	glutamate-cysteine ligase modifier subunit
20	AC091271.1	-16,67	1,64E-02	novel transcript

Table AX5: Top 20 upregulated and top 20 downregulated genes from niCD mDCs vs NC mDCs (basis)

Upregulated	Gene name	Linear Fold Change	pvalue	Gene description
1	PRRG4	239,20	4,71E-10	proline rich and Gla domain 4
2	TGM2	96,91	2,50E-05	transglutaminase 2
3	CASZ1	86,09	9,49E-04	castor zinc finger 1
4	LAD1	79,43	3,43E-04	ladinin 1
5	RETREG1	43,56	1,71E-02	reticulophagy regulator 1
6	MYO7B	40,90	3,18E-03	myosin VIIB
7	OPTN	37,91	3,47E-02	optineurin
8	RHOBTB3	35,83	2,97E-03	Rho related BTB domain containing 3
9	SLC22A23	35,81	7,75E-04	solute carrier family 22 member 23
10	SLC6A12	33,25	3,94E-02	solute carrier family 6 member 12
11	TNFRSF4	26,76	1,39E-09	TNF receptor superfamily member 4
12	S1PR1	25,15	1,64E-02	sphingosine-1-phosphate receptor 1
13	EXTL3	23,96	8,23E-03	exostosin like glycosyltransferase 3
14	CD200	21,80	5,45E-03	CD200 molecule
15	KANK1	21,78	9,68E-03	KN motif and ankyrin repeat domains 1
16	ECE1	18,52	1,21E-02	endothelin converting enzyme 1
17	CCDC28B	18,45	1,40E-02	coiled-coil domain containing 28B
18	P2RX1	18,05	1,62E-02	purinergic receptor P2X 1
19	ITPR3	15,88	8,09E-03	inositol 1,4,5-trisphosphate receptor type 3
20	ANKRD22	15,63	4,89E-02	ankyrin repeat domain 22
Downregulated	**Gene name**	**Linear Fold Change**	**pvalue**	**Gene description**
1	CD1E	-81,46	3,90E-10	CD1e molecule
2	PLPBP	-56,76	2,42E-09	pyridoxal phosphate binding protein
3	GAS2L3	-43,70	9,91E-08	growth arrest specific 2 like 3
4	AC007384.1	-38,41	3,99E-05	novel transcript
5	CTSZ	-33,33	3,93E-04	cathepsin Z
6	ACP5	-28,78	5,11E-09	acid phosphatase 5, tartrate resistant
7	HEATR5B	-26,05	2,38E-05	HEAT repeat containing 5B
8	AL357093.2	-25,85	7,35E-04	novel transcript, antisense to FOXN3
9	Z93241.1	-24,54	3,49E-03	RNA, U12 small nuclear
10	GSTM4	-23,71	6,08E-04	glutathione S-transferase mu 4
11	C17orf107	-23,17	2,67E-04	chromosome 17 open reading frame 107
12	RAB4A	-22,66	1,78E-04	RAB4A, member RAS oncogene family
13	COMMD8	-22,53	2,66E-03	COMM domain containing 8
14	CCL20	-21,87	2,74E-03	C-C motif chemokine ligand 20
15	RSAD2	-21,56	1,52E-03	radical S-adenosyl methionine domain containing 2
16	HES1	-20,51	1,42E-06	hes family bHLH transcription factor 1
17	DPP3	-20,40	8,33E-03	dipeptidyl peptidase 3
18	LIPE-AS1	-20,31	2,29E-04	LIPE antisense RNA 1
19	ITGAM	-20,07	4,44E-04	integrin subunit alpha M
20	BLVRB	-20,07	3,31E-07	biliverdin reductase B

Table AX6: Top 20 upregulated and top 20 downregulated genes from iCD mDCs vs NC mDCs (basis)

Upregulated	Gene name	Linear Fold Change	pvalue	Gene description
1	DHRS9	77,68	4,22E-02	dehydrogenase/reductase 9
2	LBH	70,16	3,19E-02	LBH regulator of WNT signaling pathway
3	UQCC1	65,49	1,24E-04	ubiquinol-cytochrome c reductase complex
4	GCLM	43,94	1,82E-06	glutamate-cysteine ligase modifier subunit
5	GZMB	28,97	4,06E-03	granzyme B
6	NR6A1	27,48	4,21E-03	nuclear receptor subfamily 6 group A member 1
7	FSCN1	23,44	5,13E-06	fascin actin-bundling protein 1
8	TBC1D13	21,76	1,09E-02	TBC1 domain family member 13
9	FER	21,70	2,13E-03	FER tyrosine kinase
10	PRRG4	19,98	4,93E-04	proline rich and Gla domain 4
11	HPGD	19,45	2,90E-02	15-hydroxyprostaglandin dehydrogenase
12	SLC9A6	19,08	1,54E-02	solute carrier family 9 member A6
13	MMD	18,65	6,85E-03	monocyte to macrophage differentiation associated
14	TFB1M	18,20	1,33E-03	transcription factor B1, mitochondrial
15	ARMC7	17,30	6,84E-04	armadillo repeat containing 7
16	ZFYVE27	16,88	1,94E-03	zinc finger FYVE-type containing 27
17	PTGIR	16,41	4,09E-02	prostaglandin I2 receptor
18	USP42	15,13	3,18E-03	ubiquitin specific peptidase 42
19	ERMP1	14,98	5,39E-03	endoplasmic reticulum metallopeptidase 1
20	TIAM2	14,94	5,59E-03	T cell lymphoma invasion and metastasis 2
Downregulated	**Gene name**	**Linear Fold Change**	**pvalue**	**Gene description**
1	CD1E	-92,83	2,63E-10	CD1e molecule
2	JCHAIN	-73,05	4,71E-02	joining chain of multimeric IgA and IgM
3	AL512646.1	-59,74	2,24E-02	WDR45-like (WDR45L) pseudogene
4	PLPBP	-39,04	9,35E-08	pyridoxal phosphate binding protein
5	A2M	-38,38	1,48E-05	alpha-2-macroglobulin
6	OXCT1	-36,93	1,71E-04	3-oxoacid CoA-transferase 1
7	HEATR5B	-34,19	6,80E-06	HEAT repeat containing 5B
8	AL357093.2	-27,55	7,40E-04	novel transcript, antisense to FOXN3
9	XPO5	-26,99	1,40E-03	exportin 5
10	DERL3	-26,76	1,32E-02	derlin 3
11	AC007384.1	-25,84	3,29E-04	novel transcript
12	ANKS1A	-25,51	7,16E-04	ankyrin repeat and sterile alpha motif domain containing 1A
13	GAS2L3	-25,07	7,68E-06	growth arrest specific 2 like 3
14	DNASE1L3	-24,81	1,02E-06	deoxyribonuclease 1 like 3
15	MRS2	-24,30	5,24E-03	magnesium transporter MRS2
16	INTS6L	-24,30	2,51E-04	integrator complex subunit 6 like
17	ZCCHC17	-24,20	3,80E-06	zinc finger CCHC-type containing 17
18	RAB4A	-23,64	1,89E-04	RAB4A, member RAS oncogene family
19	COMMD8	-23,07	3,02E-03	COMM domain containing 8
20	BLVRB	-22,41	2,23E-07	biliverdin reductase B

Table AX7: Top 20 upregulated and top 20 downregulated genes from iCD mDCs vs niCD mDCs (basis)

Upregulated	Gene name	Linear Fold Change	pvalue	Gene description
1	AC009570.2	683,06	9,55E-04	novel transcript
2	JCHAIN	389,62	6,52E-05	joining chain of multimeric IgA and IgM
3	IGHA1	299,10	2,19E-05	immunoglobulin heavy constant alpha 1
4	IFI27	144,14	5,40E-03	interferon alpha inducible protein 27
5	HDC	104,49	1,45E-03	histidine decarboxylase
6	IKZF3	87,00	1,62E-04	IKAROS family zinc finger 3
7	GOLM1	61,51	7,21E-03	golgi membrane protein 1
8	TNFRSF11A	56,65	2,07E-05	TNF receptor superfamily member 11a
9	KRT1	48,78	3,21E-02	keratin 1
10	KIAA1671	40,30	3,86E-03	KIAA1671
11	DLC1	40,13	3,97E-02	DLC1 Rho GTPase activating protein
12	RETREG1	36,14	1,36E-03	reticulophagy regulator 1
13	CASZ1	35,45	2,81E-04	castor zinc finger 1
14	PTPRF	34,36	1,04E-02	protein tyrosine phosphatase receptor type F
15	FANCF	28,15	4,22E-02	FA complementation group F
16	HEG1	27,31	4,14E-03	heart development protein with EGF like domains 1
17	P2RX1	26,17	1,37E-04	purinergic receptor P2X 1
18	PIGR	24,62	3,05E-03	polymeric immunoglobulin receptor
19	AC109925.2	24,32	1,02E-02	novel transcript, antisense to HPGDS
20	MYO7B	23,92	4,39E-04	myosin VIIB
Downregulated	**Gene name**	**Linear Fold Change**	**pvalue**	**Gene description**
1	RPS26P15	-46,52	7,16E-05	ribosomal protein S26 pseudogene 15
2	SFTPD	-30,67	6,21E-03	surfactant protein D
3	CTSZ	-28,86	1,30E-06	cathepsin Z
4	SEZ6L	-16,30	4,91E-02	seizure related 6 homolog like
5	IKZF4	-11,86	4,40E-03	IKAROS family zinc finger 4
6	FABP4	-10,93	4,42E-02	fatty acid binding protein 4
7	MELK	-10,16	3,67E-02	maternal embryonic leucine zipper kinase
8	FAM200A	-9,43	1,94E-02	family with sequence similarity 200 member A
9	HIST1H2BG	-8,81	2,29E-02	histone cluster 1 H2B family member g
10	BLOC1S4	-8,56	5,00E-02	biogenesis of lysosomal organelles complex 1 subunit4
11	TYMS	-8,26	1,47E-04	thymidylate synthetase
12	MN1	-7,69	4,20E-02	MN1 proto-oncogene, transcriptional regulator
13	STK16	-7,48	3,73E-03	serine/threonine kinase 16
14	FECH	-7,04	1,51E-02	ferrochelatase
15	CDT1	-6,54	2,77E-02	chromatin licensing and DNA replication factor 1
16	RRM2	-6,36	1,79E-02	ribonucleotide reductase regulatory subunit M2
17	AC099489.3	-6,29	4,13E-02	novel transcript, antisense to a novel protein gene
18	MTIF2	-5,67	3,70E-02	mitochondrial translational initiation factor 2
19	THUMPD2	-5,61	3,36E-02	THUMP domain containing 2
20	AC099489.1	-5,31	4,80E-03	novel lipoprotein amino terminal region containing prot

Table AX8: Top 20 upregulated and top 20 downregulated genes from niUC mDCs vs NC mDCs (basis)

Upregulated	Gene name	Linear Fold Change	pvalue	Gene description
1	AC009570.2	458,08	7,14E-04	novel transcript
2	JCHAIN	232,17	6,55E-05	joining chain of multimeric IgA and IgM
3	IFI27	156,79	1,97E-03	interferon alpha inducible protein 27
4	ALOX15B	84,00	4,87E-03	arachidonate 15-lipoxygenase type B
5	TCEA3	78,15	2,78E-02	transcription elongation factor A3
6	TNFRSF11A	71,81	1,27E-06	TNF receptor superfamily member 11a
7	IGHA1	69,95	5,36E-04	immunoglobulin heavy constant alpha 1
8	CTSK	64,63	1,56E-02	cathepsin K
9	PRRG4	59,77	1,78E-11	proline rich and Gla domain 4
10	PIGR	55,79	4,62E-05	polymeric immunoglobulin receptor
11	CASZ1	50,25	1,59E-05	castor zinc finger 1
12	IKZF3	48,83	3,73E-04	IKAROS family zinc finger 3
13	TGM2	46,34	1,69E-07	transglutaminase 2
14	PTPRF	43,48	2,90E-03	protein tyrosine phosphatase receptor type F
15	GOLM1	43,01	7,44E-03	golgi membrane protein 1
16	CLDN7	42,83	1,96E-05	claudin 7
17	CKAP4	39,39	3,51E-03	cytoskeleton associated protein 4
18	DLC1	38,97	2,57E-02	DLC1 Rho GTPase activating protein
19	CNKSR3	35,99	1,55E-03	CNKSR family member 3
20	EIF5AP2	34,78	9,65E-03	eukaryotic translation initiation factor 5Apseudogene2
Downregulated	**Gene name**	**Linear Fold Change**	**pvalue**	**Gene description**
1	AC092287.1	-25,05	7,08E-04	novel transcript, antisense to SMG1
2	CD209	-20,14	2,13E-03	CD209 molecule
3	LINC02029	-19,39	2,98E-05	long intergenic non-protein coding RNA 2029
4	LETM2	-16,35	5,53E-03	leucine zipper and EF-hand containing transmembrane protein 2
5	AL390957.1	-14,29	6,97E-06	novel transcript
6	APBA1	-13,25	1,74E-02	amyloid beta precursor protein binding family A me1
7	AC024145.1	-13,02	3,42E-03	novel transcript to ITPR2
8	PLB1	-12,62	2,18E-03	phospholipase B1
9	KLF3P1	-12,60	2,14E-02	Kruppel like factor 3 pseudogene 1
10	ELAVL4	-12,22	1,57E-04	ELAV like RNA binding protein 4
11	AC243960.3	-11,98	5,18E-04	novel transcript
12	PRAM1	-11,78	6,85E-04	PML-RARA regulated adaptor molecule 1
13	FCER1A	-11,19	2,17E-06	Fc fragment of IgE receptor Ia
14	TM7SF2	-9,68	2,68E-02	transmembrane 7 superfamily member 2
15	IGF1	-9,33	2,62E-03	insulin like growth factor 1
16	CXCL10	-9,15	2,55E-02	C-X-C motif chemokine ligand 10
17	AC129492.7	-8,98	2,35E-02	novel transcript, TEC
18	AF213884.3	-8,92	6,51E-03	novel transcript, antisense NFKB1
19	GUCY1B1	-8,73	7,55E-03	guanylate cyclase 1 soluble subunit beta 1
20	TRIT1	-8,48	3,00E-02	tRNA isopentenyltransferase 1

Table AX9: Top 20 upregulated and top 20 downregulated genes from iUC mDCs vs NC mDCs (basis)

Upregulated	Gene name	Linear Fold Change	pvalue	Gene description
1	FPR1	4,74	1,39E-03	formyl peptide receptor 1
2	FSCN1	4,52	5,30E-04	fascin actin-bundling protein 1
3	CTSZ	4,33	2,10E-02	cathepsin Z
4	TBC1D4	3,99	5,81E-03	TBC1 domain family member 4
5	S100B	3,85	5,82E-03	S100 calcium binding protein B
6	AC025048.4	3,56	7,44E-03	novel transcript
7	WFDC21P	3,50	1,73E-02	WAP four-disulfide core domain 21, pseudogene
8	MIDN	3,38	6,90E-05	midnolin
9	CYP1B1	3,37	3,24E-03	cytochrome P450 family 1 subfamily B member 1
10	NCOA7	3,35	9,02E-03	nuclear receptor coactivator 7
11	TCF4	3,13	1,52E-03	transcription factor 4
12	CALCRL	3,07	3,01E-03	calcitonin receptor like receptor
13	IDO1	2,73	1,43E-02	indoleamine 2,3-dioxygenase 1
14	IFITM3	2,59	4,31E-03	interferon induced transmembrane protein 3
15	MTHFR	2,58	4,46E-04	methylenetetrahydrofolate reductase
16	MAP3K14	2,56	2,30E-02	mitogen-activated protein kinase kinase kinase 14
17	MT2A	2,54	8,08E-03	metallothionein 2A
18	VHL	2,41	1,02E-02	von Hippel-Lindau tumor suppressor
19	REST	2,35	4,11E-03	RE1 silencing transcription factor
20	HNRNPA0	2,32	4,45E-02	heterogeneous nuclear ribonucleoprotein A0
Downregulated	**Gene name**	**Linear Fold Change**	**pvalue**	**Gene description**
1	TPSD1	-48,66	3,46E-02	tryptase delta 1
2	FCER1A	-11,72	1,39E-06	Fc fragment of IgE receptor Ia
3	ALOX5AP	-8,54	6,23E-06	arachidonate 5-lipoxygenase activating protein
4	CD82	-6,50	5,52E-03	CD82 molecule
5	NSMCE1	-6,33	1,28E-04	NSE1 homolog, SMC5-SMC6 complex component
6	CD207	-5,68	1,59E-03	CD207 molecule
7	DNASE1L3	-4,87	1,24E-04	deoxyribonuclease 1 like 3
8	DDIT3	-4,49	5,13E-05	DNA damage inducible transcript 3
9	ANXA1	-4,28	7,09E-09	annexin A1
10	AXL	-4,01	4,36E-06	AXL receptor tyrosine kinase
11	CD9	-3,94	3,69E-02	CD9 molecule
12	GALNT6	-3,90	3,36E-03	polypeptide N-acetylgalactosaminyltransferase 6
13	ACSL4	-3,89	4,71E-04	acyl-CoA synthetase long chain family member 4
14	MMP12	-3,84	3,66E-02	matrix metallopeptidase 12
15	C1QC	-3,83	1,41E-02	complement C1q C chain
16	SDS	-3,82	2,51E-03	serine dehydratase
17	CD1E	-3,75	1,11E-03	CD1e molecule
18	RGS2	-3,72	9,17E-06	regulator of G protein signaling 2
19	MS4A6A	-3,60	2,14E-03	membrane spanning 4-domains A6A
20	SLC43A3	-3,47	4,74E-04	solute carrier family 43 member 3

Table AX10: Top 20 upregulated and top 20 downregulated genes from iUC mDCs vs niUC mDCs (basis)

Upregulated	Gene name	Linear Fold Change	pvalue	Gene description
1	IFI27	995,27	3,98E-04	interferon alpha inducible protein 27
2	DHRS9	161,64	1,21E-03	dehydrogenase/reductase 9
3	GPRC5A	106,74	1,28E-04	G protein-coupled receptor class C group 5 member A
4	RAB27B	92,32	1,46E-02	RAB27B, member RAS oncogene family
5	GATA2	82,29	4,98E-02	GATA binding protein 2
6	FERMT2	56,53	3,76E-02	fermitin family member 2
7	PVT1	50,89	1,19E-03	Pvt1 oncogene
8	RRAGB	50,46	4,55E-03	Ras related GTP binding B
9	NRP1	48,49	3,96E-04	neuropilin 1
10	PINK1	46,17	4,72E-05	PTEN induced kinase 1
11	IGHA1	46,13	6,38E-03	immunoglobulin heavy constant alpha 1
12	FAM174A	44,97	1,37E-04	family with sequence similarity 174 member A
13	ACOX3	44,58	1,67E-03	acyl-CoA oxidase 3, pristanoyl
14	SH2D2A	43,60	3,02E-04	SH2 domain containing 2A
15	HPGDS	39,27	1,95E-02	hematopoietic prostaglandin D synthase
16	AC092164.1	39,19	1,82E-02	novel transcript
17	HDC	37,69	1,76E-02	histidine decarboxylase
18	YOD1	32,75	2,80E-03	YOD1 deubiquitinase
19	AC109925.2	31,07	9,09E-03	novel transcript, antisense to HPGDS
20	AC009630.4	30,52	3,90E-02	novel transcript
Downregulated	**Gene name**	**Linear Fold Change**	**pvalue**	**Gene description**
1	CTSK	-88,42	2,41E-02	cathepsin K
2	HIST1H2BG	-46,96	1,10E-04	histone cluster 1 H2B family member g
3	NKX3-1	-42,95	2,14E-03	NK3 homeobox 1
4	SEZ6L	-39,71	1,30E-02	seizure related 6 homolog like
5	MELK	-28,77	3,72E-03	maternal embryonic leucine zipper kinase
6	LCLAT1	-24,63	1,01E-03	lysocardiolipin acyltransferase 1
7	SFTPD	-22,94	1,67E-02	surfactant protein D
8	TLR6	-19,37	3,58E-02	toll like receptor 6
9	ZNF420	-19,02	4,30E-02	zinc finger protein 420
10	BPGM	-18,50	4,63E-03	bisphosphoglycerate mutase
11	AC234781.2	-16,15	2,47E-02	Twinfilin-1, pseudogene
12	WNT5B	-14,42	4,02E-02	Wnt family member 5B
13	TDRKH	-14,21	3,72E-02	tudor and KH domain containing
14	CABLES2	-13,22	3,24E-02	Cdk5 and Abl enzyme substrate 2
15	RPS26P15	-12,47	1,31E-02	ribosomal protein S26 pseudogene 15
16	FABP4	-12,19	4,48E-02	fatty acid binding protein 4
17	FAM200A	-10,52	1,93E-02	family with sequence similarity 200 member A
18	GINS2	-9,18	4,85E-02	GINS complex subunit 2
19	LHFPL6	-8,73	4,25E-02	LHFPL tetraspan subfamily member 6
20	DNASE2	-8,71	8,49E-03	deoxyribonuclease 2, lysosomal

Table AX11: Top 20 upregulated and top 20 downregulated genes from niUC mDCs vs niCD mDCs (basis)

Upregulated	Gene name	Linear Fold Change	pvalue	Gene description
1	IFI27	185,79	3,31E-02	interferon alpha inducible protein 27
2	CLDN7	74,13	1,45E-03	claudin 7
3	GPRC5A	66,66	7,86E-03	G protein-coupled receptor class C group 5 member A
4	IGFBP4	64,94	1,87E-03	insulin like growth factor binding protein 4
5	AL512646.1	52,35	1,81E-02	WDR45-like (WDR45L) pseudogene
6	HSPG2	45,40	1,94E-02	heparan sulfate proteoglycan 2
7	IGHA1	39,21	4,39E-02	immunoglobulin heavy constant alpha 1
8	PLPBP	33,83	1,05E-07	pyridoxal phosphate binding protein
9	INTS6L	33,66	2,31E-05	integrator complex subunit 6 like
10	HEATR5B	29,76	5,81E-06	HEAT repeat containing 5B
11	HEXD	24,71	4,33E-05	hexosaminidase D
12	RAB4A	22,83	1,10E-04	RAB4A, member RAS oncogene family
13	SUN1	22,74	1,96E-03	Sad1 and UNC84 domain containing 1
14	GALE	22,73	4,71E-04	UDP-galactose-4-epimerase
15	ZCCHC17	21,65	3,09E-06	zinc finger CCHC-type containing 17
16	TUBB2A	21,19	2,51E-03	tubulin beta 2A class Iia
17	GAS2L3	20,05	1,51E-05	growth arrest specific 2 like 3
18	CD1E	19,79	1,13E-05	CD1e molecule
19	AC007384.1	19,63	5,37E-04	novel transcript
20	RPRD1B	19,47	1,82E-03	regulation of nuclear pre-mRNA domain containing 1B
Downregulated	**Gene name**	**Linear Fold Change**	**pvalue**	**Gene description**
1	HPGDS	-66,27	3,86E-02	hematopoietic prostaglandin D synthase
2	UMPS	-12,95	3,37E-02	uridine monophosphate synthetase
3	TM6SF1	-11,24	2,64E-03	transmembrane 6 superfamily member 1
4	CCDC92	-10,85	3,19E-02	coiled-coil domain containing 92
5	MCM3	-10,63	1,13E-02	minichromosome maintenance complex component 3
6	SLC29A1	-10,50	3,83E-02	solute carrier family 29 member 1
7	APOOL	-10,03	1,64E-02	apolipoprotein O like
8	MUL1	-8,88	2,96E-02	mitochondrial E3 ubiquitin protein ligase 1
9	TTBK2	-8,31	3,85E-02	tau tubulin kinase 2
10	NAT9	-7,88	1,58E-02	N-acetyltransferase 9 (putative)
11	MTRR	-7,84	6,89E-03	5-methyltetrahydrofolate-homocysteine methyltransferase reductase
12	RNF213-AS1	-7,75	4,97E-02	RNF213 antisense RNA 1
13	LEO1	-7,07	1,94E-02	Paf1/RNA polymerase II complex component
14	RNF14	-6,97	5,21E-03	ring finger protein 14
15	TIAM2	-6,75	3,54E-02	T cell lymphoma invasion and metastasis 2
16	PARP11	-6,62	3,51E-02	poly(ADP-ribose) polymerase family member 11
17	COPS7B	-6,34	2,68E-02	COP9 signalosome subunit 7B
18	MAK16	-6,18	3,95E-02	MAK16 homolog
19	RGS18	-6,17	3,70E-02	regulator of G protein signaling 18
20	ERG28	-6,16	4,40E-02	ergosterol biosynthesis 28 homolog

Table AX12: Top 20 upregulated and top 20 downregulated genes from iUC mDCs vs iCD mDCs (basis)

5.5 Shared differentially expressed genes between UC, CD and NC under non-inflammatory and inflammatory conditions

Overlapping SDE genes in non-inflamed IBD	
Gene name	**Description**
MYADM	myeloid associated differentiation marker
CDT1	chromatin licensing and DNA replication factor 1

Table AX13: List of the two shared statistical significant differentially expressed genes between all comparisons from figure R56. SDE, statistical significant differentially expressed.

Overlapping SDE genes in inflamed IBD			
Gene name	**Description**	**Gene name**	**Description**
ACP5	acid phosphatase 5, tartrate resistant	**GSTM4**	glutathione S-transferase mu 4
AP003392.3	novel transcript, antisense to HYOU1	**HMGCS1**	3-hydroxy-3-methylglutaryl-CoA synthase 1
ARL4A	ADP ribosylation factor like GTPase 4A	**HSPB1**	heat shock protein family B (small) member 1
BIRC3	baculoviral IAP repeat containing 3	**IDH3A**	isocitrate dehydrogenase (NAD(+)) 3 alpha
CCL3	C-C motif chemokine ligand 3	**KBTBD8**	kelch repeat and BTB domain containing 8
CCNG2	cyclin G2	**METTL26**	methyltransferase like 26
CD1E	CD1e molecule	**NAA25**	N(alpha)-acetyltransferase 25, NatB auxiliary subunit
CD302	CD302 molecule	**NDUFS8**	NADH:ubiquinone oxidoreductase core subunit S8
CDYL	chromodomain Y like	**NKIRAS1**	NFKB inhibitor interacting Ras like 1
CSF1R	colony stimulating factor 1 receptor	**NUB1**	negative regulator of ubiquitin like proteins 1
DNAJB5	DnaJ heat shock protein family	**PAPSS2**	3'-phosphoadenosine 5'-phosphosulfate synthase 2
DNASE1L3	deoxyribonuclease 1 like 3	**PPIF**	peptidylprolyl isomerase F
ERP29	endoplasmic reticulum protein 29	**PSAP**	prosaposin
FCGRT	Fc fragment of IgG receptor and transporter	**RGCC**	regulator of cell cycle
GALE	UDP-galactose-4-epimerase	**SREBF2**	sterol regulatory element binding transcription factor 2
GAS2L3	growth arrest specific 2 like	**ST3GAL2**	ST3 beta-galactoside alpha-2,3-sialyltransferase 2
GAS7	growth arrest specific 7	**TXN**	thioredoxin
GIGYF1	GRB10 interacting GYF protein 1	**ZFP36**	ZFP36 ring finger protein
GLO1	glyoxalase I		

Table AX14: List of the 37 shared statistical significant differentially expressed genes between all comparisons from figure R58. SDE, statistical significant differentially expressed.

5.6 Conventional DC subset categorization of mLPDCs

The gene expression profile of mDCs was used to identify the cDC subtype of sorted mLPDCs. Since the markers CD141 and CD1c are used to distinguisch cDC1 and cDC2 DCs respectively, surface expression in 3.11.2 already established, that mLPDCs are a mixture of cDC1 and cDC2 cells. However, some critical genes used for cDC1 identification like XCR1 are not present, and BATF3 was only measured in mininmal amounts.

Publication 1						
Identifier	**DCsubytpe**					
	pDC	**cDC1**	**cDC2**	**DN DC**		**mLPDCs**
CD11c	-	+	+	+		+++
CD1c		-	+	-		+++
XCR1		+	-	-		-
CD123	+	-	-	-		-
BATF3		+	-			-/+
ID2		+	-			+++
NOTCH-L		+	-			-
CLEC9A		+	-			-
CADM1		+	-			+
NOTCH2		-	+			++
ZEB2		-	+			+++
CLEC10A		-	+			-
CD101		-	+			-
Publication 2						
Identifier	**DC subtype**					
		cDC1	**cDC2**			**mLPDCs**
CD103		+	+			++
SIRPα		-	+			++
CD1c		-	+			+++
CD141		+	-			++
CD209		-	+			+
IRF4		-	+			+++
IRF8		+	-			+++
BCL6		+	-			++
BLIMP1		-	+			+++
CD26		+	-			-/+
CD101		-	+			+

Table AX15: cDC classification of mDCs. Identification of cDC subgroups is based on human intestinal dendritic cells. A prerequisite for all cells is that they are CD45+ and negative for CD3-, CD14-, CD16-, CD19-, CD56- and CD64-. Green tiles show according mLPDC gene expression. cDC1/2, conventional dendritic cell 1/2; pDC, plasmacytoid dendritic cell; mLPDCs, myeloid lamina propria DCs; DN, double negative DCs (CD1c-/XCR1-)

Publication 1: (Caër and Wick 2020)

Publication 2: (Sun, Nguyen, and Gommerman 2020)

6.0 Citations

Aden, K., A. Breuer, A. Rehman, H. Geese, F. Tran, J. Sommer, G. H. Waetzig, et al. 2016. 'Classic IL-6R Signalling Is Dispensable for Intestinal Epithelial Proliferation and Repair'. *Oncogenesis* 5 (11): e270. https://doi.org/10.1038/oncsis.2016.71.

Aden, Konrad, Ateequr Rehman, Maren Falk-Paulsen, Thomas Secher, Jan Kuiper, Florian Tran, Steffen Pfeuffer, et al. 2016. 'Epithelial IL-23R Signaling Licenses Protective IL-22 Responses in Intestinal Inflammation'. *Cell Reports* 16 (8): 2208–18. https://doi.org/10.1016/j.celrep.2016.07.054.

Aguilera, Mònica, Trevor Darby, and Silvia Melgar. 2014. 'The Complex Role of Inflammasomes in the Pathogenesis of Inflammatory Bowel Diseases – Lessons Learned from Experimental Models'. *Cytokine & Growth Factor Reviews*, Special issue: Innate Sensing and Response to Pathogens, 25 (6): 715–30. https://doi.org/10.1016/j.cytogfr.2014.04.003.

Alam, Muhammad S. 2018. 'Proximity Ligation Assay (PLA)'. *Current Protocols in Immunology* 123 (1): e58. https://doi.org/10.1002/cpim.58.

Allison, J P, and L L Lanier. 1987. 'Structure, Function, and Serology of the T-Cell Antigen Receptor Complex'. *Annual Review of Immunology* 5 (1): 503–40. https://doi.org/10.1146/annurev.iy.05.040187.002443.

Arampatzidou, Maria, André Schütte, Gunnar C. Hansson, Paul Saftig, and Klaudia Brix. 2012. 'Effects of Cathepsin K Deficiency on Intercellular Junction Proteins, Luminal Mucus Layers, and Extracellular Matrix Constituents in the Mouse Colon'. *Biological Chemistry* 393 (12): 1391–1403. https://doi.org/10.1515/hsz-2012-0204.

Auray, Gaël, Stephanie C. Talker, Irene Keller, Sylvie Python, Markus Gerber, Matthias Liniger, Llilianne Ganges, Rémy Bruggmann, Nicolas Ruggli, and Artur Summerfield. 2020. 'High-Resolution Profiling of Innate Immune Responses by Porcine Dendritic Cell Subsets in Vitro and in Vivo'. *Frontiers in Immunology* 11 (July). https://doi.org/10.3389/fimmu.2020.01429.

Ayala-Fontánez, Nilmarie, David C Soler, and Thomas S McCormick. 2016. 'Current Knowledge on Psoriasis and Autoimmune Diseases'. *Psoriasis (Auckland, N.Z.)* 6 (February): 7–32. https://doi.org/10.2147/PTT.S64950.

Bain, Calum C., and Allan McI Mowat. 2012. 'CD200 Receptor and Macrophage Function in the Intestine'. *Immunobiology* 217 (6): 643–51. https://doi.org/10.1016/j.imbio.2011.11.004.

Baizabal-Carvallo, José Fidel, and Marlene Alonso-Juarez. 2020. 'The Link between Gut Dysbiosis and Neuroinflammation in Parkinson's Disease'. *Neuroscience* 432 (April): 160–73. https://doi.org/10.1016/j.neuroscience.2020.02.030.

Bala, Pramod Akula, James Foster, Lucia Carvelli, and L. Keith Henry. 2013. 'SLC6 Transporters: Structure, Function, Regulation, Disease Association and Therapeutics'. *Molecular Aspects of Medicine* 34 (2–3): 197–219. https://doi.org/10.1016/j.mam.2012.07.002.

Barceló-Batllori, Sílvia, Muriel André, Catherine Servis, Nicole Lévy, Osamu Takikawa, Pierre Michetti, Marc Reymond, and Emanuela Felley-Bosco. 2002. 'Proteomic Analysis of Cytokine Induced Proteins in Human Intestinal Epithelial Cells: Implications for Inflammatory Bowel Diseases'. *Proteomics* 2 (5): 551–60. https://doi.org/10.1002/1615-9861(200205)2:5<551::AID-PROT551>3.0.CO;2-O.

Barnes, Michael J., and Fiona Powrie. 2009. 'Regulatory T Cells Reinforce Intestinal Homeostasis'. *Immunity* 31 (3): 401–11. https://doi.org/10.1016/j.immuni.2009.08.011.

Baumgart, D. C., S. Thomas, I. Przesdzing, D. Metzke, C. Bielecki, S. M. Lehmann, S. Lehnardt, et al. 2009. 'Exaggerated Inflammatory Response of Primary Human Myeloid Dendritic Cells to Lipopolysaccharide in Patients with Inflammatory Bowel Disease'. *Clinical & Experimental Immunology* 157 (3): 423–36. https://doi.org/10.1111/j.1365-2249.2009.03981.x.

Beaulieu, Sylvie, Davide F. Robbiani, Xixuan Du, Elaine Rodrigues, Ralf Ignatius, Yang Wei, Paul Ponath, et al. 2002. 'Expression of a Functional Eotaxin (CC Chemokine Ligand 11) Receptor

CCR3 by Human Dendritic Cells'. *Journal of Immunology (Baltimore, Md.: 1950)* 169 (6): 2925–36. https://doi.org/10.4049/jimmunol.169.6.2925.

Becker, Christoph, Heike Dornhoff, Clemens Neufert, Massimo C. Fantini, Stefan Wirtz, Sabine Huebner, Alexei Nikolaev, et al. 2006. 'Cutting Edge: IL-23 Cross-Regulates IL-12 Production in T Cell-Dependent Experimental Colitis'. *Journal of Immunology (Baltimore, Md.: 1950)* 177 (5): 2760–64. https://doi.org/10.4049/jimmunol.177.5.2760.

Bekiaris, Vasileios, Emma K. Persson, and William W. Agace. 2014. 'Intestinal Dendritic Cells in the Regulation of Mucosal Immunity'. *Immunological Reviews* 260 (1): 86–101. https://doi.org/10.1111/imr.12194.

Benchimol, Eric I., Gilaad G. Kaplan, Anthony R. Otley, Geoffrey C. Nguyen, Fox E. Underwood, Astrid Guttmann, Jennifer L. Jones, et al. 2017. 'Rural and Urban Residence During Early Life Is Associated with Risk of Inflammatory Bowel Disease: A Population-Based Inception and Birth Cohort Study'. *The American Journal of Gastroenterology* 112 (9): 1412–22. https://doi.org/10.1038/ajg.2017.208.

Bernardo, David, María Chaparro, and Javier P. Gisbert. 2018. 'Human Intestinal Dendritic Cells in Inflammatory Bowel Diseases'. *Molecular Nutrition & Food Research* 62 (7): e1700931. https://doi.org/10.1002/mnfr.201700931.

Bernstein, Charles N., Abraham Eliakim, Suliman Fedail, Michael Fried, Richard Gearry, Khean-Lee Goh, Saeed Hamid, et al. 2016. 'World Gastroenterology Organisation Global Guidelines Inflammatory Bowel Disease: Update August 2015'. *Journal of Clinical Gastroenterology* 50 (10): 803–18. https://doi.org/10.1097/MCG.0000000000000660.

Bhandage, Amol K., Zhe Jin, Sergiy V. Korol, Qiujin Shen, Yu Pei, Qiaolin Deng, Daniel Espes, Per-Ola Carlsson, Masood Kamali-Moghaddam, and Bryndis Birnir. 2018. 'GABA Regulates Release of Inflammatory Cytokines From Peripheral Blood Mononuclear Cells and CD4+ T Cells and Is Immunosuppressive in Type 1 Diabetes'. *EBioMedicine* 30 (April): 283–94. https://doi.org/10.1016/j.ebiom.2018.03.019.

Bhatia, M., C. Landolfi, F. Basta, G. Bovi, R. Devi Ramnath, A. Capezzone de Joannon, and A. Guglielmotti. 2008. 'Treatment with Bindarit, an Inhibitor of MCP-1 Synthesis, Protects Mice against Trinitrobenzene Sulfonic Acid-Induced Colitis'. *Inflammation Research: Official Journal of the European Histamine Research Society ... [et Al.]* 57 (10): 464–71. https://doi.org/10.1007/s00011-008-7210-y.

Bosteels, Cedric, Katrijn Neyt, Manon Vanheerswynghels, Mary J. van Helden, Dorine Sichien, Nincy Debeuf, Sofie De Prijck, et al. 2020. 'Inflammatory Type 2 CDCs Acquire Features of CDC1s and Macrophages to Orchestrate Immunity to Respiratory Virus Infection'. *Immunity* 52 (6): 1039-1056.e9. https://doi.org/10.1016/j.immuni.2020.04.005.

Brandtzaeg, P., H. Kiyono, R. Pabst, and M. W. Russell. 2008. 'Terminology: Nomenclature of Mucosa-Associated Lymphoid Tissue'. *Mucosal Immunology* 1 (1): 31–37. https://doi.org/10.1038/mi.2007.9.

Brazil, Jennifer C., Miguel Quiros, Asma Nusrat, and Charles A. Parkos. 2019. 'Innate Immune Cell-Epithelial Crosstalk during Wound Repair'. *The Journal of Clinical Investigation* 129 (8): 2983–93. https://doi.org/10.1172/JCI124618.

Bridgewood, Charlie, Adewonuola Alase, Abdulla Watad, Miriam Wittmann, Richard Cuthbert, and Dennis McGonagle. 2019. 'The IL-23p19/EBI3 Heterodimeric Cytokine Termed IL-39 Remains a Theoretical Cytokine in Man'. *Inflammation Research: Official Journal of the European Histamine Research Society ... [et Al.]* 68 (6): 423–26. https://doi.org/10.1007/s00011-019-01235-x.

Brooks, C F, and M Moore. 1988. 'Differential MHC Class II Expression on Human Peripheral Blood Monocytes and Dendritic Cells.' *Immunology* 63 (2): 303–11.

Brown, Chrysothemis C., Herman Gudjonson, Yuri Pritykin, Deeksha Deep, Vincent-Philippe Lavallée, Alejandra Mendoza, Rachel Fromme, et al. 2019. 'Transcriptional Basis of Mouse and Human Dendritic Cell Heterogeneity'. *Cell* 179 (4): 846-863.e24. https://doi.org/10.1016/j.cell.2019.09.035.

Buechler, C., M. Ritter, E. Orsó, T. Langmann, J. Klucken, and G. Schmitz. 2000. 'Regulation of Scavenger Receptor CD163 Expression in Human Monocytes and Macrophages by Pro- and Antiinflammatory Stimuli'. *Journal of Leukocyte Biology* 67 (1): 97–103.

Buhner, Sabine, and Michael Schemann. 2012. 'Mast Cell-Nerve Axis with a Focus on the Human Gut'. *Biochimica Et Biophysica Acta* 1822 (1): 85–92. https://doi.org/10.1016/j.bbadis.2011.06.004.

Bull, D M, and M A Bookman. 1977. 'Isolation and Functional Characterization of Human Intestinal Mucosal Lymphoid Cells.' *Journal of Clinical Investigation* 59 (5): 966–74.

Busch, Svenja, Marina Talamini, Steffen Brenner, Amr Abdulazim, Daniel Hänggi, Michael Neumaier, Marcel Seiz-Rosenhagen, and Tina Fuchs. 2019. 'Circulating Monocytes and Tumor-Associated Macrophages Express Recombined Immunoglobulins in Glioblastoma Patients'. *Clinical and Translational Medicine* 8 (June). https://doi.org/10.1186/s40169-019-0235-8.

Caër, Charles, and Mary Jo Wick. 2020. 'Human Intestinal Mononuclear Phagocytes in Health and Inflammatory Bowel Disease'. *Frontiers in Immunology* 11: 410. https://doi.org/10.3389/fimmu.2020.00410.

Carbone, Federico, Giorgia Bodini, Matteo Brunacci, Aldo Bonaventura, Alessandra Vecchiè, Luca Liberale, Mattia Crespi, et al. 2018. 'Reduction in TIMP-2 Serum Levels Predicts Remission of Inflammatory Bowel Diseases'. *European Journal of Clinical Investigation* 48 (10): e13002. https://doi.org/10.1111/eci.13002.

Carter, LauraL, Lynette A. Fouser, Jason Jussif, Lori Fitz, Bija Deng, Clive R. Wood, Mary Collins, Tasuku Honjo, Gordon J. Freeman, and Beatriz M. Carreno. 2002. 'PD-1:PD-L Inhibitory Pathway Affects Both CD4(+) and CD8(+) T Cells and Is Overcome by IL-2'. *European Journal of Immunology* 32 (3): 634–43. https://doi.org/10.1002/1521-4141(200203)32:3<634::AID-IMMU634>3.0.CO;2-9.

Caux, C., C. Massacrier, B. Vanbervliet, B. Dubois, C. Van Kooten, I. Durand, and J. Banchereau. 1994. 'Activation of Human Dendritic Cells through CD40 Cross-Linking'. *The Journal of Experimental Medicine* 180 (4): 1263–72. https://doi.org/10.1084/jem.180.4.1263.

Cella, M., A. Engering, V. Pinet, J. Pieters, and A. Lanzavecchia. 1997. 'Inflammatory Stimuli Induce Accumulation of MHC Class II Complexes on Dendritic Cells'. *Nature* 388 (6644): 782–87. https://doi.org/10.1038/42030.

Cerovic, Milica, Gianluigi Forloni, and Claudia Balducci. 2019. 'Neuroinflammation and the Gut Microbiota: Possible Alternative Therapeutic Targets to Counteract Alzheimer's Disease?' *Frontiers in Aging Neuroscience* 11 (October). https://doi.org/10.3389/fnagi.2019.00284.

Chapuy, Laurence, Marwa Bsat, Heena Mehta, Manuel Rubio, Keiko Wakahara, Vu Quang Van, Nobuyasu Baba, et al. 2014. 'Basophils Increase in Crohn Disease and Ulcerative Colitis and Favor Mesenteric Lymph Node Memory TH17/TH1 Response'. *The Journal of Allergy and Clinical Immunology* 134 (4): 978-981.e1. https://doi.org/10.1016/j.jaci.2014.05.025.

Chehboun, Salma, Jérémie Labrecque-Carbonneau, Sarah Pasquin, Yasmine Meliani, Bouchra Meddah, Walter Ferlin, Mukut Sharma, Aurélie Tormo, Jean-François Masson, and Jean-François Gauchat. 2017. 'Epstein-Barr Virus-Induced Gene 3 (EBI3) Can Mediate IL-6 Trans-Signaling'. *The Journal of Biological Chemistry* 292 (16): 6644–56. https://doi.org/10.1074/jbc.M116.762021.

Chen, Xu'e, Zhijian Tan, Qing Yue, Houjun Liu, Zhixiang Liu, and Jiawen Li. 2006. 'The Expression of Interleukin-23 (P19/P40) and Interleukin-12 (P35/P40) in Psoriasis Skin'. *Journal of Huazhong University of Science and Technology. Medical Sciences = Hua Zhong Ke Ji Da Xue Xue Bao. Yi Xue Ying De Wen Ban = Huazhong Keji Daxue Xuebao. Yixue Yingdewen Ban* 26 (6): 750–52. https://doi.org/10.1007/s11596-006-0635-z.

Chen, Zhiqi, Kai Yu, Fang Zhu, and Reginald Gorczynski. 2016. 'Over-Expression of CD200 Protects Mice from Dextran Sodium Sulfate Induced Colitis'. *PLOS ONE* 11 (2): e0146681. https://doi.org/10.1371/journal.pone.0146681.

Chu, Chung-Ching, Niwa Ali, Panagiotis Karagiannis, Paola Di Meglio, Ania Skowera, Luca Napolitano, Guillermo Barinaga, et al. 2012. 'Resident CD141 (BDCA3)+ Dendritic Cells in Human Skin

Produce IL-10 and Induce Regulatory T Cells That Suppress Skin Inflammation'. *The Journal of Experimental Medicine* 209 (5): 935–45. https://doi.org/10.1084/jem.20112583.

Ciorba, Matthew A., Ellen E. Bettonville, Keely G. McDonald, Richard Metz, George C. Prendergast, Rodney D. Newberry, and William F. Stenson. 2010. 'Induction of IDO-1 by Immunostimulatory DNA Limits Severity of Experimental Colitis'. *Journal of Immunology (Baltimore, Md.: 1950)* 184 (7): 3907–16. https://doi.org/10.4049/jimmunol.0900291.

Clevers, Hans. 2013. 'The Intestinal Crypt, a Prototype Stem Cell Compartment'. *Cell* 154 (2): 274–84. https://doi.org/10.1016/j.cell.2013.07.004.

Collin, Matthew, Naomi McGovern, and Muzlifah Haniffa. 2013. 'Human Dendritic Cell Subsets'. *Immunology* 140 (1): 22–30. https://doi.org/10.1111/imm.12117.

Collison, Lauren W., Creg J. Workman, Timothy T. Kuo, Kelli Boyd, Yao Wang, Kate M. Vignali, Richard Cross, David Sehy, Richard S. Blumberg, and Dario A. A. Vignali. 2007. 'The Inhibitory Cytokine IL-35 Contributes to Regulatory T-Cell Function'. *Nature* 450 (7169): 566–69. https://doi.org/10.1038/nature06306.

Corthësy, Blaise. 2009. 'Secretory Immunoglobulin A: Well beyond Immune Exclusion at Mucosal Surfaces'. *Immunopharmacology and Immunotoxicology* 31 (2): 174–79. https://doi.org/10.1080/08923970802438441.

Cossarizza, Andrea, Hyun-Dong Chang, Andreas Radbruch, Andreas Acs, Dieter Adam, Sabine Adam-Klages, William W. Agace, et al. 2019. 'Guidelines for the Use of Flow Cytometry and Cell Sorting in Immunological Studies (Second Edition)'. *European Journal of Immunology* 49 (10): 1457–1973. https://doi.org/10.1002/eji.201970107.

Cryan, John F., Kenneth J. O'Riordan, Caitlin S. M. Cowan, Kiran V. Sandhu, Thomaz F. S. Bastiaanssen, Marcus Boehme, Martin G. Codagnone, et al. 2019. 'The Microbiota-Gut-Brain Axis'. *Physiological Reviews* 99 (4): 1877–2013. https://doi.org/10.1152/physrev.00018.2018.

Cuvelier, A., J. Bourguignon, J. F. Muir, J. P. Martin, and R. Sesboüé. 1996. 'Substitution of Carbonate by Acetate Buffer for IgG Coating in Sandwich ELISA'. *Journal of Immunoassay* 17 (4): 371–82. https://doi.org/10.1080/01971529608005799.

Dalton, Jane E., Sheena M. Cruickshank, Charlotte E. Egan, Rainy Mears, Darren J. Newton, Elizabeth M. Andrew, Beth Lawrence, et al. 2006. 'Intraepithelial Gammadelta+ Lymphocytes Maintain the Integrity of Intestinal Epithelial Tight Junctions in Response to Infection'. *Gastroenterology* 131 (3): 818–29. https://doi.org/10.1053/j.gastro.2006.06.003.

David, Lawrence A., Corinne F. Maurice, Rachel N. Carmody, David B. Gootenberg, Julie E. Button, Benjamin E. Wolfe, Alisha V. Ling, et al. 2014. 'Diet Rapidly and Reproducibly Alters the Human Gut Microbiome'. *Nature* 505 (7484): 559–63. https://doi.org/10.1038/nature12820.

De Vadder, Filipe, Petia Kovatcheva-Datchary, Daisy Goncalves, Jennifer Vinera, Carine Zitoun, Adeline Duchampt, Fredrik Bäckhed, and Gilles Mithieux. 2014. 'Microbiota-Generated Metabolites Promote Metabolic Benefits via Gut-Brain Neural Circuits'. *Cell* 156 (1–2): 84–96. https://doi.org/10.1016/j.cell.2013.12.016.

Debeljak, Nataša, Laurie Feldman, Kerry L. Davis, Radovan Komel, and Arthur J. Sytkowski. 2006. 'Variability in the Immunodetection of His-Tagged Recombinant Proteins'. *Analytical Biochemistry* 359 (2): 216–23. https://doi.org/10.1016/j.ab.2006.09.017.

Deepak, Parakkal, and Edward V Loftus. 2016. 'Ustekinumab in Treatment of Crohn's Disease: Design, Development, and Potential Place in Therapy'. *Drug Design, Development and Therapy* 10 (November): 3685–98. https://doi.org/10.2147/DDDT.S102141.

Deng, Zhenling, Ziyang Jing, Yanhong Guo, Junfan Ma, Huige Yan, Zhan Shi, Hui Deng, et al. 2021. 'Expression of Immunoglobulin G in Human Proximal Tubular Epithelial Cells'. *Molecular Medicine Reports* 23 (5). https://doi.org/10.3892/mmr.2021.11966.

Deng, Zhenling, Xinyao Wang, Yue Liu, Xinyu Tian, Shaohui Deng, Yingchun Sun, Song Wang, et al. 2020. 'Single-Cell RNA Sequencing Confirms IgG Transcription and Limited Diversity of VHDJH Rearrangements in Proximal Tubular Epithelial Cells'. *Scientific Reports* 10 (1): 19657. https://doi.org/10.1038/s41598-020-75013-9.

Detry, Sammy, Katarzyna Składanowska, Marnik Vuylsteke, Savvas N. Savvides, and Yehudi Bloch. 2019. 'Revisiting the Combinatorial Potential of Cytokine Subunits in the IL-12 Family'. *Biochemical Pharmacology* 165 (July): 240–48. https://doi.org/10.1016/j.bcp.2019.03.026.

Di Meglio, Paola, Federica Villanova, and Frank O. Nestle. 2014. 'Psoriasis'. *Cold Spring Harbor Perspectives in Medicine* 4 (8). https://doi.org/10.1101/cshperspect.a015354.

Di Virgilio, Francesco. 2005. 'Purinergic Mechanism in the Immune System: A Signal of Danger for Dendritic Cells'. *Purinergic Signalling* 1 (3): 205–9. https://doi.org/10.1007/s11302-005-6312-z.

Doyle, Chloe, Kirstie Bertram, Jake Rhodes, Anthony Cunningham, Grahame Ctercteko, Scott Byrne, and Andrew Harman. 2021. 'A NOVEL LANGERIN EXPRESSING TYPE 2-CONVENTIONAL DENDRITIC CELL IS SIGNIFICANTLY DECREASED IN CROHN'S DISEASE'. *Inflammatory Bowel Diseases* 27 (Supplement_1): S32–33. https://doi.org/10.1093/ibd/izaa347.076.

Duan, Linna, and Eric Mukherjee. 2016. 'Janeway's Immunobiology, Ninth Edition'. *The Yale Journal of Biology and Medicine* 89 (3): 424–25.

Dunphy, Gillian, Sinéad M. Flannery, Jessica F. Almine, Dympna J. Connolly, Christina Paulus, Kasper L. Jønsson, Martin R. Jakobsen, Michael M. Nevels, Andrew G. Bowie, and Leonie Unterholzner. 2018. 'Non-Canonical Activation of the DNA Sensing Adaptor STING by ATM and IFI16 Mediates NF-KB Signaling after Nuclear DNA Damage'. *Molecular Cell* 71 (5): 745-760.e5. https://doi.org/10.1016/j.molcel.2018.07.034.

Dykes, Iain M., and Costanza Emanueli. 2017. 'Transcriptional and Post-Transcriptional Gene Regulation by Long Non-Coding RNA'. *Genomics, Proteomics & Bioinformatics* 15 (3): 177–86. https://doi.org/10.1016/j.gpb.2016.12.005.

Dzionek, A., A. Fuchs, P. Schmidt, S. Cremer, M. Zysk, S. Miltenyi, D. W. Buck, and J. Schmitz. 2000. 'BDCA-2, BDCA-3, and BDCA-4: Three Markers for Distinct Subsets of Dendritic Cells in Human Peripheral Blood'. *Journal of Immunology (Baltimore, Md.: 1950)* 165 (11): 6037–46. https://doi.org/10.4049/jimmunol.165.11.6037.

Eden, Eran, Roy Navon, Israel Steinfeld, Doron Lipson, and Zohar Yakhini. 2009. 'GOrilla: A Tool for Discovery and Visualization of Enriched GO Terms in Ranked Gene Lists'. *BMC Bioinformatics* 10 (1): 48. https://doi.org/10.1186/1471-2105-10-48.

Eftychi, Christina, Robin Schwarzer, Katerina Vlantis, Laurens Wachsmuth, Marijana Basic, Prerana Wagle, Markus F. Neurath, Christoph Becker, André Bleich, and Manolis Pasparakis. 2019. 'Temporally Distinct Functions of the Cytokines IL-12 and IL-23 Drive Chronic Colon Inflammation in Response to Intestinal Barrier Impairment'. *Immunity* 51 (2): 367-380.e4. https://doi.org/10.1016/j.immuni.2019.06.008.

Eguchi, Yutaka, Tateo Itoh, and Jun-ichi Tomizawa. 1991. 'Antisense Rna'. *Annual Review of Biochemistry* 60 (1): 631–52. https://doi.org/10.1146/annurev.bi.60.070191.003215.

Ellinghaus, David, Jörn Bethune, Britt-Sabina Petersen, and Andre Franke. 2015. 'The Genetics of Crohn's Disease and Ulcerative Colitis--Status Quo and Beyond'. *Scandinavian Journal of Gastroenterology* 50 (1): 13–23. https://doi.org/10.3109/00365521.2014.990507.

Ellis, Jason S., F. Betul Guloglu, Danielle M. Tartar, Christine M. Hoeman, Cara L. Haymaker, Jason A. Cascio, Xiaoxiao Wan, et al. 2010. 'APCs Expressing High Levels of Programmed Death Ligand 2 Sustain the Development of CD4 T Cell Memory'. *Journal of Immunology (Baltimore, Md.: 1950)* 185 (6): 3149–57. https://doi.org/10.4049/jimmunol.1000810.

Elshal, Mohamed F., Alia M. Aldahlawi, Omar I. Saadah, and J. Philip McCoy. 2015. 'Reduced Dendritic Cells Expressing CD200R1 in Children with Inflammatory Bowel Disease: Correlation with Th17 and Regulatory T Cells'. *International Journal of Molecular Sciences* 16 (12): 28998–10. https://doi.org/10.3390/ijms161226143.

Engman, Carl, Yesica Garciafigueroa, Brett Eugene Phillips, Massimo Trucco, and Nick Giannoukakis. 2018. 'Co-Stimulation-Impaired Bone Marrow-Derived Dendritic Cells Prevent Dextran Sodium Sulfate-Induced Colitis in Mice'. *Frontiers in Immunology* 9: 894. https://doi.org/10.3389/fimmu.2018.00894.

Ernst, Matthias, Stefan Thiem, Paul M. Nguyen, Moritz Eissmann, and Tracy L. Putoczki. 2014. 'Epithelial Gp130/Stat3 Functions: An Intestinal Signaling Node in Health and Disease'. *Seminars in Immunology* 26 (1): 29–37. https://doi.org/10.1016/j.smim.2013.12.006.

Fagarasan, Sidonia, Shimpei Kawamoto, Osami Kanagawa, and Keiichiro Suzuki. 2010. 'Adaptive Immune Regulation in the Gut: T Cell-Dependent and T Cell-Independent IgA Synthesis'. *Annual Review of Immunology* 28: 243–73. https://doi.org/10.1146/annurev-immunol-030409-101314.

Fallarino, Francesca, Carine Asselin-Paturel, Carmine Vacca, Roberta Bianchi, Stefania Gizzi, Maria Cristina Fioretti, Giorgio Trinchieri, Ursula Grohmann, and Paolo Puccetti. 2004. 'Murine Plasmacytoid Dendritic Cells Initiate the Immunosuppressive Pathway of Tryptophan Catabolism in Response to CD200 Receptor Engagement'. *Journal of Immunology (Baltimore, Md.: 1950)* 173 (6): 3748–54. https://doi.org/10.4049/jimmunol.173.6.3748.

Ferdinande, L., P. Demetter, C. Perez-Novo, A. Waeytens, J. Taildeman, I. Rottiers, P. Rottiers, M. De Vos, and C. A. Cuvelier. 2008. 'Inflamed Intestinal Mucosa Features a Specific Epithelial Expression Pattern of Indoleamine 2,3-Dioxygenase'. *International Journal of Immunopathology and Pharmacology* 21 (2): 289–95. https://doi.org/10.1177/039463200802100205.

Fingleton, Barbara. 2017. 'Matrix Metalloproteinases as Regulators of Inflammatory Processes'. *Biochimica et Biophysica Acta (BBA) - Molecular Cell Research*, Matrix Metalloproteinases, 1864 (11, Part A): 2036–42. https://doi.org/10.1016/j.bbamcr.2017.05.010.

Flores, Rafael R., Eun Kim, Liqiao Zhou, Chenjie Yang, Jing Zhao, Andrea Gambotto, and Paul D. Robbins. 2015. 'IL-Y, a Synthetic Member of the IL-12 Cytokine Family, Suppresses the Development of Type 1 Diabetes in NOD Mice'. *European Journal of Immunology* 45 (11): 3114–25. https://doi.org/10.1002/eji.201445403.

Francisco, Loise M., Victor H. Salinas, Keturah E. Brown, Vijay K. Vanguri, Gordon J. Freeman, Vijay K. Kuchroo, and Arlene H. Sharpe. 2009. 'PD-L1 Regulates the Development, Maintenance, and Function of Induced Regulatory T Cells'. *The Journal of Experimental Medicine* 206 (13): 3015–29. https://doi.org/10.1084/jem.20090847.

Frenkel, Svetlana, Charles N. Bernstein, Michael Sargent, Qin Kuang, Wenxin Jiang, John Wei, Bhooma Thiruvahindrapuram, Elizabeth Spriggs, Stephen W. Scherer, and Pingzhao Hu. 2019. 'Genome-Wide Analysis Identifies Rare Copy Number Variations Associated with Inflammatory Bowel Disease'. *PloS One* 14 (6): e0217846. https://doi.org/10.1371/journal.pone.0217846.

Fuchs, Tina, Martin Hahn, Lukas Ries, Sophie Giesler, Svenja Busch, Chunlin Wang, Jian Han, et al. 2018. 'Expression of Combinatorial Immunoglobulins in Macrophages in the Tumor Microenvironment'. *PLoS ONE* 13 (9). https://doi.org/10.1371/journal.pone.0204108.

Gehlert, Thomas, Odile Devergne, and Gerald Niedobitek. 2004. 'Epstein-Barr Virus (EBV) Infection and Expression of the Interleukin-12 Family Member EBV-Induced Gene 3 (EBI3) in Chronic Inflammatory Bowel Disease'. *Journal of Medical Virology* 73 (3): 432–38. https://doi.org/10.1002/jmv.20109.

Geiss, Gary K., Roger E. Bumgarner, Brian Birditt, Timothy Dahl, Naeem Dowidar, Dwayne L. Dunaway, H. Perry Fell, et al. 2008. 'Direct Multiplexed Measurement of Gene Expression with Color-Coded Probe Pairs'. *Nature Biotechnology* 26 (3): 317–25. https://doi.org/10.1038/nbt1385.

Genua, Marco, Alessandro Sgambato, and Silvio Danese. 2015. 'Editorial: CCR7 Is Required for Leukocyte Egression in an Experimental Model of Crohn's Disease-like Ileitis'. *Journal of Leukocyte Biology* 97 (6): 1000–1002. https://doi.org/10.1189/jlb.5CE0215037RR.

Gevers, Dirk, Subra Kugathasan, Lee A. Denson, Yoshiki Vázquez-Baeza, Will Van Treuren, Boyu Ren, Emma Schwager, et al. 2014. 'The Treatment-Naive Microbiome in New-Onset Crohn's Disease'. *Cell Host & Microbe* 15 (3): 382–92. https://doi.org/10.1016/j.chom.2014.02.005.

Ginhoux, Florent, Martin Guilliams, and Shalin H. Naik. 2016. 'Editorial: Dendritic Cell and Macrophage Nomenclature and Classification'. *Frontiers in Immunology* 7: 168. https://doi.org/10.3389/fimmu.2016.00168.

Gol-Ara, Maryam, Farhad Jadidi-Niaragh, Reza Sadria, Gholamreza Azizi, and Abbas Mirshafiey. 2012. 'The Role of Different Subsets of Regulatory T Cells in Immunopathogenesis of Rheumatoid Arthritis'. *Arthritis* 2012. https://doi.org/10.1155/2012/805875.

Goncharov, N. V., P. I. Popova, P. P. Avdonin, I. V. Kudryavtsev, M. K. Serebryakova, E. A. Korf, and P. V. Avdonin. 2020. 'Markers of Endothelial Cells in Normal and Pathological Conditions'. *Biochemistry (Moscow), Supplement Series A: Membrane and Cell Biology* 14 (3): 167–83. https://doi.org/10.1134/S1990747819030140.

Gracz, Adam D., Megan K. Fuller, Fengchao Wang, Linheng Li, Matthias Stelzner, James C.Y. Dunn, Martin G. Martin, and Scott T. Magness. 2013. 'CD24 and CD44 Mark Human Intestinal Epithelial Cell Populations with Characteristics of Active and Facultative Stem Cells'. *Stem Cells (Dayton, Ohio)* 31 (9): 2024–30. https://doi.org/10.1002/stem.1391.

Grage-Griebenow, E., H. D. Flad, and M. Ernst. 2001. 'Heterogeneity of Human Peripheral Blood Monocyte Subsets'. *Journal of Leukocyte Biology* 69 (1): 11–20.

Granot, Tomer, Takashi Senda, Dustin J. Carpenter, Nobuhide Matsuoka, Joshua Weiner, Claire L. Gordon, Michelle Miron, et al. 2017. 'Dendritic Cells Display Subset and Tissue-Specific Maturation Dynamics over Human Life'. *Immunity* 46 (3): 504–15. https://doi.org/10.1016/j.immuni.2017.02.019.

Guilliams, Martin, Charles-Antoine Dutertre, Charlotte L. Scott, Naomi McGovern, Dorine Sichien, Svetoslav Chakarov, Sofie Van Gassen, et al. 2016. 'Unsupervised High-Dimensional Analysis Aligns Dendritic Cells across Tissues and Species'. *Immunity* 45 (3): 669–84. https://doi.org/10.1016/j.immuni.2016.08.015.

Gunten, Stephan von, and Bruce S. Bochner. 2008. 'Basic and Clinical Immunology of Siglecs'. *Annals of the New York Academy of Sciences* 1143 (November): 61–82. https://doi.org/10.1196/annals.1443.011.

Guseva, Daria, Katrin Holst, Beate Kaune, Martin Meier, Lydia Keubler, Silke Glage, Manuela Buettner, et al. 2014. 'Serotonin 5-HT7 Receptor Is Critically Involved in Acute and Chronic Inflammation of the Gastrointestinal Tract'. *Inflammatory Bowel Diseases* 20 (9): 1516–29. https://doi.org/10.1097/MIB.0000000000000150.

Gutierrez, Olga, Carlos Pipaon, Naohiro Inohara, Ana Fontalba, Yasunori Ogura, Felipe Prosper, Gabriel Nunez, and Jose L. Fernandez-Luna. 2002. 'Induction of Nod2 in Myelomonocytic and Intestinal Epithelial Cells via Nuclear Factor-Kappa B Activation'. *The Journal of Biological Chemistry* 277 (44): 41701–5. https://doi.org/10.1074/jbc.M206473200.

Haniffa, Muzlifah, Amanda Shin, Venetia Bigley, Naomi McGovern, Pearline Teo, Peter See, Pavandip Singh Wasan, et al. 2012. 'Human Tissues Contain CD141hi Cross-Presenting Dendritic Cells with Functional Homology to Mouse CD103+ Nonlymphoid Dendritic Cells'. *Immunity* 37 (1): 60–73. https://doi.org/10.1016/j.immuni.2012.04.012.

Hansen, Morten, Özcan Met, Niels Bent Larsen, Mette Marie Rosenkilde, Mads Hald Andersen, Inge Marie Svane, and Gertrud Malene Hjortø. 2016. 'Autocrine CCL19 Blocks Dendritic Cell Migration toward Weak Gradients of CCL21'. *Cytotherapy* 18 (9): 1187–96. https://doi.org/10.1016/j.jcyt.2016.06.010.

Hanžel, Jurij, and Geert R. D'Haens. 2020. 'Anti-Interleukin-23 Agents for the Treatment of Ulcerative Colitis'. *Expert Opinion on Biological Therapy* 20 (4): 399–406. https://doi.org/10.1080/14712598.2020.1697227.

Hasegawa, Hideaki, Izuru Mizoguchi, Yukino Chiba, Mio Ohashi, Mingli Xu, and Takayuki Yoshimoto. 2016. 'Expanding Diversity in Molecular Structures and Functions of the IL-6/IL-12 Heterodimeric Cytokine Family'. *Frontiers in Immunology* 7: 479. https://doi.org/10.3389/fimmu.2016.00479.

Hasegawa, Hitoshi, and Takuya Matsumoto. 2018. 'Mechanisms of Tolerance Induction by Dendritic Cells In Vivo'. *Frontiers in Immunology* 9 (February). https://doi.org/10.3389/fimmu.2018.00350.

Helander, Herbert F., and Lars Fändriks. 2014. 'Surface Area of the Digestive Tract - Revisited'. *Scandinavian Journal of Gastroenterology* 49 (6): 681–89. https://doi.org/10.3109/00365521.2014.898326.

Hildner, Kai, Brian T. Edelson, Whitney E. Purtha, Mark Diamond, Hirokazu Matsushita, Masako Kohyama, Boris Calderon, et al. 2008. 'Batf3 Deficiency Reveals a Critical Role for CD8α+ Dendritic Cells in Cytotoxic T Cell Immunity'. *Science* 322 (5904): 1097–1100. https://doi.org/10.1126/science.1164206.

Hohl, Tobias M., Amariliz Rivera, Lauren Lipuma, Alena Gallegos, Chao Shi, Mathias Mack, and Eric G. Pamer. 2009. 'Inflammatory Monocytes Facilitate Adaptive CD4 T Cell Responses during Respiratory Fungal Infection'. *Cell Host & Microbe* 6 (5): 470–81. https://doi.org/10.1016/j.chom.2009.10.007.

Hong, Guini, Wenjing Zhang, Hongdong Li, Xiaopei Shen, and Zheng Guo. 2014. 'Separate Enrichment Analysis of Pathways for Up- and Downregulated Genes'. *Journal of the Royal Society Interface* 11 (92). https://doi.org/10.1098/rsif.2013.0950.

Hou, Jason K., Hashem El-Serag, and Selvi Thirumurthi. 2009. 'Distribution and Manifestations of Inflammatory Bowel Disease in Asians, Hispanics, and African Americans: A Systematic Review'. *The American Journal of Gastroenterology* 104 (8): 2100–2109. https://doi.org/10.1038/ajg.2009.190.

Houghton, A. McGarry, William O. Hartzell, Clinton S. Robbins, F. Xavier Gomis-Rüth, and Steven D. Shapiro. 2009. 'Macrophage Elastase Kills Bacteria within Murine Macrophages'. *Nature* 460 (7255): 637–41. https://doi.org/10.1038/nature08181.

Hounnou, G., C. Destrieux, J. Desmé, P. Bertrand, and S. Velut. 2002. 'Anatomical Study of the Length of the Human Intestine'. *Surgical and Radiologic Anatomy: SRA* 24 (5): 290–94. https://doi.org/10.1007/s00276-002-0057-y.

Hu, Shi, Shuaiyi Liang, Huaizu Guo, Dapeng Zhang, Hui Li, Xiaoze Wang, Weili Yang, et al. 2013. 'Comparison of the Inhibition Mechanisms of Adalimumab and Infliximab in Treating Tumor Necrosis Factor α-Associated Diseases from a Molecular View'. *The Journal of Biological Chemistry* 288 (38): 27059–67. https://doi.org/10.1074/jbc.M113.491530.

Hughes, Catherine E., and Robert J. B. Nibbs. 2018. 'A Guide to Chemokines and Their Receptors'. *The Febs Journal* 285 (16): 2944–71. https://doi.org/10.1111/febs.14466.

Hurst, Tara Patricia, Amr Aswad, Timokratis Karamitros, Aris Katzourakis, Adrian L. Smith, and Gkikas Magiorkinis. 2019. 'Interferon-Inducible Protein 16 (IFI16) Has a Broad-Spectrum Binding Ability Against SsDNA Targets: An Evolutionary Hypothesis for Antiretroviral Checkpoint'. *Frontiers in Microbiology* 10 (July). https://doi.org/10.3389/fmicb.2019.01426.

Iwata, Makoto, Asami Hirakiyama, Yuko Eshima, Hiroyuki Kagechika, Chieko Kato, and Si-Young Song. 2004. 'Retinoic Acid Imprints Gut-Homing Specificity on T Cells'. *Immunity* 21 (4): 527–38. https://doi.org/10.1016/j.immuni.2004.08.011.

Jalili, Roxana, Joe Horecka, James R. Swartz, Ronald W. Davis, and Henrik H. J. Persson. 2018. 'Streamlined Circular Proximity Ligation Assay Provides High Stringency and Compatibility with Low-Affinity Antibodies'. *Proceedings of the National Academy of Sciences of the United States of America* 115 (5): E925–33. https://doi.org/10.1073/pnas.1718283115.

Jang, Myoung Ho, Nagako Sougawa, Toshiyuki Tanaka, Takako Hirata, Takachika Hiroi, Kazuo Tohya, Zijin Guo, et al. 2006. 'CCR7 Is Critically Important for Migration of Dendritic Cells in Intestinal Lamina Propria to Mesenteric Lymph Nodes'. *Journal of Immunology (Baltimore, Md.: 1950)* 176 (2): 803–10. https://doi.org/10.4049/jimmunol.176.2.803.

Jiang, Lingling, Yingying Shen, Danfeng Guo, Diya Yang, Jiajun Liu, Xuefeng Fei, Yunshan Yang, et al. 2016. 'EpCAM-Dependent Extracellular Vesicles from Intestinal Epithelial Cells Maintain Intestinal Tract Immune Balance'. *Nature Communications* 7 (October): 13045. https://doi.org/10.1038/ncomms13045.

Johansen, F.-E., and C. S. Kaetzel. 2011. 'Regulation of the Polymeric Immunoglobulin Receptor and IgA Transport: New Advances in Environmental Factors That Stimulate PIgR Expression and Its Role in Mucosal Immunity'. *Mucosal Immunology* 4 (6): 598–602. https://doi.org/10.1038/mi.2011.37.

Johansson, Malin E.V., and Gunnar C. Hansson. 2016. 'Immunological Aspects of Intestinal Mucus and Mucins'. *Nature Reviews. Immunology* 16 (10): 639–49. https://doi.org/10.1038/nri.2016.88.

Jostins, Luke, Stephan Ripke, Rinse K Weersma, Richard H Duerr, Dermot P McGovern, Ken Y Hui, James C Lee, et al. 2012. 'Host-Microbe Interactions Have Shaped the Genetic Architecture of Inflammatory Bowel Disease'. *Nature* 491 (7422): 119–24. https://doi.org/10.1038/nature11582.

Kabeerdoss, Jayakanthan, Prabavathi Jayakanthan, Srinivasan Pugazhendhi, and Balakrishnan S. Ramakrishna. 2015. 'Alterations of Mucosal Microbiota in the Colon of Patients with Inflammatory Bowel Disease Revealed by Real Time Polymerase Chain Reaction Amplification of 16S Ribosomal Ribonucleic Acid'. *The Indian Journal of Medical Research* 142 (1): 23–32. https://doi.org/10.4103/0971-5916.162091.

Kåhrström, Christina Tobin, Nonia Pariente, and Ursula Weiss. 2016. 'Intestinal Microbiota in Health and Disease'. *Nature* 535 (7610): 47. https://doi.org/10.1038/535047a.

Källberg, Eva, and Tomas Leanderson. 2008. 'A Subset of Dendritic Cells Express Joining Chain (J-Chain) Protein'. *Immunology* 123 (4): 590–99. https://doi.org/10.1111/j.1365-2567.2007.02733.x.

Kaplan, Gilaad G. 2015. 'The Global Burden of IBD: From 2015 to 2025'. *Nature Reviews. Gastroenterology & Hepatology* 12 (12): 720–27. https://doi.org/10.1038/nrgastro.2015.150.

Karpus, Olga N., B. Florien Westendorp, Jacqueline L. M. Vermeulen, Sander Meisner, Jan Koster, Vanesa Muncan, Manon E. Wildenberg, and Gijs R. van den Brink. 2019. 'Colonic CD90+ Crypt Fibroblasts Secrete Semaphorins to Support Epithelial Growth'. *Cell Reports* 26 (13): 3698-3708.e5. https://doi.org/10.1016/j.celrep.2019.02.101.

Karsunky, Holger, Miriam Merad, Antonio Cozzio, Irving L. Weissman, and Markus G. Manz. 2003. 'Flt3 Ligand Regulates Dendritic Cell Development from Flt3+ Lymphoid and Myeloid-Committed Progenitors to Flt3+ Dendritic Cells in Vivo'. *The Journal of Experimental Medicine* 198 (2): 305–13. https://doi.org/10.1084/jem.20030323.

Kashani, Amir, and David A. Schwartz. 2019. 'The Expanding Role of Anti–IL-12 and/or Anti–IL-23 Antibodies in the Treatment of Inflammatory Bowel Disease'. *Gastroenterology & Hepatology* 15 (5): 255–65.

Khader, Shabaana A., Sarah L. Gaffen, and Jay K. Kolls. 2009. 'Th17 Cells at the Cross Roads of Innate and Adaptive Immunity against Infectious Diseases at the Mucosa'. *Mucosal Immunology* 2 (5): 403–11. https://doi.org/10.1038/mi.2009.100.

Khor, Bernard, Agnès Gardet, and Ramnik J. Xavier. 2011. 'Genetics and Pathogenesis of Inflammatory Bowel Disease'. *Nature* 474 (7351): 307–17. https://doi.org/10.1038/nature10209.

Kida, Hiroshi, Michael L. Mucenski, Angela R. Thitoff, Timothy D. Le Cras, Kwon-Sik Park, Machiko Ikegami, Werner Müller, and Jeffrey A. Whitsett. 2008. 'GP130-STAT3 Regulates Epithelial Cell Migration and Is Required for Repair of the Bronchiolar Epithelium'. *The American Journal of Pathology* 172 (6): 1542–54. https://doi.org/10.2353/ajpath.2008.071052.

Kim, Myunghoo, Carolina Galan, Andrea A. Hill, Wan-Jung Wu, Hannah Fehlner-Peach, Hyo Won Song, Deborah Schady, et al. 2018. 'Critical Role for the Microbiota in CX3CR1+ Intestinal Mononuclear Phagocyte Regulation of Intestinal T Cell Responses'. *Immunity* 49 (1): 151-163.e5. https://doi.org/10.1016/j.immuni.2018.05.009.

Kirsner, J. B. 1988. 'Historical Aspects of Inflammatory Bowel Disease'. *Journal of Clinical Gastroenterology* 10 (3): 286–97. https://doi.org/10.1097/00004836-198806000-00012.

Kis-Toth, Katalin, Ildiko Bacskai, Peter Gogolak, Anett Mazlo, Istvan Szatmari, and Eva Rajnavolgyi. 2013. 'Monocyte-Derived Dendritic Cell Subpopulations Use Different Types of Matrix

Metalloproteinases Inhibited by GM6001'. *Immunobiology* 218 (11): 1361–69. https://doi.org/10.1016/j.imbio.2013.06.012.

Kleijmeer, M., G. Ramm, D. Schuurhuis, J. Griffith, M. Rescigno, P. Ricciardi-Castagnoli, A. Y. Rudensky, et al. 2001. 'Reorganization of Multivesicular Bodies Regulates MHC Class II Antigen Presentation by Dendritic Cells'. *The Journal of Cell Biology* 155 (1): 53–63. https://doi.org/10.1083/jcb.200103071.

Klement, Eyal, Regev V. Cohen, Jonathan Boxman, Aviva Joseph, and Shimon Reif. 2004. 'Breastfeeding and Risk of Inflammatory Bowel Disease: A Systematic Review with Meta-Analysis'. *The American Journal of Clinical Nutrition* 80 (5): 1342–52. https://doi.org/10.1093/ajcn/80.5.1342.

Koller, Felicitas L., E. Ashley Dozier, Ki Taek Nam, Mei Swee, Timothy P. Birkland, William C. Parks, and Barbara Fingleton. 2012. 'Lack of MMP10 Exacerbates Experimental Colitis and Promotes Development of Inflammation-Associated Colonic Dysplasia'. *Laboratory Investigation; a Journal of Technical Methods and Pathology* 92 (12): 1749–59. https://doi.org/10.1038/labinvest.2012.141.

Krammer, H. J., S. T. Karahan, W. Sigge, and W. Kühnel. 1994. 'Immunohistochemistry of Markers of the Enteric Nervous System in Whole-Mount Preparations of the Human Colon'. *European Journal of Pediatric Surgery: Official Journal of Austrian Association of Pediatric Surgery ... [et Al] = Zeitschrift Fur Kinderchirurgie* 4 (5): 274–78. https://doi.org/10.1055/s-2008-1066117.

Kristiansen, M., J. H. Graversen, C. Jacobsen, O. Sonne, H. J. Hoffman, S. K. Law, and S. K. Moestrup. 2001. 'Identification of the Haemoglobin Scavenger Receptor'. *Nature* 409 (6817): 198–201. https://doi.org/10.1038/35051594.

Kugathasan, S, L J Saubermann, L Smith, D Kou, J Itoh, D G Binion, A D Levine, R S Blumberg, and C Fiocchi. 2007. 'Mucosal T-cell Immunoregulation Varies in Early and Late Inflammatory Bowel Disease'. *Gut* 56 (12): 1696–1705. https://doi.org/10.1136/gut.2006.116467.

Kulkarni, Neeraja, Manisha Pathak, and Girdhari Lal. 2017. 'Role of Chemokine Receptors and Intestinal Epithelial Cells in the Mucosal Inflammation and Tolerance'. *Journal of Leukocyte Biology* 101 (2): 377–94. https://doi.org/10.1189/jlb.1RU0716-327R.

Kurashima, Yosuke, Daiki Yamamoto, Sean Nelson, Satoshi Uematsu, Peter B. Ernst, Toshinori Nakayama, and Hiroshi Kiyono. 2017. 'Mucosal Mesenchymal Cells: Secondary Barrier and Peripheral Educator for the Gut Immune System'. *Frontiers in Immunology* 8 (December). https://doi.org/10.3389/fimmu.2017.01787.

Lakschevitz, Flavia S., Siavash Hassanpour, Ayala Rubin, Noah Fine, Chunxiang Sun, and Michael Glogauer. 2016. 'Identification of Neutrophil Surface Marker Changes in Health and Inflammation Using High-Throughput Screening Flow Cytometry'. *Experimental Cell Research* 342 (2): 200–209. https://doi.org/10.1016/j.yexcr.2016.03.007.

Landsverk, Ole J. B., Anett H. Ottesen, Axel Berg-Larsen, Silke Appel, and Oddmund Bakke. 2012. 'Differential Regulation of MHC II and Invariant Chain Expression during Maturation of Monocyte-Derived Dendritic Cells'. *Journal of Leukocyte Biology* 91 (5): 729–37. https://doi.org/10.1189/jlb.0311150.

Lange, Katrina M. de, Loukas Moutsianas, James C. Lee, Christopher A. Lamb, Yang Luo, Nicholas A. Kennedy, Luke Jostins, et al. 2017. 'Genome-Wide Association Study Implicates Immune Activation of Multiple Integrin Genes in Inflammatory Bowel Disease'. *Nature Genetics* 49 (2): 256–61. https://doi.org/10.1038/ng.3760.

Langer, Victoria, Eugenia Vivi, Daniela Regensburger, Thomas H. Winkler, Maximilian J. Waldner, Timo Rath, Benjamin Schmid, et al. 2019. 'IFN-**γ** Drives Inflammatory Bowel Disease Pathogenesis through VE-Cadherin–Directed Vascular Barrier Disruption'. *The Journal of Clinical Investigation* 129 (11): 4691–4707. https://doi.org/10.1172/JCI124884.

Lehtimäki, Sari, Sari Tillander, Anne Puustinen, Sampsa Matikainen, Tuula Nyman, Nanna Fyhrquist, Terhi Savinko, et al. 2010. 'Absence of CCR4 Exacerbates Skin Inflammation in an Oxazolone-Induced Contact Hypersensitivity Model'. *The Journal of Investigative Dermatology* 130 (12): 2743–51. https://doi.org/10.1038/jid.2010.208.

Li, A., M. L. Varney, and R. K. Singh. 2001. 'Expression of Interleukin 8 and Its Receptors in Human Colon Carcinoma Cells with Different Metastatic Potentials'. *Clinical Cancer Research: An Official Journal of the American Association for Cancer Research* 7 (10): 3298–3304.

Li, Rui, Rui Zhou, Hui Wang, Weidong Li, Mingxin Pan, Xueqing Yao, Wanqi Zhan, et al. 2019. 'Gut Microbiota-Stimulated Cathepsin K Secretion Mediates TLR4-Dependent M2 Macrophage Polarization and Promotes Tumor Metastasis in Colorectal Cancer'. *Cell Death & Differentiation* 26 (11): 2447–63. https://doi.org/10.1038/s41418-019-0312-y.

Li, Tengda, Mingli Gu, Peng Liu, Yun Liu, Jie Guo, Weiwei Zhang, Cheng Qian, and Anmei Deng. 2018. 'Clinical Significance of Decreased Interleukin-35 Expression in Patients with Psoriasis'. *Microbiology and Immunology*, May. https://doi.org/10.1111/1348-0421.12605.

Liang, Yanfang, Qianqian Chen, Wenjing Du, Can Chen, Feifei Li, Jingying Yang, Jianyu Peng, et al. 2016. 'Epstein-Barr Virus-Induced Gene 3 (EBI3) Blocking Leads to Induce Antitumor Cytotoxic T Lymphocyte Response and Suppress Tumor Growth in Colorectal Cancer by Bidirectional Reciprocal-Regulation STAT3 Signaling Pathway'. *Mediators of Inflammation* 2016: 3214105. https://doi.org/10.1155/2016/3214105.

Lin, Lihui, Gaoshi Zhou, Peng Chen, Ying Wang, Jing Han, Minhu Chen, Yao He, and Shenghong Zhang. 2020. 'Which Long Noncoding RNAs and Circular RNAs Contribute to Inflammatory Bowel Disease?' *Cell Death & Disease* 11 (6): 1–15. https://doi.org/10.1038/s41419-020-2657-z.

Lindroos, Josefine, Lars Svensson, Hanne Norsgaard, Paola Lovato, Kristian Moller, Peter H. Hagedorn, Gunnar Marius Olsen, and Tord Labuda. 2011. 'IL-23-Mediated Epidermal Hyperplasia Is Dependent on IL-6'. *The Journal of Investigative Dermatology* 131 (5): 1110–18. https://doi.org/10.1038/jid.2010.432.

Liu, Jimmy Z., Suzanne van Sommeren, Hailiang Huang, Siew C. Ng, Rudi Alberts, Atsushi Takahashi, Stephan Ripke, et al. 2015. 'Association Analyses Identify 38 Susceptibility Loci for Inflammatory Bowel Disease and Highlight Shared Genetic Risk across Populations'. *Nature Genetics* 47 (9): 979–86. https://doi.org/10.1038/ng.3359.

Liu, Zhanju, Praveen K. Yadav, Xiaorong Xu, Jingling Su, Chi Chen, Maochun Tang, Hui Lin, et al. 2011. 'The Increased Expression of IL-23 in Inflammatory Bowel Disease Promotes Intraepithelial and Lamina Propria Lymphocyte Inflammatory Responses and Cytotoxicity'. *Journal of Leukocyte Biology* 89 (4): 597–606. https://doi.org/10.1189/jlb.0810456.

Loh, Gunnar, and Michael Blaut. 2012. 'Role of Commensal Gut Bacteria in Inflammatory Bowel Diseases'. *Gut Microbes* 3 (6): 544–55. https://doi.org/10.4161/gmic.22156.

Loktionov, Alexandre. 2019. 'Eosinophils in the Gastrointestinal Tract and Their Role in the Pathogenesis of Major Colorectal Disorders'. *World Journal of Gastroenterology* 25 (27): 3503–26. https://doi.org/10.3748/wjg.v25.i27.3503.

Lozano, Rafael, Mohsen Naghavi, Kyle Foreman, Stephen Lim, Kenji Shibuya, Victor Aboyans, Jerry Abraham, et al. 2012. 'Global and Regional Mortality from 235 Causes of Death for 20 Age Groups in 1990 and 2010: A Systematic Analysis for the Global Burden of Disease Study 2010'. *Lancet (London, England)* 380 (9859): 2095–2128. https://doi.org/10.1016/S0140-6736(12)61728-0.

Lundberg, Kristina, Frida Rydnert, Lennart Greiff, and Malin Lindstedt. 2014. 'Human Blood Dendritic Cell Subsets Exhibit Discriminative Pattern Recognition Receptor Profiles'. *Immunology* 142 (2): 279–88. https://doi.org/10.1111/imm.12252.

Lynch, Susan V., and Oluf Pedersen. 2016. 'The Human Intestinal Microbiome in Health and Disease'. *The New England Journal of Medicine* 375 (24): 2369–79. https://doi.org/10.1056/NEJMra1600266.

Ma, X., and G. Trinchieri. 2001. 'Regulation of Interleukin-12 Production in Antigen-Presenting Cells'. *Advances in Immunology* 79: 55–92. https://doi.org/10.1016/s0065-2776(01)79002-5.

Maaser, Christian, Laurence J. Egan, Mark P. Birkenbach, Lars Eckmann, and Martin F. Kagnoff. 2004. 'Expression of Epstein-Barr Virus-Induced Gene 3 and Other Interleukin-12-Related Molecules by Human Intestinal Epithelium'. *Immunology* 112 (3): 437–45. https://doi.org/10.1111/j.1365-2567.2004.01895.x.

Mabbott, N. A., D. S. Donaldson, H. Ohno, I. R. Williams, and A. Mahajan. 2013. 'Microfold (M) Cells: Important Immunosurveillance Posts in the Intestinal Epithelium'. *Mucosal Immunology* 6 (4): 666–77. https://doi.org/10.1038/mi.2013.30.

MacDonald, Kelli P. A., David J. Munster, Georgina J. Clark, Andrzej Dzionek, Juergen Schmitz, and Derek N. J. Hart. 2002. 'Characterization of Human Blood Dendritic Cell Subsets'. *Blood* 100 (13): 4512–20. https://doi.org/10.1182/blood-2001-11-0097.

Macho-Fernandez, Elise, Ekaterina P. Koroleva, Cody M. Spencer, Michael Tighe, Egidio Torrado, Andrea M. Cooper, Yang-Xin Fu, and Alexei V. Tumanov. 2015. 'Lymphotoxin Beta Receptor Signaling Limits Mucosal Damage through Driving IL-23 Production by Epithelial Cells'. *Mucosal Immunology* 8 (2): 403–13. https://doi.org/10.1038/mi.2014.78.

Macosko, Evan Z., Anindita Basu, Rahul Satija, James Nemesh, Karthik Shekhar, Melissa Goldman, Itay Tirosh, et al. 2015. 'Highly Parallel Genome-Wide Expression Profiling of Individual Cells Using Nanoliter Droplets'. *Cell* 161 (5): 1202–14. https://doi.org/10.1016/j.cell.2015.05.002.

MacPherson, Gordon, Simon Milling, Ulf Yrlid, Lesley Cousins, Emma Turnbull, and Fang-Ping Huang. 2004. 'Uptake of Antigens from the Intestine by Dendritic Cells'. *Annals of the New York Academy of Sciences* 1029 (December): 75–82. https://doi.org/10.1196/annals.1309.010.

Maecker, Holden T., J. Philip McCoy, and Robert Nussenblatt. 2012. 'Standardizing Immunophenotyping for the Human Immunology Project'. *Nature Reviews. Immunology* 12 (3): 191–200. https://doi.org/10.1038/nri3158.

Magnusson, Maria K, Siggeir F Brynjólfsson, Anders Dige, Heli Uronen-Hansson, Lars G. Börjesson, Jonas L. Bengtsson, Sigurdur Gudjonsson, et al. 2016. 'Macrophage and Dendritic Cell Subsets in IBD: ALDH+ Cells Are Reduced in Colon Tissue of Patients with Ulcerative Colitis Regardless of Inflammation'. *Mucosal Immunology* 9 (1): 171–82. https://doi.org/10.1038/mi.2015.48.

Mahida, Y. R., A. M. Galvin, T. Gray, S. Makh, M. E. McALINDON, H. F. Sewell, and D. K. Podolsky. 1997. 'Migration of Human Intestinal Lamina Propria Lymphocytes, Macrophages and Eosinophils Following the Loss of Surface Epithelial Cells'. *Clinical & Experimental Immunology* 109 (2): 377–86. https://doi.org/10.1046/j.1365-2249.1997.4481346.x.

Majorek, Karolina A, Misty L Kuhn, Maksymilian Chruszcz, Wayne F Anderson, and Wladek Minor. 2014. 'Double Trouble—Buffer Selection and His-Tag Presence May Be Responsible for Nonreproducibility of Biomedical Experiments'. *Protein Science : A Publication of the Protein Society* 23 (10): 1359–68. https://doi.org/10.1002/pro.2520.

Mankertz, Joachim, and Jörg-Dieter Schulzke. 2007. 'Altered Permeability in Inflammatory Bowel Disease: Pathophysiology and Clinical Implications'. *Current Opinion in Gastroenterology* 23 (4): 379–83. https://doi.org/10.1097/MOG.0b013e32816aa392.

Manning, Alicia A., Lei Zhao, Ziwen Zhu, Huaping Xiao, Chase G. Redington, Vivi A. Ding, Theodore Stewart-Hester, et al. 2018. 'IL-39 Acts as a Friend to Pancreatic Cancer'. *Medical Oncology (Northwood, London, England)* 36 (1): 12. https://doi.org/10.1007/s12032-018-1236-y.

Manousou, P, G Kolios, V Valatas, I Drygiannakis, L Bourikas, K Pyrovolaki, I Koutroubakis, H A Papadaki, and E Kouroumalis. 2010. 'Increased Expression of Chemokine Receptor CCR3 and Its Ligands in Ulcerative Colitis: The Role of Colonic Epithelial Cells in in Vitro Studies'. *Clinical and Experimental Immunology* 162 (2): 337–47. https://doi.org/10.1111/j.1365-2249.2010.04248.x.

Marinho, Fabio V., Sulayman Benmerzoug, Stephanie Rose, Priscila C. Campos, João T. Marques, André Báfica, Glen Barber, Bernhard Ryffel, Sergio C. Oliveira, and Valerie F.J. Quesniaux. 2018. 'The CGAS/STING Pathway Is Important for Dendritic Cell Activation but Is Not Essential to Induce Protective Immunity against Mycobacterium Tuberculosis Infection'. *Journal of Innate Immunity* 10 (3): 239–52. https://doi.org/10.1159/000488952.

Marinkovich, M. P., T. B. Taylor, D. R. Keene, R. E. Burgeson, and J. J. Zone. 1996. 'LAD-1, the Linear IgA Bullous Dermatosis Autoantigen, Is a Novel 120-KDa Anchoring Filament Protein Synthesized by Epidermal Cells'. *The Journal of Investigative Dermatology* 106 (4): 734–38. https://doi.org/10.1111/1523-1747.ep12345782.

Martin, Gary R., Charlene M. Blomquist, Kimiora L. Henare, and Frank R. Jirik. 2019. 'Stimulator of Interferon Genes (STING) Activation Exacerbates Experimental Colitis in Mice'. *Scientific Reports* 9 (1): 14281. https://doi.org/10.1038/s41598-019-50656-5.

Martin, Jerome C., Christie Chang, Gilles Boschetti, Ryan Ungaro, Mamta Giri, John A. Grout, Kyle Gettler, et al. 2019. 'Single-Cell Analysis of Crohn's Disease Lesions Identifies a Pathogenic Cellular Module Associated with Resistance to Anti-TNF Therapy'. *Cell* 178 (6): 1493-1508.e20. https://doi.org/10.1016/j.cell.2019.08.008.

Martinez-Sanchez, Mariana E., Leonor Huerta, Elena R. Alvarez-Buylla, and Carlos Villarreal Luján. 2018. 'Role of Cytokine Combinations on CD4+ T Cell Differentiation, Partial Polarization, and Plasticity: Continuous Network Modeling Approach'. *Frontiers in Physiology* 9 (August). https://doi.org/10.3389/fphys.2018.00877.

Matsuno, Hiroshi, Hisako Kayama, Junichi Nishimura, Yuki Sekido, Hideki Osawa, Soumik Barman, Takayuki Ogino, et al. 2017. 'CD103+ Dendritic Cell Function Is Altered in the Colons of Patients with Ulcerative Colitis'. *Inflammatory Bowel Diseases* 23 (9): 1524–34. https://doi.org/10.1097/MIB.0000000000001204.

Matteoli, Gianluca, Elisa Mazzini, Iliyan D. Iliev, Erika Mileti, Francesca Fallarino, Paolo Puccetti, Marcello Chieppa, and Maria Rescigno. 2010. 'Gut CD103+ Dendritic Cells Express Indoleamine 2,3-Dioxygenase Which Influences T Regulatory/T Effector Cell Balance and Oral Tolerance Induction'. *Gut* 59 (5): 595–604. https://doi.org/10.1136/gut.2009.185108.

Maynard, Craig L., and Casey T. Weaver. 2009. 'Intestinal Effector T Cells in Health and Disease'. *Immunity* 31 (3): 389–400. https://doi.org/10.1016/j.immuni.2009.08.012.

McAlindon, M. E., T. Gray, A. Galvin, H. F. Sewell, D. K. Podolsky, and Y. R. Mahida. 1998. 'Differential Lamina Propria Cell Migration via Basement Membrane Pores of Inflammatory Bowel Disease Mucosa'. *Gastroenterology* 115 (4): 841–48.

McDonald, Keely G., Jacquelyn S. McDonough, Brian K. Dieckgraefe, and Rodney D. Newberry. 2010. 'Dendritic Cells Produce CXCL13 and Participate in the Development of Murine Small Intestine Lymphoid Tissues'. *The American Journal of Pathology* 176 (5): 2367–77. https://doi.org/10.2353/ajpath.2010.090723.

McNamee, Eóin N., Joanne C. Masterson, Marisol Veny, Colm B. Collins, Paul Jedlicka, Fergus R. Byrne, Gordon Y. Ng, and Jesús Rivera-Nieves. 2015. 'Chemokine Receptor CCR7 Regulates the Intestinal TH1/TH17/Treg Balance during Crohn's-like Murine Ileitis'. *Journal of Leukocyte Biology* 97 (6): 1011–22. https://doi.org/10.1189/jlb.3HI0614-303R.

Mellor, Andrew L., Henrique Lemos, and Lei Huang. 2017. 'Indoleamine 2,3-Dioxygenase and Tolerance: Where Are We Now?' *Frontiers in Immunology* 8 (October). https://doi.org/10.3389/fimmu.2017.01360.

Melo-Gonzalez, Felipe, Thomas M. Fenton, Cecilia Forss, Catherine Smedley, Anu Goenka, Andrew S. MacDonald, David J. Thornton, and Mark A. Travis. 2018. 'Intestinal Mucin Activates Human Dendritic Cells and IL-8 Production in a Glycan-Specific Manner'. *The Journal of Biological Chemistry* 293 (22): 8543–53. https://doi.org/10.1074/jbc.M117.789305.

Menzies-Gow, Andrew, Sun Ying, Ian Sabroe, Victoria L. Stubbs, Dulce Soler, Timothy J. Williams, and A. Barry Kay. 2002. 'Eotaxin (CCL11) and Eotaxin-2 (CCL24) Induce Recruitment of Eosinophils, Basophils, Neutrophils, and Macrophages as Well as Features of Early- and Late-Phase Allergic Reactions Following Cutaneous Injection in Human Atopic and Nonatopic Volunteers'. *Journal of Immunology (Baltimore, Md.: 1950)* 169 (5): 2712–18. https://doi.org/10.4049/jimmunol.169.5.2712.

Mifflin, R. C., I. V. Pinchuk, J. I. Saada, and D. W. Powell. 2011. 'Intestinal Myofibroblasts: Targets for Stem Cell Therapy'. *American Journal of Physiology - Gastrointestinal and Liver Physiology* 300 (5): G684–96. https://doi.org/10.1152/ajpgi.00474.2010.

Mills, Steven, and Michael J. Stamos. 2007. 'Colonic Crohn's Disease'. *Clinics in Colon and Rectal Surgery* 20 (4): 309–13. https://doi.org/10.1055/s-2007-991030.

Moller, Frederik Trier, Vibeke Andersen, Jan Wohlfahrt, and Tine Jess. 2015. 'Familial Risk of Inflammatory Bowel Disease: A Population-Based Cohort Study 1977-2011'. *The American Journal of Gastroenterology* 110 (4): 564–71. https://doi.org/10.1038/ajg.2015.50.

Mölzer, Christine, Sucharita P. Shankar, Vlad Masalski, May Griffith, Lucia Kuffová, and John V. Forrester. 2019. 'TGF-B1-Activated Type 2 Dendritic Cells Promote Wound Healing and Induce Fibroblasts to Express Tenascin c Following Corneal Full-Thickness Hydrogel Transplantation'. *Journal of Tissue Engineering and Regenerative Medicine* 13 (9): 1507–17. https://doi.org/10.1002/term.2853.

Moon, Byul, Suk-Jin Yang, Seong Min Park, Sang-Hyun Lee, Kyu Sang Song, Eun-Jeong Jeong, Mijin Park, Jang-Seong Kim, Young Il Yeom, and Jung-Ae Kim. 2020. 'LAD1 Expression Is Associated with the Metastatic Potential of Colorectal Cancer Cells'. *BMC Cancer* 20 (December). https://doi.org/10.1186/s12885-020-07660-0.

Mora, J. R., and U. H. von Andrian. 2008. 'Differentiation and Homing of IgA-Secreting Cells'. *Mucosal Immunology* 1 (2): 96–109. https://doi.org/10.1038/mi.2007.14.

Mowat, Allan M., and William W. Agace. 2014. 'Regional Specialization within the Intestinal Immune System'. *Nature Reviews. Immunology* 14 (10): 667–85. https://doi.org/10.1038/nri3738.

Muller, Paul Andrew, Balázs Koscsó, Gaurav Manohar Rajani, Korey Stevanovic, Marie-Luise Berres, Daigo Hashimoto, Arthur Mortha, et al. 2014. 'Crosstalk between Muscularis Macrophages and Enteric Neurons Regulates Gastrointestinal Motility'. *Cell* 158 (2): 300–313. https://doi.org/10.1016/j.cell.2014.04.050.

Müller, Stephanie I., Antonie Friedl, Isabel Aschenbrenner, Julia Esser-von Bieren, Martin Zacharias, Odile Devergne, and Matthias J. Feige. 2019. 'A Folding Switch Regulates Interleukin 27 Biogenesis and Secretion of Its α-Subunit as a Cytokine'. *Proceedings of the National Academy of Sciences* 116 (5): 1585–90. https://doi.org/10.1073/pnas.1816698116.

Murillo-Rincon, Andrea P., Alexander Klimovich, Eileen Pemöller, Jan Taubenheim, Benedikt Mortzfeld, René Augustin, and Thomas C. G. Bosch. 2017. 'Spontaneous Body Contractions Are Modulated by the Microbiome of Hydra'. *Scientific Reports* 7 (1): 15937. https://doi.org/10.1038/s41598-017-16191-x.

Muzaki, A R B M, P Tetlak, J Sheng, S C Loh, Y A Setiagani, M Poidinger, F Zolezzi, K Karjalainen, and C Ruedl. 2016. 'Intestinal CD103+CD11b− Dendritic Cells Restrain Colitis via IFN-γ-Induced Anti-Inflammatory Response in Epithelial Cells'. *Mucosal Immunology* 9 (2): 336–51. https://doi.org/10.1038/mi.2015.64.

Nagasawa, Maho, Balthasar A. Heesters, Chantal M.A. Kradolfer, Lisette Krabbendam, Itziar Martinez-Gonzalez, Marjolein J.W. de Bruijn, Korneliusz Golebski, et al. 2019. 'KLRG1 and NKp46 Discriminate Subpopulations of Human CD117+CRTH2− ILCs Biased toward ILC2 or ILC3'. *Journal of Experimental Medicine* 216 (8): 1762–76. https://doi.org/10.1084/jem.20190490.

Nandagopal, Saravanan, Dan Wu, and Francis Lin. 2011. 'Combinatorial Guidance by CCR7 Ligands for T Lymphocytes Migration in Co-Existing Chemokine Fields'. *PLoS ONE* 6 (3). https://doi.org/10.1371/journal.pone.0018183.

Ng, Siew C., Hai Yun Shi, Nima Hamidi, Fox E. Underwood, Whitney Tang, Eric I. Benchimol, Remo Panaccione, et al. 2017. 'Worldwide Incidence and Prevalence of Inflammatory Bowel Disease in the 21st Century: A Systematic Review of Population-Based Studies'. *Lancet (London, England)* 390 (10114): 2769–78. https://doi.org/10.1016/S0140-6736(17)32448-0.

Niess, Jan Hendrik, Frank Leithäuser, Guido Adler, and Jörg Reimann. 2008. 'Commensal Gut Flora Drives the Expansion of Proinflammatory CD4 T Cells in the Colonic Lamina Propria under Normal and Inflammatory Conditions'. *Journal of Immunology (Baltimore, Md.: 1950)* 180 (1): 559–68. https://doi.org/10.4049/jimmunol.180.1.559.

Okumura, Ryu, and Kiyoshi Takeda. 2017. 'Roles of Intestinal Epithelial Cells in the Maintenance of Gut Homeostasis'. *Experimental & Molecular Medicine* 49 (5): e338. https://doi.org/10.1038/emm.2017.20.

Olivares-Villagómez, Danyvid, and Luc Van Kaer. 2018. 'Intestinal Intraepithelial Lymphocytes: Sentinels of the Mucosal Barrier'. *Trends in Immunology* 39 (4): 264–75. https://doi.org/10.1016/j.it.2017.11.003.

O'Sullivan, Shane, John F. Gilmer, and Carlos Medina. 2015. 'Matrix Metalloproteinases in Inflammatory Bowel Disease: An Update'. *Mediators of Inflammation* 2015. https://doi.org/10.1155/2015/964131.

Page-McCaw, Andrea, Andrew J. Ewald, and Zena Werb. 2007. 'Matrix Metalloproteinases and the Regulation of Tissue Remodelling'. *Nature Reviews. Molecular Cell Biology* 8 (3): 221–33. https://doi.org/10.1038/nrm2125.

Perry, Justin S. A., Sho Morioka, Christopher B. Medina, J. Iker Etchegaray, Brady Barron, Michael H. Raymond, Christopher D. Lucas, Suna Onengut-Gumuscu, Eric Delpire, and Kodi S. Ravichandran. 2019. 'Interpreting an Apoptotic Corpse as Anti-Inflammatory Involves a Chloride Sensing Pathway'. *Nature Cell Biology* 21 (12): 1532–43. https://doi.org/10.1038/s41556-019-0431-1.

Plumptre, Isabella, Daniel Knabel, and Kenneth Tomecki. 2018. 'Pyoderma Gangrenosum: A Review for the Gastroenterologist'. *Inflammatory Bowel Diseases* 24 (12): 2510–17. https://doi.org/10.1093/ibd/izy174.

Pochard, Camille, Sabrina Coquenlorge, Julie Jaulin, Nicolas Cenac, Nathalie Vergnolle, Guillaume Meurette, Marie Freyssinet, Michel Neunlist, and Malvyne Rolli-Derkinderen. 2016. 'Defects in 15-HETE Production and Control of Epithelial Permeability by Human Enteric Glial Cells From Patients With Crohn's Disease'. *Gastroenterology* 150 (1): 168–80. https://doi.org/10.1053/j.gastro.2015.09.038.

Quigley, Eamonn M. M. 2011. 'Microflora Modulation of Motility'. *Journal of Neurogastroenterology and Motility* 17 (2): 140–47. https://doi.org/10.5056/jnm.2011.17.2.140.

Ramnath, Divya, Elizabeth E. Powell, Glen M. Scholz, and Matthew J. Sweet. 2017. 'The Toll-like Receptor 3 Pathway in Homeostasis, Responses to Injury and Wound Repair'. *Seminars in Cell & Developmental Biology* 61 (January): 22–30. https://doi.org/10.1016/j.semcdb.2016.08.014.

Ramnath, Divya, Kathryn Tunny, Daniel M. Hohenhaus, Claire M. Pitts, Anne-Sophie Bergot, P. Mark Hogarth, John A. Hamilton, et al. 2015. 'TLR3 Drives IRF6-Dependent IL-23p19 Expression and P19/EBI3 Heterodimer Formation in Keratinocytes'. *Immunology and Cell Biology* 93 (9): 771–79. https://doi.org/10.1038/icb.2015.77.

Rao, Meenakshi, and Michael D. Gershon. 2016. 'The Bowel and beyond: The Enteric Nervous System in Neurological Disorders'. *Nature Reviews Gastroenterology & Hepatology* 13 (9): 517–28. https://doi.org/10.1038/nrgastro.2016.107.

Rapp, Moritz, Maximilian W. M. Wintergerst, Wolfgang G. Kunz, Viola K. Vetter, Max M. L. Knott, Dominik Lisowski, Sascha Haubner, et al. 2019. 'CCL22 Controls Immunity by Promoting Regulatory T Cell Communication with Dendritic Cells in Lymph Nodes'. *The Journal of Experimental Medicine* 216 (5): 1170–81. https://doi.org/10.1084/jem.20170277.

Ray, Prabir, Nandini Krishnamoorthy, Timothy B. Oriss, and Anuradha Ray. 2010. 'Signaling of C-Kit in Dendritic Cells Influences Adaptive Immunity'. *Annals of the New York Academy of Sciences* 1183 (January): 104–22. https://doi.org/10.1111/j.1749-6632.2009.05122.x.

Reis e Sousa, Caetano. 2006. 'Dendritic Cells in a Mature Age'. *Nature Reviews. Immunology* 6 (6): 476–83. https://doi.org/10.1038/nri1845.

Ricciuto, Amanda, Binita M. Kamath, and Anne M. Griffiths. 2018. 'The IBD and PSC Phenotypes of PSC-IBD'. *Current Gastroenterology Reports* 20 (4): 16. https://doi.org/10.1007/s11894-018-0620-2.

Rimoldi, Monica, Marcello Chieppa, Valentina Salucci, Francesca Avogadri, Angelica Sonzogni, Gianluca M. Sampietro, Angelo Nespoli, Giuseppe Viale, Paola Allavena, and Maria Rescigno. 2005. 'Intestinal Immune Homeostasis Is Regulated by the Crosstalk between Epithelial Cells and Dendritic Cells'. *Nature Immunology* 6 (5): 507–14. https://doi.org/10.1038/ni1192.

Riol-Blanco, Lorena, Noelia Sánchez-Sánchez, Ana Torres, Alberto Tejedor, Shuh Narumiya, Angel L. Corbí, Paloma Sánchez-Mateos, and José Luis Rodríguez-Fernández. 2005. 'The Chemokine Receptor CCR7 Activates in Dendritic Cells Two Signaling Modules That Independently Regulate Chemotaxis and Migratory Speed'. *Journal of Immunology (Baltimore, Md.: 1950)* 174 (7): 4070–80. https://doi.org/10.4049/jimmunol.174.7.4070.

Rodewald, H. R., and T. N. Sato. 1996. 'Tie1, a Receptor Tyrosine Kinase Essential for Vascular Endothelial Cell Integrity, Is Not Critical for the Development of Hematopoietic Cells'. *Oncogene* 12 (2): 397–404.

Rosario, Maria, Nathanael L. Dirks, Catherine Milch, Asit Parikh, Michael Bargfrede, Tim Wyant, Eric Fedyk, and Irving Fox. 2017. 'A Review of the Clinical Pharmacokinetics, Pharmacodynamics, and Immunogenicity of Vedolizumab'. *Clinical Pharmacokinetics* 56 (11): 1287–1301. https://doi.org/10.1007/s40262-017-0546-0.

Roth, Lee, Swati Srivastava, Moshit Lindzen, Aldema Sas-Chen, Michal Sheffer, Mattia Lauriola, Yehoshua Enuka, et al. 2018. 'SILAC Identifies LAD1 as a Filamin-Binding Regulator of Actin Dynamics in Response to EGF and a Marker of Aggressive Breast Tumors'. *Science Signaling* 11 (515). https://doi.org/10.1126/scisignal.aan0949.

Ruder, Barbara, and Christoph Becker. 2020. 'At the Forefront of the Mucosal Barrier: The Role of Macrophages in the Intestine'. *Cells* 9 (10). https://doi.org/10.3390/cells9102162.

Sallusto, F, M Cella, C Danieli, and A Lanzavecchia. 1995. 'Dendritic Cells Use Macropinocytosis and the Mannose Receptor to Concentrate Macromolecules in the Major Histocompatibility Complex Class II Compartment: Downregulation by Cytokines and Bacterial Products.' *Journal of Experimental Medicine* 182 (2): 389–400. https://doi.org/10.1084/jem.182.2.389.

Sanz, Ignacio, Chungwen Wei, Scott A. Jenks, Kevin S. Cashman, Christopher Tipton, Matthew C. Woodruff, Jennifer Hom, and F. Eun-Hyung Lee. 2019. 'Challenges and Opportunities for Consistent Classification of Human B Cell and Plasma Cell Populations'. *Frontiers in Immunology* 10. https://doi.org/10.3389/fimmu.2019.02458.

Schmidt, Carsten, Thomas Giese, Bianca Ludwig, Ina Mueller-Molaian, Thomas Marth, Stefan Zeuzem, Stefan C. Meuer, and Andreas Stallmach. 2005. 'Expression of Interleukin-12-Related Cytokine Transcripts in Inflammatory Bowel Disease: Elevated Interleukin-23p19 and Interleukin-27p28 in Crohn's Disease but Not in Ulcerative Colitis'. *Inflammatory Bowel Diseases* 11 (1): 16–23. https://doi.org/10.1097/00054725-200501000-00003.

Scholz, Glen M., Jacqueline E. Heath, Katrina A. Walsh, and Eric C. Reynolds. 2018. 'MEK-ERK Signaling Diametrically Controls the Stimulation of IL-23p19 and EBI3 Expression in Epithelial Cells by IL-36γ'. *Immunology and Cell Biology* 96 (6): 646–55. https://doi.org/10.1111/imcb.12029.

Schröder-Braunstein, Jutta, Judith Gras, Benedikt Brors, Sonja Schwarz, Timea Szikszai, Felix Lasitschka, Guido Wabnitz, et al. 2014. 'Initiation of an Inflammatory Response in Resident Intestinal Lamina Propria Cells -Use of a Human Organ Culture Model'. *PloS One* 9 (5): e97780. https://doi.org/10.1371/journal.pone.0097780.

Schurch, Nicholas J., Pietá Schofield, Marek Gierliński, Christian Cole, Alexander Sherstnev, Vijender Singh, Nicola Wrobel, et al. 2016. 'How Many Biological Replicates Are Needed in an RNA-Seq Experiment and Which Differential Expression Tool Should You Use?' *RNA (New York, N.Y.)* 22 (6): 839–51. https://doi.org/10.1261/rna.053959.115.

Scott, C. L., C. C. Bain, P. B. Wright, D. Sichien, K. Kotarsky, E. K. Persson, K. Luda, et al. 2015. 'CCR2(+)CD103(-) Intestinal Dendritic Cells Develop from DC-Committed Precursors and Induce Interleukin-17 Production by T Cells'. *Mucosal Immunology* 8 (2): 327–39. https://doi.org/10.1038/mi.2014.70.

Seegert, D, P Rosenstiel, H Pfahler, P Pfefferkorn, S Nikolaus, and S Schreiber. 2001. 'Increased Expression of IL-16 in Inflammatory Bowel Disease'. *Gut* 48 (3): 326–32. https://doi.org/10.1136/gut.48.3.326.

Segura, Elodie. 2016. 'Review of Mouse and Human Dendritic Cell Subsets'. *Methods in Molecular Biology (Clifton, N.J.)* 1423: 3–15. https://doi.org/10.1007/978-1-4939-3606-9_1.

Sengupta, N., and T. T. MacDonald. 2007. 'The Role of Matrix Metalloproteinases in Stromal/Epithelial Interactions in the Gut'. *Physiology (Bethesda, Md.)* 22 (December): 401–9. https://doi.org/10.1152/physiol.00027.2007.

Shaikh, Tamim H. 2017. 'Copy Number Variation Disorders'. *Current Genetic Medicine Reports* 5 (4): 183–90. https://doi.org/10.1007/s40142-017-0129-2.

Shaw, Souradet Y., James F. Blanchard, and Charles N. Bernstein. 2010. 'Association between the Use of Antibiotics in the First Year of Life and Pediatric Inflammatory Bowel Disease'. *The American Journal of Gastroenterology* 105 (12): 2687–92. https://doi.org/10.1038/ajg.2010.398.

Shi, Jishu, Shelly Aono, Wuyuan Lu, Andre J. Ouellette, Xueyou Hu, Yingbiao Ji, Lei Wang, et al. 2007. 'A Novel Role for Defensins in Intestinal Homeostasis: Regulation of IL-1beta Secretion'. *Journal of Immunology (Baltimore, Md.: 1950)* 179 (2): 1245–53. https://doi.org/10.4049/jimmunol.179.2.1245.

Simonetti, Sonia, Amairelys B. Barroeta Seijas, Ambra Natalini, Sara Vitale, Daniele Runci, Alessandra Soriani, Antonio Di Virgilio, et al. 2019. 'Dendritic Cells Modulate C-Kit Expression on the Edge between Activation and Death'. *European Journal of Immunology* 49 (4): 534–45. https://doi.org/10.1002/eji.201847683.

Sina, Christian, Simone Lipinski, Olga Gavrilova, Konrad Aden, Ateequr Rehman, Andreas Till, Andrea Rittger, et al. 2013. 'Extracellular Cathepsin K Exerts Antimicrobial Activity and Is Protective against Chronic Intestinal Inflammation in Mice'. *Gut* 62 (4): 520–30. https://doi.org/10.1136/gutjnl-2011-300076.

Sivanesan, Durga, Claudine Beauchamp, Christiane Quinou, Jonathan Lee, Sylvie Lesage, Sylvain Chemtob, John D. Rioux, and Stephen W. Michnick. 2016. 'IL23R (Interleukin 23 Receptor) Variants Protective against Inflammatory Bowel Diseases (IBD) Display Loss of Function Due to Impaired Protein Stability and Intracellular Trafficking'. *The Journal of Biological Chemistry* 291 (16): 8673–85. https://doi.org/10.1074/jbc.M116.715870.

Skubitz, K. M., K. D. Campbell, and A. P. Skubitz. 1996. 'CD66a, CD66b, CD66c, and CD66d Each Independently Stimulate Neutrophils'. *Journal of Leukocyte Biology* 60 (1): 106–17. https://doi.org/10.1002/jlb.60.1.106.

Smillie, Christopher S., Moshe Biton, Jose Ordovas-Montanes, Keri M. Sullivan, Grace Burgin, Daniel B. Graham, Rebecca H. Herbst, et al. 2019. 'Intra- and Inter-Cellular Rewiring of the Human Colon during Ulcerative Colitis'. *Cell* 178 (3): 714-730.e22. https://doi.org/10.1016/j.cell.2019.06.029.

Smith, Paul J., and Pratip K. Chattopadhyay. 2016. 'Re-Visiting Fc-Receptor Blocking Maneuvers in Man'. *Cytometry. Part A: The Journal of the International Society for Analytical Cytology* 89 (11): 975–77. https://doi.org/10.1002/cyto.a.22998.

Stagg, Andrew J. 2018. 'Intestinal Dendritic Cells in Health and Gut Inflammation'. *Frontiers in Immunology* 9 (December). https://doi.org/10.3389/fimmu.2018.02883.

Strbo, Natasa, Natalie Yin, and Olivera Stojadinovic. 2014. 'Innate and Adaptive Immune Responses in Wound Epithelialization'. *Advances in Wound Care* 3 (7): 492–501. https://doi.org/10.1089/wound.2012.0435.

Sturm, Andreas, Daniel C. Baumgart, Johanna Harder d'Heureuse, Angelika Hotz, Bertram Wiedenmann, and Axel U. Dignass. 2005. 'CXCL8 Modulates Human Intestinal Epithelial Cells through a CXCR1 Dependent Pathway'. *Cytokine* 29 (1): 42–48. https://doi.org/10.1016/j.cyto.2004.09.007.

Sun, Tian, Albert Nguyen, and Jennifer L. Gommerman. 2020. 'Dendritic Cell Subsets in Intestinal Immunity and Inflammation'. *The Journal of Immunology* 204 (5): 1075–83. https://doi.org/10.4049/jimmunol.1900710.

Swee, Mei, Carole L. Wilson, Ying Wang, John K. McGuire, and William C. Parks. 2008. 'Matrix Metalloproteinase-7 (Matrilysin) Controls Neutrophil Egress by Generating Chemokine Gradients'. *Journal of Leukocyte Biology* 83 (6): 1404–12. https://doi.org/10.1189/jlb.0108016.

Szikszai, Timea, Felix Lasitschka, Thomas Giese, Matthias Greulich, Young-Seon Lee, Juliane Ilse, Serin Schiessling, et al. 2015. 'Standardization of a Human Organ Culture Model of Intestinal Inflammation and Its Application for Drug Testing'. *Journal of Immunological Methods* 421 (June): 96–103. https://doi.org/10.1016/j.jim.2014.12.014.

Takenaka, Maisa C., Marcia G. Guereschi, and Alexandre S. Basso. 2017. 'Neuroimmune Interactions: Dendritic Cell Modulation by the Sympathetic Nervous System'. *Seminars in Immunopathology* 39 (2): 165–76. https://doi.org/10.1007/s00281-016-0590-0.

Teodosio, Cristina, Andrea Mayado, Laura Sánchez-Muñoz, José M. Morgado, María Jara-Acevedo, Ivan Álvarez-Twose, Andrés C. García-Montero, et al. 2015. 'The Immunophenotype of Mast Cells and Its Utility in the Diagnostic Work-up of Systemic Mastocytosis'. *Journal of Leukocyte Biology* 97 (1): 49–59. https://doi.org/10.1189/jlb.5RU0614-296R.

Tezuka, Hiroyuki, and Toshiaki Ohteki. 2019. 'Regulation of IgA Production by Intestinal Dendritic Cells and Related Cells'. *Frontiers in Immunology* 10: 1891. https://doi.org/10.3389/fimmu.2019.01891.

Tong, Honglian, Yoshiyuki Miyazaki, Masanori Yamazaki, Hiromitsu Hara, Herman Waldmann, Shohei Hori, and Hiroki Yoshida. 2010. 'Exacerbation of Delayed-Type Hypersensitivity Responses in EBV-Induced Gene-3 (EBI-3)-Deficient Mice'. *Immunology Letters* 128 (2): 108–15. https://doi.org/10.1016/j.imlet.2010.01.001.

Trombetta, E. Sergio, and Ira Mellman. 2005. 'Cell Biology of Antigen Processing in Vitro and in Vivo'. *Annual Review of Immunology* 23: 975–1028. https://doi.org/10.1146/annurev.immunol.22.012703.104538.

Trzpis, Monika, Pamela M.J. McLaughlin, Lou M.F.H. de Leij, and Martin C. Harmsen. 2007. 'Epithelial Cell Adhesion Molecule'. *The American Journal of Pathology* 171 (2): 386–95. https://doi.org/10.2353/ajpath.2007.070152.

Tsai, Shih Han, Makoto Kinoshita, Takashi Kusu, Hisako Kayama, Ryu Okumura, Kayo Ikeda, Yosuke Shimada, et al. 2015. 'The Ectoenzyme E-NPP3 Negatively Regulates ATP-Dependent Chronic Allergic Responses by Basophils and Mast Cells'. *Immunity* 42 (2): 279–93. https://doi.org/10.1016/j.immuni.2015.01.015.

Turpin, Williams, Osvaldo Espin-Garcia, Wei Xu, Mark S. Silverberg, David Kevans, Michelle I. Smith, David S. Guttman, et al. 2016. 'Association of Host Genome with Intestinal Microbial Composition in a Large Healthy Cohort'. *Nature Genetics* 48 (11): 1413–17. https://doi.org/10.1038/ng.3693.

Unterholzner, Leonie, Sinead E. Keating, Marcin Baran, Kristy A. Horan, Søren B. Jensen, Shruti Sharma, Cherilyn M. Sirois, et al. 2010. 'IFI16 Is an Innate Immune Sensor for Intracellular DNA'. *Nature Immunology* 11 (11): 997–1004. https://doi.org/10.1038/ni.1932.

Vaine, Christine A., and Roy J. Soberman. 2014. 'The CD200–CD200R1 Inhibitory Signaling Pathway'. *Advances in Immunology* 121: 191–211. https://doi.org/10.1016/B978-0-12-800100-4.00005-2.

Valent, Peter, Sabine Cerny-Reiterer, Harald Herrmann, Irina Mirkina, Tracy I. George, Karl Sotlar, Wolfgang R. Sperr, and Hans-Peter Horny. 2010. 'Phenotypic Heterogeneity, Novel Diagnostic Markers, and Target Expression Profiles in Normal and Neoplastic Human Mast Cells'. *Best Practice & Research. Clinical Haematology* 23 (3): 369–78. https://doi.org/10.1016/j.beha.2010.07.003.

Vanhove, Wiebe, Paul M. Peeters, Dominiek Staelens, Anica Schraenen, Jan Van der Goten, Isabelle Cleynen, Sebastiaan De Schepper, et al. 2015. 'Strong Upregulation of AIM2 and IFI16 Inflammasomes in the Mucosa of Patients with Active Inflammatory Bowel Disease'. *Inflammatory Bowel Diseases* 21 (11): 2673–82. https://doi.org/10.1097/MIB.0000000000000535.

Vavricka, Stephan R., Michael Scharl, Martin Gubler, and Gerhard Rogler. 2014. 'Biologics for Extraintestinal Manifestations of IBD'. *Current Drug Targets* 15 (11): 1064–73. https://doi.org/10.2174/1389450115666140908125453.

Veenbergen, S, P Li, HC Raatgeep, DJ Lindenbergh-Kortleve, Y Simons-Oosterhuis, A Farrel, LMM Costes, et al. 2019. 'IL-10 Signaling in Dendritic Cells Controls IL-1β-Mediated IFNγ Secretion by Human CD4+ T Cells: Relevance to Inflammatory Bowel Disease'. *Mucosal Immunology* 12 (5): 1201–11. https://doi.org/10.1038/s41385-019-0194-9.

Versteven, Maarten, Johan M. J. Van den Bergh, Elly Marcq, Evelien L. J. Smits, Viggo F. I. Van Tendeloo, Willemijn Hobo, and Eva Lion. 2018. 'Dendritic Cells and Programmed Death-1 Blockade: A Joint Venture to Combat Cancer'. *Frontiers in Immunology* 9 (March). https://doi.org/10.3389/fimmu.2018.00394.

Vignali, Dario A. A., and Vijay K. Kuchroo. 2012. 'IL-12 Family Cytokines: Immunological Playmakers'. *Nature Immunology* 13 (8): 722–28. https://doi.org/10.1038/ni.2366.

Villadangos, José A., Petra Schnorrer, and Nicholas S. Wilson. 2005. 'Control of MHC Class II Antigen Presentation in Dendritic Cells: A Balance between Creative and Destructive Forces'. *Immunological Reviews* 207 (October): 191–205. https://doi.org/10.1111/j.0105-2896.2005.00317.x.

Vinish, Monika, Weihua Cui, Eboni Stafford, Leon Bae, Hal Hawkins, Robert Cox, and Tracy Toliver-Kinsky. 2016. 'Dendritic Cells Modulate Burn Wound Healing by Enhancing Early Proliferation'. *Wound Repair and Regeneration: Official Publication of the Wound Healing Society [and] the European Tissue Repair Society* 24 (1): 6–13. https://doi.org/10.1111/wrr.12388.

Vogt, R. F., D. L. Phillips, L. O. Henderson, W. Whitfield, and F. W. Spierto. 1987. 'Quantitative Differences among Various Proteins as Blocking Agents for ELISA Microtiter Plates'. *Journal of Immunological Methods* 101 (1): 43–50. https://doi.org/10.1016/0022-1759(87)90214-6.

Wang, Ge-Fei, Jian-An Ren, Song Liu, Jun Chen, Guo-Sheng Gu, Xin-Bo Wang, Chao-Gang Fan, and Jie-Shou Li. 2012. 'Clinical Characteristics of Non-Perianal Fistulating Crohn's Disease in China: A Single-Center Experience of 184 Cases'. *Chinese Medical Journal* 125 (14): 2405–10.

Wang, X., X. Liu, Y. Zhang, Z. Wang, G. Zhu, G. Han, G. Chen, et al. 2016. 'Interleukin (IL)-39 [IL-23p19/Epstein–Barr Virus-induced 3 (Ebi3)] Induces Differentiation/Expansion of Neutrophils in Lupus-prone Mice'. *Clinical and Experimental Immunology* 186 (2): 144–56. https://doi.org/10.1111/cei.12840.

Wang, Xiaoqian, Yinxiang Wei, He Xiao, Xiaoling Liu, Yu Zhang, Gencheng Han, Guojiang Chen, et al. 2016. 'A Novel IL-23p19/Ebi3 (IL-39) Cytokine Mediates Inflammation in Lupus-like Mice'. *European Journal of Immunology* 46 (6): 1343–50. https://doi.org/10.1002/eji.201546095.

Waugh, David J. J., and Catherine Wilson. 2008. 'The Interleukin-8 Pathway in Cancer'. *Clinical Cancer Research: An Official Journal of the American Association for Cancer Research* 14 (21): 6735–41. https://doi.org/10.1158/1078-0432.CCR-07-4843.

Wechter, Todd, Abigail Cline, and Steven R. Feldman. 2018. 'Targeting P19 as a Treatment Option for Psoriasis: An Evidence-Based Review of Guselkumab'. *Therapeutics and Clinical Risk Management* 14: 1489–97. https://doi.org/10.2147/TCRM.S177127.

West, Nathaniel R., Ahmed N. Hegazy, Benjamin M. J. Owens, Samuel J. Bullers, Bryan Linggi, Sofia Buonocore, Margherita Coccia, et al. 2017. 'Oncostatin M Drives Intestinal Inflammation and Predicts Response to Tumor Necrosis Factor-Neutralizing Therapy in Patients with Inflammatory Bowel Disease'. *Nature Medicine* 23 (5): 579–89. https://doi.org/10.1038/nm.4307.

Wetzel, Alexandra, Bettina Scholtka, Christian Gerecke, and Burkhard Kleuser. 2020. 'Epigenetic Histone Modulation Contributes to Improvements in Inflammatory Bowel Disease via EBI3'. *Cellular and Molecular Life Sciences: CMLS* 77 (23): 5017–30. https://doi.org/10.1007/s00018-020-03451-9.

Williams, E. J., S. Haque, C. Banks, P. Johnson, P. Sarsfield, and N. Sheron. 2000. 'Distribution of the Interleukin-8 Receptors, CXCR1 and CXCR2, in Inflamed Gut Tissue'. *The Journal of Pathology* 192 (4): 533–39. https://doi.org/10.1002/1096-9896(2000)9999:9999<::AID-PATH732>3.0.CO;2-X.

Wolf, Anna Maria, Dominik Wolf, Holger Rumpold, Alexander R. Moschen, Arthur Kaser, Peter Obrist, Dietmar Fuchs, et al. 2004. 'Overexpression of Indoleamine 2,3-Dioxygenase in Human Inflammatory Bowel Disease'. *Clinical Immunology (Orlando, Fla.)* 113 (1): 47–55. https://doi.org/10.1016/j.clim.2004.05.004.

Wolf, Marie, Selene M. Clay, Siyu Zheng, Peipei Pan, and Matilda F. Chan. 2019. 'MMP12 Inhibits Corneal Neovascularization and Inflammation through Regulation of CCL2'. *Scientific Reports* 9 (August). https://doi.org/10.1038/s41598-019-47831-z.

Wu, Yang, Zhigang Tian, and Haiming Wei. 2017. 'Developmental and Functional Control of Natural Killer Cells by Cytokines'. *Frontiers in Immunology* 8. https://doi.org/10.3389/fimmu.2017.00930.

Xue, Xiang, and Daniel M. Falcon. 2019. 'The Role of Immune Cells and Cytokines in Intestinal Wound Healing'. *International Journal of Molecular Sciences* 20 (23). https://doi.org/10.3390/ijms20236097.

Yamazaki, Sayuri, and Ralph M. Steinman. 2009. 'Dendritic Cells as Controllers of Antigen-Specific Foxp3+ Regulatory T Cells'. *Journal of Dermatological Science* 54 (2): 69–75. https://doi.org/10.1016/j.jdermsci.2009.02.001.

Yang, Bin, Jutamas Suwanpradid, Roberto Sanchez-Lagunes, Hae Woong Choi, Peter Hoang, Donghai Wang, Soman N. Abraham, and Amanda S. MacLeod. 2017. 'IL-27 Facilitates Skin Wound Healing through Induction of Epidermal Proliferation and Host Defense'. *The Journal of Investigative Dermatology* 137 (5): 1166–75. https://doi.org/10.1016/j.jid.2017.01.010.

Yoo, Bryan B., and Sarkis K. Mazmanian. 2017. 'The Enteric Network: Interactions between the Immune and Nervous Systems of the Gut'. *Immunity* 46 (6): 910–26. https://doi.org/10.1016/j.immuni.2017.05.011.

Yoon, Juhan, Akihiko Terada, and Hirohito Kita. 2007. 'CD66b Regulates Adhesion and Activation of Human Eosinophils'. *Journal of Immunology (Baltimore, Md.: 1950)* 179 (12): 8454–62. https://doi.org/10.4049/jimmunol.179.12.8454.

Yoshie, Osamu, and Kouji Matsushima. 2015. 'CCR4 and Its Ligands: From Bench to Bedside'. *International Immunology* 27 (1): 11–20. https://doi.org/10.1093/intimm/dxu079.

Yoshimura-Uchiyama, C., M. Iikura, M. Yamaguchi, H. Nagase, A. Ishii, K. Matsushima, K. Yamamoto, M. Shichijo, K. B. Bacon, and K. Hirai. 2004. 'Differential Modulation of Human Basophil Functions through Prostaglandin D2 Receptors DP and Chemoattractant Receptor-Homologous Molecule Expressed on Th2 Cells/DP2'. *Clinical & Experimental Allergy* 34 (8): 1283–90. https://doi.org/10.1111/j.1365-2222.2004.02027.x.

Zanello, Galliano, Ashleigh Goethel, Katharina Forster, Kaoru Geddes, Dana J. Philpott, and Kenneth Croitoru. 2013. 'Nod2 Activates NF-KB in CD4+ T Cells but Its Expression Is Dispensable for T Cell-Induced Colitis'. *PloS One* 8 (12): e82623. https://doi.org/10.1371/journal.pone.0082623.

Zhang, Chenhong, Menghui Zhang, Shengyue Wang, Ruijun Han, Youfang Cao, Weiying Hua, Yuejian Mao, et al. 2010. 'Interactions between Gut Microbiota, Host Genetics and Diet Relevant to Development of Metabolic Syndromes in Mice'. *The ISME Journal* 4 (2): 232–41. https://doi.org/10.1038/ismej.2009.112.

Zhu, Yuzhen, Jun Dai, Xiaoying Yao, Guanjun Dong, Hui Zhang, Fenglian Yan, Chunxia Li, Xuehui Li, Huabao Xiong, and Chuanping Si. 2018. '[IL-16 aggravates dextran sulfate sodium (DSS)-induced mouse inflammatory bowel disease by promoting M1 polarization of macrophages]'. *Xi Bao Yu Fen Zi Mian Yi Xue Za Zhi = Chinese Journal of Cellular and Molecular Immunology* 34 (8): 695–701.

Zimmerman, Noah P., Rebecca A. Vongsa, Michael K. Wendt, and Michael B. Dwinell. 2008. 'Chemokines and Chemokine Receptors in Mucosal Homeostasis at the Intestinal Epithelial Barrier in Inflammatory Bowel Disease'. *Inflammatory Bowel Diseases* 14 (7): 1000–1011. https://doi.org/10.1002/ibd.20480.

Danksagung

Hiermit bedanke ich mich bei Herrn Prof. Dr. Tobias Dick für die Betreuung dieser Doktorarbeit.

Ebenso bedanke ich mich bei Herrn Prof. Dr. Stefan Meuer für die Möglichkeit diese Doktorarbeit am Institut für Immunologie anfertigen zu dürfen und die Unterstützung meiner Ziele.

Besonderer Dank geht an Frau Dr. Jutta Schröder-Braunstein für die wissenschaftliche Betreuung dieser Doktorarbeit, der Tatsache mir stets entgegengekommen zu sein und zu jeder Zeit ein offenes Ohr gehabt zu haben.

Danke auch an alle Mitarbeiter:innen und ex Mitarbeiter:innen der AG Meuer/Schröder-Braunstein die einen Teil meines Weges gemeinsam mit mir verbracht haben.

Danke auch an alle Kolleg:innen der Labore Samstag, Giese, Wabnitz, Kirschfink und Nakchbandi für den regen Austausch und etliche lustige Momente.

Ganz besonderer Dank gebührt meiner Familie und meiner Frau, welche den Schaffensprozess aus nächster Nähe verfolgen durften.